Helices by hydrogen bonding : folding and stacking of chiral supramolecular scaffolds

Helices by Hydrogen Bonding

Folding and Stacking of Chiral Supramolecular Scaffolds

Helices by Hydrogen Bonding

Folding and Stacking of Chiral Supramolecular Scaffolds

PROEFSCHRIFT

ter verkrijging van de graad van doctor aan de Technische Universiteit Eindhoven, op gezag van de Rector Magnificus, prof.dr. R.A. van Santen, voor een commissie aangewezen door het College voor Promoties in het openbaar te verdedigen op woensdag 12 mei 2004 om 14.00 uur

door

Judith Johanna van Gorp

geboren te Eindhoven

Dit proefschrift is goedgekeurd door de promotoren:

prof.dr. E.W. Meijer
en
prof.dr. S.C. Zimmerman

Copromotor:

dr. J.A.J.M. Vekemans

This research has been financially supported by the Council for Chemical Sciences of the Netherlands Organization for Scientific Research (NWO-CW).

Omslagontwerp: Judith J. van Gorp

Druk: Universiteitsdrukkerij, Technische Universiteit Eindhoven

CIP-DATA LIBRARY TECHNISCHE UNIVERSITEIT EINDHOVEN

Gorp, Judith J. van

Helices by hydrogen bonding : folding and stacking of chiral supramolecular scaffolds / by Judith J. van Gorp. – Eindhoven : Technische Universiteit Eindhoven, 2004.
Proefschrift. – ISBN 90-386-2995-8
NUR 913
Trefwoorden: supramoleculaire chemie / chiraliteit / vloeibare kristallen ; discoten / helixconformatie ; opvouwbaarheid / inter- en intramoleculaire waterstofbruggen
Subject headings: supramolecular chemistry / chirality / liquid crystals ; discotics / helix conformation ; folding / inter- and intramolecular hydrogen bonding

'Achter iedere deur die ik open doe,
doe jij een andere deur weer dicht.
En zo blijf je verborgen,
nooit wordt er meer dan
een tip van de sluier
opgelicht.'

Een tip van de sluier
Boudewijn de Groot / Lennaert Nijgh

Contents

Chapter 1

Amplification of chirality in supramolecular architectures

Abstract: *Chirality provides spatial architectures with unique properties. Living systems rely on the exclusive choice by nature of one enantiomer over the other as builing block for defined biomolecules with embedded chirality. When chirality is transferred to a higher level of organization, it governs the three-dimensional shape of the molecules of life. Similarly, small bits of chiral information have been incorporated in artificial systems to control the shape of complex, supramolecular, architectures. This implies that in these synthetic supramolecular systems, chirality in one of the building blocks may order the entire architecture. In those cases chirality is said to be amplified, resulting in an induced circular dichroism effect (ICD).*

The 'sergeants and soldiers' effect describes how one chiral element imposes its twist sense on a large 'platoon' of achiral fragments. Initially, the effect was recognized in stiff macromolecules. These results appeal to the imagination, and inspire to adapt the principle to supramolecular helices of discotics. In this chapter it is explained why and how induced CD effects (the 'sergeants and soldiers effect', 'majority rules expression', and 'chiral solvation phenomenon'), serve as a probe for the inherent chirality of supramolecular architectures, and for cooperativity in the non-covalent interactions. Quantification in the form of an association constant and a cooperative length, allows comparison of a variety of helical supramolecular columns of discotics. Amplification of chirality has also been expressed in concave supramolecular assemblies, displaying an exciting 'chiral memory'. This shows that the principle is generally applicable to probe chiral order in supramolecular architectures, both in self-assemblies and in folded macromolecules.

1.1 Stereochemistry in conformational studies

'*One chiral molecule imposing its twist sense on hundreds of achiral ones*', an appealing idea indeed, touching on the intriguing issues of the origin of life and the relevance of the interaction of light with matter. Mark Green and co-workers materialized this thought in stiff macromolecules, poly(*n*-alkylisocyanates), in which one chiral side chain, the 'sergeant', imposed its preferential twist sense on a 'platoon' of achiral monomeric units, the 'soldiers'.[1] The imagination is challenged even further by the expression of the 'sergeants and soldiers' principle, or amplification of chirality, in dynamic supramolecular columns of C_3-symmetrical discotics, firstly described by Anja Palmans *et al.*.[2] This initiated the exploration of the apparent strength of stereochemistry in revealing the structure and behavior of supramolecular architectures.

Nowadays, the appeal to introduce stereochemical subtleties within conformational research topics is widely recognized. Synthetic architectures approach slowly but steadily the size and functionality of natural macromolecules, via molecular, macromolecular, and supramolecular pathways.[3] However, some hurdles had to be taken before stereochemical and conformational interests were united. Already in the late 19th century, Jacobus Henricus van 't Hoff was especially intrigued by stereochemical issues.[4,5] This first Nobel laureate in chemistry, initially put forward the concept of a tetrahedral carbon atom (1875) to rationalize Louis Pasteur's findings, concerning the two different chiroptical crystals of sodium ammonium tartrate (1848). The overwhelming impact he had on stereochemistry, in particular in the Netherlands,[6] is illustrated by the work of J. M. Bijvoet, who established the absolute configuration of stereoisomers (1951).[7] It was proven by anomalous X-ray diffraction that before (1906) the right relative configuration system had been chosen, rendering it unnecessary to view half a century of stereochemical formulas 'via a mirror'.[8] At the same time (1951), Linus Pauling firstly proposed the α-helical conformation for polypeptide chains.[9] Although he shared the chemistry building with John G. Kirkwood,[10] a crystallographer certainly aware of Bijvoet's results, it appears as if, at that time, Pauling could not care less about the absolute configuration of his amino acids, let alone the handedness of his helical molecular models![11] Finally, John Kendrew and co-workers (1960) could relate the accurate right handedness of the helix build from correctly *S*-assigned amino acids, by revealing the presence of α-helices in an actual protein (myoglobin).[12] Many 'hot' issues concerning either the structure of complex architectures and/or their stereochemistry were already recognized immediately after the establishment of both chemical fields, and details keep being revealed every day.[13]

It seems only logical, that in this period (1950's) the techniques ORD (optical rotatory dispersion) and CD (circular dichroism) were rediscovered to perform structural studies on complex architectures. The ORD technique studies chiroptical properties of materials by the wavelength dependency of their

refractive index, which corresponds to their capability to rotate plane polarized light (Biot, 1820's).[14] Pierre Curie and his description of circularly polarized light (1893),[15] initiated the development of the CD technique (Aimé Cotton, 1895).[16] Using CD, the difference in absorption between right- and left-handed circularly polarized light is determined. CD made it possible to observe directly the absorption of the chromophores of specific moieties in the molecules, while ORD merely gives an overall signal originating from contributions of all CD bands. Refocusing on the α-helical example, the specific ellipticity at 220 nm is proportional to the α-helix content of the protein under investigation.[17]

Because CD was used in molecular chemistry, as well as in biochemistry, it was naturally implemented as a tool in supramolecular chemistry. As described above, the structure needs to be optically active to be studied with CD, which means incorporation of a stereocenter, and of a chromophore (180-800 nm). Molecular chirality reveals small local ordering concerning configuration and conformation of individual molecules. Chiral, isolated chromophores preferentially absorb one of the helical components of light, expressed in a typical Cotton effect. For biomacromolecules, the stereochemistry does not only relate to the primary, covalent chromophores, but also to secondary and tertiary structures, that are well-defined and inherently chiral. Supramolecular chirality has become a probe in recognizing order in supramolecular architectures. In contrast to molecular chirality studies, usually chromophores are used that are non-chiral themselves, while the stereocenter is located distantly (e.g. in a UV inactive, alkyl chain). In a disordered environment (isolated or in a disordered aggregate), such elements do not show preferential interaction with either right- or left-handed circularly polarized light. However, in an ordered architecture with an intrinsic overall chiral conformation (for example a helix), the distant stereocenters are ordered, which enables them to bias one handedness in the ordered architecture.[13d] Chirality is said to be transferred from the distant stereocenters to the chromophores, giving rise to an induced CD effect (ICD).[18] In other words, the chiral information 'travels' from the stereocenter to the chromophore along various structural elements and (non-) covalent bonds. The chiral information and the resulting ICD effect are changed by the specific impact of each encountered element and bond. Similarly, a story changes, when it is passed on from one person to the other, and so to the next generation.

The 'ordered architectures' containing a combination of 'chromophores' and 'stereocenters' indeed cover the broad range of structures implied by the universality of the terms they are denoted with. Supramolecular chemistry allows for a large variety of combinations, as building blocks are not only combined via covalent bonds, as in (macro)molecular chemistry, but also via non-covalent interactions.[19a] Whereas host-guest chemistry has been utilized frequently since its introduction by the Nobel laureates in supramolecular chemistry,[19b] hydrogen bonding has been found crucial for the behavior and properties of ordered architectures. It may increase overall directionality in the non-

covalent interactions, among which π-π stacking and solvophobic effects. Natural hydrogen bonding is encountered in macromolecules (e.g. Paulings helix),[9] as well as in self-assembled systems (e.g. tobacco mosaic virus).[20] Synthetic imitations of both types of architectures require a specific approach to enable investigation with CD spectroscopy, and the focus will be on self-assembled supramolecular architectures, columnar as well as concave ones.

Valuable structural information is obtained when the distant stereocenter is covalently linked to the chromophore. When no stereocenters are incorporated in the building blocks (*R*), 50 % of the helices is left handed, and 50 % right handed (Figure 1.1, situation A). *P* and *M* helices are mirror images and therefore enantiomers. Preference towards one helical sense can be induced by stereocenters in the supramolecular building blocks (*R** and *S**, Figure 1.1, left). This preference serves as a driving force accounting for an energy difference between the left- and right-handed helical diastereomers. For example, the *S** stereocenter might have a strong preference for incorporation in the *P* helix and the *R** stereocenter for incorporation in the *M* helix (Figure 1.1, situation B). Upon self-assembly of the mirror-image *R** or *S** building blocks, mirror-image supramolecular architectures are obtained (M-R* and P-S*). In case of a helix reversal, the diastereomer of M-R* would be formed, which is P-R*. However, it is energetically unfavorable to do so. Similarly, the occurance of M-S*, which is the diastereomer of P-S*, is limited. In case of non-covalent connection of *R** or *S** stereocenters (host/guest or acid/base interactions, chiral solvation) the supramolecular assemblies themselves contain no chiral building blocks and one of the enantiomers in situation A is preferred (Figure 1.1).

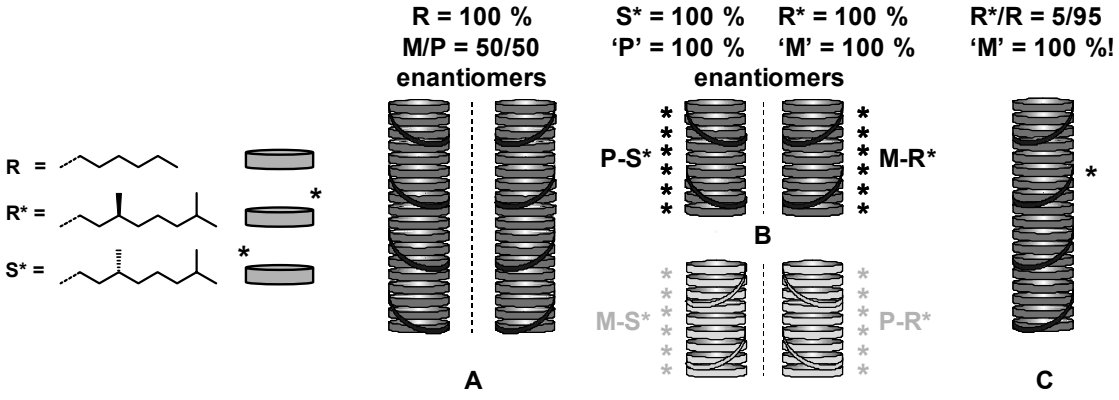

Figure 1.1. *Illustration of general aspects, using disks as supramolecular building blocks. Situation A: Achiral disks (R) yield an enantiomeric mixture of P and M helices. Situation B: Chiral disks yield exclusively one handedness, for example R* disks give M helices, while S* disks yield P helices. Situation C: A mixture of 5 % chiral disks (R*) and 95 % achiral disks (R) yields a fully chiral assembly. This is called the sergeants and soldiers effect.*

Four ICD phenomena have been encountered: the sergeants and soldiers effect, the majority rules expression, chiral solvation, and the chiral memory effect (Figure 1.1, situation C; *vide infra*). This has created a picture of cooperativity in non-covalent interactions, transferring chirality from stereocenters to chromophores, neighboring molecules, and supramolecular aggregates.

1.2 Amplification of chirality in columnar supramolecular architectures

1.2.1 C_3-Symmetrical discotics

The first example of amplification of chirality in supramolecular self-assemblies, described by Anja Palmans of our group, comprises inherently helical columns of C_3-symmetrical discotics.[2,21,22] This inherent helicity arises from its components **1** and **2a**, which are not flat, but 'propeller'-like, which prevents free rotation in the stack (Figure 1.2). The information necessary for adopting this 'propeller', and hence inherently chiral architecture, is embedded in the chemical structure of the components. Three amide functionalities at the benzene-1,3,5-tricarboxamide core are twisted out of the plane of the central benzene ring in order to achieve intermolecular hydrogen bonding from one disk to the other, inducing a tilt of the (intramolecular hydrogen bonded) bipyridinyl-gallic wedges.

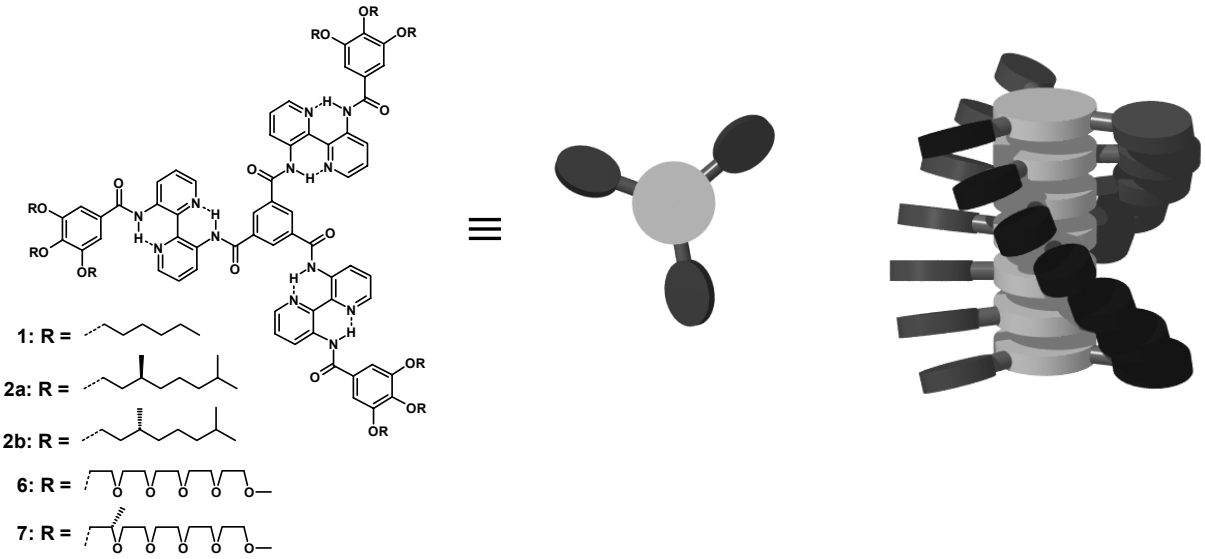

Figure 1.2. *Bipyridine based C_3-symmetrical disks and a cartoon representing their helical supramolecular stacking.*

In achiral compounds (hexyl side chains, **1**) an equal amount of *P* and *M* helical enantiomers is present (Figure 1.1, situation A). However, preference towards one helical sense can be induced by steric interactions of a stereocenter in a chiral side chain (RO = (*S*)-3,7-dimethyloctyloxy, **2a**). This serves as a driving force accounting for an energy difference between the left- and right-handed helical diastereomers (Figure 1.1, situation B). This sterical ordering locates the stereocenters regularly (according to the preferred handedness) along the column, enabling chirality to be transferred from the CD-silent chiral side chains to the bipyridinyl chromophores, resulting in a Cotton effect. Now, chiral amplification (Figure 1.1, situation C) implies that in a mixed stack of achiral and chiral propellers, **1** and **2a**, the chiral propellers (sergeants) impose their preferred twist sense on the achiral ones (soldiers). Indeed, addition of a small amount of chiral **2a** to a solution of

achiral **1** (10^{-5} M in heptane), instantaneously produces a Cotton effect, implying a random distribution of chiral and achiral molecules, **1/2a**. A dynamic process, in which molecules are exchanged, gives access to a cooperatively assembled stack. Nonetheless, an inherent chirality, or helicity, in both the optically inactive **1,** and in the optically active propeller **2a** stays insuperable for chiral amplification.

1.2.2 Inherent helicity

Inherent chirality implies that chiral information is present in the supramolecular building block itself (e.g. propeller-like conformation), and is not depending on the steric restrictions introduced by the stereocenters. In helical columns relying on the steric restrictions of the stereocenters, amplification of chirality is impossible, since achiral, planar disks, lacking the steric ordering, rotate freely about the columnar axis.[23] In these cases self-assembly is non-cooperative: steric ordering of the stereocenter in the side chain simultaneously induces helicity itself, along with a preferential twist sense. Thomas Katz *et al.* applied bulky helicene substituents to induce helicity in phthalocyanine stacks,[24] while Arno Kraft *et al.* used citronellol derived side chains to achieve this in tetrazole assemblies.[25]

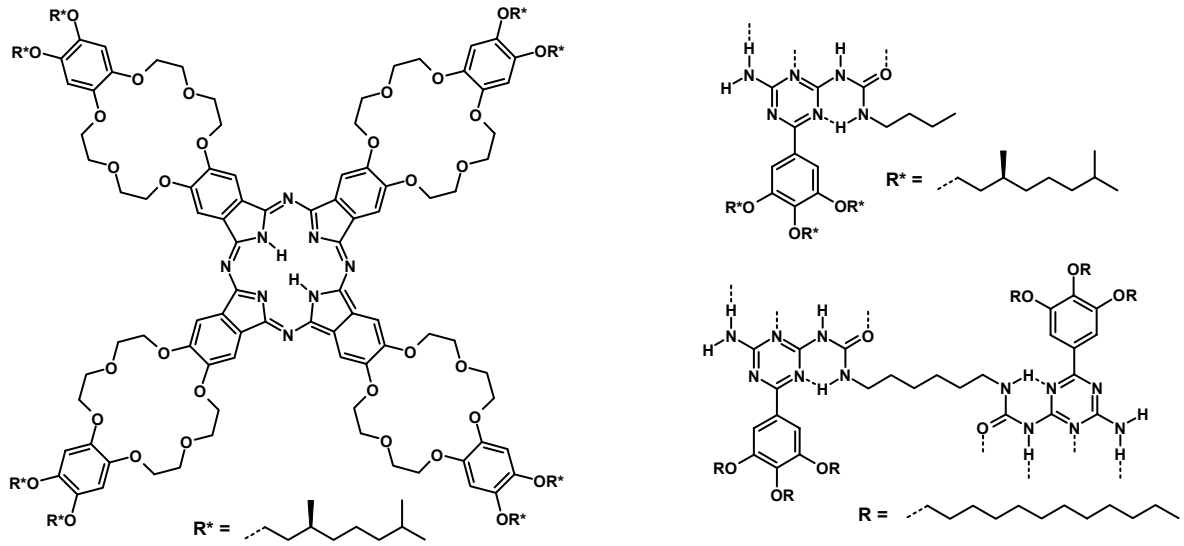

Figure 1.3. *Chemical structures of a phthalocyanine equipped with crown ether and (S)-3,7-dimethyloctyloxy moieties (left), and of monofunctional (top right) and bifunctional (bottom right) triazines.*

The non-inherently chiral behavior is illustrated clearly in phthalocyanines equipped with crown ether and (*S*)-3,7-dimethyloctyloxy moieties, developed by Roeland Nolte and coworkers (Figure 1.3, left).[26] In these phthalocyanines, the stacking seemed not only non-cooperative, but even anti-cooperative. It was reasoned that at least two sergeants have to stack on top of each other before steric interactions due to the side-chain stereocenters become operative. Notably, the inherent chirality of

the columns is induced when steric restrictions are enforced upon covalent linkage of the phthalocyanine units, together with complexation of potassium ions to the crown ethers.

Similarly, steric restrictions induce helicity in columns of ureidotriazine[27] or ureidopyrimidinone[28] moieties (Figure 1.3, right, and Figure 1.4). Two 'monofunctional' halves dimerize to give discotics, which rotate freely in the non-helical stacks that are formed in apolar solution. Stereocenters (methyls in (*S*)-3,7-dimethyloctyloxy moieties) cannot induce the steric restrictions needed to express supramolecular chirality. However, when two 'halves' are connected via a short alkyl spacer, inherently helical, hydrogen bonded polymers are formed, since the spacers prevent free rotation of the discotics. Chirality is induced in a stack of achiral bifunctional triazine structures via cooperative interactions with a chiral monofunctional triazine.[27] The sergeants and soldiers effect is also demonstrated by mixtures of chiral and achiral bifunctional 'Upy's'.[28]

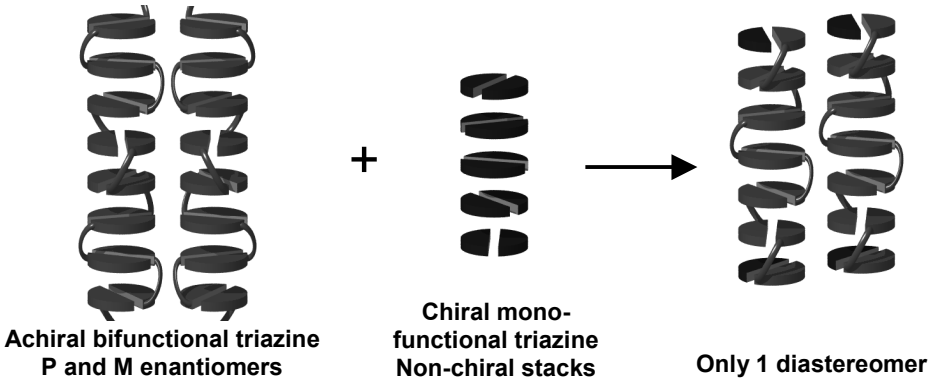

Figure 1.4. *Schematic representation of a chiral monofunctional ureidotriazine, that imposes its preferential twist sense on a stack of achiral bifunctional ureidotriazines.*

1.2.3 Quantifying amplification and comparing different C_3-symmetrical structures

Before amplification of chirality is quantified, the intensities of the CD signals themselves need to be compared. The molar ellipticity $\Delta\varepsilon$ [l/mol.cm], corrects the Cotton effect CD [mdeg] for the concentration c [M] and the path length l [cm] according to $\Delta\varepsilon = CD/(c \times l \times 32{,}980)$. The CD intensity [mdeg] might also be related to the UV absorption [O.D.] to give the g value ($g = \Delta\varepsilon/\varepsilon$). When CD and UV spectra are recorded using the same sample (c and l), g equals to CD/(UV*32,980)). Amplification of chirality is quantified by the length of one twist sense between helical reversals, defined as the cooperative length L_C. In inherently chiral stacks of propellers **1**/**2a** amplification of chirality occurs efficiently. L_C corresponds to ~ 80 molecules, as calculated by a model proposed by Edsko Havinga.[2,21] By introducing on average 1 molecule of chiral **2a** per 80 molecules achiral **1**, the sergeant **2a** is able to totally dictate the helical sense of the stack. The association constant ($K_{ass} \sim 10^8$ l/mol) determines the average length of the columns DP ($DP = 2 \times \sqrt{(K_{ass} \times \text{concentration})}$).[13d,30] Naturally, the actual amplification or 'number of sergeants' needed, will be determined by the average

length of the columns, when this length is smaller than the cooperative length. Abovementioned values for L_C and K_{ass} are based on the experimental finding that below 10^{-5} M concentration dependency sets in.[29] This means that the cooperative length L_C corresponds to the number average degree of polymerization DP at 10^{-5} M (1.9×10^{-4} M: DP = 275, 1.9×10^{-5} M: DP = 80, 1.9×10^{-6} M: DP = 20). Full expression of chirality was obtained with 5 % sergeants, 4 times more than needed theoretically (1.25 %), due to a statistical distribution of the sergeants over the soldiers and disconnection of the different segments by thermal motion, expressed in 'movement of the persistence length over the column'.

The inherent chirality induced by merely the intermolecularly hydrogen bonded central benzene-1,3,5-tricarboxamide unit, is illustrated by the even more pronounced chiral amplification in 'small' disks **3/4** (Figure 1.5). These small disks are substituted with single octyloxy chains (**3**) or ((*S*)-3,7-dimethyloctyloxy) chains (**4**), featuring a cooperative length L_C of 200 and an association constant K_{ass} of 5×10^8 l/mol.[13d,31] The limiting factor of DP on the full expression of amplification is illustrated by the concentration dependency (8×10^{-5} M: 2 % sergeant, DP = 400; 6×10^{-6} M: 5 % sergeant, DP = 100). Also, imposition of chirality on achiral sorbyl substituted disk **5** by chiral **4** occurs to a similar extent (3.3×10^{-5} M, 5 % sergeant).[32] The conversion and degree of polymerization for pure sorbyl disk **5** are similar to those of a 2/1 mixture of sorbyl disk **5** and achiral disk **3**. This indicates a dynamic exchange of the disks in the (polymerizing) stack. What is more, presence of chiral **4** upon polymerization of sorbyl disk **5**, allows formation of polymerized stacks of achiral disks **5** with a preferred handedness![33] From these results it might be concluded that intermolecular amide-mediated hydrogen bonding by itself is decisive in expressing supramolecular chirality and its amplification. However, from Chapters 2 and 3 in this thesis it follows that it is the subtle interplay of the different non-covalent interactions, together with the degree of remoteness of the chiral center, that determines the actual aggregation processes.[34]

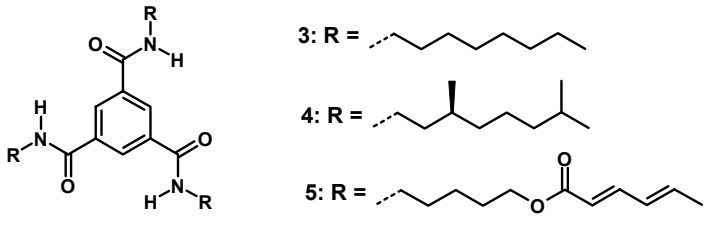

Figure 1.5. *Chemical structures of 'small' disks **3**, **4**, and **5**.*

Polar solvents, in particular water, affect the delicate hydrogen bonding interactions, rendering use of a combination of hydrogen bonding and 'hydrophobic' interactions, as encountered in proteins, inevitable. In oligo(ethylene oxide) substituted propellers **6/7** (Figure 1.1), the bipyridyl-gallic wedges

account for such 'hydrophobic effect', shielding the hydrogen bonding interactions at the benzene-1,3,5-tricarboxamide core from the polar solvent.[13d,35] In water itself, the 'hydrophobic effect' is responsible for strong aggregation ($K_{ass} \sim 10^8$ l/mol, DP = 200 at 10^{-4} M), although it cannot shield the structuring hydrogen bonds completely. Even at low temperatures (5 °C), the Cotton effect has not become constant and relatively much chiral compound (25-30 %) is needed for full expression of chirality, expressed in a low cooperative length ($L_C \sim 12$). However, in *n*-butanol at low temperatures (5 °C) the solvent does not interfere, and the fine tuning of intermolecular hydrogen bonding, and hence amplification of supramolecular chirality, is complete ($L_C \sim 400$, $K_{ass} \sim 5\times10^8$ l/mol). Whereas amplification of chirality is determined by the cooperative length at 10^{-4} M (DP = 450, 1 % sergeants), the number average degree of polymerization becomes the limiting factor upon dilution (DP = 140, and 5 % sergeants at 10^{-5} M).

1.3 Related phenomena in supramolecular C_3-symmetrical stacks

1.3.1 Majority rules

As mentioned before, the term 'sergeants and soldiers' was introduced by Mark Green[1,36] to describe the behavior in poly(*n*-alkylisocyanates). The stiff polymers adopt, due to their rigid backbones, an extended helical conformation with long stretches of one handedness (the cooperative length L_C), separated by high energy reversals. The replacement of a hydrogen by a methyl or a deuterium in only ~10 % of the side-chains was sufficient to induce full expression of chirality. Other phenomena were revealed to daylight by these rigid polymer structures as well, among which the expression of the 'majority rules'.[37a] The high energetic cost of a helix reversal gives rise to a non-linear relationship between the enantiomeric excess and the Cotton effect. Many monomers have to adopt their energetically less favored helical sense (many small costs), before a helix reversal is induced (one big cost). As a result, the Cotton effect of a random 2,6-dimethylheptylisocyanate copolymer with an *R*/*S* ratio of 56/44 (enantiomeric excess e.e. = 12) was indistinguishable from that of a nearly enantiomerically pure *R* sample. More recently it has been shown that the majority rules effect is unaffected upon 'dilution' with achiral units i.e. the majority rules effect in an *R*/*S* copolymer is similar to that in a *R*/*S*/achiral terpolymer.[37b] Gratifyingly, the majority rules principle has been found to apply also to the supramolecular stacks of propellers **2a** (*S*) and **2b** (*R*), although an e.e. of ~30 (25 °C) is needed to obtain effects similar to those of enantiomerically pure samples.[38] With a theoretical model of the majority rules principle,[13e] 'helix reversal' penalties and 'screw sense mismatch' penalties could be determined and compared to those of poly(*n*-alkylisocyanate) systems.

1.3.2 Chiral solvation

Another phenomenon encountered in stiff poly(*n*-alkylisocyanates) is 'chiral solvation', by which is meant that the helical sense could not only be biased by covalently linked alkyl chains, but also by

chiral solvents.[39] Presumably, the first layer of solvent around the supramolecular aggregate is actively involved in the aggregation processes.[40] 'Chiral solvation' could be applied to achiral bipyridinyl disks, to polar **6**/**7**, as well as to apolar **1**/**2**. The Cotton effect of **6** in (*S*)-(-)-2-methyl-1-butanol ($g = 2\times10^{-3}$) is similar to that of **7** in *n*-butanol ($g = 3\times10^{-3}$).[13d] The CD spectra of **1** in (*R*)-(-)-2,6-dimethyloctane and (*S*)-(+)-2,6-dimethyloctane are mirror images of each other, while g values are lower than those obtained with **2** (containing covalently linked chiral alkyl chains) in dodecane (**1** and *R* solvent: $g = -8.5\times10^{-4}$, **1** and *S* solvent: $g = +5.3\times10^{-4}$, **2a** in dodecane $g = -1.5\times10^{-3}$).[21] The many bulky solvent chains disfavor the energetically most favorable packing of the molecules and thus lower the Cotton effect.[40,41] Also, in chiral solvation, the stereocenter is placed far away from the core and is not connected covalently to the molecules, so a smaller influence can be expected.

1.3.3 Chiral induction via auxiliaries

Whereas in chiral solvation chirality is transferred via generic, 'weak' van der Waals interactions, better results are expected when 'stronger' or 'more directional' non-covalent interactions are used to relate the stereocenter to the chromophore in the self-assembly. Hicham Fenniri and co-workers established communication between amino acids and nanotubes of rosette structures (containing six heterobicyclic hydrogen-bonded bases)[42] via electrostatic interactions to benzo crown ether substituents (Figure 1.6).[43] Only when all crown-ether sites are occupied, chirality is transferred to give an 'induced CD effect' (ICD). In other words, the system does not behave according to the sergeants and soldiers principle.[44] Similar to non-cooperative columnar stacks mentioned above,[24-26] the chiral promoters themselves are essential for the stability of the helical columnar aggregate in dilute solutions (0.04 mM). In combination with the 'autocatalytic pathway' by which the self-assemblies are formed, this allowed for a 'majority rules related behavior'. The addition of an excess of D-alanine (0.4 mM, 10 eq.) to a preequilibrated solution of the heterobicyclic crown ether moiety (0.04 mM) and L-alanine (0.4 M, 5 eq.) afforded a CD spectrum similar to that obtained for the heterobicyclic crown ether (0.04 mM) and D-alanine. The dominant promoter D-alanine induces preferential binding of its congeners to the nanotubes' stereoselective platforms. Thereby it shifts the *M*/*P* equilibrium to the *P* nanotubes, rendering the recessive promoter L-alanine obsolete.[44]

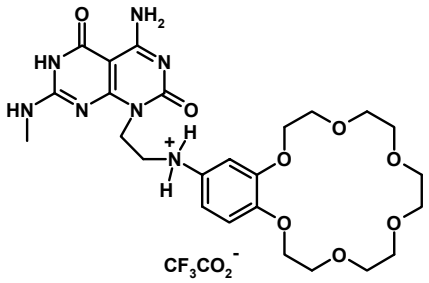

Figure 1.6. *Chemical structure of a heterobicyclic hydrogen-bonded base with a crown ether unit.*

Similar self-assembled nanocolumns have been developed by Giovanni Gottarelli and coworkers.[45] Apolar guanosine derivatives[46] form helical octamers of two stacked G quartets,[47,48] and eventually helical columns,[49] upon extraction of potassium salts from the aqueous into the organic layer, as indicated by the observed Cotton effect. Next to enantioselective extraction of chiral potassium salts by the octamer and polymer, the polymer induces a Cottton effect in an achiral potassium chromophore.[50] Although the authors frequently use CD spectroscopy in establishing the shape of the supramolecular architectures,[51] no examples of amplification of chirality are reported yet.[52]

1.4 Concave supramolecular architectures

1.4.1 Amplification of chirality in double rosettes

In the Netherlands, David Reinhoudt already opened up the field of supramolecular chemistry in the early crown ether period.[53] Recently, the focus is on hydrogen-bonded double rosettes built up out of 3 dimelamines **8** and 6 barbiturate units **9** or cyanurate units **10** (Figure 1.7).[54] These concave architectures are applied in enantioselective guest recognition[55] and in nanotechnology.[56,57] Chiral centers in either one of the building blocks quantitatively induce one handedness (*M* or *P* diastereomers) in the helical twist that the two rosette motifs make.[58] In dimelamine/barbiturate assemblies exchange of components is fast, and amplification of chirality occurs under thermodynamically controlled conditions. Although a distinct positive deviation from linearity is observed, full expression of chirality is not achieved unless all dimelamines in the assembly are chiral (The amplification of chirality is 20% ($\Delta\varepsilon_{rel} \sim 85$) in a rosette with 2 chiral dimelamines ($\Delta\varepsilon_{rel} = 100$) and 1 achiral dimelamine ($\Delta\varepsilon_{rel} = 0$)). In dimelamine/cyanurate rosettes, amplification of chirality occurs under kinetically controlled conditions. Inversion of the handedness is remarkably slow, since it happens via complete dissociation of the dimelamine components, which are strongly bound via 12 hydrogen bonds to the cyanurates.[59] This rationalizes observation of a much lower amplification when using chiral dimelamines (32 %, ($\Delta\varepsilon_{rel} = 72$) in a 40/60 mixture of chiral and achiral components), than when using chiral cyanurates (46 %, $\Delta\varepsilon_{rel} = 86$).[60] In the latter case, full expression of supramolecular chirality is obtained with 60% chiral compound.

Kinetic models have been developed, to simulate chiral amplification in dynamic systems in general. When interconversion between helical states and exchange of the chiral components occurs via the same process, the thermodynamical end value $\Delta\varepsilon_{therm}$ is limited to a maximum. Assemblies without chiral components are at all times present as a racemic mixture. However, when exchange of chiral components is much faster than switching of the handedness, no intrinsic limit exists for $\Delta\varepsilon_{therm}$. Theoretically, with less than 1% chiral compound, the preferred chirality could be imposed on over 99 % of the assemblies. The observant authors already noted that this model could apply to the columnar

stacks of discotics **1-7**. Slow switching of the handedness could correspond to processes relating to the cooperative length L_C (cooperative helix reversal of hundreds of molecules), and exchange of chiral components to actions of one chiral disk (e.g. 'hopping' of a chiral disk from one column to the other).[60]

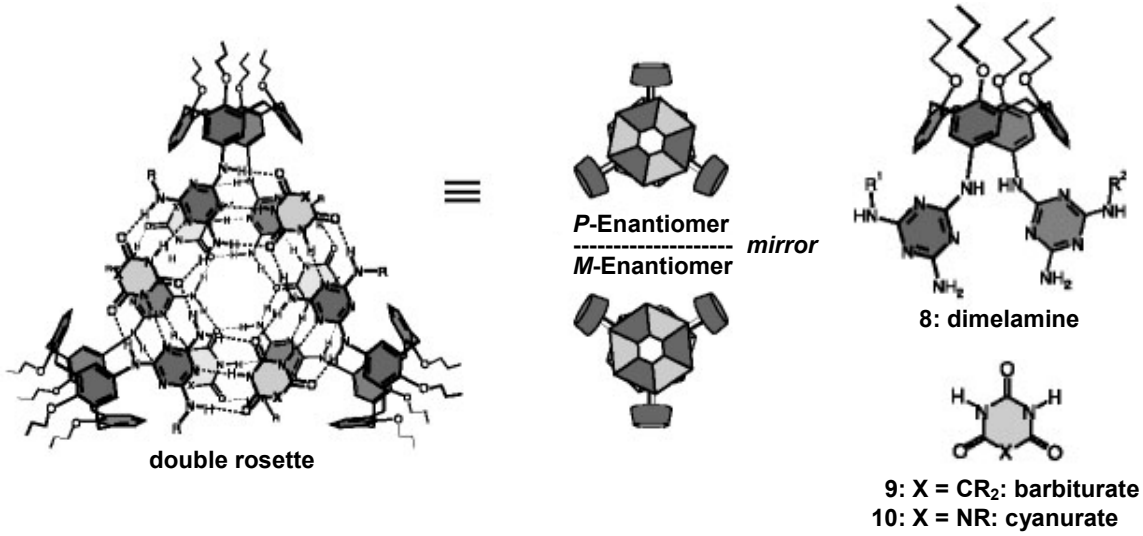

Figure 1.7. *Chemical structure of a double rosette (left), containing 3 dimelamine units **8** (top right) and 6 barbiturates **9** (X = CR_2) or cyanurates **10** (X = NR) (bottom right), together with a schematic representation of the P and M enantiomers of a complex containing achiral building blocks (middle).*

1.4.2 Chiral memory

The low dissociation rate of a dimelamine from the double-rosette structure allows -in combination with the stronger binding of melamines to cyanurates than to barbiturates- occurance of a 'chiral memory' phenomenon.[59,61] Upon exchange of chiral barbiturates with achiral cyanurates, double rosettes maintain their preferred handedness! Since they no longer contain chiral components, the *M* and *P* assemblies have become mirror images, and thus, enantiomers. Racemization is sufficiently slow (4.5 days at 20 °C) to isolate single *M* or *P* enantiomers, and its half time increases with another two orders of magnitude upon ring-closing metathesis of the three dimelamine units. On the other hand, raising temperature and addition of an *R* or *S* barbiturate 'racemization catalyst' speed up the racemization process.

In contrast to examples discussed above, no 'majority rules' related phenomena could be observed in double-rosette architectures.[62] This effect can only arise when *R* and *S* components are statistically mixed. Clearly, the *R* and *S* dimelamines are phase separated[63] in homochiral double rosettes. This results in a linear relationship between the enantiomeric excess and the Cotton effect in titration experiments with the *M* and *P* assemblies. Also, formation of well-defined assemblies is generally only observed when both melamine and cyanurate components contain unidirectional information for the induction of either *M* or *P* chirality. When dimelamines with *M* preference and cyanurates with *P*

preference are mixed (or vice versa), no CD effect is observed, and ^{1}H-NMR spectroscopy reveals formation of multiple disordered aggregates.

Notably, the authors did not report experiments in which achiral dimelamines are exposed to mixtures of *R* and *S* cyanurates or barbiturates. However, dimelamine units were equipped with two primary amine functionalities, enabling acid/base interaction with chiral carboxylic acids,[64] or chiral carboxylic diacids.[65] The cooperative recognition process yielded a considerable diastereomeric excess (d.e. = 21[64]; d.e. = 90[65]), although results were strongly dependent on the specific structures of the host (dimelamine) and the guest (chiral acid). In case of two-point hydrogen bonding interactions,[65] the diastereomeric excess was memorized, yielding an optically active assembly of individual achiral components (90 % e.e. (enantiomeric excess), half life time ~ 1 week).

Several other examples of the chiral memory effect are known,[66] in which the host retains the chiral information of chiral guests, after their replacement with achiral molecules. Takuzo Aida *et al.* initiated this field with their saddle-shaped porphyrin complex (Figure 1.8, left), that forms diastereoisomeric complexes with two equivalents of either *R*- or *S*-mandeleic acid. [66a] In acetic acid, the half life of optical activity is as long as 200 h. Interestingly, the mandelate-porphyrin complex could be 'photoswitched'. Upon excitation by visible light, the complex lost its optical activity. However, when the light was switched off, the optical purity automatically reverted to the initial value. Similarly, the cerium(IV) double decker porphyrin of Seiji Shinkai *et al.* preferably forms one diastereomeric complex with two equivalents of a chiral diacid.[66c] After removal of the chiral guests, the chiral memory could be preserved for 3 days at 0 °C. Another example is the hydrogen-bonded dimeric capsule ('softball') of Julius Rebek Jr. *et al.* (Figure 1.8, right).[67,68] The capsule preserves induced supramolecular chirality of its original chiral guest upon replacement by its enantiomeric counterpart, by an achiral guest, or even upon complete removal of guests (50 % d.e./e.e.). The imagination of the authors associates this to a ghost of the chiral guest, still present in the host; or in my view 'the genie in the bottle'.

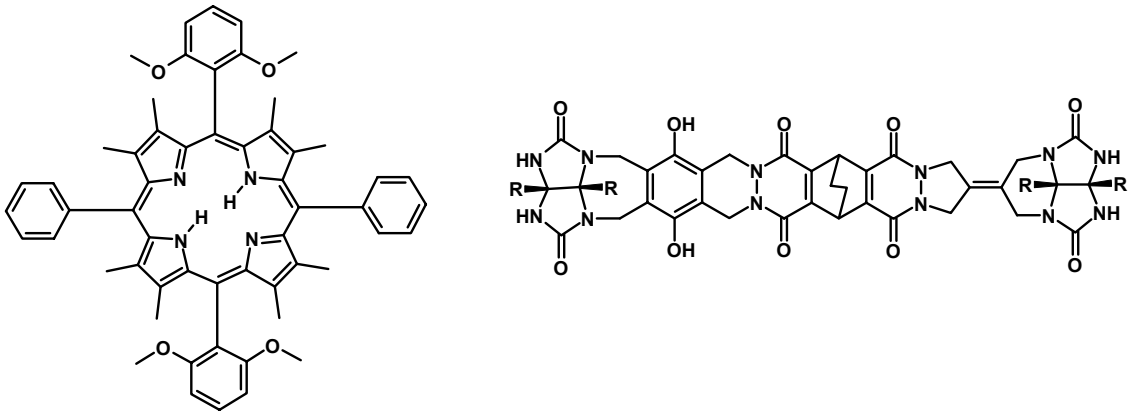

Figure 1.8. *Chemical structure of one half of a saddle-shaped porphyrin complex (left) and one half of a dimeric capsule (right), both capable of memorizing chirality of removed chiral guests.*

1.5 Back to polymeric systems

The phenomena (most importantly sergeants and soldiers) firstly noticed by Mark Green in stiff poly(*n*-alkylisocyanates) (Figure 1.9, left), are not only applicable to various dynamic self-assembled systems, but also to various rather flexible oligo- and polymeric structures. Oligo(ethylene oxide) substituted *m*-phenylene ethynylenes of Jeffrey Moore and co-workers (Figure 1.9, middle), fold into a racemic mixture of left- and right-handed helices in acetonitrile solution.[69] Homochirality was obtained by complexation of chiral terpenes in the apolar cavity of the helix,[70] or by an optically active tether in the main chain.[71,72] However, in analogy to the work of Mark Green on stiff poly(*n*-alkylisocyanates), stereocenters in the side chain efficiently express supramolecular chirality in flexible *m*-PE's.[73] Cotton effects of co-oligomers containing both chiral and achiral units display a positive non-linear dependence on the percentage of chiral side chains.[74,75] This illustrates cooperativity in the folding. However, the sergeants and soldiers effect is not very strong. Approximately 15 % chiral side chains was needed to obtain half the Cotton effect of the homochiral oligomers.[13d] Upon addition of water to acetonitrile, cooperative stacking of helices occurs,[76] allowing a modest intermolecular amplification of chirality from chiral to achiral helices. On average 50 % chiral oligomer was needed for a full bias of the helicity of achiral oligomers.[13d] Amplification does not seem limited by aggregate size, but by the small directing power of the generic solvophobic effect and diastereomeric impurity of the chiral helices. Folding and stacking coincide for chiral alkyl substituted *m*-PE's in alkanes.[77] Regrettably, no sergeants and soldiers experiments have been performed. Denaturation experiments indicate that the formation of supramolecular columns stabilizes in a cooperative fashion the chiral helical conformation of the individual oligomers, although the time dependent folding behavior might hamper amplification of chirality.[78]

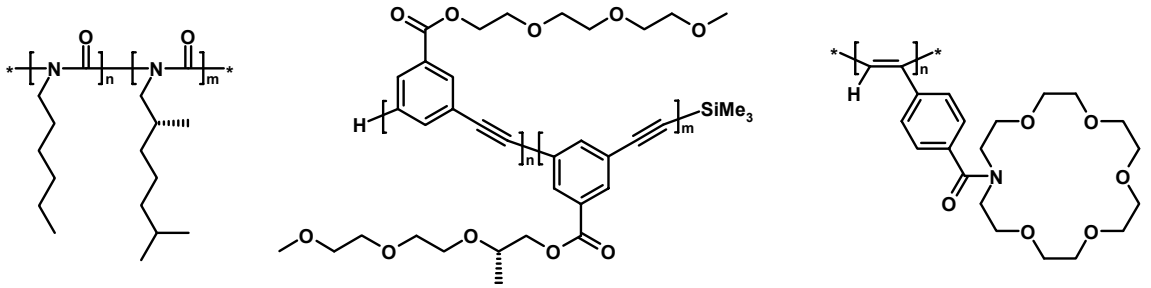

Figure 1.9. *Chemical structures of a poly(n-alkylisocyanate) (left), a m-phenylene ethynylene polymer (middle), and a crown ether functionalized poly(phenylacetylene) (right), all capable of amplification of chirality.*

Amplification of chirality in helical polymers was reviewed recently by Eiji Yashima,[79,80] focusing on functionalized phenylacetylene backbone chromophores,[81] that target chiral guest molecules via acid/base[82] or host/guest[83] interactions. Chiral solvation was observed in polysilanes,[84] while the helical sense was memorized by acid functionalized poly(phenylacetylenes) upon replacement of the

chiral amines with achiral guests.[82c,d] Expression of the sergeants and soldiers effect was illustrated by induction of a one-handed helix by 0.1 eq. L-alanine to a crown ether functionalized poly(phenylacetylene) (Figure 1.9, right).[83a,b] The induced Cotton effect of the polymer upon complexation with a 5 % e.e. L-alanine mixture was indistinguishable from the one upon complexation with enantiomerically pure L-alanine, demonstrating 'majority rules'. Even a very low e.e. (0.005 %) in L-alanine could be detected. Again, this indicates the high cooperativity in the non-covalent bonding interactions, justifying future application of these systems as sensors of a tiny chiral imbalance in biologically important chiral molecules.

More general, these examples certainly illustrate the combined strength of supramolecular chemistry and stereochemistry. On one hand, chirality helps in revealing the structure, conformation, and interactions in a supramolecular architecture, while on the other hand, the supramolecular architecture enables detection of minor 'traces of chirality'. One way or the other, by combining both, new insights are gathered for the creation of large, dynamic systems, able to adapt their shape, and thus their function, to the environment.

1.6 Aim of the thesis

Self-assembled architectures may open new opportunities in both the fields of biology and materials science. Indeed, supramolecular chemistry allows rapid formation of, nano-sized, and complex architectures, which may adopt stable and compact conformations, despite their non-covalent, reversible nature. A supramolecular architecture needs an optimal balance between stability and reversibility. When non-covalent interactions are too strong, movement of building blocks might be hampered by kinetic factors. The ordered thermodynamic equilibrium situation might become difficult to reach.

To find an optimal balance between the stability and the reversibility in the supramolecular architecture, an optimal balance between non-covalent interactions in the architecture has to be achieved. The focus will be on hydrogen bonding in combination with π-π stacking. To judge the contribution of each specific secondary interaction, a thorough understanding of the relationship between the chemical structure and material properties (liquid crystallinity, gel formation) is essential. Therefore, a coherent molecular picture is needed over the complete concentration range from bulk to isolated molecule. To achieve this, the supramolecular architectures are investigated in the solid state (DSC, optical microscopy, X-ray), in the concentrated gel phase (AFM, SANS), as well as in dilute solution, where isolated supramolecular architectures are present. To recognize, and to determine the degree of ordering in, supramolecular architectures, supramolecular chirality is incorporated via information in the chiral peripheral chains. Circular dichroism spectroscopy is the appropriate tool that will generate insight into and understanding of the behavior of new chiral assemblies.

In supramolecular architectures, the helix has been recognized as an extremely valuable shape, in view of its key role in expressing functions of natural macromolecules. It is known that C_3-symmetrical discotics suitably self-assemble into helical stacks. Their ease of synthesis invites to vary intermolecular hydrogen bonding and π-π stacking interactions, enabling investigation of their respective contributions to the supramolecular aggregation processes. Especially intermolecular hydrogen bonding is expected to play a crucial role in the formation of helical stacks. Therefore, comparison of weaker (amide) and stronger (urea) hydrogen bonding, might give detailed information about the optimal strength of non-covalent interactions to be used in supramolecular assemblies. This information is then used, to redesign the chemical structure in order to improve material properties.

The information can also be used to design new structures, displaying new features and properties. A keen sense of 'weak' and 'strong' in intermolecular hydrogen bonding is useful in designing 'foldamers'. These synthetic macromolecules make use of multiple 'weak' cooperative intramolecular interactions, similar to natural macromolecules, such as the α-helix. Two different foldamers, based on intramolecular urea hydrogen bonding, are designed, and synthesized, after which their self-assembly is investigated. We wish to demonstrate that the one containing 'strong' hydrogen bonding (based on the C_3-symmetrical discotics), folds uncontrolled, since kinetic factors prevent the movement into the most ordered conformation. The foldamer with multiple 'weak' hydrogen bonding units (ureidophthalimide) is supposed to fold instantaneously into its thermodynamically stable, most ordered, helical conformation.

In our view, the approach described above could significantly contribute to the development of complex, dynamic systems, able to adapt their shape, and thus their function, to the changing environment. As an illustration, such systems could be useful in supramolecular electronics, where mesoscopic ordering of dyes is essential.

1.7 Outline of the thesis

Recently, C_3-symmetrical discotics have been developed, in which a combination of intermolecular hydrogen bonding and π-π stacking induces self-assembly into helical columns. The influence of changes in these delicately balanced non-covalent interactions on the stability and reversibility of the architectures, is studied in Chapters 2 and 3 wherein a series of twelve C_3-symmetrical discotics, varying in hydrogen bonding unit (amide, urea), π-π stacking (alkyl, gallic, bipyridinyl), and chirality, is compared. In Chapter 2 it is shown that a broad range of combinations of these non-covalent interactions gives rise to helical columns, indeed. Thermotropic columnar mesophases, fibers on the surface, and gels in apolar solvents, are described in great detail. However, distinct differences between the various C_3-symmetrical disks are revealed in Chapter 3, using optical techniques on dilute solutions (temperature dependent time resolved fluorescence and sergeants and soldiers CD measurements).[34] Urea stacks are much more rigid than the amide ones, and hysteresis is involved in

the transformation of an ill-defined urea aggregate, into a well-defined, chiral helix. As a result of the rigidity of the urea stacks, participation of the linear *n*-heptane to the supramolecular stacking of bipyridinyl urea disks in a branched solvent (2,2,4-trimethylpentane) could be demonstrated.

Asymmetry in the abovementioned discotics in principle allows incorporation of the 'secondary' helices in 'tertiary architectures' by introduction of functionalities that bring about extra order. In Chapter 4 it is shown that monoamide diurea discotics self-assemble into helical architectures by specific amide-amide and urea-urea interactions.[85] An attempt to transfer these specific intermolecular hydrogen bonding interactions in *m*-phenylene-ureido foldamers failed since non-covalent interactions are so strong, that oligomers are kinetically hampered to reach their most ordered conformation.

Nonetheless, the foldamer approach is a strategy towards helix formation closer to nature than the self-assembly strategy. In Chapter 5 it is described how 'weak' multiple intramolecular hydrogen bonding interactions are successfully applied to create a polymeric helix.[86] Next to the design, synthesis, and characterization of a polymeric ureidophthalimide (~ 30 units), the isolation of pure oligomers (dimer up to octamer) is described, enabling the identification of individual intra- and intermolecular folding processes from CD measurements in different solvents. With this molecular picture of the poly-ureidophthalimide helix in mind, we wish to develop new biological applications (membrane ion channel, water soluble 'carrier') and new materials (ordered dyes, molecular wires). In Chapter 6, a preliminary exploration is undertaken to regularly incorporate an anthraquinone dye in the poly-ureidophthalimide backbone. Regular helical positioning of the dye may offer opportunities for efficient charge transport in supramolecular electronics.

1.8 References and Notes

(1) Green, M.M.; Reidy, M. P.; Johnson, R.D.; Darling, G.; O'Leary, D.J.; Wilson, G. *J. Am. Chem. Soc.* **1989**, *111*, 6452–6454.

(2) Palmans, A.R.A.; Vekemans, J.A.J.M.; Havinga, E.E.; Meijer, E.W. *Angew. Chem. Int. Ed. Engl.* **1997**, *36*, 2648–2651.

(3) (a) Elemans, J.A.A.W.; Rowan, A.E.; Nolte, R.J.M. *J. Mater. Chem.* **2003**, *13*, 2661–2670. (b) Schalley, C.A.; Lützen, A.; Albrecht, M. *Chem. Eur. J.* **2004**, *10*, 1072–1080.

(4) Meijer, E. W. *Angew. Chem. Int. Ed.* **2001**, *40*, 3783 – 3789.

(5) (a) van 't Hoff, J.H.; *Arch. Neerl. Sci. Exactes Nat.* **1874**, *9*, 445–454. (b) van 't Hoff, J.H.; *Bull. Soc. Chim. Fr.* **1875**, *23*, 295–301.

(6) Other examples: Stereochemical phenomena in triene cyclization leading to the Woodward and Hoffmann rules are described by L.J. Oosterhoff and E. Havinga: (a) Havinga, E.; Schlatmann, J.L. M.A. *Tetrahedron* **1961**, *16*, 146–152. Dutch resolution technique: (b) Vries, T.; Wynberg, H.; van Echten, E.; Koek, J.; ten Hoeve, W.; Kellogg, R.M.; Broxtermann, Q.B.; Minnaard, A.; Kaptein, B.; van der Sluis, S.; Hulshof, L.; Kooistra, J. *Angew. Chem.* **1998**, *110*, 2591–2496. 10 Years citronellol in helical columns; from Nijmegen 1993 to Eindhoven 2003: (c) van Nostrum, C.F.; Bosman, A.W.; Gelinck, G.H.; Picken, S.J.; Schouten, P.G.; Warman, J.M.; Schouten A.-J.; Nolte, R.J.M. *J. Chem. Soc., Chem. Commun.* **1993**, 1120–1122; (d) van Gorp, J.J.; Vekemans, J.A.J.M.; Meijer, E.W. *Mol. Cryst. Liq. Cryst*. **2003**, *397*, 491-505.

(7) Bijvoet, J.M.; Peerdeman, A.F.; van Bommel, A.J. *Nature* **1951**, *168*, 271–272.

(8) M.A. Rosanoff first suggested (+)-glyceraldehyde to be D in 1906: (a) Solomons, T.W.G. *Organic Chemistry; 5th ed.,* John Wiley & Sons, inc., New York, **1992**. According to ref. 11 E. Fisher first suggested the right absolute configuration of (+)-tartaric acid: (b) Fischer, E. *Ber. Dtsch. Chem. Ges.* **1896**, *29*, 1377 – 1683.

(9) Pauling, L.; Corey, R.B.; Branson, H.R. *Proc. Natl. Acad. Sci. USA* **1951**, *37*, 205–211.

(10) Wood, W.W.; Ficket, W.; Kirkwood, J.G. *J. Chem. Phys.* **1952**, *20*, 561–568.

(11) Dunitz, J.D. *Angew. Chem. Int. Ed.* **2001**, *40*, 4167 – 4173.

(12) Kendrew, J.C.; Dickerson, R.E.; Strandberg, B.E.; Hart, R.G.; Davies, D.R.; Phillips, D.C.; Shore, V.C. *Nature* **1960**, *185*, 422–427.

(13) For example, the first helix-coil transition was recognized in poly-γ-benzyl-L-glutamate (1954), while the corresponding theory was developed by Zimm and Bragg (1959). Still new models for the transition are developed and optimized. See: (a) Doty, P.; Holtzer, A.M.; Bradbury, J.H.; Blout. E.R.; *J. Am. Chem. Soc.* **1954**, *76*, 4493–3394. (b) Zimm, B.H.; Bragg, J.K. *J. Chem. Phys.* **1959**, *31*, 526–535. (c) Luthey-Schulten, Z.; Ramirez, B.E.; Wolynes, P.G. *Phys. Chem.* **1995**, *99*, 2177–2185. (d) Brunsveld, L. *Thesis: Supramolecular chirality, from molecules to helical assemblies in polar media*; Eindhoven University of Technology: Eindhoven, **2001**. (e) van Gestel, J. *Thesis: Theory of helical supramolecular polymers*; Eindhoven University of Technology: Eindhoven, **2003**.
Also, phenomena related to 'majority rules' were recognized in 1957 in copolymers of D- and L-peptides. (f) Downie, A.R.; Elliot, A.; Hanby, W.E., Malcolm B.R. *Proc. R. Soc. London* **1957**, *A242*, 325–340.

(14) See reference 13d and references therein.

(15) Curie, P. *J. Phys.* **1893**, *3*, 393.

(16) Cotton, A. *C. R. Acad. Sci. Paris* **1895**, *120*, 337–347.

(17) (a) Zhou, N.E.; Kay, C.M.; Hodges, R.S. *Biochemistry* **1992**, *31*, 5739–5746. (b) Janssen, H.M. *Thesis: Chiral ethylene oxide derivatives in supramolecular assemblies*; Eindhoven University of Technology: Eindhoven, **1997**.

(18) The term induced circular dichroism (ICD) was originally proposed by H. Falk for the phenomenon of asymmetry transfer from chiral solvents to achiral chromophores: (a) Falk, H.; Jungwirth, W.; Müller, N. *Monatsh. Chem.* **1984**, *115*, 455–466. (b) Borovkov, V.V.; Hembury, G.A.; Inoue, Y. *Angew. Chem. Int. Ed.* **2003**, *42*, 5310–5314.

(19) (a) Lehn, J.-M. *Angew. Chem. Int. Ed. Engl.* **1988**, 27, 91–116. (b) Pedersen, C.J. *J. Am. Chem. Soc.* **1967**, *89*, 2495–2496 and 7017–7036.

(20) (a) Klug, A. *Angew. Chem.* **1983**, *95*, 579 – 596. (b) Stryer, L.; *Biochemistry*, 4th ed, W. H. Freeman & Company: New York, **1995**.

(21) Palmans, A.R.A. *Thesis: Supramolecular structures based on the intramolecular H-bonding in the 3,3'-di(acylamino)-2,2'-bipyridine unit*; Eindhoven University of Technology: Eindhoven, **1997**.

(22) (a) Palmans, A.R.A.; Vekemans, J.A.J.M.; Fischer, H.; Hikmet, R.A.; Meijer, E.W. *Chem. Eur. J.* **1997**, *3*, 300–307. (b) Palmans, A.R.A.; Vekemans, J.A.J.M.; Hikmet, R.A.; Fisher, H.; Meijer, E.W. *Adv. Mater.* **1998**, *10*, 873–876. (c) Meijer, E.W.; Vekemans, J.A.J.M.; Palmans, A.R.A.; Breure, P.; de Kraker, J.; Brunsveld, L. *Polym. Prepr.* **2000**, *41(1)*, 902–903.

(23) Brunsveld, L.; Meijer, E.W.; Rowan, A.E.; Nolte, R.J.M. *Top. Stereochem.* **2003**, *24*, 373–423.
(24) Fox, J.M.; Katz, T.J.; van Elshocht, S.; Verbiest, T.; Kauranen, M.; Persoons, A., Thongpanchang, T.; Krauss, T.; Brus, L. *J. Am. Chem. Soc.* **1999**, *121*, 3453–3459.
(25) Kraft, A.; Osterod, F.; Fröhlich, R. *J. Org. Chem.* **1999**, *64*, 6425–6433.
(26) (a) Engelkamp, H.; Middelbeek, S.; Nolte, R.J.M. *Science* **1999**, *284*,785–788. (b) van Nostrum, D.F.; Picken, S.J.; Nolte, R.J.M. *Angew. Chem. Int. Ed. Engl.* **1994**, *33*, 2173–2175.
(27) Hirschberg, J.H.K.K.; Brunsveld, L.; Ramzi, A.; Vekemans, J.A.J.M.; Sijbesma, R.P.; Meijer, E.W. *Nature* **2000**, *407*, 167–170.
(28) Hirschberg, J.H.K.K.; Koevoets, R.A.; Sijbesma, R.P.; Meijer, E.W. *Chem. Eur. J.* **2003**, *9*, 4222–4231.
(29) The number average degree of polymerization also depends on temperature. The results are discussed in the corresponding references.
(30) The degree of polymerization calculated from the association constant K_{ass} has an error of around 10 %, but still is in excellent agreement with values from a model of van der Schoot *et al.*, based on the standard theory of linear self-assembly modified by adopting a two-state model for the molecules in the aggregates, to account for the cooperative transition. See references 13d and 13e.
(31) Brunsveld L.; Schenning, A.P.H.J.; Broeren, M.A.C.; Janssen, H.M.; Vekemans, J.A.J.M.; Meijer, E.W. *Chem. Lett.* **2000**, 292–293.
(32) Masuda, M.; Jonkheijm. P.; Sijbesma, R.P.; Meijer, E.W. *J. Am. Chem. Soc.* **2003**, *125*, 15935–15940.
(33) Andy Wilson, results to be published.
(34) van Gorp, J.J.; Vekemans, J.A.J.M.; Meijer, E.W. *J. Am. Chem. Soc.* **2002**, *124*, 14759–14769.
(35) Brunsveld, L.; Zhang, H.; Glasbeek, M.; Vekemans, J.A.J.M.; Meijer, E.W. *J. Am. Chem. Soc.* **2000**, *122*, 6175–6182.
(36) Green, M.M.; Peterson, N.C.; Sato, T.; Teramoto, A.; Cook, R.; Lifson, S. *Science* **1995**, *268*, 1860–1866.
(37) (a) Green, M.M.; Garetz, B.A.; Munoz, B.; Chang, H.P.; Hoke, S.; Cooks, R.G. *J. Am. Chem. Soc.* **1995**, *117*, 4181–4182. (b) Jha, S.K.; Cheon, K.-S.; Green, M.M.; Selinger, J.V. *J. Am. Chem. Soc.* **1999**, *121*, 1665–1673.
(38) Anja Palmans, Bram Titulaer, results to be published.
(39) (a) Green, M.M.; Khatri, C.A.; Peterson, N.C.; *J. Am. Chem. Soc.* **1993**, *115*, 4941–4942. (b) Khatri, C.A.; Pavlova, Y.; Green, M.M.; Morawetz, H. *J. Am Chem. Soc*. **1997**, *119*, 6991–6995.
(40) In Chapter 3 this will be confirmed by the observation of a 'solvent shell' of linear *n*-heptane around large urea disks **2f** in bulky *iso*-octane.
(41) In apolar and polar large amide disks **1**, mixtures of chiral (branched) and achiral (linear) disks give larger CD effects than the pure chiral disks. See references 13d and 21.
(42) Fenniri, H.; Mathivana, P.; Vidale, K.L.; Sherman, D.M.; Hallenga, K.; Wood, K.V.; Stowell, J.G. *J. Am. Chem. Soc.* **2001**, *123*, 3854 – 3855.
(43) Fenniri, H.; Deng, B.-L.; Ribbe, A.E.; Hallenga, K.; Jacob, J.; Thiyagarajan, P. *Proc. Natl. Acad. Sci. USA* **2002**, *99*, 6487 – 6492.
(44) Fenniri, H.; Deng, B.-L.; Ribbe, A.E. *J. Am. Chem. Soc.* **2002**, *124*, 11064 – 11072
(45) Bonazzi, S.; Capobianco, M.; DeMorais, M.M.; Garbesi, A.; Gottarelli, G.; Mariani, P.; Ponzi Bossi, M.G.; Spada, G.P.; Tondelli, L. *J. Am. Chem. Soc.* **1991**, *113*, 5809–5816.
(46) Gottarelli, G.; Masiero, S.; Spada, G.P. *J. Chem. Soc., Chem. Commun.* **1995**, 2555–2557.
(47) Marlow, A.L.; Mezzina, E.; Spada, G.P.; Masiero, S.; Davis, J.T.; Gottarelli, G. *J. Org. Chem.* **1999**, *64*, 5116–5123.
(48) Forman, S.L.; Fettinger, J.C.; Pieraccini, S.; Gottarelli, G.; Davis, J.T. *J. Am. Chem. Soc.* **2000**, *122*, 4060–4067.
(49) Mezzina, E.; Mariani, P.; Itri, R.; Masiero, S.; Pieraccini, S.; Spada, G.P.; Spinozzi, F.; Davis, J.T.; Gottarelli, G. *Chem. Eur. J.* **2001**, *7*, 388–395.
(50) Andrisano, V.; Gottarelli, G. Masiero, S.; Heijene, E.H.; Pieraccini, S.; Spada, G.P. *Angew. Chem. Int. Ed.* **1999**, *38,* 2386–2388.
(51) Giorgi T.; Lena S.; Mariani P.; Cremonini M.A; Masiero S.; Pieraccini S.; Rabe J.P; Samori P.; Spada G.P.; Gottarelli G. *J. Am. Chem. Soc.* **2003**, *125*, 14741–14749.
(52) Sergeants and soldiers effect in barbituric acid and triaminopyridine with a chiral lysine side chain: Vidale, K.L.; Fenniri, H. *Abstracts of Papers, ACS National Meeting*, *Chicago Aug.* **2001**.
(53) Reinhoudt, D.N.; Gray, R.T. *Tetrahedron Lett.* **1975**, 2105–2108.
(54) Vreekamp, R.H.; van Duynhoven, J.P.M.; Hubert, M.; Verboom, W.; Reinhoudt, D.N. *Angew. Chem. Int. Ed. Engl.* **1996**, *35*, 1215–1218.
(55) Ishi-I, T.; Mateos-Timoneda, M.A.; Timmerman, P.; Crego-Calama, M.; Reinhoudt, D.N.; Shinkai, S. *Angew. Chem. Int. Ed.* **2003**, *42*, 2300–2305.

(56) (a) Klok, H.-A.; Jolliffe, K.A.; Schauer, C.L.; Prins, L.J.; Spatz, J.P.; Möller, M.; Timmerman, P.; Reinhoudt, D.N. *J. Am. Chem. Soc.* **1999**, *121*, 7154–7155. (b) Schönherr, H.; Paraschiv, V.; Zapotoczny, S.; Crego-Calama, M.; Timmerman, P.; Frank, C.W.; Vansco, G.J.; Reinhoudt, D.N. *Proc. Natl. Acad. Sci. USA* **2002**, *99*, 5024–5029.
(57) Choi, I.S.; Li, X.; Simanek, E.E.; Akaba, R.; Whitesides, G.M. *Chem. Mater.* **1999**, *11*, 684–690.
(58) Prins, L.J.; Huskens, J.; de Jong, F.; Timmerman, P.; Reinhoudt, D.N. *Nature* **1999**, *398*, 498–502.
(59) Prins, L.J.; De Jong, F.; Timmerman, P.; Reinhoudt, D.N. *Nature* **2000**, *408*, 181–184.
(60) Prins, L.J.; Timmerman, P.; Reinhoudt, D.N. *J. Am. Chem. Soc.* **2001**, *123*, 10153–10163.
(61) Prins, L.J.; Verhage, J. J.; de Jong, F.; Timmerman, P.; Reinhoudt, D.N. *Chem. Eur J.* **2002**, *8*, 2302–2313.
(62) Prins, L.J.; Hulst, R.; Timmerman, P.; Reinhoudt, D.N. *Chem. Eur. J.* **2002**, *8*, 2288–2301.
(63) Similar enantiomeric self sorting in solution in a racemic mixture of D- and L-isoguanosines: (a) Shi, X.; Fettinger, J.C.; Cai, M.; Davis, J.T. *Angew. Chem. Int. Ed.* **2000**, *39*, 3124–3127. (b) Shi, X.; Fettinger, J.C.; Davis, J.T. *J. Am. Chem. Soc.* **2001**, *123*, 6738–6739.
(64) Ishi-i, T.; Crego-Calama, M.; Timmerman, P.; Reinhoudt, D.N.; Shinkai, S. *Angew. Chem. Int. Ed.* **2002**, *41*, 1924–1929.
(65) Ishi-i, T.; Crego-Calama, M.; Timmerman, P.; Reinhoudt, D.N.; Shinkai, S. *J. Am. Chem. Soc.* **2002**, *124*, 14631–14641.
(66) ionic porphyrin complex: (a) Furusho, Y.; Kimura, T.; Mizuno, Y.; Aida, T. *J. Am. Chem. Soc.* **1997**, *119*, 5267–5268. ionic polymeric system: (b) Yashima, E.; Maeda, K.;Okamoto, Y. *Nature* **1999**, *399*, 499–451. cerium double decker porphyrin: (c) Sugasaki, A.; Ikeda, M.; Takeushi, M.; Robertson, A.; Shinkai, S. *J. Chem. Soc. Perkin Trans. 1* **1999**, 3259–3264. metallo assembly: (d) Ziegler, M.; Davis, A.V.; Johnson, D.W.; Raymond, K.N. *Angew. Chem. Int. Ed.* **2003**, *42*, 665–668.
(67) Rivera, J.M.; Craig, S.L.; Martín, T.; Rebek, J.Jr. *Angew. Chem. Int. Ed.* **2000**, *39*, 2130–2132.
(68) Amino acid side groups induce chirality in tetraurea calixarene capsules, sensing chiral guests: Castellano, R.K.; Nuckolls, C.; Rebek, J.Jr. *J. Am. Chem. Soc.* **1999**, *121*, 11156–11163.
(69) (a) Nelson, J.C.; Saven, J.G.; Moore, J.S.; Wolynes, P.G. *Science* **1997**, *277*, 1793–1796. (b) Hill, D.J.; Mio, M.J.; Prince, R.B.; Hughes, T.S.; Moore, J.S. *Chem. Rev.* **2001**, *101*, 3893-4011.
(70) Prince, R.B.; Barnes, S.A.; Moore, J.S. *J. Am. Chem. Soc.* **2000**, *122*, 2758–2762.
(71) Gin, M.S.; Yokozawa, T.; Prince, R.B.; Moore, J.S. *J. Am. Chem. Soc.* **1999**, *121*, 2643–2644.
(72) Gin, M.S.; Moore, J.S. *Org. Lett.* **2000**, *2*, 135–138.
(73) Prince, R.B.; Brunsveld, L.; Meijer, E.W.; Moore, J.S. *Angew. Chem. Int. Ed.* **2000**, *39*, 228–230.
(74) Prince, R.B.; Moore, J.S.; Brunsveld, L.; Meijer, E.W. *Chem. Eur. J.* **2001**, *7*, 4150–4154.
(75) Similar behavior has also been called 'domino effect': (a) Inai, Y.; Tagawa, K.; Takasu, A.; Hirabayasi, T.; Oshikawa, T.; Yamashita, M. *J. Am. Chem. Soc.* **2000**, *122*, 11731–11732. (b) Maeda, K.; Okamoto, Y. *Polym. J.* **1998**, *30*, 100–105.
(76) Brunsveld, L.; Meijer, E.W.; Prince, R.B.; Moore, J.S. *J. Am. Chem. Soc.* **2001**, *123*, 7978–7984.
(77) Brunsveld, L.; Prince, R.B.; Meijer, E.W.; Moore, J.S. *Org. Lett.* **2000**, *2*, 1525–1528.
(78) See urea disks in Chapter 3.
(79) (a) Yashima, E.; Maeda, K.; Nishimura, T. *Chem. Eur. J.* **2004**, *10*, 42–51.
(80) Other reviews: (a) Tsukube, H.; Shinoda, S. *Chem. Rev.* **2002**, *102*, 2389–2403. (b) Okamoto, Y.; Nakano, T. *Chem. Rev.* **1994**, *94*, 349–372. (c) Nakano, T., Okamoto, Y. *Chem. Rev.* **2001**, *101*, 4013–4038.
(81) Yashima, E.; Matsushima, T.; Okamoto, Y. *J. Am. Chem. Soc.* **1995**, *117*, 11596–11597.
(82) (a) Yashima, E.; Matsushima, T.; Okamoto, Y. *J. Am. Chem. Soc.* **1997**, *119*, 6345–6359. (b) Yashima, E.; Maeda, K.; Okamoto, Y.; *Nature* **1999**, *399*, 449–451. (c) Morino, K.; Maeda, K.; Okamoto, Y.; Yashima, E.; Sato, T. *Chem. Eur. J.* **2002**, *8*, 5112–5120. (d) Ashida, Y.; Sato, T.; Morino, K.; Maeda, K.; Okamoto, Y.; Yashima, E. *Macromolecules* **2003**, *36*, 3345–3350. (e) Ishikawa, M.; Maeda, K.; Mitsutsuji, Y.; Yahima, E. *J. Am. Chem. Soc.* **2004**, *126*, 732–733.
(83) crown ether: (a) Nonokawa, R.; Yahima, E. *J. Am. Chem. Soc.* **2003**, *125*, 1278–1283. (b) Nonokawa, R.; Yahima, E. *J. Polym. Sci. Part A* **2003**, *41*, 1004–1013. (b) Nishimura, T.; Ohsawa, S.; Maeda, K.; Yashima, E. *Chem. Commun.* **2004**, 646 –647. cyclodextrin: (c) Yashima, E.; Maeda, K.; Sato, O. *J. Am. Chem. Soc.* **2001**, *123*, 8159–8160.
(84) (a) Dellaportas, P.; Jones, R.G.; Holder, S.J. *Macromol. Rapid Commun.* **2002**, *23*, 99–103. (b) Nakashima, H.; Koe, J.R.; Torimitsu, K.; Fujiki, M. *J. Am. Chem. Soc.* **2001**, *123*, 4847–4848.
(85) van Gorp, J.J.; Vekemans, J.A.J.M.; Meijer E.W. *Mol. Cryst. Liq. Cryst.* **2003**, *397*, 491–505.
(86) van Gorp, J.J.; Vekemans, J.A.J.M.; Meijer E.W. *Chem. Commun.* **2004**, 60-61.

Chapter 2

Columnar mesophases, fibers, and organic gels from discotic triamides and triureas

Abstract: *Hydrogen-bonded C_3-symmetrical discotics that associate into helical stacks are described. Structural mutation on these molecules has been performed to elucidate the contribution of the different secondary interactions (hydrogen bonding, π-π stacking) to the ordering of the disks into columnar mesophases. Twelve C_3-symmetrical molecules have been investigated, six of which contain three central amide functionalities (**1a-f**) and six of which contain three central urea groups (**2a-f**). Peripheral groups of the disks are 'small', 'medium' or 'large', half of them being achiral and the other half being chiral. A detailed investigation of the formation and ordering of elongated stacks has been performed in the solid phase (TOPM, DSC, X-ray), on the surface (AFM), and in the gel phase (SANS, IR). Urea discotics are hard to investigate in the solid phase due to their low degradation temperature (140 °C), compared to their isotropization point (> 220 °C). However, systematic X-ray studies of the six achiral compounds (**1a,c,e** and **2a,c,e**) have displayed a variety of thermotropic columnar phases. Most compounds feature an ordered hexagonal phase (Col_{ho} for **1a**, **1e**, **2c**, and **2e**); while small urea **2a** forms tetragonally ordered columns (Col_{tet}). Medium amide **1c** shows two low energy transitions from an ordered hexagonal phase (Col_{ho}), to disordered rectangular (Col_{rd}), and disordered hexagonal phases (Col_{hd}). In contrast to all other disks, these medium amide discotics **1c/d** do not form gels in apolar solvents. Small urea disk **2a** shows a minimal gel concentration as low as 1.2 mg/ml, while for large urea disk **2f** a network of fibers with lengths up to 2 μm has been visualized on the surface.*

2.1 Introduction

Self-assembly may open new possibilities in both the fields of biology and materials science, since it enables the rapid formation of nano-sized, complex architectures, adopting stable and compact conformations, despite their non-covalent, reversible nature.[1] A vast number of these structures is known, that contain strong (self-)complementary and unidirectional intermolecular interactions to enforce one-, two-, or three-dimensional self-assembled architectures.[2] In this respect, the helix has been recognized as a valuable entity, because of flexibility in its propagation direction, together with compact order perpendicular to that.[3] For the self-assembled systems to be successful, ordered architectures must not only be formed in the solid or liquid crystalline phase,[4a] the lyotropic organic gel phase,[4b-d] but also in dilute solution.[4e] In this chapter the focus is on the liquid crystalline phase and gel phase, while the behavior in dilute solution will be discussed in Chapter 3.

In the liquid crystalline phase, X-ray diffraction measurements disclose ordering of mesogens in one, two, or three dimensions. For columnar and/or helical structures these are, respectively, low-order nematic phases (N_D and N_C), lamellar phases (e.g. D_{LC}), and columnar phases (Figure 2.1), among which highly ordered hexagonal phases (Col_h), tetragonal phases (Col_{tet}), and various rectangular packing motifs (Col_r).[5] In the direction of the columns, ordered, as well as disordered situations are encountered.

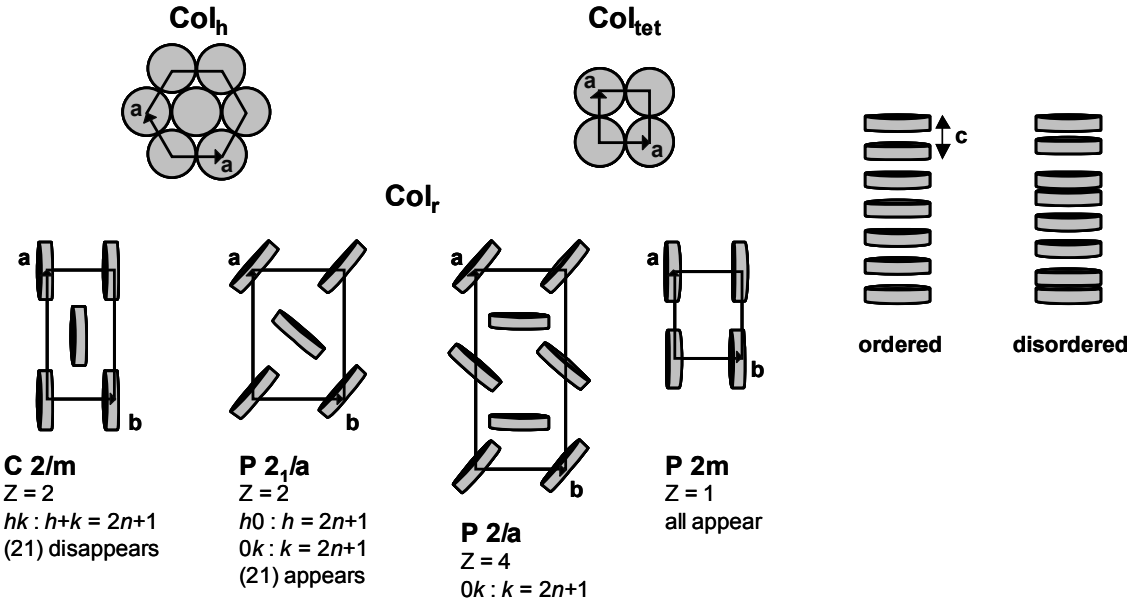

Figure 2.1. *Schematic representation of various columnar phases: hexagonal (Col_h), tetragonal (Col_{tet}), and rectangular (Col_r); ordered, as well as disordered.*

The self-assembled systems have been applied in so-called organogels,[6] for example those of the well-known cyanuric acid / melamine motifs.[2a, 6a] In an organogel the liquid is prevented from flowing by a continuous, three-dimensional, entangled network of fibers of low molecular weight

organogelators.[7] These are held together solely by non-covalent forces, including hydrogen bonding, π-π stacking and solvophobic interactions. Much effort is being put into the design of new organogelators,[8] but even when the basic requirements of gel formation are met (supramolecular aggregation and cross-link formation), external factors (concentration, temperature, solvent and stoichiometry) can prevent gel formation.[9] Irreversible precipitation of fibers is induced, similar to irreversible aggregation of proteins in case of neuro-degenerative diseases, such as Alzheimer's and Creutzfeldt-Jakob's disease.[10] To increase insight into the supramolecular aggregation phenomena, the exact nature and relative importance of the secondary interactions need to be studied.

For this purpose, discotic molecules[11] were selected as highly suitable building blocks for the formation of cylindrically shaped fibers. Both solvophobic effects and π-π stacking[12a-c] as well as hydrogen bonding[12d,e] are used to assemble the disc-like entities. Remarkably, hydrogen bonding is also used to preorganize the core of the disk,[12f,g] or even to form the disk by bringing together multiple precursors.[12h-l] The discotic structures cover a broad range of rotational symmetries (e.g. ranging from C_2 to C_6), but from an esthetic and practical point of view, C_3-symmetrical compounds were found highly attractive,[12e,g,k,l,m-r] especially those containing a 1,3,5-benzenetricarboxamide unit.[13,14] For disks consisting of such a tricarboxamide unit and short 2-methoxyethyl side chains, the single crystal X-ray structure shows conformationally unique π-stacked rods supported by a triple helical network of hydrogen bonds (pitch: 21.7 Å, inter disk distance: 3.62 Å), with a rectangular packing.[15a] Rheological studies on organogels of 3,7-dimethyloctyl substituted tricarboxamides in linear apolar solvents (C_n), show that the columnar, flexible supramolecular structures display a pronounced viscoelasticity, similar to that in fully entangled linear polymer systems. However, a peculiar mechanism for entanglement release is observed, like described for aqueous threadlike micellar systems.[16]

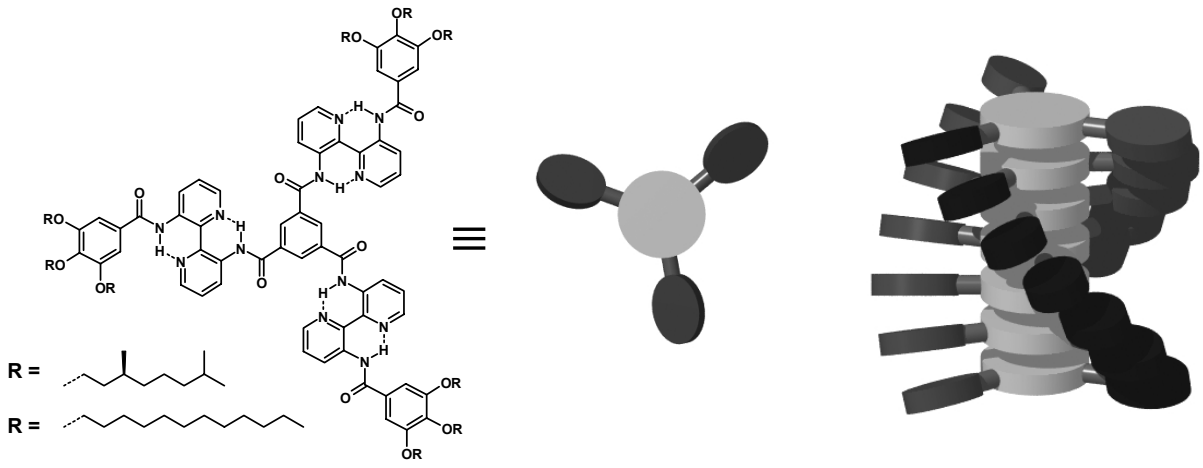

Figure 2.2. *The first bipyridine based C_3-symmetrical disks and a cartoon representing their helical supramolecular stacking.*

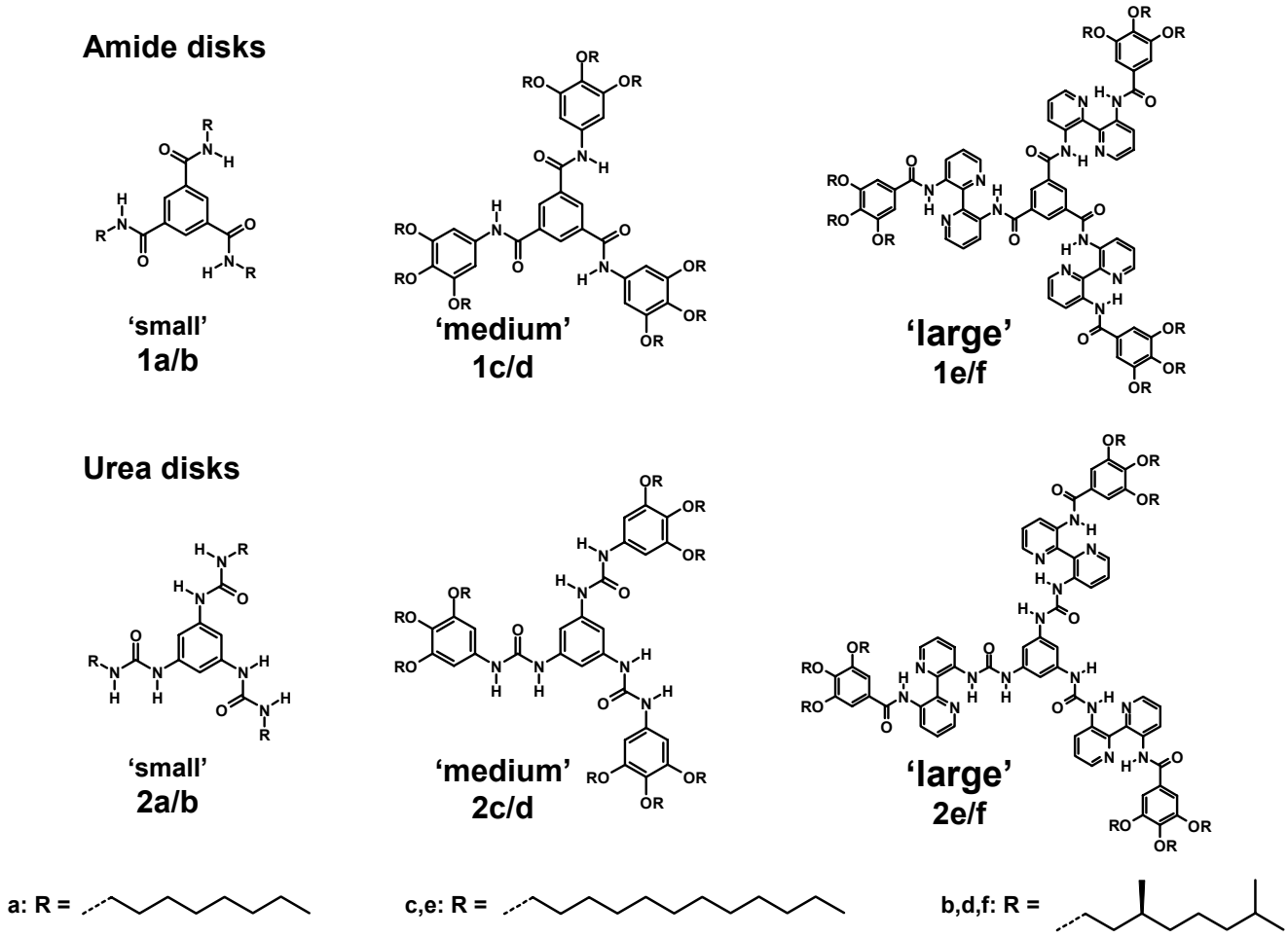

Figure 2.3. *Overview of twelve C_3-symmetrical disks, containing central amides **(1a-f)** or ureas **(2a-f)**. The peripheral groups of the disks are 'small' **(1a/b** and **2a/b)**, 'medium' **(1c/d** and **2c/d)** or 'large' **(1e/f** and **2e/f)**. Half of the disks are achiral **(1a/c/e** and **2a/c/e)**; the other half is chiral **(1b/d/f** and **2b/d/f)**.*

Recently, various C_3-symmetrical columnar supramolecular architectures relying on hydrogen bonding in combination with π-π stacking were reported.[17,18] The first representatives of this class of C_3-symmetrical self-assembled structures were built up convergently by the stepwise acylation of 2,2'-bipyridine-3,3'-diamine (Figure 2.2).[17] The bipyridinyl parts are planar and preorganized due to their intramolecular hydrogen bonding; the gallic moieties are equipped with alkyl groups, inducing phase separation; while the assemblies feature a threefold array of intermolecular hydrogen bonds via the central 1,3,5-benzenetricarboxamide unit. Order is not only observed in the solid or liquid crystalline phase,[17a] the lyotropic organic gel phase,[17b] but also in dilute solution[17c] (Chapter 3). In the wide thermotropic liquid crystalline window (9-355 °C), as well as in the concentrated lyotropic phase (0.21 M), an ordered hexagonal packing was observed, together with a strong X-ray reflection at

17.6 Å, assigned to the pitch.[17a,b] Enlargement of the central aromatic core with six methoxy groups or three pyrazine rings gives stronger but less ordered π-π stacks.[17d]

To what extent both intermolecular hydrogen bonding and π-π interactions contribute to the cooperative, helical self-assembly is an intriguing question. That both secondary interactions can work hierarchically, is for example elucidated by the stepwise growth of analogous disks equipped with oligo(ethylene oxide) tails into chiral columns in polar media.[18] In apolar media, with hydrophobic peripheral tails, such a stepwise aggregation is not observed and both secondary interactions are proposed coming to expression almost simultaneously.

To unravel the features governing self-assembly in apolar media, various π-π interacting groups and hydrogen bonding units are combined to afford a series of C_3-symmetrical disks (Figure 2.3). The π-π interactions are strengthened in the series by using 'small' alkyl tails (**1a/b**, **2a/b**), 'medium' gallic groups (**1c/d**, **2c/d**), and 'large' bipyridinyl-gallic groups (**1e/f**, **2e/f**). The intermolecular hydrogen bonding amide moieties in **1a-f** are substituted by urea ones in **2a-f**. Because a urea has two protons prone to hydrogen bonding -where an amide has only one-, the urea hydrogen bond is considered stronger and more rigid. In this chapter, the behavior of twelve C_3-symmetrical disks is compared in the solid, liquid crystalline state, and in the gel phase. Previously, the properties of **1a/b**[13-16] and **1e/f**[17] have been described, while all the other members of the library are novel.

2.2 Synthesis and characterization of discotic triamides and triureas

2.2.1 Synthesis

Triamides **1a-f** were formed by threefold reaction of trimesyl chloride with amines **3a-f**, of which the chiral ones **3b**[19], **3d**[20] and **3f**[17] are based on the (*S*)-3,7-dimethyloctyl unit (Scheme 2.1). The syntheses of compounds **1a/b** and **1e/f** have been described before.[14a,17] Triamides **1c** and **1d** were obtained in reasonable yield after column chromatography (86 % and 70 % for **1c** and **1d**, respectively). The triureas **2a-f** were obtained by threefold reaction of amines **3a-f** with 1,3,5-benzenetriisocyanate (**5**). The latter was synthesized in 90 % yield by treatment of trimesyl chloride with sodium azide, and subsequent thermolysis of trimesyl azide (**4**)[21] to induce the Curtius rearrangement.[22] The urea disks were obtained in satisfactory yield after washing with the appropriate solvent (yields for **2a**: 70 %, **2b**: 68 %, **2c**: 87 %, **2d**: 78 %, **2e**: 75 % and **2f**: 87 %).

2.2.2 Order in the solid state

All C_3-symmetrical amide disks **1a-f** show liquid crystallinity, most of them over a broad temperature range (Table 2.1). Optical microscopy and DSC of the achiral medium compound **1c** shows that the thermotropic liquid crystalline window expands from –4 °C (44 kJ/mol) to 178 °C (27

Scheme 2.1. *Synthesis of disc-shaped amides **1a-f** and ureas **2a-f**.*

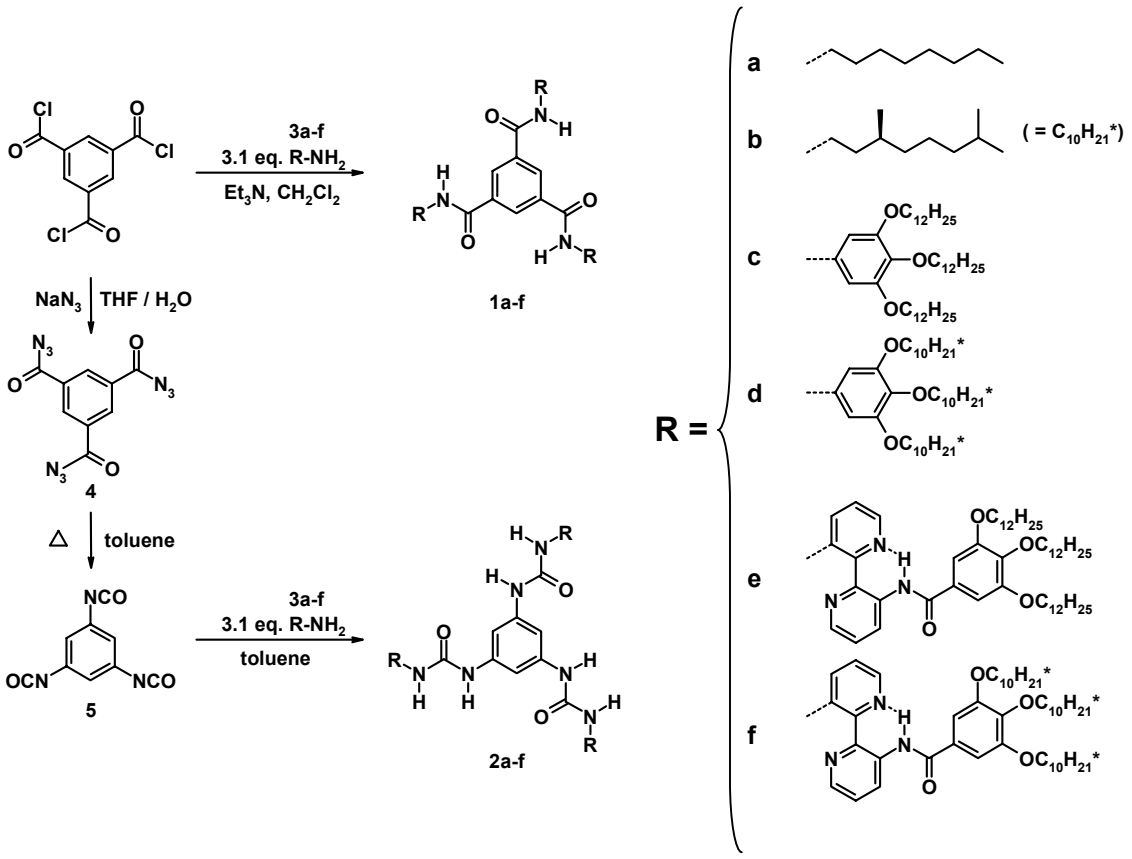

kJ/mol). Three phases are found (Figure 2.6), separated by small transitions at 61 °C (4.2 kJ/mol) and 98 °C (2.1 kJ/mol). In case of the chiral compound **1d** a small (<1 kJ/mol) crystalline-crystalline transition is found at lower temperatures (0 °C). Compound **1d** enters the liquid crystalline phase at 96 °C (1.8 kJ/mol) and becomes already isotropic at 113 °C (15 kJ/mol). Typical focal conic structures are found for the amide disks **1a-f**, pointing to a helical columnar structure (Figure 2.4).

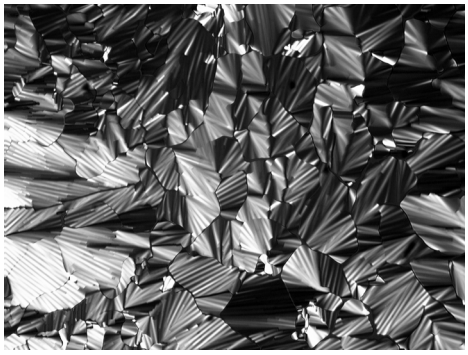

Figure 2.4. *Typical focal conic structure found in the liquid crystalline phase for achiral medium amide disk **1c** (172 °C, after shortly pressing the sample between two glass plates; see also Figure 2.6).*

The disc-shaped ureas **2a-f** are difficult to study in the pure form, due to degradation of these compounds above 140 °C, which is lower than the isotropization temperature (>220 °C). However, observed transitions are also reported in Table 2.1. Furthermore, infrared spectroscopy shows that hydrogen bonding occurs in the ordered (liquid) crystalline phases (Table 2.2), indicated by the typically low wavenumber positions of the carbonyl vibrations.[13a/b]

Table 2.1.[a] *Transition temperatures T [°C] and corresponding enthalpies ΔH [kJ/mol] of disc-shaped amides **1a-f** and ureas **2a-f**.*

No.	K	T (*ΔH*)	M	T (*ΔH*)	I	No.	K	T (*ΔH*)	M	T (*ΔH*)	I
1a[b]	Col_{ho}	102 (*19*)	Col_{ho}	204 (*17*)	•	**2a**	Col_{tet}	122 *(8.1)*	Col_{tet}	215[f]	•
1b[c]	•	119 (*16*)	•	236 (*21*)	•	**2b**	•	100 *(2.1)*	•	-	•
1c	•	-4 (*44*)	$Col_{ho,rd,hd}$	178 (*27*)	•	**2c**	Col_h	53 *(65)*	Col_h	228[f]	•
1d	•	96 (*1.8*)	•	113 (*15*)	•	**2d**	-[e]	-	•	215[f]	-
1e[d]	•	9 (*56*)	Col_{ho}	355 (*27*)[f]	•	**2e**	-[g]	-45	Col_{ho}	-	-
1f[d]	-[e]	-	Col_{ho}	373 (*28*)[f]	•	**2f**	-[g]	-60	Col_{ho}	190[f]	-

[a] • = phase is observed; - = phase is not observed; K = crystalline phase; M = unidentified mesophase; Col = columnar phase (see text for details); I = isotropic phase. [b] Reference 13c. [c] Reference 14a. [d] Reference 23. [e] Cooling the sample down to –80 °C did not show any transition. [f] The clearing is accompanied by decomposition of the sample making the data less reliable. [g] A T_g is observed.

Table 2.2. *Wavenumbers σ [cm^{-1}] of the carbonyl stretch vibrations of amides **1a-f** and ureas **2a-f** in the solid state.*

Compound	**1a**[a]	**1c**	**1e**[b]	Compound	**2a**	**2c**	**2e**
σ solid state	1640	1682	1668	σ solid state	1632	1641	1670
		1664					1623

[a] Reference 24. [b] Reference 23.

The thermotropic mesophases of the achiral amide disks (**1a,c,e**) and urea disks (**2a,c,e**) have been characterized using X-ray diffraction. Firstly, the thermotropic ordered columnar hexagonal phase (Col_{ho}) of large amide disk **1e** was reconfirmed.[23] The ratio between the diffraction spacings of the <100>, <110>, and <210> reflections of 1 / $^1/_{\sqrt{3}}$ / $^1/_{\sqrt{7}}$, typical for a hexagonal phase, is clearly visible (Figure 2.5, Table 2.3). The reflection at d = 3.3 Å (2θ = 26.7, 25 °C) is assigned to be the inter disk distance, and indicates that the phase is ordered.[15,25] Finally, an intense reflection is observed at d = 17.6 Å (2θ = 5.0, 25 °C), which is assigned to the pitch of the helix. Upon raising temperature from 25 °C to 150 °C, the sample is annealed, and the spectrum more resolved. As expected, the inter column and inter disk distances increase. However, for the pitch this trend was not observed, indicating that by annealing the order in the system is increased even further.

The resolved spectrum for large amide disk **1e** contrasts with the broad reflections obtained for large urea disk **2e**. Nevertheless, a similarly ordered hexagonal phase (Col_{ho}) was assigned (see Experimental section). It was tried to improve spectral data by using the chiral compound, which

flowed more easily, but only the reflection assigned to the pitch sharpened. Measurements after longer annealing times (several hours at 100 °C) might be helpful. As expected, the inter column distance is somewhat larger for urea **2e** (41.1 Å), than for amide **1e** (39.5 Å) (25 °C, Table 2.4). More remarkable are the smaller pitch (and inter disk distance) for urea **2e** (15.7 Å), compared to that of amide **1e** (17.6 Å).

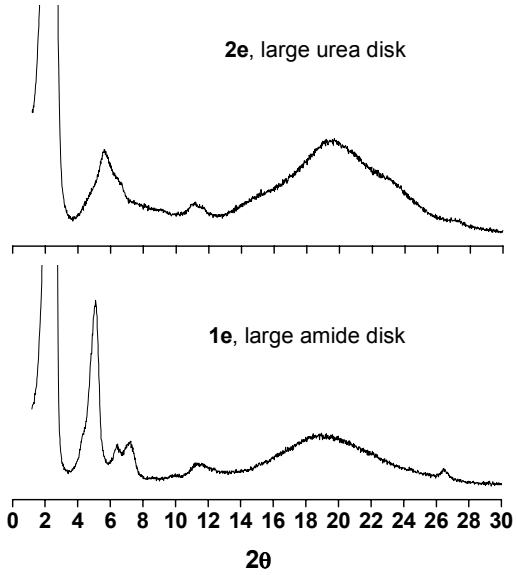

Figure 2.5. *X-ray spectra of achiral large amide disk **1e** (bottom) and urea disk **2e** (top) at 100 °C (Bragg: d [Å] = λ/2sinθ, λ = 1.54056 Å, see Experimental section).*

Table 2.3. *Diffraction spacings and molecular dimensions [Å] obtained for achiral large amide **1e**;* a *[Å] = inter column distance,* pitch *[Å] = pitch,* c *[Å] = inter disk distance.*

reflection	<100>	a	<110>	<200>	pitch	<210>	<300>	<400>	<410>	halo	c
ratio	1		1/√3	1/2		1/√7	1/3	1/4	1/√21		
Col_{ho}	35.88		20.72	17.94		13.56	11.96	8.97	7.83		
25 °C	*34.22*	*39.51*			*17.59*	*13.54*	*11.94*	*8.68*	*7.51*	*4.48*	*3.33*
50 °C	*35.88*	*41.46*			*17.87*	*13.76*	*12.20*	*8.86*	*7.54*	*4.60*	*3.35*
100 °C	*35.88*	*41.46*	*20.53*	*18.28*	*17.31*	*13.80*	*12.23*	*8.93*	*7.81*	*4.69*	*3.37*
150 °C	*36.18*	*41.77*	*20.34*	*18.24*	*17.12*	*13.76*	*12.27*	-	*7.81*	*4.76*	*3.39*

Also medium urea **2c** gave a broad, unresolved spectrum, even in the crystalline phase (25 °C). However, also here the reflections correspond to those of a hexagonal packing (a = 33.3 Å, pitch = 15.4 Å, 25 °C). No inter disk distance could be discerned. On the other hand, a complex behavior was observed for medium amide disk **1c**. The three phases observed in the DSC scan can unarguably be assigned as ordered hexagonal (Col_{ho}, -4 to 61 °C), disordered rectangular (Col_{rd}, 61 to 98 °C), and disordered hexagonal (Col_{hd}, 98 to 178 °C) phases (Figure 2.6). It has to be noted that the inter column distance in the ordered hexagonal phase is much larger (a = 39.5 Å), than in the disordered hexagonal phase (35.6 Å). Where in previous cases (**1e/f**, **2e/f**, **2c**) intense reflections for the pitch were observed, only the rectangular phase of **1c** showed such reflection (d = 15.5 Å).

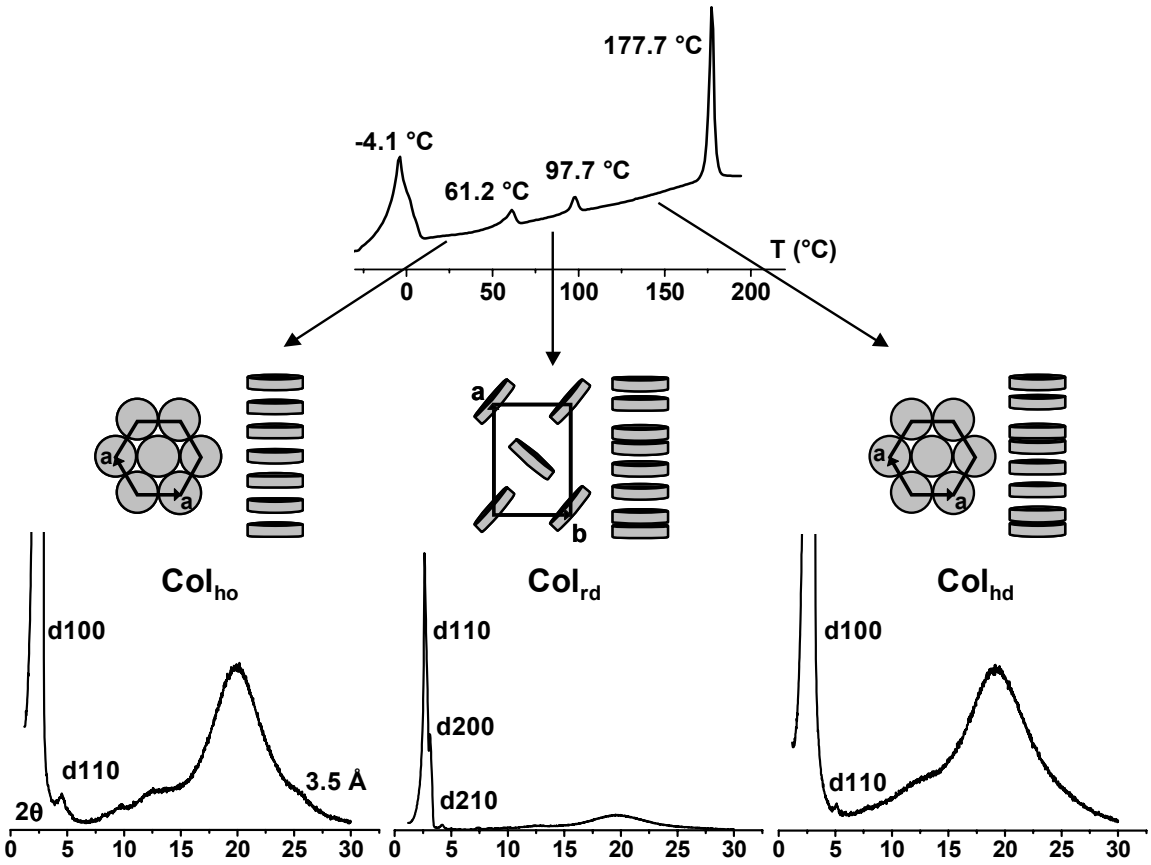

Figure 2.6. *Solid phase behavior of medium amide disk **1c** (see Figure 2.3 for the texture at 172 °C). DSC reveals 3 mesophases (top): Col_{ho}, Col_{rd}, and Col_{hd}, determined by X-ray analyisis (bottom), and illustrated by schematic representations (middle).*

Small amide and urea disks show a single mesophase. For small amide **1a**, this is an ordered hexagonal one, in the crystalline (25 °C), as well as in the liquid crystalline (140 °C) phase. Remarkably, the broad reflections of small urea **2a**, correspond to a tetragonal packing. Similar to large disks **1e** and **2e**, the inter column distance of urea **2a** is somewhat larger than of **1a** (Table 2.4, 25 °C, 17.8 Å for **1a**, and 20.6 Å for **2a**), while the pitch might be significantly smaller (see experimental section, 15.4 Å for **1a**, and 14.5 Å for **2a**).

CPK models of the disks were used to derive the radius of the aromatic core (Figure 2.7 and 2.8). For example, a radius (r) of 9.8 Å was calculated for the medium urea disk and of 16 Å for the large urea disk (see 2.2.3). Estimating the cross section to twice this radius (d_O) corresponds to experimental values (Table 2.4), although, due to the C_3-symmetrical nature, the cross section might also be estimated somewhat smaller (d_Δ). Taking into account the propeller like, rather than circular shape of the molecules, the inter column distance a, derived from X-ray data, was compared to the sum of the diameter d_O, and the length of one extended side chain l.

Table 2.4. *Molecular dimensions derived from X-ray data for amide compounds **1a/c/e/f** and urea compounds **2a/c/e/f** at 25 °C; together with a CPK estimate of the cross section of the disks (Figure 2.7); a [Å] = inter column distance, c [Å] = inter disk distance, d_O+l [Å] = cross section, d_O [Å] = coss section of the aromatic core, and l [Å] = the length of one extended side chain.*

No.	**1a**	**1c**	**1e**	**1f**[a]
d_O+*l*	18	33	43	38
a	17.8	39.5 / 35.6	39.5	38
pitch	15.4	-	17.6	17.4
c	3.47	3.47 / -	3.33	3.5

No.	**2a**	**2c**	**2e**	**2f**
d_O+*l*	21	35	47	42
a	20.6	33.3	41.1	38.6
pitch	-	15.4	15.7	14.8
c	-	-	3.31	3.25

[a] Reference 23.

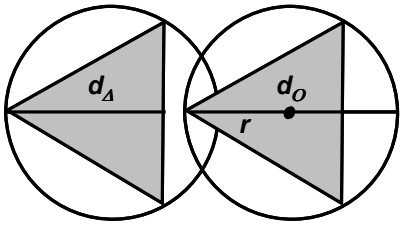

Figure 2.7. *Schematic representation of the position of two adjacent C_3-symmetrical disks; the gray triangles represent the aromatic cores of the disks, of which d_Δ is the perpendicular bisector, r the radius, and d_O the diameter of the corresponding circle.*

2.2.3 Self-assembly in the gel phase

A property inherent to the presence of elongated, columnar stacks is the possibility to form macroscopic organogels. These gels were made by dissolving the compounds in hot apolar solvents and subsequent cooling. When the jar could be turned over without product movement, the substance was judged a gel. Minimal gel concentrations were determined by this method (Table 2.5). Medium amide disk **1c** is not able to form a gel in apolar solvents. The triureas **2** generally display lower minimal concentrations than the corresponding amides **1**; especially the small urea compound **2a** performs well in this respect.

Table 2.5. *Minimal gel concentrations (concentration [mg/ml]; concentration [M]; solvent) of amides **1a-f** and ureas **2a-f**.*

	Amide (**1**)	Urea (**2**)
'small' (**a**)	55 mg/ml[a] 8.8×10^{-2} M hexane	1.2 mg/ml 2.0×10^{-3} M toluene
'medium' (**c**)	-	174 mg/ml 8.1×10^{-2} M heptane
'large' (**e**)	37 mg/ml[b] 1.4×10^{-2} M dodecane	17 mg/ml 6.2×10^{-3} M dodecane

[a] **1b** in reference 13b. [b] Reference 23.

Macroscopic order of the large disc-shaped molecules **1e/f** and **2e/f** in the gel was proven by their birefringence in optical microscopy. In birefringent solutions of 'large' amide disks **1e** in concentrations varying from 56 mg/ml (2.9×10^{-2} M) to 207 mg/ml (0.11 M) an N_c phase is present. Concentrated samples (407 mg/ml, 0.21 M) show hexagonal packing of the columns as well as a helical superstructure, indicative of a D_{ho} phase.[23] For the urea disks, both in case of the achiral compound **2e** (17 mg/ml, 6.2×10^{-3} M) and in case of chiral compound **2f** (57 mg/ml, 2.3×10^{-2} M), focal conic structures were found in dodecane, indicative of a columnar phase.

Where for small and large amide disks **1a** and **1e** it is obvious from different techniques, such as IR and NMR spectroscopy, that intermolecular hydrogen bonding -and hence aggregation- remains present in (dilute) apolar solutions, for medium amide disks **1c** this is not the case. IR gives two carbonyl vibrations in both the solid state (1682 and 1664 cm^{-1}, Table 2.2) and in heptane solution (1670 and 1650 cm^{-1}, Table 2.6), indicating the presence of both hydrogen-bonded aggregates and molecularly dissolved species. On the other hand, for urea disks **2c** and **2e** the positions of the single carbonyl vibration are similar in the solid state and in 10^{-4} M heptane solution, indicating hydrogen bonding and aggregation in solution. Small urea **2a** is only sparingly soluble in heptane (10^{-3} M, 40 °C) and shows a carbonyl vibration that is significantly higher in heptane than in the solid state (1736 *vs.* 1632, respectively). However, in toluene, a 10^{-4} M solution gives a similar NH stretch vibration as found in the solid state (3310 *vs.* 3302 cm^{-1}, respectively).

Table 2.6. *Wavenumbers σ [cm^{-1}] of the carbonyl stretch vibrations of amides **1a-f** and ureas **2a-f** in 10^{-4} M heptane solution.*

Compound	**1a**[a]	**1c**	**1e**
σ 10^{-4} M heptane	1640	1670 1650	1669

Compound	**2a**	**2c**	**2e**
σ 10^{-4} M heptane	1736	1641	1670 1624

[a] Reference 24.

Macroscopic gelation is supposed to originate from a network of fibers present in apolar solutions of amides **1a/b** and **1e/f** or ureas **2a-f**. For the medium and large molecules (**1d**, and **2d/f**) this network can be visualized by atomic force microscopy (AFM) and small angle neutron scattering (SANS). With these techniques, also the dimensions of the aggregates can be verified. Both AFM and SANS should give cross sections of about 20 *(d_O)* - 35 *(d_O+l)* Å for medium urea **2d** and 32 *(d_O)* - 42 (d_O+l) Å for large urea **2f** (Table 2.4, Figures 2.7 and 2.8).

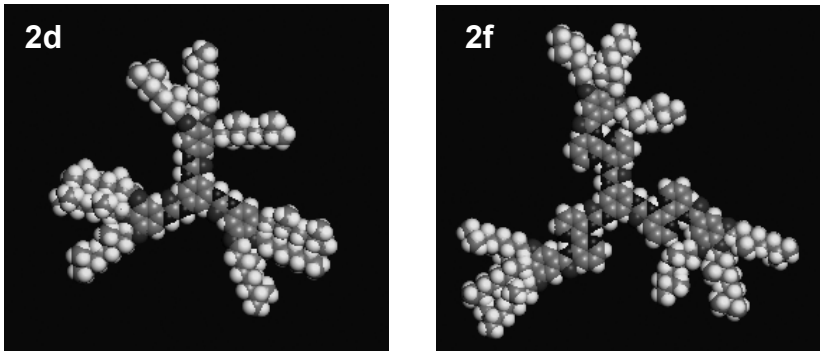

Figure 2.8. *CPK models of medium **2d** (left) and large **2f** (right) urea disks.*

For the medium amide **1d**, no network was found (Figure 2.9). This was expected, in view of their inability to form a viscous solution. In contrast, the triurea molecules **2d** and **2f** did show gel formation, and a network of fibers was observed in the AFM scans, indeed. In case of the large urea **2f**, the fibers are as long as 2 μm. With an inter disk distance of 3.5 Å, this would correspond to columns consisting of as much as 5,700 molecules!

Formation of the network occurs *via* physical cross-link points. At these points several strands, which are lying next to each other, split up and continue separately, to rejoin some other strands later on (Figure 2.9). In an area where several strands are aligned parallel, the width of one strand can be estimated by dividing the total width by the number of strands. In this way, a width of 4.2 nm is calculated (Table 2.7).

However, the height profile of the structures can also be considered. For the medium amide **1d**, the height of the plateaus (3.1 nm) is constant over the sample, although no special architecture is formed. The heights of the medium and large urea fibers **2d** and **2f** are 2.2 and 3.2 nm. As expected, the smaller molecule displays the smallest height.

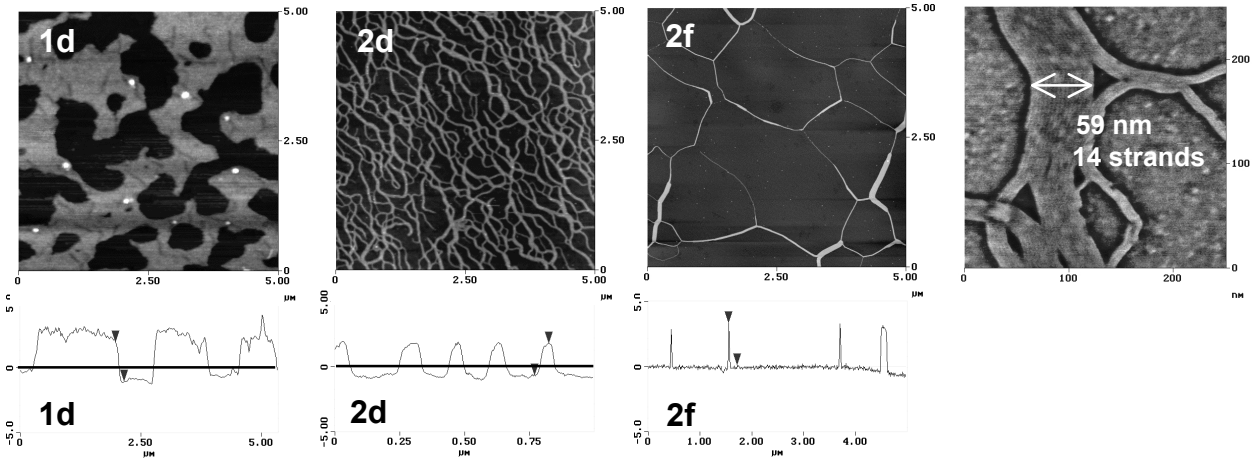

Figure 2.9. *AFM pictures (top) and height profiles (bottom) of medium amide disk **1d** (far left), medium urea disk **2d** (middle left) and large urea disk **2f** (middle right) as well as a physical cross-link point of large urea disk **2f** (far right).*

A technique to investigate the shape and dimensions of aggregates in the actual solution is small angle neutron scattering (SANS). In the plot of the scattering intensity against the scattering vector, the combination of a linear curve with a slope of -1 (in the intermediate angle area) with a symmetrical side maximum (in the large angle area) indicates the presence of cylindrical aggregates. Indeed, this situation applies to 6 mg/ml solutions of the medium and large urea disks **2d** and **2f** in dodecane-*d26*, in which case the length of the aggregate is at least 150 nm (Figure 2.10). At very low scattering vectors the curve of medium urea **2d** positively deviates from linearity. Since these systems reveal thermo-reversible gel formation this deviation must be attributed to the presence of columnar clusters that represent the physical cross-links in the gel. From the position of the side maximum the radius of the cross section 'R_c' can be determined using the formula '$R_c \sim 4.48/q_{max}$'. The radius of the large urea disk **2f** (39 Å) is indeed larger than that of the medium one **2d** (33 Å). Finally, medium amide disk **1d** is investigated as a reference (Figure 2.10). In contrast to the medium urea disk **2d** no linear curve with a slope of -1 and no side maximum are observed. Obviously, in this case no elongated stacks are formed.

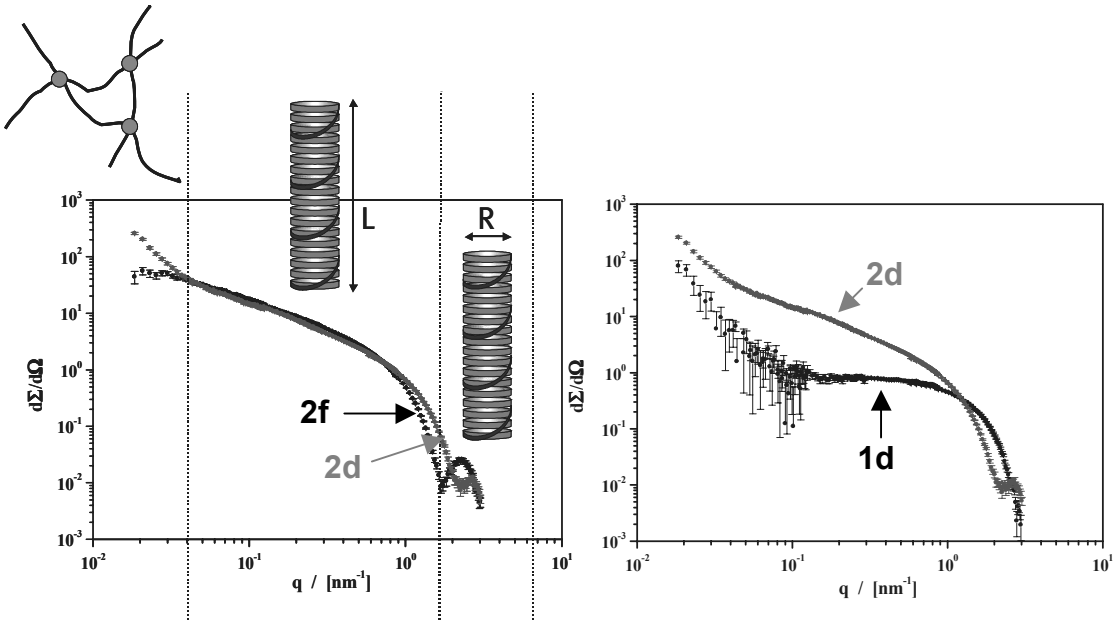

Figure 2.10. *SANS data of medium urea disk **2d** (gray line), large urea disk **2f** (left black line) and medium amide disk **1d** (right black line).*

Table 2.7. *Cross sections [Å] of medium urea **2d**, large urea **2f** and large amide **1f** determined with different techniques; d_O+l [Å] = cross section, d_O [Å] = coss section of the aromatic core, and l [Å] = the length of one extended side chain.*

	CPK d_O	AFM (height)	CPK d_O+l	AFM (width)	SANS	X-ray
medium (**2d**)	20	22	30		33	33.3 (**2c**)
large (**2f**)	32	32	42	42	39	38.6
large (**1f**)[a]	28		38			38

[a] Reference 23.

2.3 Thermotropic and lyotropic columnar phases involving amide or urea hydrogen bonding

From the results above it is clear that all investigated disks form columnar structures in their liquid crystalline phases. Most of the disks (**1a/e/f**, **2c/e/f**) show a hexagonal packing of the columns, but tetragonal (**2a**) and rectangular (**1c**) lattices are also observed. Obviously, a minor structural variation in the molecule (an extra NH group) may dramatically disturb the subtle interactions between molecules building a columnar aggregate, and thus the interactions between those aggregates (e.g. amide **1a**: Col_{ho}, and urea **2a**: Col_{tet}). On the other hand, all columnar phases are highly ordered, and differences in positioning of the columns are relatively small. This is illustrated by the sequence of phases encountered for medium amide **1c** upon raising temperature (Col_{ho}, Col_{rd}, and Col_{hd}), in which the phases are only separated by low energetic transitions (2-4 kJ/mol). To the best of my knowledge, rectangular column packing for discotics remains rare,[11b,15] which makes the interconversions between hexagonal and rectangular phases displayed by medium amide **1c**, the more remarkable.[26]

The disks that show a hexagonal packing (**1a/e/f**, **2c/e/f**), are ordered (inter disk distance c of ~ 3.4 Å) and show a clear reflection corresponding to the pitch (15-18 Å). From the fact that both achiral and chiral compounds show these reflections, it can be concluded that the individual columns are inherently helical, and therefore chiral. In an annealed sample of large amide **1e** (150 °C), the ratio between pitch (17.1 Å) and inter disk distance (3.4 Å) is exactly 5, indicating that the pitch consists of 5 molecules. This would imply that the disks are rotated 72 ° with respect to each other. The situation is comparable to that in a tricarboxamide disk with short 2-methoxyethyl side chains, where the ratio between pitch (21.7 Å) and inter disk distance (3.62 Å) is 6, implying a rotation of 60 ° between two disks. According to single crystal X-ray data, the mean planes of the three amide units make on average an angle of 41.5 ° with the central aryl mean plane. As a consequence, amide dipoles point ~60 ° from the column axis.[15]

In case of the small, medium, as well as large disks, the X-ray spectra of ureas **2** are much broader and less resolved than those of corresponding amides **1**. This might be explained by the fact that ureas **2** cannot align spontaneously, like amides **1**. Large amide **1e** gave a well resolved spectrum, just after

smearing it on the X-ray sample plate. Also, the spectrum of branched, chiral **2f**, was better resolved than that of linear, achiral **2e**. Furthermore, the ureas cannot be heated into the isotropic phase, to be annealed, because of degradation problems. Therefore, very long annealing times will have to be applied. On the molecular level, the lack of spontaneous alignment of urea disks, might be caused by stronger intermolecular hydrogen bonding between molecules (6 NH for ureas **2**, instead of 3 NH for amides **1**), giving rise to more strongly bound aggregates. The small pitch of large urea **2e** (15.7 Å), compared to that of large amide **1e** (17.6 Å) points towards such intermolecular hydrogen bonding. It seems that urea disks readily form columns, in which helicity is not perfect due to 'mistakes'. Amide hydrogen bonding seems to allow rotational freedom to repair these mistakes, while strong urea interactions might prevent the urea disks to move into their thermodynamically stable situation of maximal order. In another view, urea hydrogen bonds act as mindless hulks, very powerful in forming columnar aggregates, but slow in learning chiral information (see Chapter 3).

Because of the extra NH groups, the inter column distance of small, as well as large, urea molecules is somewhat larger than those of the corresponding amide ones (*a* for **1a**: 17.8 Å, and **2a**: 20.6 Å; *a* for **1e**: 39.5 Å, and **2e**: 41.1 Å). Remarkably, the inter column distance for medium amide **1c** is larger than that of medium urea **2c** (33.3 Å), in the ordered (39.5 Å), as well as the disordered hexagonal phase (35.6 Å). This would imply that in the ordered hexagonal phase of amide **1c**, the dodecyloxy chains are extended. However, in general, the inter column distances *a*, correspond well to the sum of the diameter of the aromatic core, and the length of one extended side chain (Table 2.4). This seems reasonable, taking into account that the molecules are propeller shaped, rather than circular (Figure 2.7). Estimations using either the diameter of the circle d_O, or the perpendicular bisector of the corresponding triangle d_Δ, for the cross section of the aromatic core, both seem reasonable. In case of large ureas **2e**, for example, d_Δ gives a lower, so better corresponding, value, than d_O (**2e**: a = 41.1 Å, $d_O + l$ = 47 Å, $d_\Delta + l$ = 39 Å).

Most of these C_3-symmetrical supramolecular architectures are retained in gels in apolar solution. For medium urea **2d** and large urea **2f**, respectively, the value for the cross section R_c of the molecule -and hence the supramolecular fiber- found in the AFM height profile (22 Å and 32 Å, respectively) corresponds well to the CPK estimate d_O (20 Å and 32 Å, respectively). The values for the cross section R_c found with AFM-width, SANS, or X-ray also correspond perfectly to the CPK estimate $d_O + l$ (Table 2.7, 33 Å and 39 Å, respectively), but are substantially larger than those found using AFM height profiles or CPK models. This can be explained, since the latter two techniques are underestimating the space occupied by the aliphatic tails. In case of CPK modeling this was done consciously by only taking into account the aromatic core d_O; in case of AFM height profiles, one can imagine that the AFM tip compresses the flexible outer shell of the fiber. Strikingly, the difference between the values found with CPK/AFM-height and AFM-width/SANS/X-ray is 10 Å, which

corresponds to the space taken up by one extended chiral alkyl chain *l* ((*S*)-3,7-dimethyloctyl: 8 × 1.25 Å = 10 Å). X-Ray studies on systems as different as large amide **1f**[23] and sugar appended organogelators[6n], have shown that solvent molecules can widen the inter-column distance by taking part in the supramolecular ordering. But in view of this striking difference of 10 Å, the influence of the solvent on the AFM and SANS measurements is most likely small in case of medium and large ureas **2d** and **2f**.

Surprisingly, medium amide disks **1c/d** do not retain their columnar structure in apolar solution, in contrast to all the other amide and urea disks (**1a/b-e/f**, **2a-f**). The variation in liquid crystalline phases for **1c**, the small liquid crystalline phase found for **1d,** the absence of a pitch reflection and/or inter disk distance in the X-ray spectrum of **1c**, and the good solubility of **1c/d** in apolar solvents, might all be indications for this behavior. Medium amide disks with inversed (nitrogen centered) amide groups do not form (chiral) aggregates either,[27] confirming the behavior found for medium amide disks **1c/d**. Generally, it depends on several factors whether aggregates are formed, among which, the strength of the hydrogen bonding, the strength of the π-π and van der Waals interactions and the mutual proportionality of the two. Apparently, the combination of π-π stacking between single aromatic rings and hydrogen bonding between amide groups is not strong enough to form helical stacks. In the small amide disks **1a/b**, strong van der Waals interactions probably account for a crystal-like packing of the alkyl tails. In the large amide disks **1e/f** strong π-π interactions are present between the planarized and preorganizing bipyridinyl rings, which stabilize the aggregate. These aspects will be addressed in Chapter 3. Where X-ray diffraction was found very suitable to identify the columnar phases (in the solid state), the formation of the columnar aggregates, and the mobility of the disks in the aggregate (in dilute solution), will be studied further using various optical techniques.

2.4 Conclusions

All C_3-symmetrical discotics investigated (small, medium, and large amides **1a-f**, and ureas, **2a-f**) form elongated, columnar aggregates, both in the solid (liquid crystalline) state and in solution (except for medium amide disks **1c/d**). This shows that a broad range of combinations of hydrogen bonding groups (amide and urea) and peripheral groups (alkyl, gallic and bipyridinyl-gallic) is compatible with the formation of helical columns. Moreover, the columns are inherently helical, as indicated by X-ray reflections, which could be assigned to the pitch and the inter disk distance. AFM and SANS made it possible to visualize micrometer long strands consisting of thousands of molecules (2 μm for **2f**), displaying the directionality of the hydrogen bonding interactions. Physical cross-link points, giving rise to gels with minimal gel concentrations as low as 1.2 mg/ml for **2a**, hold these strands together.

However, choosing a different combination of secondary interactions may drastically affect the behavior and properties of the columnar structures. In case of the small and medium disks substituting

amide by urea results in a change of columnar phase (e.g. amide **1a**: Col_{ho}, and urea **2a**: Col_{tet}). These differences were elucidated accurately by X-ray diffraction, which even showed the small difference in inter column distance (one NH group) between amide and urea (e.g. amide **1e**: 39.5 Å, and urea **2e**: 41.1 Å). Changes in the van der Waals and π-π interactions at the periphery of the molecule may also strongly influence the capacity for aggregation. Medium amide disk **1c** is not able to retain the columns in apolar solution, which might be reflected in the variety of phases displayed in the liquid crystalline phase (Col_{ho}, Col_{rd}, Col_{hd}). This phase sequence indicates that the discotic molecules, aggregated in the columnar stacks, still have freedom to move. However, this freedom seems larger for amide disks than for urea ones, as is indicated by the typical difference in X-ray spectral resolution. Whereas amide hydrogen bonding allows sufficient rotational freedom to optimize helical order, resulting in resolved spectra, urea hydrogen bonding operates like a mindless hulk, slow in the full comprehension of the beauty in the helical delicacies. Differences concerning aggregate formation and rigidity in the stack between the various amide and urea compounds, will be discussed in Chapter 3.

2.5 Experimental section

General. All starting materials were obtained from commercial suppliers and used as received. The syntheses of the following compounds have been described previously: **1a**[13], **1b**[14a], **1e**[17], **1f**[17], **3b**[19], **3c**[20], **3d**[20], **3e**[17a-b], **3f**[17], 3,4,5-tri((*S*)-3,7-dimethyloctyloxy)benzenecarbonylazide[20]. All moisture sensitive reactions were performed under an atmosphere of dry argon. Dry and ethanol-free dichloromethane was obtained by distillation from P_2O_5; dry tetrahydrofuran was obtained by distillation from Na/K/benzophenone; toluene was dried on Merck molsieves (4 Å) and triethylamine was dried over potassium hydroxide. Analytical thin layer chromatography was performed on Kieselgel F-254 precoated silica plates. Visualization was accomplished with UV light. Column chromatography was carried out on Merck silica gel 60 (70-230 mesh or 230-400 mesh ASTM) or Merck aluminum oxide 90 (70-230 mesh, activity II). ^{1}H-NMR and ^{13}C-NMR spectra were recorded on a Varian Mercury, 400 MHz for ^{1}H-NMR and 100 MHz for ^{13}C-NMR, or on a Varian Gemini, 300 MHz for ^{1}H-NMR and 75 MHz for ^{13}C-NMR. Proton chemical shifts are reported in ppm downfield from tetramethylsilane (TMS) and carbon chemical shifts in ppm downfield from TMS using the resonance of the deuterated solvent as internal standard. Elemental analyses were carried out using a Perkin Elmer 2400. Matrix assisted laser desorption/ionization mass spectra were obtained using α-cyano-4-hydroxycinnamic acid as the matrix on a PerSeptive Biosystems Voyager-DE PRO spectrometer. IR spectra were measured on a Perkin Elmer 1600 FT-IR. Optical properties and melting points were determined using a Jenaval polarization microscope with crossed polarizers equipped with a Linkham THMS 600 heating device. DSC spectra were obtained on a Perkin Elmer Pyris 1 DSC. X-Ray diffraction measurements were carried out on a Rigaku X-ray Rad 2B system with a heating stage using Ni-filtered CuKα radiation (λ = 1.54056 Å). Atomic force microscopy images were obtained on a Nanoscope IIIa from Digital Instruments Santa Barbara CA. RTESP-type tips were used. Samples were prepared by drop casting from 10^{-5} M solutions in dodecane or heptane on freshly cleaved mica / silica wafers. Small angle neutron scattering (SANS) experiments were performed at the Geesthacht Neutron Facility (GeNF) with the SANS-2 instrument located at the FRG-1 reactor of the GKSS Forschungszentrum in Geesthacht, using four instrumental settings with sample-detector distances of d = 1, 3, 9 and 21 m at a fixed wavelength of λ = 0.57 nm. A mechanical selector used for monochromatization of the neutrons was set to a wavelength resolution of $\Delta\lambda/\lambda$ = 0.08. Based on these settings, the SANS experiments covered scattering vectors $|Q| = Q = (4\pi/\lambda)\sin(\Theta/2)$ from 0.01 to 3 nm^{-1} (with Θ, the scattering angle). Solutions of the hydrogen-bonded disks in dodecane-*d26* (6 mg/ml) were measured in (HELMA) quartz cuvettes (path length 1 mm), which were kept in a temperature-controlled stage. Scattering patterns, recorded from the solutions were radially averaged, normalized to the beam intensity and finally corrected with respect to the contributions arising from instrumental background, empty cells and solvent. Finally, the scattering data obtained in relative intensities were normalized to an absolute scale (m^{-1}), using the scattering from vanadium as a secondary standard, which allowed for a conversion into the coherent scattering cross section $\frac{d\Sigma}{d\Omega}(Q)$. All data processing has been performed using the SANS data reduction and analysis software (SANDRA), developed at GKSS.

N,N',N''-Tris(3,4,5-tridodecyloxy-phenyl)benzene-1,3,5-tricarboxamide (1c). A solution of 1,3,5-benzenetricarbonyl trichloride (0.13 g, 0.50 mmol) in dry dichloromethane (5 ml) was added dropwise to a solution of 3,4,5-tridodecyloxyaniline (3c) (1.0 g, 1.6 mmol) and triethylamine (0.28 ml, 2.0 mmol) in dry dichloromethane (15 ml). After stirring overnight and evaporation of the dichloromethane the product was purified using column chromatography (silica, gradient: chloroform / dichloromethane + 0-1 %v/v methanol, R_f = 0-0.9). Finally, 1c was obtained as a white sticky solid (0.90 g, 86 %): ^{1}H-NMR ($CDCl_3$) δ 8.46 (H-ortho, s, 3H), 8.43 (NH, s, 3H), 6.92 (H'-ortho, s, 6H), 3.91 (OCH_2, m, 18H), 1.73 (OCH_2CH_2, m, 18H), 1.41 ($OCH_2CH_2CH_2$, m, 18H), 1.26 ($(CH_2)_8$, m, 144H), 0.88 (OCH_3, m, 27H); ^{13}C-NMR ($CDCl_3$) δ 163.7 (NHCO), 153.1 (C3'), 135.8, 135.1, 133.1, 128.4 (C1, C1', C2, C4'), 99.0 (C2'), 73.6, 69.0 (OCH_2), 31.9, 30.9, 30.4, 29.8, 29.8, 29.7, 29.5, 29.4, 26.2, 26.1, 22.7 (alkyl C), 14.1 (CH_3); IR (ATR): 3515, 3239, 2955, 2919, 2850, 1682, 1664, 1599, 1538, 1502, 1467, 1437, 1420, 1380, 1329, 1302, 1266, 1231, 1114, 1030, 917, 828, 720 cm^{-1}; Elemental analysis: calculated: $C_{135}H_{237}N_3O_{12}$ (2094.41): C, 77.42; H, 11.41; N, 2.01; found: C, 76.87; H, 10.60; N, 2.00; MALDI-TOF MS: calculated: 2093.81, found: 2093.56.

N,N',N''-Tris[3,4,5-tri((*S*)-3,7-dimethyloctyloxy)-phenyl]benzene-1,3,5-tricarboxamide (1d). A solution of 1,3,5-benzenetricarbonyl trichloride (0.16 g, 0.61 mmol) in dry dichloromethane (5 ml) was added dropwise to a solution of 3,4,5-tris((*S*)-3,7-dimethyloctyl)aniline (**3d**) (1.1 g, 1.9 mmol) and triethylamine (0.28 ml, 2.0 mmol) in dry dichloromethane (15 ml). After stirring overnight and evaporation of the dichloromethane the product was purified using column chromatography (silica, gradient: chloroform / dichloromethane + 0-0.25 %v/v methanol, R_f = 0-0.5). Finally, **1d** was obtained as a white sticky solid (0.78 g, 70 %): ^{1}H-NMR ($CDCl_3$) δ 8.59 (H-ortho, s, 3H), 8.19 (NH, s, 3H), 6.99 (H'-ortho, s, 6H), 4.01 (OCH_2, m, 18H), 1.88 – 0.86 (alkyl H, m,

171H); ^{13}C-NMR ($CDCl_3$) δ 163.2 (NHCO), 153.3 (C3'), 135.9, 135.4, 132.9, 128.3 (C1, C1', C2, C4'), 98.9 (C2'), 71.8, 67.4 (OCH_2), 39.4, 39.3, 37.5, 37.4, 37.3, 36.4, 29.8, 29.7, 28.0, 24.7, 22.7, 22.6, 19.6, 19.5 (alkyl C); IR (ATR): 3283, 2954, 2926, 2870, 1649, 1602, 1537, 1504, 1467, 1432, 1384, 1366, 1332, 1299, 1231, 1113, 1047, 1027, 997, 965, 914, 831, 731, 699 cm^{-1}; Elemental analysis: calculated: $C_{117}H_{201}N_3O_{12}$ (1841.92): C, 76.30; H, 11.00; N, 2.28; found: C, 75.37; H, 10.36; N, 2.31; MALDI-TOF MS: calculated: 1841.52, found: 1840.99.

N',N''',N'''''-Trioctyl-N,N'',N''''-1,3,5-benzenetriyltriurea (2a). To a solution of 1,3,5-benzenetriisocyanate (**5**) (0.14 g, 0.70 mmol) in toluene (7.0 ml, 0.1 M) a solution of N-octylamine (**3a**) (0.32 g, 2.5 mmol) in dry toluene (10 ml) was added dropwise at 80°C. After 1 h the toluene was evaporated and the product was dissolved in chloroform/methanol 2/1 (15 ml) to be poured into acetone/acetonitrile 3/1 (200 ml). Finally, filtration of the precipitate gave **2a** as a white solid (0.29 g, 70 %): ^{1}H-NMR ($CDCl_3$/CD_3OD 2/1) δ 8.00 (NH, s, residual), 7.07 (H-ortho, s, 3H), 5.80 (NH', t, residual), 3.19 (NHCH_2, t, 6H), 1.52 (NHCH$_2$CH_2, m, 6H), 1.29 ((CH$_2$)$_5$, m, 30H), 0.89 (CH$_3$, m, 9H); ^{13}C-NMR ($CDCl_3$/CD_3OD 2/1) δ 157.0 (NHCONH), 140.7 (aromatic C-NH), 102.8 (aromatic C-H), 40.0 (NH-CH$_2$), 32.1, 30.3, 29.6, 29.5, 27.2, 22.9 (alkyl C), 14.2 (CH$_3$); IR (ATR): 3302, 3112, 2921, 2851, 1632, 1556, 1466, 1252, 1200 cm^{-1}; Elemental analysis: calculated: $C_{33}H_{60}N_6O_3$ (588.87): C, 67.31; H, 10.27; N, 14.27; found: C, 66.64; H, 10.45; N, 13.82; MALDI-TOF MS: calculated: 588.47, found: 589.47.

N',N''',N'''''-Tri((*S*)-3,7-dimethyloctyl)-N,N'',N''''-1,3,5-benzenetriyltriurea (2b). To a solution of 1,3,5-benzenetriisocyanate (**5**) (0.14 g, 0.70 mmol) in toluene (7.0 ml, 0.1 M) a solution of (*S*)-3,7-dimethyloctylamine (**3b**) (0.39 g, 2.5 mmol) in dry toluene (10 ml) was added dropwise at 80°C. After 1 h the toluene was evaporated and the product was dissolved in chloroform/methanol 2/1 (7 ml) to be poured into acetonitrile/acetone 4/1 (100 ml). Finally, filtration of the precipitate gave **2b** as a white solid (0.40 g, 68 %): ^{1}H-NMR ($CDCl_3$/CD_3OD 2/1) δ 8.00 (NH, s, residual), 7.06 (H-ortho, s, 3H), 5.75 (NH', t, residual), 3.21 (NHCH_2, m, 6H), 1.53 (NHCH$_2$CH_2CH, m, 9H), 1.30 (NHCH$_2$CH$_2$CHCH_2CH_2, m, 12H), 1.16 ((CH$_3$)$_2$CHCH_2, m, 9H), 0.93, 0.91, 0.88 (CH$_3$, m, 27H); ^{13}C-NMR ($CDCl_3$/CD_3OD 2/1) δ 157.2 (NHCONH), 139.0 (aromatic C-NH), 103.0 (aromatic C-H), 39.2, 38.2, 37.3, 37.1, 36.3, 30.8, 30.5, 27.8, 24.6, 22.6, 22.5, 19.4 (alkyl C); IR (ATR): 3323, 2954, 2926, 2869, 1642, 1563, 1454, 1379, 1366, 1245, 850, 779, 732, 668 cm^{-1}; Elemental analysis: calculated: $C_{39}H_{72}N_6O_3$ (672.57): C, 69.60; H, 10.78; N, 12.49; found: C, 69.35; H, 9.92; N, 12.11; MALDI-TOF MS: calculated: 673.04, found: 673.54.

N',N''',N'''''-Tris(3,4,5-tridodecyloxy-phenyl)-N,N'',N''''-1,3,5-benzenetriyltriurea (2c). To a solution of 1,3,5-benzenetriisocyanate (**5**) (0.14 g, 0.70 mmol) in toluene (7.0 ml, 0.1 M) a solution of 3,4,5-tridodecyloxyaniline (**3c**) (1.6 g, 2.5 mmol) in dry toluene (20 ml) was added dropwise at 80°C. After stirring overnight the toluene was evaporated and the product was washed with acetone (30 ml). Filtration yielded white solid **2c** (1.3 g, 87 %): mp = 54 °C; ^{1}H-NMR ($CDCl_3$/CD_3OD 2/1) δ 8.14 (NH, s, residual), 7.96 (NH, s, residual), 7.23 (H-ortho, s, 3H), 6.69 (H'-ortho, s, 6H), 3.97 (OCH_2, m, 12H), 3.92 (OCH_2, m, 6H), 1.80 (OCH$_2$CH_2, m, 18H), 1.48 (OCH$_2$CH$_2$CH_2, m, 18H), 1.28 ((CH$_2$)$_8$, m, 144H), 0.89 (CH$_3$, m, 27H); ^{13}C-NMR ($CDCl_3$/CD_3OD 2/1) δ 153.8, 153.0 (NHCONH, C3'), 139.8 (C1), 134.5, 133.5 (C1', C4'), 103.9 (C2), 98.6 (C2'), 73.6, 68.9 (OCH_2), 31.8, 30.1, 29.5, 29.3, 29.2, 26.0, 22.5 (alkyl C), 13.8 (CH$_3$); IR (ATR): 3285, 2918, 2850, 1641, 1601, 1556, 1506, 1467, 1433, 1418, 1227, 1122, 1028, 825, 720 cm^{-1}; Elemental analysis: calculated: $C_{135}H_{240}N_6O_{12}$ (2139.42): C, 75.79; H, 11.31; N, 3.93; found: C, 75.77; H, 11.32; N, 3.86; MALDI-TOF MS: calculated: 2138.84, found: 2138.67.

N',N''',N'''''-Tris[3,4,5-tri((*S*)-3,7-dimethyloctyloxy)-phenyl]-N,N'',N''''-1,3,5-benzenetriyl-triurea (2d). To a solution of 1,3,5-benzenetriisocyanate (**5**) (0.041 g, 0.20 mmol) in toluene (2.0 ml, 0.1 M) a solution of 3,4,5-tris((*S*)-3,7-dimethyloctyloxy)aniline (**3d**) (0.40 g, 0.71 mmol) in dry toluene (10 ml) was added dropwise at 80°C. After stirring overnight the toluene was evaporated and the product was washed with dichloromethane (30 ml). Filtration yielded white sticky solid **2d** (0.30 g, 78 %): ^{1}H-NMR (toluene-*d8*/CD_3OD 2/1) δ 8.35 (NH, s, residual), 8.25 (NH, s, residual), 7.70 (H-ortho, s, 3H), 6.97 (H'-ortho, s, 6H), 4.11 (OCH_2, m, 6H), 4.02 (OCH_2, m, 12H), 2.02-0.89 (alkyl H, m, 171H); ^{13}C-NMR (toluene-*d8*/CD_3OD 2/1) δ 155.6, 155.1 (NHCONH, C3'), 142.2 (C1), 136.6, 135.8 (C1', C4'), 105.1 (C2), 100.4 (C2'), 73.2, 68.9 (OCH_2), 41.1, 40.9, 39.3, 39.2, 39.1, 38.2, 31.5, 29.6, 26.5, 24.0, 24.0, 23.9, 20.8 (alkyl C); IR (ATR): 3286, 2954, 2925, 2870, 1641, 1603, 1555, 1503, 1462, 1420, 1383, 1366, 1295, 1217, 1117, 1002, 827, 717 cm^{-1}; Elemental analysis: calculated: $C_{117}H_{204}N_6O_{12}$ (1886.93): C, 74.47; H, 10.90; N, 4.45; found: C, 74.57; H, 11.14; N, 4.42; MALDI-TOF MS: calculated: 1886.56, found: 1886.37.

N',N''',N'''''-Tris{3[3'-(3,4,5-tridodecyloxybenzoylamino)-2,2'-bipyridyl]}-N,N'',N''''-1,3,5-benzene-triyltriurea (2e). To a solution of 1,3,5-benzenetriisocyanate (5) (28 mg, 0.14 mmol) in toluene (1.9 ml, 0.072 M) a solution of 3'-(3,4,5-tridodecyloxybenzoylamino)-2,2'-bipyridine-3-amine (3e) (0.40 g, 0.47 mmol) in dry toluene (5 ml) was added at 80 °C. After 1 h the solvent was evaporated. The product was purified by washing with acetone and column chromatography (alumina (II), dichloromethane + 0.5 %v/v methanol, R_f = 0.3),

giving 2e as a white sticky solid (0.28 g, 75 %): ^{1}H-NMR (THF-*d8*) δ 13.89 (NH'CO, s, 3H), 12.57 (N*H*^{A}CONH, s, 3H), 9.23 (H4, d, 3H), 8.90 (H4', NHCON*H*^{B}, m, 6H), 8.18, 8.15 (H6, H6', d, d, 6H), 7.67 (H-ortho, s, 3H), 7.27, 7.23 (H5, H5', dd, dd, 6H), 7.18 (H'-ortho, s, 6H), 4.01 (OCH_2, m, 12H), 3.94 (OCH_2, m, 6H), 1.77 (OCH_2CH_2, m, 12H), 1.67 (OCH_2CH_2, m, 6H), 1.47 ($OCH_2CH_2CH_2$, m, 18H), 1.20 ($(CH_2)_8$, m, 144H), 0.78 (CH_3, m, 27H); ^{13}C-NMR (THF-*d8*) δ 167.0 (NHCO), 155.3, 154.9 (NHCONH, C3''), 144.1, 143.8, 143.6, 142.6, 142.2 (C2/2', C3/3', $C1_{in}$), 140.6 (C4''), 139.1 (C6/6'), 132.4, 131.5, 130.7 (C4/4', C1''), 125.4 (C5/5'), 108.5 ($C2_{in}$), 106.3 (C2''), 74.9, 71.3 (OCH_2), 33.9, 32.5, 31.8, 31.8, 31.7, 31.7, 31.7, 31.6, 31.5, 31.4, 31.4, 28.2, 24.6, 15.5 (alkyl C); IR (ATR): 3294, 3103, 2921, 2852, 1670, 1623, 1558, 1489, 1467, 1426, 1371, 1330, 1296, 1247, 1219, 1115, 1069, 1031, 1006, 859, 797, 748, 730 cm^{-1}; Elemental analysis: calculated: $C_{168}H_{261}N_{15}O_{15}$ (2731.04): C, 73.89; H, 9.63; N, 7.69; found: C, 73.46; H, 9.22; N, 7.66; MALDI-TOF MS: calculated: 2730.02, found: 2752.96 (Na-adduct).

N',N''',N''''',N''''''-Tris{3[3'-(3,4,5-tri((*S*)-3,7-dimethyloctyloxy)benzoylamino)-2,2'-bipyridyl]}-N,N'',N''''-1,3,5-benzenetriyltriurea (2f). To a solution of 1,3,5-benzenetriisocyanate (**5**) (76 mg, 0.38 mmol) a solution of 3'-[3,4,5-tri((*S*)-3,7-dimethyloctyloxy)benzoylamino]-2,2'-bipyridine-3-amine (**3f**) (1.0 g, 1.3 mmol) in dry toluene (15 ml) was added at 80 °C. After 1 h the solvent was evaporated. Washing with acetone and column chromatography (alumina (II), dichloromethane + 0.25 %v/v methanol, R_f = 0.5) purified the product. In this way 0.82 g (87 %) of white sticky solid **2f** was obtained: ^{1}H-NMR (THF-*d8*) δ 13.91 (NH'CO, s, 3H), 12.57 (N*H*^{A}CONH, s, 3H), 9.23 (H4, d, 3H), 8.90 (H4', NHCON*H*^{B}, m, 6H), 8.18, 8.16 (H6, H6', d, d, 6H), 7.64 (H-ortho, s, 3H), 7.29, 7.25 (H5, H5', dd, dd, 6H), 7.19 (H'-ortho, s, 6H), 4.05 (OCH_2, m, 12H), 3.97 (OCH_2, m, 6H), 1.85 – 0.77 (alkyl H, m, 171H); ^{13}C-NMR (THF-*d8*) δ 167.1 (NHCO), 155.3, 154.8 (NHCONH, C3''), 143.9, 143.9, 143.4, 142.6, 142.3 (C2/2', C3/3', $C1_{in}$), 140.6 (C4''), 139.1 (C6/6'), 132.5, 131.5, 130.7 (C4/4', C1''), 125.4 (C5/5'), 108.4 ($C2_{in}$), 106.3 (C2''), 73.1, 69.5 (OCH_2), 41.4, 41.3, 39.6, 39.5, 39.4, 38.6, 31.9, 31.7, 30.0, 26.8, 24.2, 24.1, 24.1, 24.0, 21.1, 21.1, 21.1 (alkyl C); IR (ATR): 3290, 3098, 2953, 2925, 2869, 1670, 1621, 1560, 1489, 1468, 1426, 1370, 1328, 1296, 1244, 1216, 1113, 1069, 994, 859, 796, 748, 731 cm^{-1}; Elemental analysis: calculated: $C_{150}H_{225}N_{15}O_{15}$ (2478.56): C, 72.69; H, 9.15; N, 8.48; found: C, 72.22; H, 8.15; N, 8.35; MALDI-TOF MS: calculated: 2477.73, found: 2500.49 (Na-adduct).

1,3,5-Benzenetricarbonyl triazide (4). A solution of 1,3,5-benzenetricarbonyl trichloride (1.0 g, 3.8 mmol) in dry tetrahydrofuran (3.5 ml) was added dropwise to a solution of NaN_3 (2.5 g, 38 mmol) in water (7.0 ml) while cooling with an ice bath. Immediately, the desired product was formed as a white solid, which was stirred in suspension for 1½ h. To the reaction mixture toluene (30 ml) and a saturated solution of $NaHCO_3$ in water (50 ml) were added respectively. After phase separation the aqueous layer was extracted twice more with toluene (2 x 20 ml). The combined organic layers were washed with saturated $NaHCO_3$ and NaCl solutions in water and dried with $MgSO_4.H_2O$. After filtration the solution of 1,3,5-benzenetricarbonyl triazide in toluene was concentrated by evaporating until a volume of 35 ml was reached. This yielded a 0.1 M solution of **4**, which was used as such: ^{1}H-NMR (toluene-*d8*) δ 8.35 (H-ortho, s, 3H); ^{13}C-NMR (toluene-*d8*) : δ 169.9 (CO), 134.6 (C-H), 132.2 (*C*-CO); IR (ATR): 3081, 2141, 1699, 1602, 1326, 1188, 742, 711 cm^{-1}.

Caution: 1,3,5-Benzenetricarbonyl triazide is explosive in the solid state under heat or pressure. Therefore, it should preferentially be kept in solution and be handled at 1 g scale maximum.

1,3,5-Benzenetriisocyanate (5). A solution of 1,3,5-benzenetricarbonyl triazide (**4**) (0.20 g, 0.70 mmol) in toluene (7.0 ml, 0.1M) was gradually heated from 60° to 100°C and stirred for 1½ h, at which point no N_2 evolved anymore. Compound **5** was formed quantitatively. The solution was cooled to 80°C and used as such: ^{1}H-NMR (toluene-*d8*) δ 5.44 (H-ortho, s, 3H); ^{13}C-NMR (toluene-*d8*) δ 137.4 (*C*-NCO), 134.9 (NCO), 118.2 (C-H); IR (ATR): 3092, 2254, 1721, 1613, 1598, 1099, 897, 852, 665 cm^{-1}.

X-ray data

Reflections for columnar phases:[5a]

d-spacings: *h*, *k*, *l*; Miller indices, *a*, *b*, *c*

Lamellar

$1/d_l^2 = l^2/c^2$

$d_{001} : d_{002} : d_{003} : d_{004}$; …. = 1 : 1/2 : 1/3 : 1/4 : ….

Hexagonal

$1/d_{hk}^2 = 4/3((h^2 + hk + k^2))/a^2)$

$d_{100} : d_{110} : d_{200} : d_{210} : d_{300} : d_{220}$: …. = 1 : 1/√3 :1/2 : 1/√7 : 1/3 : 1/√12 : ….

Tetragonal

$1/d_{hk}^2 = (h^2 + k^2)/a^2$

$d_{100} : d_{110} : d_{200} : d_{210} : d_{220} : d_{300}$: …. = 1 : 1/√2 :1/2 : 1/√5 : 1/√8 : 1/3 : ….

Rectangular

$1/d_{hk}^2 = h^2/a^2 + k^2/b^2$

Diffraction spacings [Å]

1a small achiral amide disk

reflection	<100>	pitch	<110>	<200>	<210>	<300>	<220>	<310>	<400>	halo	inter
ratio	1		1/√3	1/2	1/√7	1/3	1/√12	1/√13	1/4		disk
Col_{ho}	15.38		8.88	7.69	5.81	5.13	4.44	4.27	3.85		
25 °C	*15.38*		*8.80*	*7.62*	*5.73*	*5.06*	*4.57*	*4.38*	*3.91*		*3.47*
140 °C	*16.11*	*15.77*	*9.192*	*7.96*						*4.73*	*3.47*
180 °C	*16.35*	*19.45*	*9.34*	*8.07*						*4.73*	*3.49*

2a, small achiral urea disk

reflection	<100>	pitch	<110>	<200>	<210>	<220>	halo	inter
ratio	1		1/√2	1/2	1/√5	1/√8		disk
Col_{tet}	20.63		14.59	10.31	9.23	7.30		
25 °C	*20.63*		*14.52*		*9.15*	*7.11*	*4.23*	
140 °C	*21.85*						*4.48*	

1c, medium achiral amide disk

T	<100>	<110>	<200>	<210>	<300>	<220>	<310>	<400>	<320>			halo	inter
	1	1/√3	1/2	1/√7	1/3	1/√12	1/√13	1/4	1/√19				disk
Col_{ho}	34.22	19.75	17.11	12.93	11.41	9.88	9.49	8.55	7.85				
30	*34.22*	*19.45*	*16.85*		*10.88*		*8.96*		*7.13*			*4.43*	*3.47*
40	*34.22*	*19.71*	*16.82*		*10.75*		*9.09*		*7.12*			*4.45*	*3.47*
50	*34.22*	*19.80*				*9.11*			*7.08*			*4.47*	*3.48*
	<110>	<200>	<210>	<120>	pitch	<130>	<420>					halo	
Col_{rd}	a=56.59	b=41.45	21.5993	16.03		10.94	10.80						
$P2_1/a$													
60	*33.44*	*28.29*	*20.92*	*17.66*	*15.55*	*12.03*	*10.59*	*9.15*	*8.77*	*7.18*	*6.80*	*4.52*	
70	*33.44*	*28.29*	*21.12*	*17.59*	*15.66*	*12.00*	*10.57*	*9.15*	*8.75*	*7.13*		*4.49*	
Col_{rd}	a=56.95	b=40.83	23.3580	19.22		13.24	11.68						
$P2_1/a$													
80	*33.19*	*28.48*	*21.22*	*17.66*	*15.44*	*12.07*	*10.57*	*9.15*	*8.70*	*7.14*	*6.79*	*4.53*	
90	*33.19*	*28.66*	*21.64*	*17.52*	*15.44*	*12.00*	*10.59*		*8.70*	*7.10*		*4.56*	
	<100>	<110>	<200>	<210>	<300>	<220>	<310>	<400>	<320>			halo	inter
	1	1/√3	1/2	1/√7	1/3	1/√12	1/√13	1/4	1/√19				disk
Col_{hd}	30.87	17.82	15.43	11.67	10.29								
100	*30.87*	*17.38*	*14.82*									*4.54*	
110	*30.87*	*17.45*										*4.58*	
120	*30.87*	*17.31*										*4.60*	
130	*30.87*	*17.38*	*15.02*									*4.61*	
140	*30.87*	*17.31*	*15.17*	*11.21*								*4.64*	

2c, medium achiral urea disk

reflection	<100>	<110>	pitch	<200>	<210>	<300>	<220>	halo	inter
ratio	1	1/√3		1/2	1/√7	1/3	1/√12		disk
Col_{ho}	30.03	17.34		15.01	11.35	10.01	8.67		
25 °C	*28.85*		*15.38*		*10.06*		*8.40*	*7.32*	-
80 °C	*29.62*		*16.54*		*10.49*		*8.05*	*4.52*	-
140 °C	*30.03*		*16.66*		*10.85*	*9.65*	*8.08*	*4.60*	-

1e, large achiral amide disk

reflection	<100>	<110>	<200>	pitch	<210>	<300>	<400>	<410>	halo	inter
ratio	1	1/√3	1/2		1/√7	1/3	1/4	1/√21		disk
Col_{ho}	35.88	20.72	17.94		13.56	11.96	8.97	7.83		
25 °C	*34.22*			*17.59*	*13.54*	*11.94*	*8.68*	*7.51*	*4.48*	*3.33*
50 °C	*35.88*			*17.87*	*13.76*	*12.20*	*8.86*	*7.54*	*4.60*	*3.35*
100 °C	*35.88*	*20.53*	*18.28*	*17.31*	*13.80*	*12.23*	*8.93*	*7.81*	*4.69*	*3.37*
150 °C	*36.18*	*20.34*	*18.24*	*17.12*	*13.76*	*12.27*		*7.81*	*4.76*	*3.39*

2e, large achiral urea disk

reflection	<100>	<110>	<200>	pitch	<210>	<410>	halo	inter
ratio	1	1/√3	1/2		1/√7	1/√21		disk
Col_{ho}	36.18	20.89	18.09		13.67	7.89		
26 °C	*35.59*			*15.66*		*7.72*	*4.44*	*3.31*
50 °C	*35.88*		*17.94*	*15.88*		*7.80*	*4.49*	*3.32*
100 °C	*36.18*	*19.51*	*17.80*	*15.71*	*13.18*	*7.94*	*4.53*	*3.28*

2f, large chiral urea disk

reflection	<100>	<110>	<200>	pitch	<210>	<400>	<410>	halo	inter?	inter
ratio	1	1/√3	1/2		1/√7	1/4	1/√21			disk
Col_{ho}	34.48	19.91	17.24		13.03	8.62	7.52			
25 °C	*33.44*		*18.39*	*14.77*	*12.44*	*8.91*	*7.50*	*4.73*	*3.81*	*3.25*
50 °C	*33.69*		*17.94*	*14.98*	*12.55*	*8.96*	*7.57*	*4.75*	*3.86*	*3.26*
100 °C	*34.48*		*17.84*	*15.17*	*12.65*	*9.13*	*7.64*	*4.78*	*3.82*	*3.29*

2.6 References and notes

(1) Reviews: (a) Prins, L.J.; Reinhoudt, D.N.; Timmerman, P. *Angew. Chem. Int. Ed.* **2001**, *40*, 2382–2426. (b) Hill, D.J.; Mio, M.J.; Prince, R.J.; Hughes, T.S.; Moore, J.S. *Chem. Rev.* **2001**, *101*, 3893–4011. (c) Kato, T. *Science* **2002**, 295, 2414–2418. (d) Brunsveld, L.; Folmer, B.J.B.; Meijer, E.W.; Sijbesma, R.P. *Chem. Rev.* **2001**, *101*, 4071–4097. (e) Sherrington, D.C.; Taskinen, K.A. *Chem. Soc. Rev.* **2001**, *30*, 83–93. (f) Greig, L.M.; Philp, D. *Chem. Soc. Rev.* **2001**, *30*, 287–302. (g) Bong, D.T.; Clark, T.D.; Granja, J.R.; Ghadiri, M.R. *Angew. Chem. Int. Ed.* **2001**, *40*, 989–1011. (h) Ciferri, A. *Macromol. Rapid Commun.* **2002**, *23*, 511–529.

(2) Some examples of self-assembled architectures: cyanuric acid / melamine motifs: (a) Zerowski, J.A.; Seto, C.T.; Wierda, D.A.; Whitesides, G.M. *J. Am. Chem. Soc.* **1990**, *112*, 9025–9026. (b) Prins, L.J.; de Jong, F.; Timmerman, P.; Reinhoudt, D.N. *Nature* **2000**, *408*, 181–184. (c) Hof, F.; Nuckolls, C.; Rebek, J.Jr. *J. Am. Chem. Soc.* **2000**, *122*, 4251–4252. (d) Berl, V.; Huc, I.; Lehn, J.-M.; DeCian, A.; Fischer, J. *Eur. J. Org. Chem.* **1999**, 3089–3094. (e) Freeman, A.W.; Vreekamp, R.; Fréchet, J.-M. *J. Polym. Mater. Sci. Eng.* **1997**, *77*, 138–140. dendritic isophthalic acid: (f) Zimmerman, S.C.; Zeng, F.; Reichert, D.E.C.; Kolotuchin, S.V. *Science* **1996**, *271*, 1095–1098. gallate based columns: (g) Percec, V.; Ahn, C.-H.; Ungar, G.; Yeardley, D.J.P.; Möller, M.; Sheiko, S.S. *Nature* **1998**, *391*, 161–164. (h) Percec, V.; Holerca, M.N.; Uchida, S.; Cho, W.-D.; Ungar, G.; Lee, Y.; Yeardley, D.J.P. *Chem. Eur. J.* **2002**, *8*, 1106–1117. deoxyguanosine oligomers: (i) Gottarelli, G.; Proni, G.; Spada, G.P.; Bonazzi, S.; Garbesi, A.; Ciuchi, F.; Mariani, P. *Biopolymers* **1997**, *42*, 561–574. folic acid derivatives: (j) Kanie, K.; Nishii, M.; Yasuda, T.; Taki, T.; Ujiie, S.; Kato, T. *J. Mater. Chem.* **2002**, *11*, 2875–2886. ureidopyrimidinone: (k) Beijer, F.H.; Sijbesma, R.P.; Kooijman, H.; Spek, A.L.; Meijer, E.W. *J. Am. Chem. Soc.* **1998**, *120*, 6761–6769.

(3) Nakano, T.; Okamoto, Y. *Chem. Rev.* **2001**, *101*, 4013–4038.

(4) solid state: (a) Kishimoto, K.; Yoshio, M.; Mukai, T.; Yoshizawa, M.; Ohno, H.; Kato, T. *J. Am. Chem. Soc.* **2003**, *125*, 3196–3197. gel phase: (b) Mizoshita, N.; Hanabusa, K.; Kato, T. *Adv. Func. Mater.* **2003**, *13*, 313–317. (c) Yabuuchi, K.; Marfo-Owusu, E.; Kato, T. *Org. Biomol. Chem.* **2003**, *1*, 3464–3469. (d) Heeres, A.; van der Pol, C.; Stuart, M. Friggeri, A.; Feringa, B.L.; van Esch, J. *J. Am. Chem. Soc.* **2003**, *125*, 14252–14253. dilute solution: (e) Schenning, A.P.H.J.; van Herrikhuyzen, J.; Jonkheijm, P.; Chen, Z.; Würthner, F.; Meijer, E.W. *J. Am. Chem. Soc.* **2002**, *124*, 10252–10253.

(5) (a) Ohta, K. *Ekisho* **2002**, *6*, 61–71. (b) Dierking, I. *Textures of Liquid Crystals*; WILEY-VCH: Weinheim, **2003**. (c) Beginn, U. *Prog. Polym. Sci.* **2003**, *28*, 1049–1105.

(6) Some examples of low molecular weight organogelators: cyanuric acid / melamine motifs: (a) Lehn, J.-M.; Mascal, M.; DeCian, A.; Fisher, J. *J. Chem Soc., Chem. Commun.* **1990**, 479–481. (b) Hanabusa, K.; Miki, T.; Taguchi, Y.; Koyama, T.; Shirai, H. *J. Chem. Soc., Chem. Commun.* **1993**, 1382–1384. (c) Jeong, S.W.; Murata, K.; Shinkai, S. *Supramolec. Sci.* **1996**, *3*, 83–86. anthracene derivatives: (d) Brotin, T.; Utermöhlen, R.; Fages, F.; Bouas-Laurent, H.; Desvergne, J.-P. *J. Chem. Soc., Chem. Commun.* **1991**, 416–418. porphyrin derivatives: (e) Tamaru, S.; Takeuchi, M.; Sano, M.; Shinkai, S. *Angew. Chem. Int. Ed.* **2002**, *41*, 853–856. cyclohexane based diureas: (f) van Esch, J.; Schoonbeek F.; de Loos, M.; Kooijman, H.; Spek, A.L.; Kellogg, R.M.; Feringa, B.L. *Chem. Eur. J.* **1999**, *5*, 937–950. (g) Hanabusa, K.; Shimura, K.; Hirose, K.; Shirai, H. *Chem. Lett.* **1996**, 885–886. linear diureas: (h) Shi, C.; Huang, Z.; Kilic, S.; Xu, J.; Enick, R.M.; Beckman, E.J.; Carr, A.J.; Melendez, R.E.; Hamilton, A.D. *Science* **1999**, *286*, 1540–1543. cyclic amides: (i) Hanabusa, K.; Matsumoto, Y.; Miki, T.; Koyama, T.; Shirai, H. *J. Chem. Soc., Chem. Commun.* **1994**, 1401–1402. cyclohexane based diamides: (j) Hanabusa, K.; Yamada, M.; Kimura, M.; Shirai, H. *Angew. Chem. Int. Ed. Engl.* **1996**, *35*, 1949–1951. α-amino acid derivatives: (k) Partridge, K.S.; Smith, D.K.; Dykes G.M.; McGrail, P.T. *Chem. Commun.* **2001**, 319–320. amino sugars: (l) Yoza, K.; Amanokura, N.; Ono, Y.; Akao, T.; Shinmori, H.; Takeuchi, M.; Shinkai, S.; Reinhoudt, D.N. *Chem. Eur. J.* **1999**, *5*, 2722–2729. (m) Hafkamp, R.H.; Feiters, M.C.; Nolte, R.J.M. *J. Org. Chem.* **1999**, *64*, 412–426. sugars: (n) Sakurai, K.; Kimura, T.; Gronwald, O.; Inoue, K.; Shinkai, S. *Chem. Lett.* **2002**, 746–747. cholesterol-perylene: (o) Sugiyasu, K.; Fujita, N.; Shinkai, S. *Angew. Chem. Int. Ed.* **2004**, *43*, 1229–1233. water gelation: (p) Estroff, L.A.; Hamilton, A.D. *Chem. Rev.* **2004**, *104*, 1201–1217.

(7) (a) Flory, P.J. *Faraday Discuss. R. Soc. Chem.* **1974**, *57*, 7 – 18. (b) Tanaka, T. *Am. Sci.* **1981**, *244*, 110–123.

(8) (a) van Esch, J.H.; Feringa, B.L. *Angew. Chem. Int. Ed.* **2000**, *39*, 2263–2266. (b) Schoonbeek, F.S. *Thesis: Making it all stick together*; University of Groningen: Groningen, **2001**. (c) Lucas, L.N. *Thesis: Dithienylcyclopentene optical switches*; University of Groningen: Groningen, **2001**. (d) Terech, P.; Weiss, R. *Chem. Rev.* **1997**, *97*, 3133–3159. (e) Luboradzki, R.; Gronwald, O.; Ikeda, M.; Shinkai, S.; Reinhoudt, D.N. *Tetrahedron* **2000**, *56*, 9595–9599.

(9) Berl, V.; Schmutz, M.; Krische, M.J.; Khoury, R.G.; Lehn, J.-M. *Chem. Eur. J.* **2002**, *8*, 1227–1244.

(10) (a) Tranchant, C.; Rodier, G.; Schmitthaeusler, R.; Warren, J.M. *Rev. Neurol.* **1996**, *152*, 153–157. (b) Buxbaum, J.N.; Tagoe, C.E. *Annu. Rev. Med.* **2000***, 51*, 543–569.
(11) (a) Chandrasekhar, S.; Sadashiva, B.K.; Suresh, K.A. *Pramana* **1977**, *9*, 471–480. (b) Chandrasekhar, S.; Ranganath, G.S. *Rep. Prog. Phys.* **1990**, *53*, 57–84.
(12) π-π Stacked disks: (a) Tobe, Y.; Utsumi, N.; Kawabata, K.; Nagano, A.; Adachi, K.; Araki, S.; Sonoda, M.; Hirose, K.; Naemura, K. *J. Am. Chem. Soc.* **2002**, *124*, 5350–5364. (b) Lahiri, S.; Thompson, J.L.; Moore, J.S. *J. Am. Chem. Soc.* **2000**, *122*, 11315–11319. (c) Höger, S.; Bonrad, K.; Mourran, A.; Beginn, U.; Möller, M. *J. Am. Chem. Soc.* **2001**, *123*, 5651–5659. H-bonded disks: (d) Percec, V.; Ahn, C.H.; Bera, T.K.; Ungar, G.; Yeardley, D.J.P. *Chem. Eur. J.* **1999**, *5*, 1070–1083. (e) Bushey, M.L.; Hwang, A.; Stephens, P.W.; Nuckolls, C. *Angew. Chem. Int. Ed.* **2002**, *41*, 2828–2831. H-bond stabilized disks: (f) Paulus, W.; Ringsdorf, H.; Diele, S.; Pelzl, G. *Liq. Cryst.* **1991**, *9*, 807–819. (g) Shu, W.; Valiyaveettil, S. *Chem. Commun.* **2002**, 1350–1351. (h) Kleppinger, R.; Lillya, P.; Yang, C. *J. Am. Chem. Soc.* **1997**, *119*, 4097–4102. (i) Yang, W.; Chai, X.; Chi, L.; Liu, X.; Cao, Y.; Lu, R.; Jiang, Y.; Tang, X.; Fuchs, H.; Li, T. *Chem. Eur. J.* **1999**, *5*, 1144–1149. (j) Beginn, U.; Sheiko, S.; Möller, M. *Macromol. Chem. Phys.* **2000**, *201*, 1008–1015. (k) Suárez, M.; Lehn, J.-M.; Zimmerman, S.C.; Skoulios, A.; Heinrich, B. **1998**, *120*, 9526–9532. (l) Kraft, A.; Reichert, A.; Kleppinger, R. *Chem. Commun.* **2000**, 1015–1016. C_3- symmetrical disks: (m) Boden, N.; Bushby, R. J.; Hardy, C.; Sixl, F. *Chem. Phys. Lett.* **1986**, *123*, 359–364. (n) Pieterse, K.; van Hal, P.A.; Kleppinger, R.; Vekemans, J.A.J.M.; Janssen, R.A.J.; Meijer, E.W. *Chem. Mater.* **2001**, *13*, 2675–2679. (o) Yasuda, Y.; Takebe, Y.; Fukumoto, M.; Inada, H.; Shirota, Y. *Adv. Mater.* **1996**, *8*, 740–741. C_3- symmetrical cyclohexane: (p) Fan, E.; Yang, J.; Geib, S.J.; Stoner, T.C.; Hopkins, M.D.; Hamilton, A.D. *J. Chem. Soc., Chem. Commun.* **1995**, 1251–1252. (q) van Bommel, K.J.C.; van der Pol, C.; Muizebelt, I.; Friggeri, A.; Heeres, A.; Meetsma, A.; Feringa, B.L.; van Esch, J. *Angew. Chem. Int. Ed.* **2004**, *43,* 1663–1667. trimesic acid: (r) Kolotuchin, S.V.; Thiessen, P.A.; Fenlon, E.E.; Wilson, S.R.; Loweth, C.J.; Zimmerman, S.C. *Chem. Eur. J.* **1999**, *5*, 2537–2547.
(13) (a) Yasuda, Y.; Iishi, E.; Inada, H.; Shirota, Y. *Chem. Lett.* **1996**, 575–576. (b) Hanabusa, K.; Koto, C.; Kimura, M.; Shirai, H.; Kakehi, A. *Chem. Lett.* **1997**, 429–430. (c) Matsunaga, Y.; Miyajima, N.; Nakayasu, Y.; Sakai, S. *Bull. Chem. Soc. Jpn*. **1988**, 61, 207–210.
(14) (a) Brunsveld L.; Schenning, A.P.H.J.; Broeren, M.A.C.; Janssen, H.M.; Vekemans, J.A.J.M.; Meijer, E.W. *Chem. Lett.* **2000**, 292–293. (b) Masuda, M.; Jonkheijm. P.; Sijbesma, R.P.; Meijer, E.W. *J. Am. Chem. Soc.* **2003**, *125*, 15935–15940. (c) Palmans, A.R.A.; Vekemans, J.A.J.M.; Kooijman, H.; Spek, A.L.; Meijer, E.W. *Chem. Commun.* **1997**, 2247–2248.
(15) (a) Lightfoot, M.P.; Mair, F.S.; Pritchard, R.G.; Warren, J.E. *Chem. Commun.* **1999**, 1645–1946. (b) Gong, B.; Zheng, C.; Yan, Y. *J. Chem. Crystallogr.* **1999**, *29*, 649–652.
(16) Shikata, T.; Ogata, D.; Hanabusa, K. *J. Phys. Chem. B* **2003**, *125*, 14252–14253.
(17) (a) Palmans, A.R.A.; Vekemans, J.A.J.M.; Fischer, H.; Hikmet, R.A.; Meijer, E.W. *Chem. Eur. J.* **1997**, *3*, 300–307. (b) Palmans, A. R. A.; Vekemans, J. A. J. M.; Hikmet, R. A.; Fisher, H.; Meijer, E. W. *Adv. Mater.* **1998**, *10*, 873–876. (c) Palmans, A.R.A.; Vekemans, J.A.J.M.; Havinga, E.E.; Meijer, E.W. *Angew. Chem. Int. Ed. Engl.* **1997**, *36*, 2648–2651. (d) Meijer, E.W.; Vekemans, J.A.J.M.; Palmans, A.R.A.; Breure, P.; de Kraker, J.; Brunsveld, L. *Polym. Prepr.* **2000**, *41(1)*, 902–903.
(18) Brunsveld, L.; Zhang, H.; Glasbeek, M.; Vekemans, J.A.J.M.; Meijer, E.W. *J. Am. Chem. Soc.* **2000**, *122*, 6175–6182.
(19) Fontana, M.; Chanzy, H.; Caseri, W.R.; Smith, P.; Schenning, A.P.H.J.; Meijer, E.W.; Gröhn, F. *Chem. Mater.* **2002**, *14*, 1730–1735.
(20) Pieterse, K. *Thesis: Electron deficient materials based on azaheterocycles*; Eindhoven University of Technology: Eindhoven, **2001**.
(21) Trimesyl azide (**4**) is explosive under heat or pressure in the solid state.
(22) Ambade, A.V.; Kumar, A. *J. Polym. Sci., Part A: Polym. Chem.* **2001**, *39*, 1295–1304.
(23) Palmans, A.R.A. *Thesis: Supramolecular structures based on the intramolecular H-bonding in the 3,3'-di(acylamino)-2,2'-bipyridine unit*; Eindhoven University of Technology: Eindhoven, **1997**.
(24) Brunsveld, L. *Thesis: Supramolecular chirality, from molecules to helical assemblies in polar media*; Eindhoven University of Technology: Eindhoven, **2001**.
(25) In preliminary solid state ^{1}H-NMR a Δ (δsolid - δsolution) of –1.6 was found. This corresponds to an inter disk distance of approximately 3 Å. (a) Almut Rapp, Max-Planck Institute for Polymer Research, Mainz, Germany, results to be published. (b) Rapp, A.; Schnell, I.; Sebastiani, D.; Brown, S.P.; Percec, V.; Spiess, H.W. *J. Am. Chem. Soc.* **2003**, *125*, 13284–13297.
(26) Krishna Prasad, S.; Shankar Rao, D.S.; Chandrasekhar, S.; Kumar, S. *Mol. Cryst. Liq. Cryst*. **2003**, *396*, 121–139.
(27) See Chapter 4; van Gorp, J.J.; Vekemans, J.A.J.M.; Meijer E.W. *Mol. Cryst. Liq. Cryst*. **2003**, *397*, 491–505.

Chapter 3

C_3-Symmetrical supramolecular architectures from discotic triamides and triureas

Abstract: *Whereas in Chapter 2 the formation of elongated, helical stacks by twelve C_3-symmetrical disks (**1a-f**, **2a-f**) was investigated in the liquid crystalline and gel phase, in this chapter the focus is on dilute solution (CD, UV-Vis, (time dependent) fluorescence). The disks vary in hydrogen bonding strength (amide, urea), π-π interactions (large, medium, small) and chirality. The urea stacks behave much more rigid than the corresponding amide ones. Whereas amide disks immediately reach their thermodynamic equilibrium, kinetic factors seem to govern urea aggregation, implying that these urea disks initially form a less-defined stack, that subsequently transforms slowly into a well-defined, chiral architecture. For large urea **2e/f** various temperature dependent measurements indeed confirm this two step process. The rigidity of the urea stacks prevents a pronounced sergeants and soldiers behavior. However, it allows formation of a 'solvent shell' of linear n-heptane around stacks of large urea disks **2f**. Stack and shell as a whole, are stable in a solution of branched iso-octane. Finally, the temperature dependent behavior in CD of medium monourea compound **3**, and medium diurea compound **4**, indicates the necessity to find the optimum in strength of secondary interactions (hydrogen bonding and π-π stacking), rather than the maximum.*

3.1 Introduction

A broad field of applications, among which molecular recognition and scaffold functions, is expected for synthetic helices, because of the key role natural helices play in the expression of functions of natural macromolecules. Where natural helices persist in polar solutions; numerous examples are known of synthetic columnar architectures built out of discotics in the liquid crystalline phase,[1a-c] but examples of ordered, columnar structures in the gel phase,[1d] or even in dilute solution[1e-p] are less ample. Another outstanding aspect of the natural helix is its chirality. Next to the possibility to create cholesteric and ferrroelectric liquid crystals, chirality was recognized as a new tool in studying the self-assembly of the disks.[2] In dilute solution, supramolecular architectures can be recognized and studied by introducing supramolecular chirality via peripheral side chains. Circular dichroism spectroscopy then probes the efficiency of the transfer of chiral information from the CD silent peripheral chains to the precisely ordered chromophores in the supramolecular architecture. Moreover, transfer within the stack from chiral to achiral molecules is known ('sergeants and soldiers' principle),[3] and even transfer of chirality of a CD silent solvent to disks with CD active chromophores has been observed (chiral solvation).[4,5]

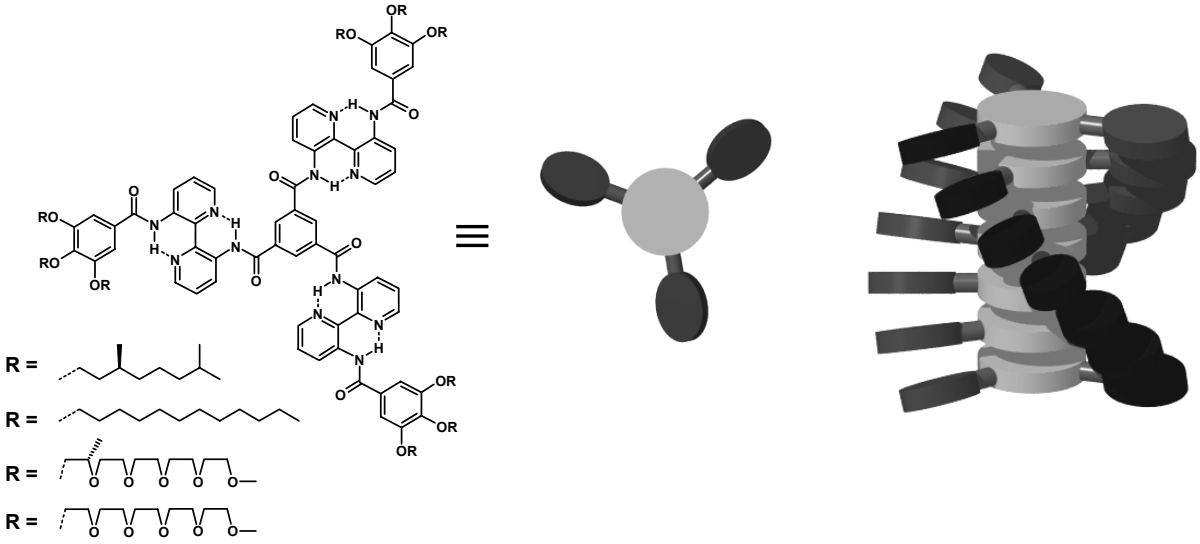

Figure 3.1. *Apolar and polar bipyridine based C_3-symmetrical disks and a cartoon representing their helical supramolecular stacking.*

Recently, various C_3-symmetrical columnar supramolecular architectures relying on hydrogen bonding in combination with π-π stacking were reported.[5-8] The first representatives of this class of C_3-symmetrical self-assembled structures were built up convergently by the stepwise acylation of 2,2'-bipyridine-3,3'-diamine (Figure 3.1).[6] The bipyridinyl parts are planar and preorganized due to their intramolecular hydrogen bonding; the gallic moieties are equipped with alkyl groups, inducing phase separation; while the assemblies feature a threefold array of intermolecular hydrogen bonds via the central 1,3,5-benzenetricarboxamide unit. Order is not only observed in the solid or liquid

crystalline phase[6a], and the lyotropic organic gel phase[6b] (Chapter 2), but also in dilute solution.[6c] Chirality in the solubilizing side chain of the constituting molecules allowed investigation of the three-dimensional structure of the aggregates using CD spectroscopy. The self-assembled stacks undergo a huge amplification of chirality[3] with one chiral molecule capable of organizing as much as eighty achiral ones in either a right- or a left-handed helical stack in dilute solution (cooperative length L_C = 80). Although the assocation constant is high (K_{ass} = 10^8 l/mol), the aggregation is still completely reversible without displaying any hysteresis. However, enlargement of the central aromatic core with methoxy groups or pyrazine rings gives stronger but less ordered π-π stacks.[6d]

To what extent both intermolecular hydrogen bonding and π-π interactions contribute to the cooperative, helical self-assembly remains an intriguing question. The fact that both secondary interactions play a role, follows from the involvement of a variety of forces in the stabilization of the native fold of natural proteins. Hydrophobicity has generally been considered the main driving force for the collapse of the random coil, whereas the well-defined 3-D structure can only arise after shielding the specific interactions such as hydrogen bonding, arene-cation and dipole-dipole interactions, from the polar environment by a hydrophobic domain.[8] For synthetic, water soluble self-assemblies, examples of a unique chiral self-assembled state,[9] as well as of a two-state folding process[8,10] are known.

C_3-symmetrical disks equipped with oligo(ethylene oxide) tails display a stepwise growth into chiral columns in polar media.[7,8] First achiral, small aggregates are generated by hydrophobicity of the core. Then, expression of the more sensitive hydrogen bonding interactions gives rise to large, chiral, self-assembled structures (Figure 3.2).

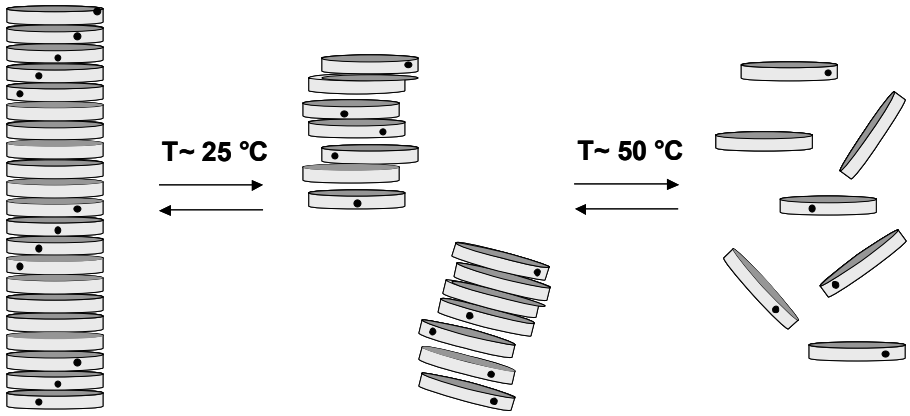

Figure 3.2. *Cartoon showing the two-step self-assembly of large ethylene oxide urea disks from single molecules via short achiral columns to long homochiral helical columns.*[8]

In apolar media, with hydrophobic peripheral tails, such a stepwise aggregation has not been observed until now for C_3-symmetrical discotics,[11] since both secondary interactions seem to be expressed simultaneously. Therefore, contributions of π-π stacking and hydrogen bonding have to be differentiated in another way. Several π-π interacting groups and hydrogen bonding units have been combined to afford a series of C_3-symmetrical disks (Figure 3.3). After all, for series of quadruply hydrogen bonded systems it was shown that both changes in π-π interactions and hydrogen bonding strength can have large influences on the behavior of the disc-like entities in dilute solution, and that valuable information follows from the comparison of the different structures.[12]

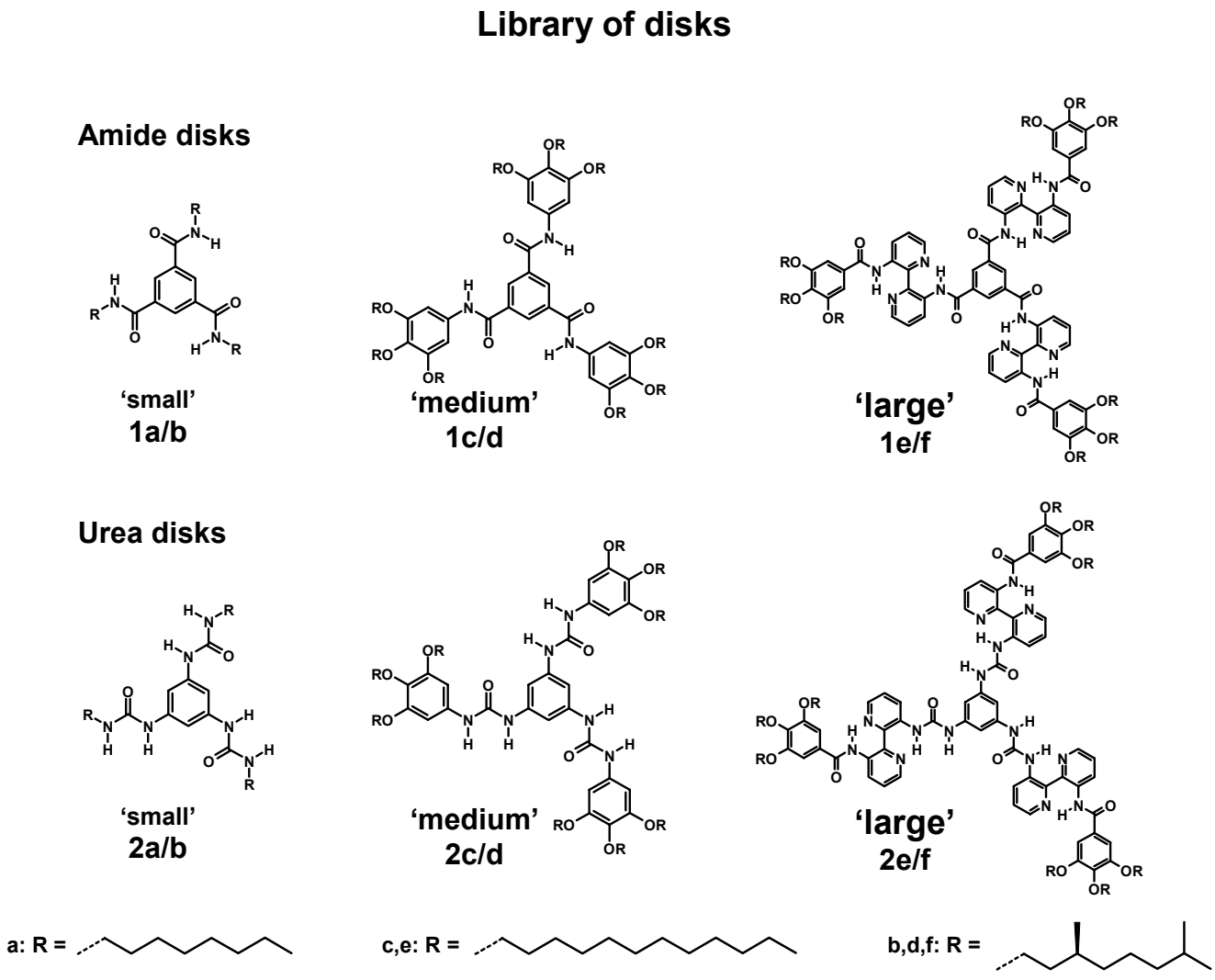

Figure 3.3. *Overview of twelve C_3-symmetrical disks, containing central amides (**1a-f**) or ureas (**2a-f**). The peripheral groups of the disks are 'small' (**1a/b** and **2a/b**), 'medium' (**1c/d** and **2c/d**) or 'large' (**1e/f** and **2e/f**). Half of the disks are achiral (**1a/c/e** and **2a/c/e**); the other half is chiral (**1b/d/f** and **2b/d/f**).*

In our case, the π-π interactions are strengthened in the series by using 'small' alkyl tails (**1a/b**, **2a/b**), 'medium' gallic groups (**1c/d**, **2c/d**), and 'large' bipyridinyl-gallic groups (**1e/f**, **2e/f**). The intermolecular hydrogen bonding amide moieties in **1a-f** are substituted by urea ones in **2a-f**. Because a urea has two protons to form hydrogen bonds -where an amide has only one-, the urea bond is considered stronger and more rigid. In this chapter, we compare the behavior of twelve C_3-symmetrical disks in dilute apolar solution. Previously, the supramolecular properties of **1a/b**[13] and **1e/f**[5,6] have been described, while the solid state and gel phase behavior of all the other members of the library has been discussed in Chapter 2. Indeed, it will be shown that contributions from either hydrogen bonding or π-π stacking follow from this comparison of the twelve disks, and that a two-step aggregation process is also possible for apolar C_3-symmetrical stacks with a changed hydrogen bonding / π-π stacking balance (large urea **2e/f**).

3.2 Supramolecular chirality

3.2.1 Self-assembly in dilute solution

To retain the helices in dilute solution (10^{-5} M), it is necessary that the solvent is only compatible with the flexible periphery of the disk (heptane), and does not interfere with the internal π-π stacking and hydrogen bonds (chloroform). Only when a supramolecular architecture is formed, chirality can be transferred from the CD silent citronnellol tails, to the chromophores in the center of the disk, resulting in a Cotton effect. Therefore, small and large chiral amide disks **1b**[13d] and **1f**[5,6c] show no Cotton effect in chloroform, while the molecules show significant effects in heptane.

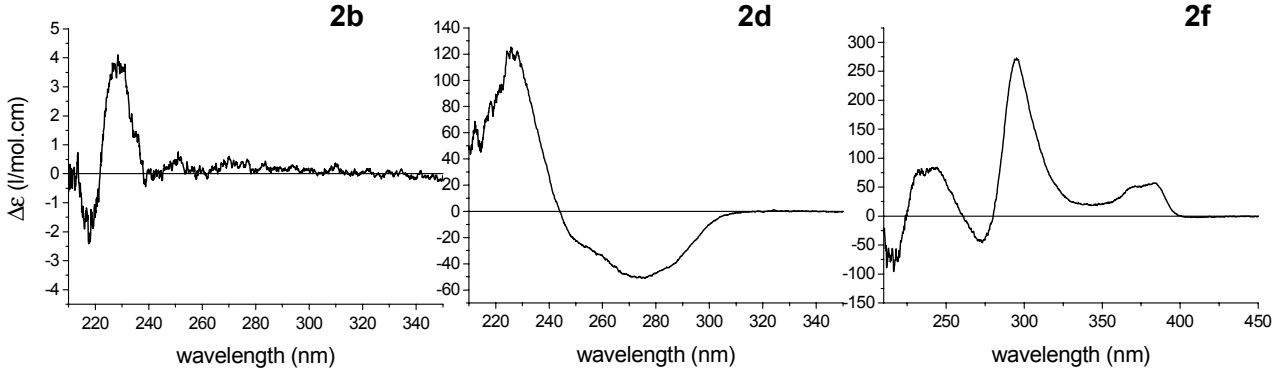

Figure 3.4. *CD spectra of small **2b** (left), medium **2d** (middle) and large **2f** (right) urea disks (**2b**: 10^{-4} M in heptane, **2d**: 10^{-5} M in dodecane, **2f**: 10^{-5} M in heptane).*

However, no Cotton effects were found in 10^{-4} and 10^{-5} M solutions of **1d** (or mixtures of **1c** and **1d**) in heptane. Similarly, the small (**2b**), medium (**2d**) and large (**2f**) urea disks were investigated (Figure 3.4). In contrast to the substantial Cotton effects shown by medium and large urea disks **2d** and **2f**, the effect produced by the small urea **2b** is only marginal (Table 3.1). Notable is the sign

inversion between the amide and urea molecules **1f** and **2f**, despite the fact that they are based on the same side chain, with the same (*S*)-configuration of the (*S*)-3,7-dimethyloctyloxy group.

Table 3.1[a]. *UV and CD data of chiral amides **1b/d/f** and ureas **2b/d/f**; λ_{max} [nm] = the absorption band most towards the red and $\varepsilon/\Delta\varepsilon$ [l/mol.cm] = the intensity of the signal.*

No.	UV		CD		No.	UV		CD	
	λ_{max}	ε	λ_{max}	$\Delta\varepsilon$		λ_{max}	ε	λ_{max}	$\Delta\varepsilon$
1b[b]	<210	9.2×10^3	224	-25.1	**2b**	224	7.4×10^3	228	+3.70
1d	308	2.1×10^4	-	-	**2d**	259	5.1×10^4	275	-51.5
1f[c]	364	3.2×10^4	369	-23.6	**2f**	357	3.1×10^4	371	+52.5
	384	2.3×10^4	387	-35.6		375	2.4×10^4	384	+57.4

[a] **1b**, **1d** and **2f** measured in heptane at ~ 10^{-5} M; **1f** and **2d** measured in dodecane at ~10^{-5} M; **2b** measured in heptane at ~ 10^{-4} M. [b] References 13d and 8. [c] Reference 5.

In order to better understand the behavior of the C_3-symmetrical amide (**1a-f**) and urea (**2a-f**) molecules, temperature dependent measurements are performed emphasizing the different maxima in the CD spectra. The Cotton effects of small amide **1b**, large amide **1f** and small urea **2b** gradually decrease upon raising the temperature until they disappear at approximately 100 °C (Table 3.2). These systems also respond immediately to changes in temperature. Upon cooling, the signal is restored at once. The medium urea **2d** shows a different behavior (Figure 3.5). The structure is retained up to very high temperatures (135 °C). At 120 °C, still one third of the original Cotton effect is present, after which the rest is lost in a sharp transition. In case of the large urea disk **2f**, an even sharper transition is observed at 75 °C. The medium urea disk **2d** shows strong hysteresis. Upon cooling, it takes 2 days before the original signal is retored, while the hysteresis only takes 1½ hours for **2f**.

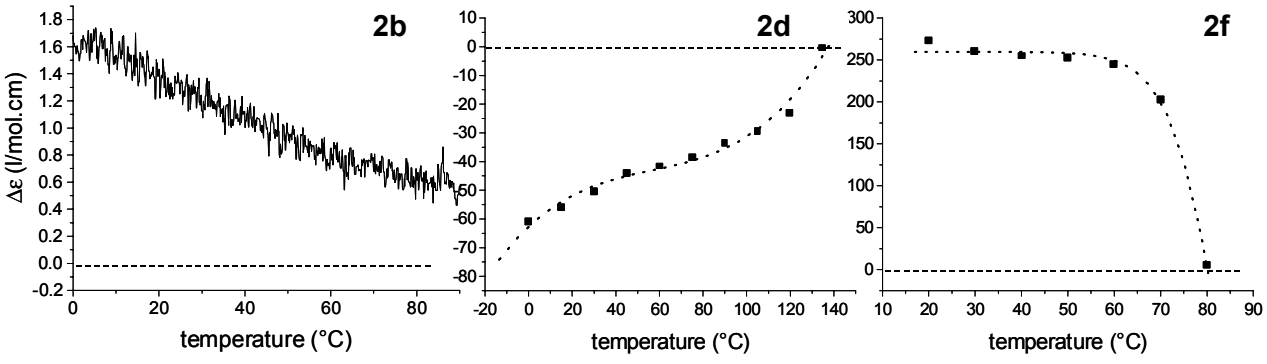

Figure 3.5. *Temperature dependent CD spectra of small **2b** (left), medium **2d** (middle) and large **2f** (right) urea disks at λ_{max} = 228, 275 and 295 nm, respectively (**2b**: 10^{-4} M in heptane, **2d**: 10^{-5} M in dodecane, **2f**: 10^{-5} M in heptane).*

Table 3.2[a]**.** *Temperature dependent CD data of amides **1b/d/f** and ureas **2b/d/f**; T [°C] = temperature of disappearance of the Cotton effect; hysteresis indicates whether kinetic factors influence the system during sample preparation and measurements.*

Compound	**1b**[b]	**1d**	**1f**[c]
T	90	-	110
hysteresis	no	-	no

Compound	**2b**	**2d**	**2f**
T	100	135	80
hysteresis	no	yes	yes

[a, b, c] See Table 3.1.

Besides UV-Vis and CD spectroscopy, the aggregation behavior of the large, bipyridinyl containing disks **1e/f** and **2e/f** could be investigated by fluoresence spectroscopy. A large Stokes shift is observed (**1f**: $\lambda_{max,UV}$ = 369 nm, $\lambda_{max,Fl}$ = 529 nm; **2f**: $\lambda_{max,UV}$ = 371 nm, $\lambda_{max,Fl}$ = 512 nm) due to double proton transfer in the diamino bipyridinyl group in the excited state, in analogy with the previously studied bipyridinyl-3,3'-diol,[14] and diacylated 2,2'-bypiridine-3,3'-diamines.[8] Unlike H-aggregates of for example π-π conjugated systems (oligo(thiophenes), oligo(phenylene vinylenes), or porphyrins,[15] but similar to J-aggregates of for example perylenes or cyanine dyes,[16a-c] fluorescence is found when the molecules **1e/f** and **2e/f** are aggregated in apolar solvents like heptane. Recently, it was found that also oxadiazole-based benzene-1,3,5-tricarboxamide disks start fluorescing upon self-assembly into fibers.[16d] In the molecularly dissolved state (chloroform) fluorescence is quenched by a factor 16 (Figure 3.6). Temperature dependent UV-Vis and fluorescence measurements show differences between large amide **1e** and large urea **2f** similar to those in CD spectroscopy (Figure 3.8). In case of amide **1e/f** intensities decrease gradually over the whole temperature window considered (0 – 140 °C), while urea **2f** shows a sharp transition at 80 °C. But clearly visible in the UV curve, this is followed by a much broader transition, which still seems not complete at 140 °C.

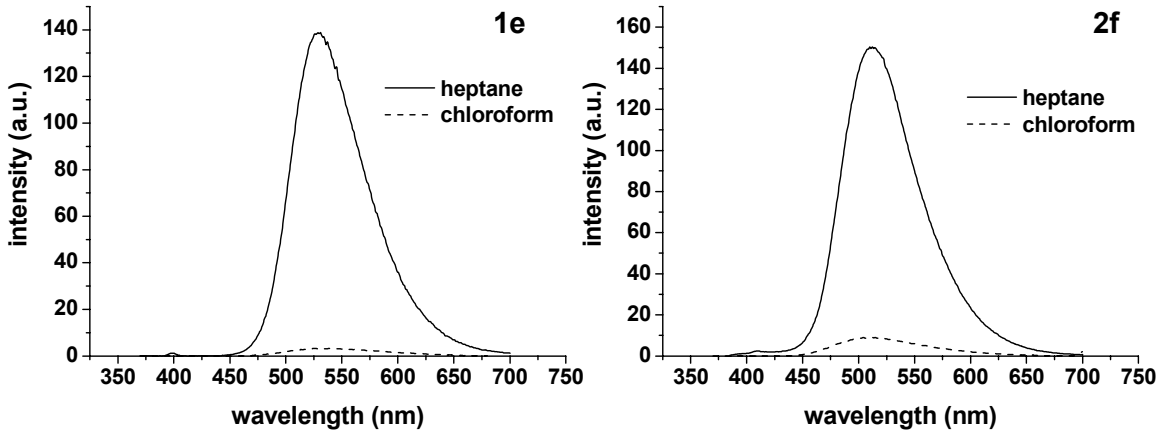

Figure 3.6. *Fluorescence spectra of large amide disk **1e** and large urea disk **2f** in heptane and chloroform (10^{-6} M in dodecane, O.D. = 0.1).*

Time resolved fluorescence measurements produced decay curves which could be fit to a biexponential function. In the biexponential decay, the slow component is regarded characteristic for

the lifetime. This slow component (aggregated state (4-5 ns)), as well as the fast one (molecularly dissolved state (0.3 ns)), of amide **1e** and urea **2f** are similar, and corresponded to values found for an ethylene oxide equipped large amide disk.[7,8] The lifetime is approximately 10 times longer in the aggregated state due to the more rigid environment of the disks which suppresses non radiative decay.

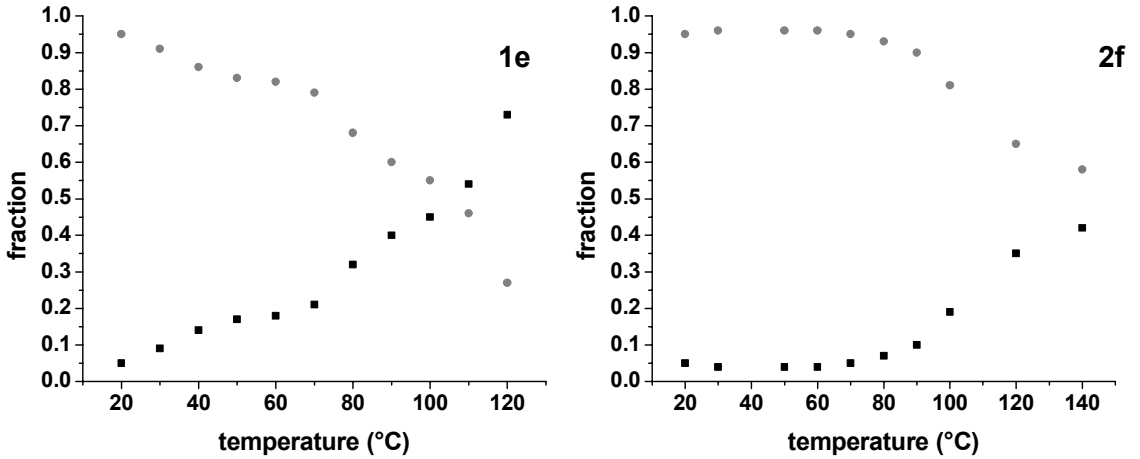

Figure 3.7. *Fraction of aggregated molecules (gray circles) and molecularly dissolved molecules (black squares) for large amide disk **1e** (left) and large urea disk **2f** (right) (10^{-6} M in dodecane).*

Upon raising temperature, rigidity diminishes, which shortens the lifetime in the aggregated state τ_2. In case of amide **1e** the fluorescence lifetime decreases gradually upon raising temperature, while in case of urea **2f** a distinct decrease at 80 °C is observed. When the lifetime data are correlated with the fractions molecularly dissolved and aggregated species (Figure 3.7, See Experimental Section), it becomes clear that in the amide case, loss of aggregates is about 75 % at 120 °C, while for the urea disk it is only 35 %.

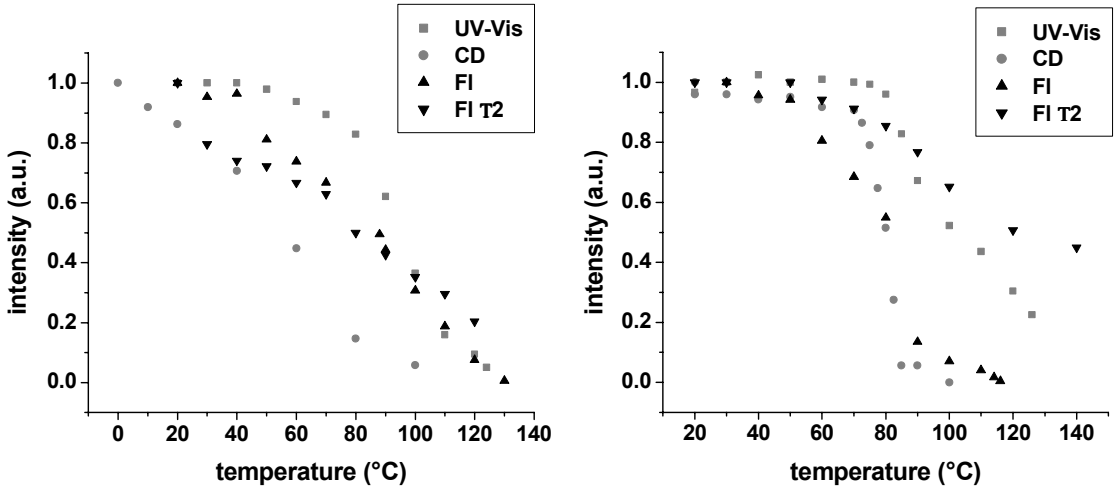

Figure 3.8. *Absorption, fluorescence, lifetime, and circular dichroism data of large amide disk **1e/f** (left) and urea disk **2f** (right) (large amide disk, UV, Fl, Fl τ_2: 7×10^{-6} M, **1e** in dodecane; CD: 2×10^{-5} M, **1f** in dodecane;[6] large urea disk, UV, CD, Fl, Fl τ_2: 7×10^{-6} M, **2f** in dodecane). Data relative to values obtained upon complete aggregation (1) and values found in the molecularly dissolved state (0).*

To clarify this difference in temperature dependent behavior between large amide **1e/f** and large urea **2f**, absorption, fluorescence, lifetime, and circular dichroism data are gathered in Figure 3.8. For the amide the transition covers the whole temperature window (0-140 °C), although the UV curve shows primarily changes in the second half of the transition, while the CD curve changes most in the first half. The UV and fluorescence lifetime curves of the urea are still following a broad transition at 140 °C, while chirality and emission are already lost at 80 °C.

3.2.2 'Solvent shell'

Recently, it was shown for large amide disk **1f**, that use of a branched solvent 2,2,4-trimethylpentane (*iso*-octane), instead of a linear one (*n*-heptane),[17] does not affect the supramolecular aggregation. What is more, chirality can be transferred from a branched, chiral solvent (*(R)*-(+)-2,6-dimethyloctane or *(S)*-(-)-2,6-dimethyloctane) to achiral amide disk **1e**,[5] indicating participation of solvent molecules to the aggregation process. Remarkably, we now found, that in case of large urea disk **2f**, the use of a branched solvent decreases the intensity of the Cotton effect substantially, compared to the use of a linear one (*n*-heptane: $\Delta\varepsilon$ = 300 l/mol·cm, *iso*-octane $\Delta\varepsilon$ = 60 l/mol·cm). The shape of the spectrum remains unchanged (Figure 3.9), while the temperature dependent behavior becomes irreversible. At 70 °C the Cotton effect disappears, and does not reappear upon cooling. Also, no chirality can be transferred from *(S)*-(-)-2,6-dimethyloctane to achiral urea disk **2e**. However, this behavior can rather be rationalized by issues related to the rigidity of the stack (vide supra), than by issues related to solvent-disk interactions.

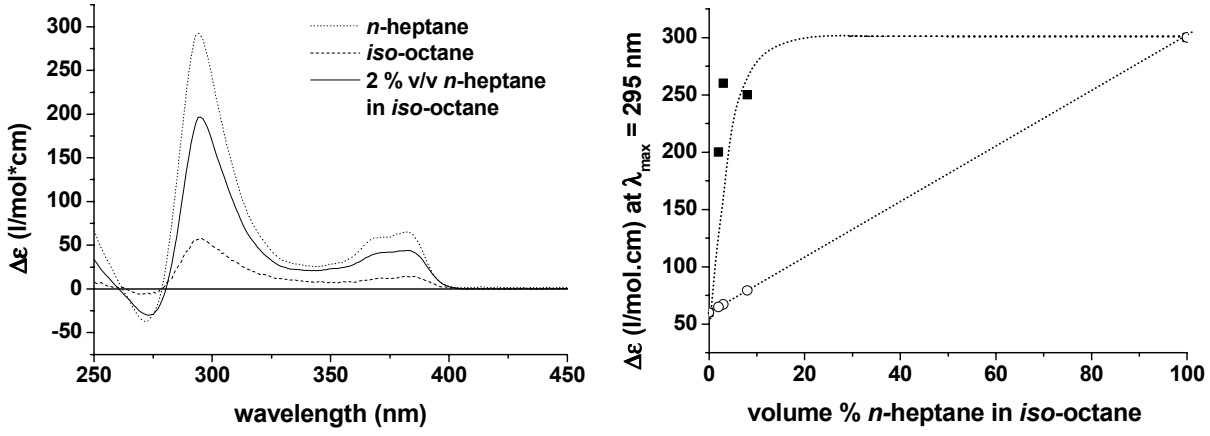

Figure 3.9. *CD-spectra of chiral large urea disk **2f** (left) in n-heptane (dotted line), iso-octane (dashed line), and an iso-octane solution containing 2 % v/v n-heptane (solid line), together with the relationship between the CD intensity at λ_{max} = 295 nm, and the percentage n-heptane (right), as found experimentally (black squares, line to guide the eye) and in case of a linear relationship (open circles).*

When *n*-heptane is added to a solution of large urea disk **2f** in *iso*-octane, the low value for Δε of 60 l/mol·cm is maintained, while the other way around, a huge non-linear dependence between the CD-intensity and the amount of *n*-heptane is found (Figure 3.9). Firstly, highly viscous solutions of 0.620 mg urea disk **2f**, in 0.50, 0.75, and 2.0 ml heptane were prepared. Secondly, these had to be dissolved in *iso*-octane (total volume: 25 ml, 10^{-5} M) using heat and/or an ultra-sonic bath. The final values for Δε of these samples are up to 30 times as high, as could be expected in case of a linear relationship between Δε and the percentage heptane. In time, the intensity of the Cotton effect remains constant. However, when the samples are heated, the stacks are clearly less stable than in a single solvent *n*-heptane or *iso*-octane solution (mix: 55 °C, *iso*-octane: 70 °C, *n*-heptane 80 °C). Also sonication induces a decrease in supramolecular ordering. Finally, the value of λ_{max} in the UV-Vis and fluorescence spectra of the mixed solvent, are identical to those found in *n*-heptane, and different to those found in *iso*-octane (Figure 3.10).

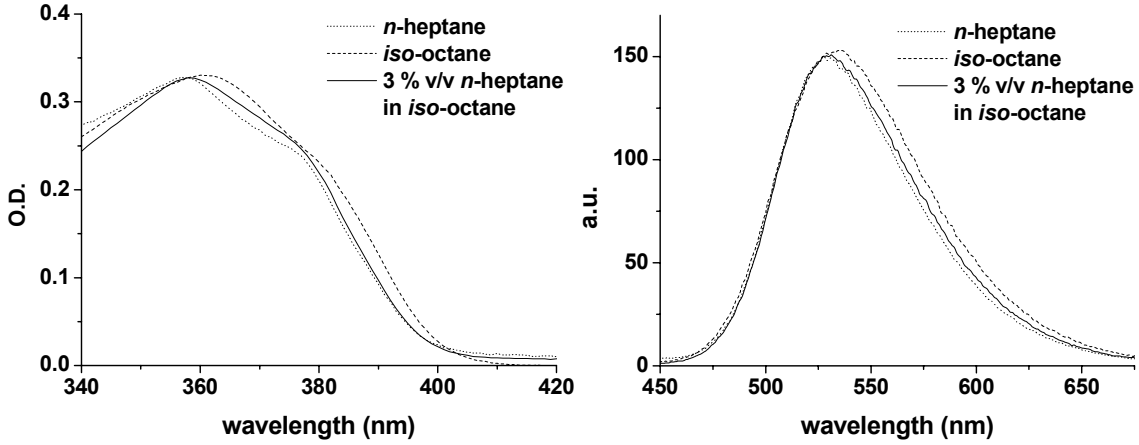

Figure 3.10. *UV (left) and fluorescence-spectra (right) of large urea disk **2f** in n-heptane (dotted line), iso-octane (dashed line), and an iso-octane solution containing 3 % v/v n-heptane (solid line).*

3.2.3 Sergeants and soldiers measurements

Both small and large amide disks **1a/b**[8] and **1e/f**[5] show a strong amplification of chirality, with one chiral molecule capable of organizing as much as 200 and 80 achiral ones, respectively, in either a right- or a left-handed helical stack. These results are interpreted as being the result of both a strong cooperative effect in the stacking and of the columns of achiral disks being inherently chiral. The insertion of a seed of chiral disk to equal amounts of *P* and *M* helices of the achiral disks induces a strong preference of one helicity over the other.

In the large ureas **2e/f** no sergeants and soldiers effect could be observed (Table 3.3). Several methods of sample preparation were applied (mixing of two solutions, heating and cooling of samples, premixing of two solids), but in all cases a linear relationship between the Cotton effect and the percentage of chiral molecules was found. Medium ureas **2c/d** did give an amplification of 2 when

the sample was prepared by premixing the two solids in chloroform, evaporating the solvent and, finally, dissolving the mixed solids in heptane at 10^{-5} M (Figure 3.11).

Upon mixing 10^{-4} M solutions of achiral small urea disk **2a** and chiral small urea disk **2b** a remarkable aggregate (Figure 3.11, squares) was formed just above room temperature (30-40 °C). Cotton effects opposite in sign and with intensities up to 5 times that of the pure chiral compound **2b** were observed. However, these initial aggregates (Figure 3.11, squares) proved not stable in time. After approximately 1 hour, the Cotton effect changed completely (Figure 3.11, dots). More than 75 % chiral compound gave the Cotton effect of the pure chiral compound **2b**, while less chiral compound gave no substantial Cotton effect.

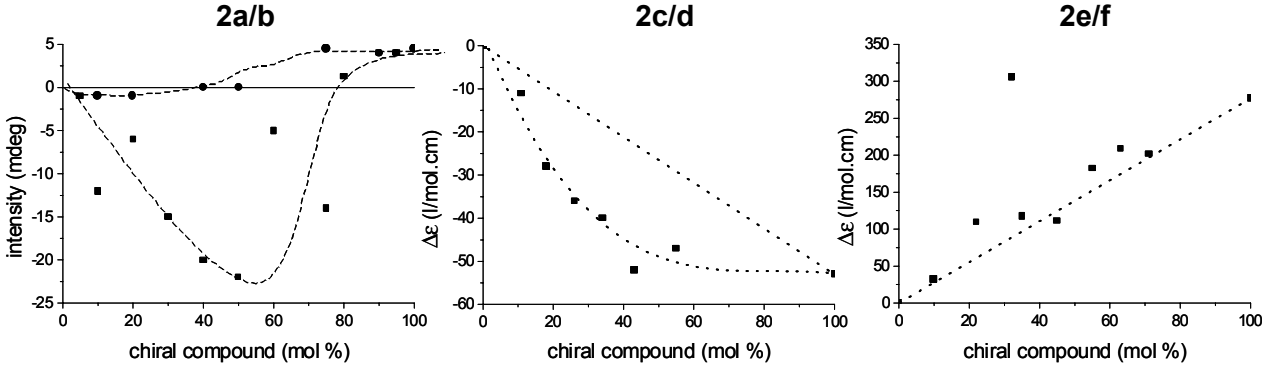

Figure 3.11. *Sergeants and soldiers measurements of small **2a/b** (left), medium **2c/d** (middle) and large **2e/f** (right) urea disks at λ_{max} = 228, 275 and 295 nm, respectively (**2a/b**: 10^{-4} M, **2c/d** and **2e/f**: 10^{-5} M in heptane).*

Table 3.3[a]**.** *Amplification of chirality of amides **1a-f** and ureas **2a-f**. Amplification of chirality = $100/c_{100}$ in which c_{100} [mol %] is the percentage chiral compound where the intensity of a sample containing 100 % chiral compound is reached. Hysteresis indicates whether kinetic factors influence the system during sample preparation and measurements.*

Compound	**1a/b**[b]	**1c/d**	**1e/f**[c]	Compound	**2a/b**	**2c/d**	**2e/f**
amplification of chirality	40	-	40	amplification of chirality	-5[d]	2	no
hysteresis	no	-	no	hysteresis	yes	yes	-

[a] **2a/b**: 10^{-4} M, all others: 10^{-5} M in heptane. [b, c] See Table 3.1. [d] At 50 % chiral compound the CD intensity is –5 times that at 100 % chiral compound.

The above findings were confirmed when amide disks **1a-f** were mixed with urea disks **2a-f**. If amplification of chirality occurs upon mixing of a chiral amide with an achiral urea (or an achiral amide with a chiral urea), this would imply that amide and urea molecules can be accommodated in one single aggregate. Upon mixing in solution 5-20 mol % of small chiral amide **1b** with small achiral urea **2a** a chiral amplification of 4 was observed (Figure 3.12). However, within 1 hour the effect disappeared, and a linear relationship was observed similar to that found in the remainder of the

concentration range (20-100 mol % **1b**). When solutions of small achiral amide **1a** and small chiral urea **2b** were mixed, no Cotton effect appeared.

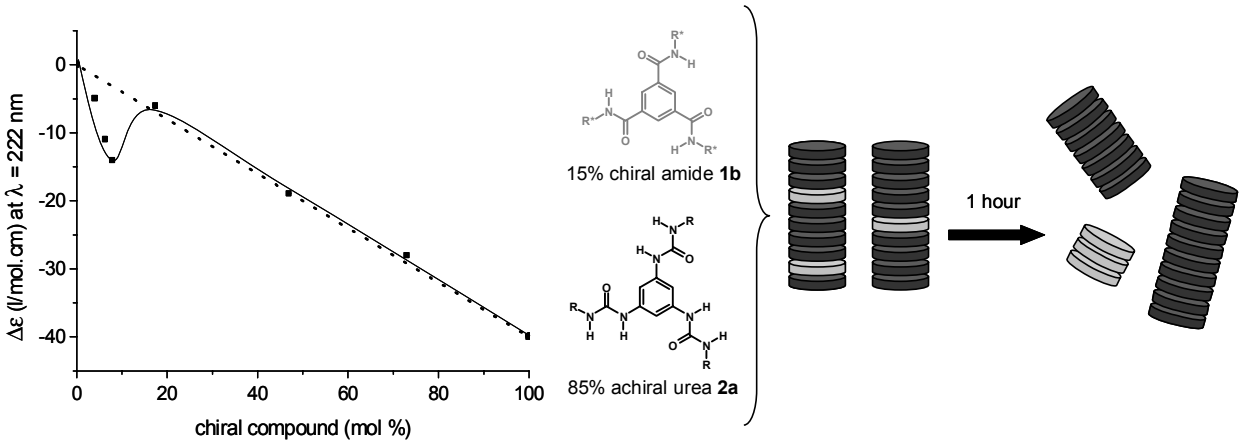

Figure 3.12. *Sergeants and soldiers measurements with small chiral amide **1b** and small achiral urea **2a** (5×10^{-5} M in heptane). The schematic representation shows the mixing of small disks. Mixing 15 % of chiral amide **1b** (gray) and 85 % of achiral urea **2a** (black) gives aggregates containing both kinds of disks (gray and black). However, in time the disks rearrange into two different stacks, containing only chiral amide **1b** (gray) or only achiral urea **2a** (black).*

Mixing medium disks **1d** and **2c** (chiral amide and achiral urea) did not give rise to any Cotton effect, independent of the type of mixing. Upon mixing large disks **1f** and **2e** (chiral amide and achiral urea), or **1e** and **2f** (achiral amide and chiral urea), a linear relationship existed between the percentage of chiral compound and the Cotton effect, implying that also large amide and urea disks are not compatible.

To investigate whether this incompatibility was caused by a 'mismatch' of intermolecular hydrogen bonding or by immiscibility of the compounds, optical microscopy studies were performed, in which two compounds were mixed in a 50 / 50 ratio in their pure form. Mixtures of achiral and chiral small ureas **2a** and **2b** gave a phase separated texture, as well as a mixture of chiral amide **1b** and achiral urea **2a**, although this was less clear. In all other cases (mixtures of small amides **1a**/**1b**, medium ureas **2c/d**, large amides **1e/f**, large ureas **2e/f**, and a mixture of large achiral amide **1e** and large chiral urea **2f**) homogeneous, liquid crystalline textures were observed.

3.2.4 Need for C_3-symmetry: mono-, di-, and triurea

From the measurements described above and in Chapter 2, we assume that the chiral aggregates of the urea disks are helical stacks, similar to the amide stacks. In a helical stack, all three wedges of the molecule are involved in formation of the supramolecular structure. To prove that this is indeed the case, we investigated a monourea (**3**) and a diurea (**4**) as reference compounds for the medium urea disk **2d**. Also, these model compounds might help understand the hysteresis in temperature dependent experiments, displayed by triurea **2d**. The CD spectrum of the monourea **3** shows no Cotton effect

(Figure 3.13). The diurea **4** does show a fair Cotton effect, but it is much smaller than that of the triurea **2d** and differs in shape, sign and maxima.

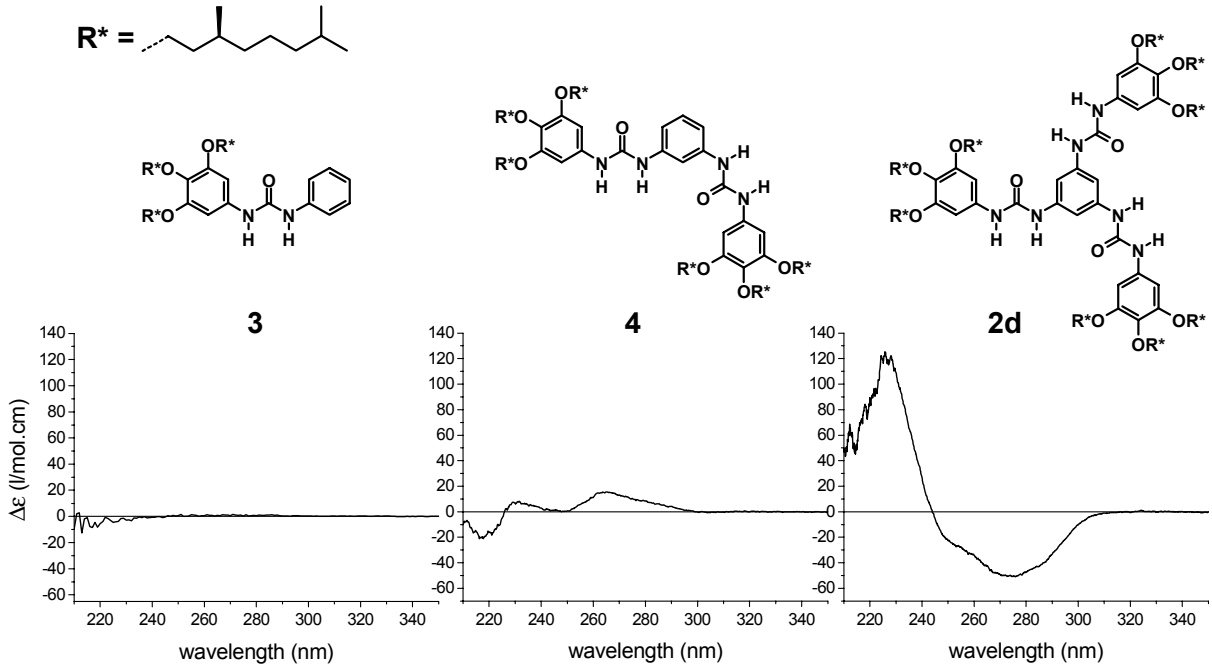

Figure 3.13. *Chemical structures and CD spectra of medium monourea **3** (left), diurea **4** (middle) and triurea **2d** (right) (10^{-5} M in heptane for **3** and **4** and in dodecane for **2d**).*

More differences between the diurea **4** and triurea **2d** become clear when inspecting the temperature dependent CD spectra (Figure 3.14). In the first place, the diurea (80 °C) is less stable upon raising temperature than the triurea (135 °C). Furthermore, upon heating the loss of signal occurs more gradually, while upon cooling the signal of the diurea is restored immediately, in contrast with that of the triurea, which displays a hysteresis of two days.

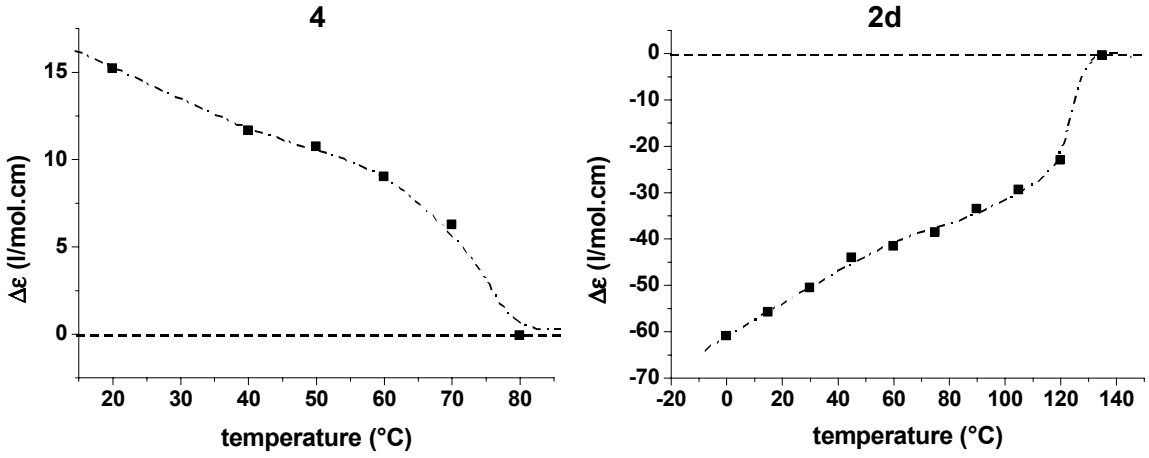

Figure 3.14. *Temperature dependent CD spectra of aggregates of medium diurea **4** (left graph) and triurea **2d** (right graph) at λ_{max} = 264 and 275 nm, respectively (10^{-5} M in heptane for **4** and in dodecane for **2d**).*

3.3 Thermodynamics versus kinetics

All investigated disks retain their helical columnar structures in apolar dilute solution, just as they are formed in the gel phase (Chapter 2). From the chiral disks, only medium amide disk **1d** fails to show a Cotton effect when brought in a dilute apolar solution, which could be expected as no gel is formed in concentrated apolar systems. Generally, it depends on several factors whether aggregates are formed, among which, the strength of the hydrogen bonding, the strength of the π-π and van der Waals interactions and the mutual proportionality of the two. Apparently, the combination of π-π stacking between single aromatic rings and hydrogen bonding between amide groups is not strong enough to form helical stacks. In the small amide disks **1a/b**, strong van der Waals interactions probably account for a crystalline like packing of the alkyl tails. Moreover, chirality is easily expressed, because the distance of the chiral center to the chromophore (center of the molecule) is small. In the large amide disks **1e/f** strong π-π interactions between the planarized and preorganizing bipyridinyl rings, stabilize the aggregate and allow chirality to be transferred a long way.

Strikingly, and in contrast to the medium amide disk **1d**, the medium urea disk **2d** does show supramolecular aggregation in solution. Apparently, in this case stronger intermolecular hydrogen bonding increases the tendency to form chiral aggregates. The CD effect produced by small urea **2b** is only marginal, also compared to that of small amide **1b**. This is in congruence with IR and gelation experiments (Chapter 2), which show that toluene is clearly a better solvent for aggregation of urea **2b** than heptane, probably due to the very low solubility of **2b** in heptane, and participation of toluene in the gel formation relying on its specific π-π stacking capabilities. However, CD measurements cannot be performed in toluene, in view of the low wavelength absorption of small urea **2b** (224 nm). The Cotton effect of large urea **2f** is comparable in size and shape to that of large amide **1f**, but opposite in sign, although both molecules are based on the same (*S*)-3,7-dimethyloctyloxy side chain, with the same (*S*)-configuration. The additional NH group in urea **2f** could cause an 'odd-even' effect, inducing a sign inversion with every atom placed between the chiral center and the center of the molecule. This odd-even effect has been observed before in the optical rotation of a series of poly(isocyanides)[18a] and polythiophenes[18b]. However, in large urea **2f** the extra NH is not positioned between the stereogenic center and the bipyridine chromophore displaying sign inversion, rendering an alternative explanation more plausible. The additional NH group in urea **2f** could slightly alter the conformation of the disks in the stack, inducing a small change in the pitch of the helix, which could suffice to change the sign of the Cotton effect produced by the helical aggregate. Indeed, X-ray measurements have confirmed that the pitch of the urea is smaller than that of the amide (Chapter 2).

Differences between amide and urea stacks become more evident when their temperature dependent CD behavior is studied. The temperature at which the Cotton effect disappears is significantly higher for medium urea **2d** (135 °C) than for small and large amides **1b** (90 °C) and **1f** (110 °C), indicating that the three additional hydrogen bonding protons of the urea indeed can strengthen the

supramolecular aggregate. Notably, the large urea disk **2f** (80 °C) cannot do so, implying that the aggregate of the large disk is less stable upon heating than that of the medium one **2d**. This can be rationalized by the fact that the intermolecular hydrogen bonds of the large urea **2f** might be weaker due to competitive (one point or bifurcated) intramolecular hydrogen bonding to the bipyridinyl groups. Furthermore, the reversible amide stacking is in contrast with the observed hysteresis of 2 days for urea **2d** and 1½ hours for urea **2f**. The amide molecules reach thermodynamical equilibrium immediately, while kinetics intervenes before the urea disks reach their thermodynamically controlled aggregation state. These findings correspond to the observation that X-ray spectra of urea disks keep getting more resolved even after very long annealing times (Chapter 2), indicating that it might even be, that the most ordered state is never reached.

Comparison of the temperature dependent CD data with UV, fluorescence and fluorescence lifetime curves, clarifies why loss of supramolecular chirality and loss of aggregation coincide in case of large amide disks **1f**, while for large ureas **2f** this takes place as a two-step process. The temperature dependent UV curve of amide **1f**, shows that loss of aggregation occurs mainly in the second part of the transition (higher temperatures), while the CD curve indicates a distinct loss of supramolecular chirality during the first part of the transition (lower temperatures). However, temperature dependent fluorescence and fluorescence lifetime measurements clearly decrease gradually (0-140 °C). On the other hand, the urea fluorescence closely follows the urea CD data, while the fluorescence lifetime transition resembles the urea UV curve. From these data it becomes obvious that loss of chirality (80 °C) and loss of aggregation (140 °C / degradation) occur not simultaneously, but subsequently. This follows also from preliminary, temperature dependent SANS data, which reveal no differences in curves recorded between 20 and 70 °C, while at 150 °C, the aggregates are much less defined and significantly smaller in size.[19] The two-step behavior[20] corresponds to that of oligo(ethylene oxide) substituted large amide disks in dilute *n*-butanol solution, which show a sharp transition at 25 °C from chiral to achiral structures, followed by a broader transition at approximately 50 °C from short achiral stacks to molecularly dissolved species (Figure 3.2).[7,8] In case of alkylated large urea **2f**, transition temperatures are higher, as no competitive hydrogen bonding by polar solvents is present.

The rigidity of stacks consisting of large urea disks **2f**, allowed formation of a 'solvent shell'. Although *n*-heptane does mix very well with *iso*-octane, the highly viscous solutions of urea **2f** in *n*-heptane dissolve only in *iso*-octane by use of heat or sonication. Indeed, this indicates that the heptane molecules tightly surround the ordered stack of large urea disks **2f**. The *iso*-octane molecules that are added later on during the preparation, will stay outside this *n*-heptane 'solvent shell' (Figure 3.15). Also UV-Vis and fluorescence spectroscopy indicate the closeness of the *n*-heptane molecules to the chromophores of the disks. The values of λ_{max} in the UV-Vis and fluorescence spectra of the mixed solvent, are identical to those found in *n*-heptane, and different from those found in *iso*-octane.

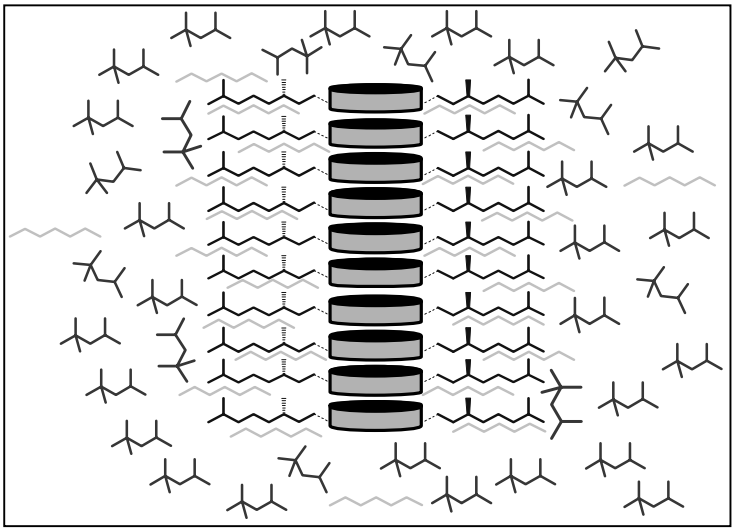

Figure 3.15. *A schematic representation of the heptane solvent shell; the stack (black/dark grey) is tightly surrounded by n-heptane molecules (light grey), while iso-octane molecules (dark grey) are only present outside the stack / heptane system.*

The presence of a shell of tightly bound solvent molecules around stacks of large urea disk **2f**, would also explain why *n*-heptane molecules cannot reach the periphery of the stack, when they are added to a solution of the stacks in *iso*-octane. In this case, the bulky *iso*-octane molecules might disturb the six, presicely placed, intermolecular urea hydrogen bonds in **2f** ($\Delta\varepsilon$ = 60 l/mol·cm).[21] Three intermolecular amide bonds in **1f** might have more freedom to rotate, and the intensity of the Cotton effect is similar in linear *n*-heptane and branched *iso*-octane.[17] On the other hand, there might be enough room for the linear *n*-heptane structures in the periphery between two tightly bound urea disks **2f** ($\Delta\varepsilon$ = 300 l/mol.cm). When all the urea disks are totally surrounded by heptane molecules, it should be possible to produce an ordered stack just like in a solution of 100% heptane ($\Delta\varepsilon$ = 300 l/mol.cm). Of course, immediately after the preparation, diffusion of some of the heptane molecules into the *iso*-octane solvent will occur. Therefore somewhat lower values are found (2 % v/v: $\Delta\varepsilon_{max}$ = 200 l/mol.cm, 3 % v/v: $\Delta\varepsilon_{max}$ = 260 l/mol.cm, 8 % v/v: $\Delta\varepsilon_{max}$ = 250 l/mol.cm), especially for the 2 % v/v solution, where the jelly aggregates needed the most heat and sonication to become totally dissolved. When the sample is heated, the ordered stacks are clearly less stable in a mixed solvent, than in a single solvent *n*-heptane or *iso*-octane solution (mix: 55 ^{o}C, *iso*-octane: 70 ^{o}C, heptane 80 ^{o}C). The higher mobility of the molecules probably increases the diffusion of heptane away from the stacks and the *iso*-octane molecules distort the stacks more easily.

Finally, it has to be noted that participation of solvent molecules to the supramolecular assembly usually is suggested after combining X-ray data with molecular modelling.[22,5] The above example illustrates that CD spectroscopy is a welcome alternative.[23]

Knowing that urea stacks **2** behave much less flexible and less reversible than amide aggregates **1**, it is not surprising that the urea disks do not show the pronounced sergeants and soldiers effect, as found in case of the amides. These sergeants and soldiers measurements are able to show clear differences between 'formally' reversible architectures and systems with a non-equilibrium character. Furthermore, sergeants and soldiers measurements give valuable information about the compatibility of the components (which might be largely different chiral and achiral molecules[4,5]), especially when the (mixing) behavior of the ureas **2** is hard to study in the solid state.

Whereas stacks of achiral and chiral large ureas **2e/f** cannot be made compatible, medium urea disks **2c/d** only can after premixing in a good solvent. However, small urea molecules **2a/b** do mix in apolar solution, although also here kinetics plays an important role. The mixed stacks, consisting of achiral and chiral molecules, undergo microphase separation within an hour, giving aggregates containing either only chiral or achiral molecules. Indeed, optical microscopy proved this phase separation between small ureas **2a/b**. In a solution containing both **2a** and **2b** probably three types of aggregates are present (Figure 3.11, circles): aggregates consisting of chiral compound **2b** (giving a small, positive Cotton effect), of achiral compound **2a** (giving no Cotton effect), and aggregates consisting of both **2a** and **2b** (giving a negative Cotton effect), the latter being kinetically favored, the former two thermodynamically. It is believed that the three methyl groups in chiral **2b** destabilize π-π interactions between the disks in such a way that no ideal packing, such as the one in achiral **2a**, can be achieved.

Similar results and explanations apply to situations where small chiral amide **1b** and achiral urea **2a** are brought together in one solution. Also in this case, an aggregate in which both chiral and achiral disks are present is not thermodynamically stable and after microphase separation (observed by microscopy) two different columnar stacks are present containing either only chiral amide **1b** or achiral urea **2a** (Figure 3.12). In the reverse case (mixing small chiral urea **2b** and achiral amide **1a**) the absence of a Cotton effect is rationalized by de marginal Cotton effect of pure chiral urea **2b**. Because medium amides **1c/d** are incapable of forming aggregates, let alone chiral ones, no amplification of chirality is to be expected upon mixing medium amide disks **1c/d** and ureas **2d/c**. Also the linear relationship between the intensity of the CD absorption and the percentage of chiral compound upon mixing large amides **1e/f** and ureas **2f/e**, shows that amide and urea molecules are virtually incompatible. As shown by optical microscopy, a small structural change (an extra methyl group or NH group), does not induce phase separation in case of medium and large molecules, where in small molecules, such a small change does lead to phase separation. Thus, a minor structural variation (an extra methyl group or NH group) in the molecule (middle or large sized) may dramatically disturb the subtle non-covalent, intermolecular interactions between molecules building a helical columnar aggregate.

Related to this, is the necessity to find the optimum in strength of secondary interactions (hydrogen bonding and π-π stacking), rather than the maximum. Only then, both order and reversibility, as well as stability, will be optimal in the supramolecular aggregate. When π-π stacking interactions overrule hydrogen bonding, or the other way around, (cooperative) order will not be expressed.[6d] Next to this, both interactions (hydrogen bonding and π-π stacking) might be balanced, but both might be very strong. In this case, the molecular conformation is trapped in a local minimum, and order will not be expressed either (see Chapter 4, section 3). Therefore, at a certain point, 'stronger' is no longer equivalent to 'better'. This is illustrated by comparison of the temperature dependent behavior of monourea **6**, diurea **7** and triurea **2d**. The one urea group in **6** does not have enough hydrogen bonding capacity to form chiral superstructures in solution. The reversible temperature dependent behavior of diurea **7** implies that the aggregate formed by its four hydrogen bonding protons is less rigid than the typical aggregate formed by triurea **2d** which shows pronounced hysteresis because of involvement of all six hydrogen bonding protons in the intermolecular hydrogen bonding.

3.4 Conclusions

All C_3-symmetrical discotics -except for medium amide disks **1c/d**- form helical, elongated, columnar aggregates, both in the solid, liquid crystalline state (Chapter 2) and in solution. This proves that formation of helical columns tolerates a broad range of combinations of hydrogen bonding groups (amide and urea) and peripheral groups (alkyl, gallic and bipyridinyl-gallic).

However, the exact behavior and properties of the supramolecular aggregate may strongly be affected by the particular combination of secondary interactions selected. Substituting amide by urea renders kinetic factors important when disks move into their thermodynamically stable, most ordered conformation. Temperature dependent CD measurements show that -unlike the reversible behavior of the amide disks- distinct hysteresis takes place upon heating and cooling samples of ureas. Furthermore, the urea compounds do not display overwhelming sergeants and soldiers effects. This indicates that the initially formed, less-defined urea stacks only slowly transform into a well-defined, thermodynamically more favorable state. Achiral urea disks behave like 'silly soldiers', with a complete focus on strong hydrogen bonding, and therefore slowly in learning the spatial subtleties offered by the stereocenters.

By comparing the CD measurements with temperature dependent fluorescence transients, the occurence of the two-step process, from disordered to ordered urea aggregates, could be demonstrated unarguably. Once the optimal structure is found, the stacks have rigid rod character, which prevents the molecules from easy rearrangement and intermixing, as occurs in the amide stacks. In case of medium urea **2d** a true rigid rod is formed, of which the constituting disks almost have to be destroyed (135 °C), before breaking up of the aggregates occurs. Rigidity in the stacks of large urea **2f**, allows

formation of a solvent shell of linear *n*-heptane around the stacks, that is stable in a solution of branched *iso*-octane.

Changes in the van der Waals and π-π interactions in the periphery of the molecule may strongly influence the capacity for aggregation (in case of **1c/d**). However, these influences are still hard to assess, because other factors, like solubility and distance of the chiral center to the chromophore, are altered simultaneously. The distinct influence of minor structural variations also accounts for the immiscibility of the amide and urea stacks, both forming similar C_3-symmetical supramolecular architectures, but in their own distinct way.

The exciting observation of intermediate stages during the formation of the helical urea aggregates can be interpreted as the folding of a supramolecular polymer, using its self-healing properties to reach or retain its most favorable conformation.[24] Valuable insights could be obtained when this mobility of the disks in the helical architectures, leading to continous reorganization and, therefore, the possibilities of self-repair, is investigated in more detail.[25]

Disks containing two urea groups (**4**), or three amide groups (**1a/b** and **1e/f**) show a reversible temperature dependent behavior, while disks containing 3 urea groups (**2c/d**, **2e/f**) show hysteresis. Indeed, these molecules illustrate the necessity to find the optimum in strength of secondary interactions (in this case intermolecular hydrogen bonding), rather than the maximum. Demands concerning order and reversibility, as well as stability, are met with in the supramolecular aggregate, in which the emphasis is on reversibility in diurea **4**, amides **1a/b**, and **1e/f**, while it is on stability in ureas **2c-f**. In Chapter 4 the design of supramolecular architectures in which the non-covalent interactions are optimally balanced will be re-encountered.[26]

*In summarizing Chapters 2 and 3, the comparison of a set of compounds (amides **1a-f** and ureas **2a-f**) over a full concentration range, from the liquid crystalline state, via the gel phase (10^{-2}, 10^{-3} M), to dilute solution (10^{-5} M), is powerful in creating a detailed picture of the aggregation behavior (Figure 3.16). Different techniques show consistent results: ordered hexagonal phases in the solid state (X-ray), relate to gels and networks of fibers (AFM, SANS), as well as to expression of supramolecular chirality (CD). Exceptional behavior is illustrated by medium amide disks **1c/d**. In the solid state (DSC, TOPM, X-Ray) a complex phase behavior is observed, which could 'confuse' the molecules, thereby rationalizing the absence of a network of fibres on the surface (AFM) and the absence of a gel phase (SANS). Since no columns are formed, supramolecular chirality is not expressed in dilute solution (CD). Also the 'hulk-like' character of urea hydrogen bonding is eminent over the whole concentration range: X-ray measurements show unresolved urea spectra due to a lack of flow and alignment; urea disks show lower minimal gel concentrations than amide ones; while time-dependent effects in CD measurements show that even in dilute solution, hydrogen bonding is mindlessly strong, hampering expression of stereochemical subtleties.*

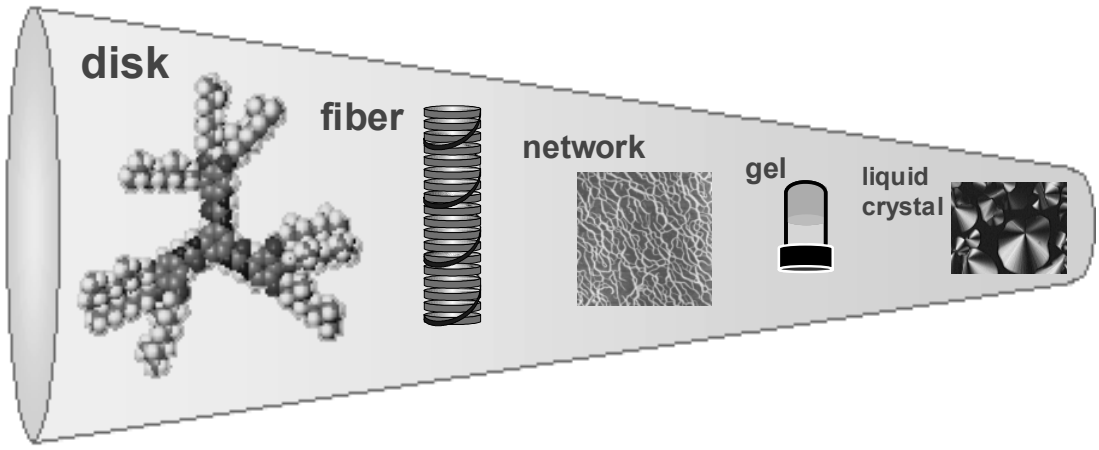

Figure 3.16. *Zooming out…, starting at the chemical structure of the discotics, via the isolated stacks, the network of fibers, and the gel to the liquid crystalline phase.*

3.5 Experimental section

General. General aspects concerning synthesis and characterization have been described in Chapter 2, as well as the synthetic procedures for amides **1a-f** and ureas **2a-f**. Synthesis of 3,4,5-tri((*S*)-3,7-dimethyloctyloxy)aniline, and 3,4,5-tri((*S*)-3,7-dimethyloctyloxy)benzenecarbonylazide have been described previously.[27] UV/Vis spectra were recorded on a Perkin Elmer Lambda 40 UV/Vis spectrometer. CD spectra were recorded on a Jasco J-600 spectropolarimeter equipped with a Jasco PTC-348WI Peltier type temperature control system. Fluorescence spectra were recorded on a Perkin Elmer LS50B luminescence spectrometer. Transient fluorescence measurements with picosecond time resolution were conducted using time-correlated single-photon-counting detection.[28]

5-(Phenylureido)-1,2,3-tris((*S*)-3,7-dimethyloctyloxy)benzene (3). To a solution of phenylisocyanate (42 mg, 0.36 mmol) in dry toluene (1 ml) a solution of 3,4,5-tri((*S*)-3,7-dimethyloctyloxy)aniline (**3d**) (0.24 g, 0.43 mmol) in dry toluene (3 ml) was added. After 1½ h the reaction mixture was precipitated in acetonitrile (50 ml). Filtration yielded **6** as a white powder (0.20 g, 82 %): ^{1}H-NMR ($CDCl_3$) δ 7.32 (H2, H3, m, 4H), 7.07 (H4, m, 1H), 6.91 (NH, s, 1H), 6.72 (NH, s, 1H), 6.58 (H'-ortho, s, 2H), 3.93 (OCH_2, m, 6H), 1.81 - 0.87 (alkyl H, m, 57H); ^{13}C-NMR ($CDCl_3$) δ 153.5 (C3', NHCONH), 138.1 (C1), 133.2 (C1', C4'), 129.2 (C3), 123.9 (C4), 120.6 (C2), 100.9 (C2'), 71.8, 67.5 (OCH_2), 39.3, 39.2, 37.5, 37.4, 37.3, 36.4, 29.8, 29.7, 28.0, 24.7, 22.7, 22.6, 22.6, 19.6, 19.5 (alkyl C); IR (ATR): 3312, 2953, 2925, 2869, 1647, 1599, 1559, 1500, 1468, 1446, 1425, 1384, 1311, 1221, 1115, 1065, 800, 743, 703 cm^{-1}; Elemental analysis: calculated: $C_{43}H_{72}N_2O_4$ (681.06): C, 75.83; H, 10.66; N, 4.11; found: C, 75.17; H, 10.41; N, 3.85; MALDI-TOF MS: calculated: 680.55, found: 680.54.

1,3-Bis[3,4,5-tris((*S*)-3,7-dimethyloctyloxy)-phenylureido]benzene (4). A solution of 3,4,5-tri((*S*)-3,7-dimethyloctyloxy)benzenecarbonylazide (0.30 g, 0.49 mmol) in dry toluene (5 ml) was heated under reflux for 2 h. The toluene was evaporated and the product redissolved in dry tetrahydrofuran (5 ml). A solution of benzene-1,3-diamine (26 mg, 0.24 mmol) in dry tetrahydrofuran (5 ml) was added. After stirring overnight at 80 °C, the tetrahydrofuran was evaporated and the product dissolved in dichloromethane (15 ml). The solution was cooled with ice, which gave a precipitate that yielded the crude product after filtration. Column chromatography (silica, chloroform + 2 %v/v methanol, R_f = 0.5) yielded white sticky solid **7** (0.10 g, 33 %): ^{1}H-NMR ($CDCl_3$ / CH_3OH) δ 7.97 (NH, s, 2H), 7.88 (NH, s, 2H), 7.43 (H2, m, 1H), 7.19 (H5, m, 1H), 7.10 (H4, m, 2H), 6.70 (H'-ortho, s, 4H), 4.00 (OCH_2, m, 8H), 3.93 (OCH_2, m, 4H), 1.88 – 0.86 (alkyl H, m, 114H); ^{13}C-NMR ($CDCl_3$ / CH_3OH) δ 153.7 (C3'), 152.9 (NHCONH), 139.3 (C1), 134.5 (C1'), 133.5 (C4'), 129.2 (C5), 113.6 (C4), 109.9 (C2), 98.6 (C2'), 71.8, 67.1 (OCH_2), 39.1, 39.1, 37.3, 37.2, 37.0, 36.2, 29.6, 29.5, 27.8, 24.5, 24.5, 22.4, 22.3, 22.3, 19.3, 19.2 (alkyl C); IR (ATR): 3311, 2953, 2926, 2869, 1645, 1602, 1558, 1506, 1491, 1468, 1426, 1384, 1298, 1226, 1199, 1115, 1001, 830, 754, 698 cm^{-1}; Elemental analysis: calculated: $C_{80}H_{138}N_4O_8$ (1284.01): C, 74.84; H, 10.83; N, 4.36; found: C, 73.86; H, 10.10; N, 4.35; MALDI-TOF MS: calculated: 1283.05, found: 1305.83 (Na-adduct).

Determination of the relation between observed fluorescence and fraction of aggregation

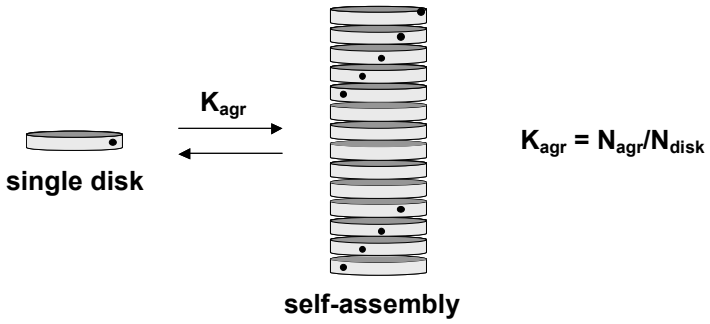

Scheme of the self-assembly of molecularly dissolved disks; N_{agr} represents the number of disks in theaggregates, and N_{disk} represents the number of molecularly dissolved disks.

Suppose a molecule is irradiated with a laser pulse which has a rectangular shaped frequency spectrum. The absorption intensity is then represented by:

$$I_{abs} = I_{laser} \int_0^\infty N_{abs}\sigma(\nu)d\nu$$

Where I_{laser} is the laser intensity N_{abs} is the density of absorbant molecules and $\sigma(\upsilon)$ is the absorption cross-section of the molecules at excitation frequency υ.
The corresponding fluorescence originating from the photoexcited sample is then equal to:

$$I_{fl} = c\phi_{fl} I_{abs} = c\phi_{fl} N_{abs} \int_0^\infty \sigma(\nu)d\nu$$

Here ϕ_{fl} is the fluorescence quantum yield, and c an arbitrary constant.
Since we have two absorbant species, the single-disk molecule and the aggregated molecule, one now can determine the relation between the observed fluorescence and the fraction of aggregation. The ratio between the fluorescence intensity arising from the aggregated species and the single disk molecules is simply: I_{agr}/I_{disk}. This ratio can be expressed as:

$$\frac{I_{agr}}{I_{disk}} = C\frac{N_{agr}}{N_{disk}} \frac{\phi_{fl,agr}\int_0^\infty \sigma_{agr}(\nu)d\nu}{\phi_{fl,disk}\int_0^\infty \sigma_{disk}(\nu)d\nu}$$

If one now considers the fluorescence quantum yields of both emissive species to be constant in the temperature range of interest, one can find a very simple relation between the observed fluorescence and fraction of aggregation.

$$\frac{I_{agr}}{I_{disk}} = C^+\frac{N_{agr}}{N_{disk}} \qquad with \qquad C^+ = C\frac{\phi_{fl,agr}\int_0^\infty \sigma_{agr}(\nu)d\nu}{\phi_{fl,disk}\int_0^\infty \sigma_{disk}(\nu)d\nu} \approx \frac{\phi_{fl,agr}\varepsilon_{\max,agr}}{\phi_{fl,disk}\varepsilon_{\max,disk}} \quad as\ a\ constant$$

Where ε is the molar extinction coefficient.

3.6 References and notes

(1) solid state: (a) Praefcke, K.; Eckert, A. *Mol. Cryst. Liq. Cryst.* **2003**, *396*, 265–299. (b) Chandrasekhar, S. *Handbook of liquid crystals: Low molecular weight Liquid Crystals II*; Vol. 2B, 749–780; Demus, D.; Goodby, J.; Gray, G.W.; Spiess, H.W., Vill, V. (Eds.), WILEY-VCH: Weinheim, **1998**. (c) Kato, T. *Handbook of liquid crystals: Low molecular weight Liquid Crystals II*; Vol. 2B, 969–979; Demus, D.; Goodby, J.; Gray, G.W.; Spiess, H.W.; Vill, V. (Eds.), WILEY-VCH: Weinheim, **1998**. gel phase: (d) Usol'tseva, N.; Praefcke, K.; Smirnova, A.; Blunk, D. *Liq. Cryst.* **1999**, *26*, 1723–1734. dilute solution (e) Prins, L.J.; de Jong, F.; Timmerman, P.; Reinhoudt, D.N. *Nature* **2000**, *408*, 181–184. (f) Russell, K.C.; Lehn, J.-M.; Kyritsakas, N.; DeCian, A.; Fisher, J. *New. J. Chem.* **1998**, 123–128. (g) Guo, Y.-M.; Oike, H.; Aida, T. *J. Am. Chem. Soc.* **2004**, *126*, 716–717. (h) Tabei, J.; Nomura, R.; Sanda, F.; Masuda, T. *Macromolecules* **2004**, *37*, 1175–1179. (i) Cheuk, K.K.L.; Lam, J.W.Y.; Ming Lai, L.; Dong, Y.; Tang, B.Z. *Macromolecules* **2003**, *36*, 9752–9762. (j) Yashima, E.; Maeda, K.; Okamoto, Y. *Nature* **1999**, *399*, 449–451. (k) Mayer, S.; Maxein, G.; Zentel, R. *Macromolecules* **1998**, *31*, 8522–8525. (l) Gu, H.; Nakamura, Y.; Sato, T.; Teramoto, A.; Green, M.M.; Jha, S.K.; Andreola, C.; Reidy, M.P. *Macromolecules* **1998**, *31*, 6362–6368. (m) Schlitzer, D.S.; Novak, B.M. *J. Am. Chem. Soc.* **1998**, *120*, 2196–2197. (n) Green, M.M.; Peterson, N.C.; Sato, T.; Teramoto, A.; Cook, R.; Lifson, S. *Science* **1995**, *268*, 1860–1866. (o) Moore, J.S.; Gorman, C.B.; Grubbs, R.H. *J. Am. Chem. Soc* **1991**, *113*, 1704–1712. (p) Langeveld-Voss, B.M.W.; Waterval, R.J.M.; Janssen, R.A.J.; Meijer, E.W. *Macromolecules* **1999**, *32*, 227–230.

(2) (a) Fechtenkötter, A.; Tchebotareva, N.; Watson, M.; Müllen, K. *Tetrahedron* **2001**, *57*, 3769–3783. (b) Engelkamp, H.; Middelbeek, S.; Nolte, R.J.M. *Science* **1999**, *284*, 785–788. (c) Tamaru, S.; Uchino, S.; Takeuchi, M.; Ikeda, M.; Hatano, T.; Shinkai, S. *Tetrahedron Lett.* **2002**, *43*, 3751–3755.

(3) Green, M.M.; Reidy, M.P.; Johnson, R.D.; Darling, G.; O'Leary, D.J.; Wilson, G. *J. Am. Chem. Soc.* **1989**, *111*, 6452–6454.

(4) Tamaru, S.; Uchino, S.; Takeuchi, M.; Ikeda, M.; Hatano, T.; Shinkai, S. *Tetrahedron Lett.* **2002**, *43*, 3751–3755.

(5) Palmans, A.R.A. *Thesis: Supramolecular structures based on the intramolecular H-bonding in the 3,3'-di(acylamino)-2,2'-bipyridine unit*; Eindhoven University of Technology: Eindhoven, **1997**.

(6) (a) Palmans, A.R.A.; Vekemans, J.A.J.M.; Fischer, H.; Hikmet, R.A.; Meijer, E.W. *Chem. Eur. J.* **1997**, *3*, 300–307. (b) Palmans, A.R.A.; Vekemans, J.A.J.M.; Hikmet, R.A.; Fisher, H.; Meijer, E.W. *Adv. Mater.* **1998**, *10*, 873–876. (c) Palmans, A.R.A.; Vekemans, J.A.J.M.; Havinga, E.E.; Meijer, E.W. *Angew. Chem. Int. Ed. Engl.* **1997**, *36*, 2648–2651. (d) Meijer, E.W.; Vekemans, J.A.J.M.; Palmans, A.R.A.; Breure, P.; de Kraker, J.; Brunsveld, L. *Polym. Prepr.* **2000**, *41(1)*, 902–903.

(7) Brunsveld, L.; Zhang, H.; Glasbeek, M.; Vekemans, J.A.J.M.; Meijer, E.W. *J. Am. Chem. Soc.* **2000**, *122*, 6175–6182.

(8) Brunsveld, L. *Thesis: Supramolecular chirality, from molecules to helical assemblies in polar media*; Eindhoven University of Technology: Eindhoven, **2001**; and references therein.

(9) Kilbinger, A.F.M.; Schenning, A.P.H.J.; Goldoni, F.; Feast, W.J.; Meijer, E.W. *J. Am. Chem. Soc.* **2000**, *122*, 1820–1821.

(10) (a) Prince, R.B.; Brunsveld, L.; Meijer, E.W.; Moore, J.S. *Angew. Chem. Int. Ed.* **2000**, *39*, 228–231. (b) Hirschberg, J.H.K.K.; Brunsveld, L.; Ramzi, A.; Vekemans, J.A.J.M.; Sijbesma, R.P.; Meijer, E.W. *Nature* **2000**, *407*, 167–170.

(11) Apolar oligo(phenylene ethynylenes), as well as polythiophenes show a strong time-dependence due to intermolecular aggregation, evidenced by small spectral changes in the UV spectrum and an increasing CD intensity. In these two examples, intermolecular aggregation into columns of stacked helices was found to play an important role in the expression of the twist sense bias and is subject to hysteresis. See ref. 8 and Langeveld-Voss, B.M.W. *Thesis: Chiral polythiophenes*; Eindhoven University of Technology: Eindhoven, **1999**.

(12) In ureidotriazine units with trialkoxyphenyl groups, transfer of chirality from a monofunctional, chiral chain stopper to a bifunctional achiral unit occurs. In similar, more strongly hydrogen-bonded, ureidopyrimidinone structures, such transfer is not present. Also, increasing the amount of aromatic moieties (π-π stacking) in monofunctional ureidotriazine moieties with trialkoxyphenyl groups, increases the tendency to form helical, supramolecular architectures. See: Hirschberg, J.H.K.K. *Thesis: Supramolecular Polymers*; Eindhoven University of Technology: Eindhoven, **2001**, and Schenning, A.P.H.J. ; Jonkheijm, P.; Peeters, E.; Meijer, E.W. *J. Am. Chem. Soc.* **2001**, *123*, 409–416.

(13) (a) Yasuda, Y.; Iishi, E.; Inada, H.; Shirota, Y. *Chem. Lett.* **1996**, 575–576. (b) Hanabusa, K.; Koto, C.; Kimura, M.; Shirai, H.; Kakehi, A. *Chem. Lett.* **1997**, 429–430. (c) Matsunaga, Y.; Miyajima, N.; Nakayasu, Y.; Sakai, S. *Bull. Chem. Soc. Jpn*. **1988**, *61*, 207–210. (d) Brunsveld L.; Schenning, A.P.H.J.; Broeren, M.A.C.; Janssen, H.M.; Vekemans, J.A.J.M.; Meijer, E.W. *Chem. Lett.* **2000**, 292–293. (e)

Lightfoot, M.P.; Mair, F.S.; Pritchard, R.G.; Warren, J.E. *Chem. Commun.* **1999**, 1645–1946. (f) Shikata, T.; Ogata, D.; Hanabusa, K. *J. Phys. Chem. B* **2003**, *108*, 508–514.

(14) (a) Toele, P.; Zhang, H.; Glasbeek, M. *J. Phys. Chem. A.* **2002**, 106, 3651–3658. (b) Glasbeek, M.; Toele, P.; Zhang, H. *J. Lumines.* **2001**, 623–625. (c) Prosposito, P.; Marks, D.; Zhang, H.; Glasbeek, M. *J. Phys. Chem. A* **1998**, *102*, 8894–8902. (d) Eyal, M.; Reisfeld, R.; Chernyak, V.; Kaczmarek, L.; Grabowska, A. *Chem. Phys. Lett*. **1991**, *176*, 531–535. (e) Bulska, H. *Chem. Phys. Lett.* **1983**, *98*, 398–402.

(15) (a) Schenning, A.P.H.J.; Kilbinger, A.F.M.; Biscarini, F.; Cavallini, M.; Cooper, H.J.; Berrick, P.J.; Feast, J.; Lazzaroni, R.; Leclère, Ph.; McDonnel, L.A.; Meijer, E.W.; Meskers, S.C.J. *J. Am. Chem. Soc.* **2002**, *124*, 1269–1275. (b) Schenning, A.P.H.J.; Tsipis, A.C.; Meskers, S.C.J.; Beljonne, D.; Meijer, E.W.; Bredas, J.L. *Chem. Mater*. **2002**, *14*, 1362–1368. (c) Aratani, N.; Osuka, A. *Bull. Chem. Soc. Jpn.* **2001**, *74*, 1361–1379.

(16) (a) Shirakawa, M.; Kawano, S.; Fujita, N.; Sada, K.; Shinkai, S.J. *Org. Chem.* **2003**, *68*, 5037–5044. (b) Würthner, F.; Thalacker, C.; Sautter, A.; Schärtl, W.; Ibach, W.; Hollricher, O. *Chem. Eur. J.* **2000**, *6*, 3971–3886. (c) Lydon, J. *Curr. Opin. Colloid Interface Sci.* **1998**, *3*, 458–466. (d) Ryu, S.Y.; Kim, S.; Seo, J.; Kim, Y.-W.; Kwon, O.-H., Jang, D.-J.; Park, S.Y. *Chem. Commun.* **2004**, 70–71.

(17) Coolen, B.F.; van de Broek, P.R.; Langelaan, M.L.P.. *Quarterly report Laboratory of Macromolecular and Organic Chemistry*; Eindhoven University of Technology:Eindhoven, **2002**, 7-2, and **2003**, 8–1.

(18) (a) Amabilino, D.B.; Ramos, E.; Serrano, J.-L.; Sierra, T.; Veciana, J. *J. Am. Chem. Soc.* **1998**, *120*, 9126 – 9134. (b) Ramos Lermo, E.; Langeveld-Voss, B.M.W.; Janssen, R.A.J.; Meijer, E.W. *Chem. Commun.* **1999**, 791–792.

(19) Kleppinger, R. *Quarterly report Laboratory of Macromolecular and Organic Chemistry*; Eindhoven University of Technology: Eindhoven, **2002**, 7–2.

(20) Badjić, J.D.; Cantrill, S.J.; Stoddart, J.F. *J. Am. Chem. Soc.* **2004**, *126*, 2288–2289.

(21) Irreversible temperature dependent behavior might be caused by initial retainment of the solid state conformation: Jiang, H.; Dolain, C.; Léger, J.-M.; Gornitzka, H.; Huc, I. *J. Am. Chem. Soc.* **2004**, *126*, 1034–1035.

(22) Sakurai, K.; Kimura, T.; Gronwald, O.; Inoue, K.; Shinkai, S. *Chem. Lett.* **2001**, 746–747.

(23) Borovkov, V.V.; Hembury, G.A.; Inoue, Y. *Angew. Chem. Int. Ed.* **2003**, *42*, 5310–5314.

(24) (a) Hill, D.J.; Mio, M.J.; Prince, R.J.; Hughes, T.S.; Moore, J.S. *Chem. Rev.* **2001**, *101*, 3893–4011. (b) Brunsveld, L.; Folmer, B.J.B.; Meijer, E.W.; Sijbesma, R.P. *Chem. Rev.* **2001**, *101*, 4071–4097. (c) Berl, V.; Schmutz, M.; Krische, M.J.; Khoury, R.G.; Lehn, J.-M. *Chem. Eur. J.* **2002**, *8*, 1227–1244.

(25) solid state NMR; macrocycle: (a) Fischer, M; Lieser, G.; Rapp, A.; Schnell, I.; Mamdouh, W.; De Feyter, S.; De Schryver, F.C.; Höger, S. *J. Am. Chem. Soc.* **2004**, 126, 214–222. hexabenzocoronene: (b) Brown, S.P.; Schnell, I.; Brand, J.D.; Müllen, K.; Spiess, H.W. *Phys. Chem. Chem. Phys.* **2000**, *2*, 1735–1745. (c) Ochsenfeld, C.; Brown, S.P.; Schnell, I.; Gauss, J.; Spiess, H.W. *J. Am. Chem. Soc.* **2001**, *123*, 2597–2606. dendron: (d) Rapp, A.; Schnell, I.; Sebastiani, D.; Brown, S.P.; Percec, V.; Spiess, H.W. *J. Am. Chem. Soc.* **2003**, *125*, 13284–13297. isocytosine: (e) Schnell. I.; Langer, B.; Söntjens, S.H.M.; van Genderen, M.H.P.; Sijbesma, R.P.; Spiess, H.W. *J. Magn. Reson.* **2001**, *150*, 57–70. pyramidics: (f) Luz, Z.; Poupko, R; Wachtel, E.J. *Mol. Cryst. Liq. Cryst.* **2003**, *397*, 67–77. (g) Zimmerman, H; Bader, V.; Poupko, R.; Wachtel, E.J.; Luz, Z. *J. Am. Chem. Soc.* **2002**, *124*, 15286–15301.

(26) van Gorp, J.J.; Vekemans, J.A.J.M.; Meijer E.W. *Mol. Cryst. Liq. Cryst*. **2003**, *397*, 491–505.

(27) Pieterse, K. *Thesis: Electron deficient materials based on azaheterocycles*; Eindhoven University of Technology: Eindhoven, **2001**.

(28) Lifetime measurements were performed using the picosecond fluorescence setup described previously: Middelhoek, E.R.; van der Meulen, P.; Verhoeven, J.W.; Glasbeek, M. *Chem. Phys.* **1995**, *198*, 373–380.

Chapter 4

From inter- to intramolecular hydrogen bonding; designing folded helices from self-assembled ones

Abstract: *Medium-sized chiral urea disk **2d** forms helical, rigid rod-like architectures in dilute solution, while medium-sized chiral, carbonyl centered amide disk **1d** is unable to express supramolecular chirality (Chapter 3). To elucidate this remarkable difference in more detail, chiral (**1h**) and achiral (**1g**) C_3-symmetrical nitrogen centered amide disks are investigated with optical polarizing microscopy, differential scanning calorimetry and UV-Vis / circular dichroism spectroscopy. Similar to the carbonyl centered amide disks **1c/d**, order is only observed for achiral nitrogen centered disk **1h** in the liquid crystalline phase. Using the same techniques, two asymmetrical monoamide diurea disks are studied, one containing 6 'chiral urea' groups (**3**) and the other containing 3 'chiral amide' centers (**4**). These compounds do show chiral supramolecular aggregation in dilute apolar solutions, featuring hysteresis in experiments investigating thermoreversibility, similar to C_3-symmetrical triurea compounds **2d**. Furthermore, CD measurements of monoamide diureas **3** and **4** indicate that the helical aggregate self-assembles via amide-amide and urea-urea hydrogen bonding, offering opportunities to order single functionalities on 'chiral urea' disk **3** in a helical stack. An attempt was made to apply the asymmetry in the helical folding of oligomeric meta-phenylene-ureido structures **5**. In order to elongate the structures via a stepwise approach, next to 1,3,5-trisubstituted benzene building blocks with two different functionalities **6/7**, ones with three different substituents **8/9** have been synthesized also. Tetra-, penta-, and hexaureas **5h-j** are expected to have the necessary length to complete one turn of a helix. However, they show strong but undirectional intermolecular interactions, despite the specific amide-amide and urea-urea intermolecular hydrogen bonding interactions displayed by monoamide diurea disks **3** and **4**. This prevents endgroup reactivity, purification and characterization. NOESY ^{1}H-NMR cannot reveal any preferential conformation for monourea oligomer **5c**, diurea oligomer **5e** or triurea oligomer **5g**.*

4.1 Introduction

4.1.1 Tertiary architectures

Various discotic molecules are known, that contain sufficient information (hydrogen bonding and π-π stacking interactions) to form helical architectures,[1] reminiscent of natural α-helices.[2] However, biological functions are expressed by more complicated, tertiary architectures, of which the α-helices might just constitute a small part.[3] Therefore, it is desirable to bring the synthetic helices to the next level of order. For example, bundles of intertwined helices,[4] display similarities to the coiled coil structures of keratin, myosin, or tropocollagene.[3]

In case of C_3-symmetrical discotics, non-covalent interactions required for the formation of such a synthetic tertiary architecture can be introduced via desymmetrization of the disk. This renders the disks asymmetrical, meaning that the three wedges are no longer identical (Figure 4.1).[5] Previously, asymmetry has been introduced at the periphery of the molecule. For large[6] oligo(ethylene oxide) amide disks it was shown that a terpyridine ligand caused selective dimerization upon addition of Fe^{2+}. The capability of chiral amplification, as in the corresponding non-functionalized disk, was maintained.[7] Another example deals with a large disk containing one achiral alkyl wedge, and two chiral oligo(ethylene oxide) wedges (Figure 4.1, right).[8] Both in apolar as well as in polar solutions, substantial Cotton effects were observed, indicating that various tertiary architectures, most probably coiled coils, can be formed. In these coils either the alkyl chains, or the oligo(ethylene oxide) chains are shielded from the solvent.

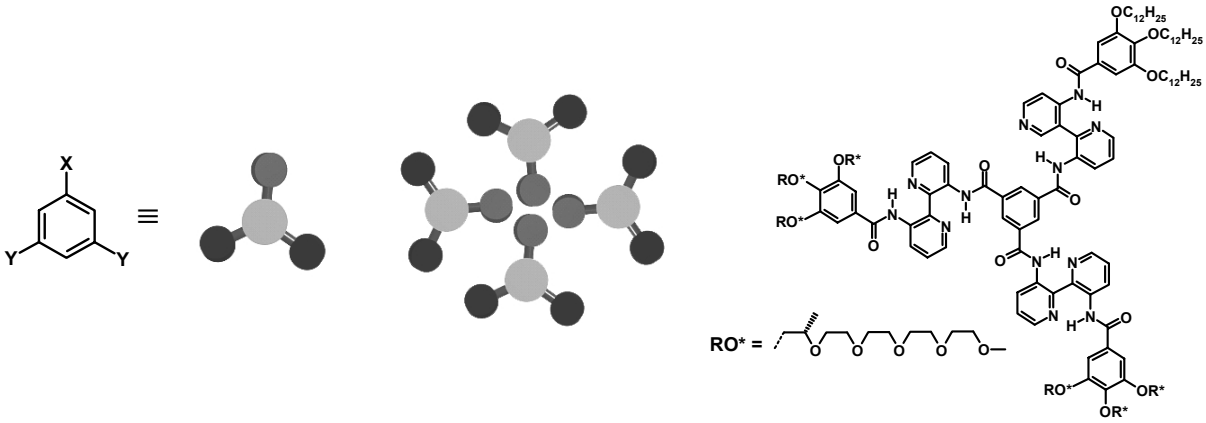

Figure 4.1. *Schematical representation of an asymmetrical disk with two different wedges X in gray, and Y in black, and it's hypothetical aggregate (left); together with the chemical structure of a disk with one apolar and two polar wedges (right).*

However, it proved difficult to synthesize such large asymmetrical architectures via an efficient route. The conversion of 3,5-bis(methoxycarbonyl)benzoic acid[9] to the 3,5-dicarboxy-1-benzenecarboxamide moiety proceeds under standard saponification conditions. But in the next step, thionyl chloride does not only convert the acid groups to acid chlorides, but also converts part of the carboxamide functions to imidoyl chlorides.[10] To overcome this problem, not benzene-1,3,5-

tricarboxylic acid, but benzene-1,3,5-triamine,[11] may be used as an aromatic core, in order to obtain 'medium' or 'large' (aromatically substituted) asymmetrical disks. Commercial 3,5-dinitroaniline could prove to be a suitable starting material.

Next to the intertwined helical bundles, asymmetrical disks might be applied to mimic other examples of higher order architectures in nature, such as the tobacco mosaic virus. [3,12] It is built via stepwise self-assembly in which a templating effect plays an important role. These processes have been copied in synthetic analogues, formed by initial self-assembly of units into disks, followed by stacking of disks into columns.[13] 1,3-Diureidopyrimidinone units have been applied successfully in the formation of hexameric cycles, bound via quadruple hydrogen bonding.[14] However, in covalent foldamers[15] based on monomers derived from large bipyridinyl benzene-1,3,5-tricarboxamides, non-directional π-π interactions were found to overrule directional hydrogen bonding, required for a cyclic conformation.[8]

4.1.2 Design of asymmetrical disks and *meta*-phenylene-ureido oligomers

Apart from introduction of asymmetry at the periphery of the molecule, different hydrogen bonding groups can be combined in one discotic entity. Medium-sized discotics based on gallic acid derivatives (Figure 4.2, Chapter 3) were focused on, because large differences have been found between the amide disks **1c/d** and the urea disks **2c/d**. 'Medium' carbonyl centered triamides **1c/d** are not capable of retaining their columnar structure in apolar solution, and order is only found in the liquid crystalline phase of triamide **1c**. On the other hand, the 'medium' triurea **2c/d** forms rigid rod-like structures at concentrations as low as 10^{-5} M.

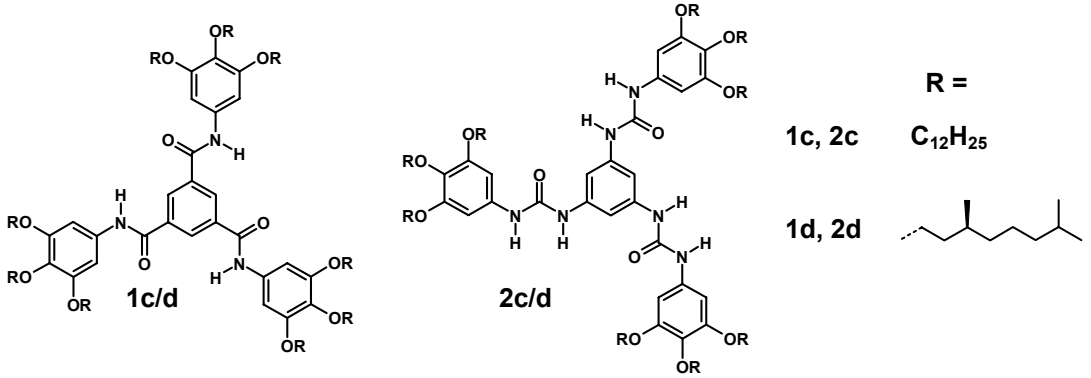

Figure 4.2. *Chemical structures of carbonyl centered triamides **1c/d** (left), and triureas **2c/d** (right).*

To rule out any influences caused by the difference in connectivity (carbonyl or nitrogen), nitrogen centered triamides **1g/h** have been synthesized and investigated (Figure 4.3). At the same time, asymmetrical 'medium' structures **3** and **4**, each containing one amide and two urea groups, have been studied to better understand the differences in self-assembly between triamides **1c/d** and triureas **2c/d**. Monoamide diurea disk **3** contains 6 chiral centers, which are connected to the central benzene ring

via the urea groups, while monoamide diurea disk **4** is equipped with 3 'chiral amide' functionalities. This enables us to investigate separately the aggregation of the amide or the urea groups of these asymmetrical disks with circular dichroism spectroscopy. From these data, information concerning the conformation of the asymmetrical disks in the supramolecular aggregate can be derived. From the absence of chiral amplification upon mixing a chiral amide with an achiral urea (Chapter 3), it could be judged that amide groups in one disk do not form intermolecular hydrogen bonds with urea groups in the other. This is what we wish to verify in asymmetrical disks **3** and **4**.

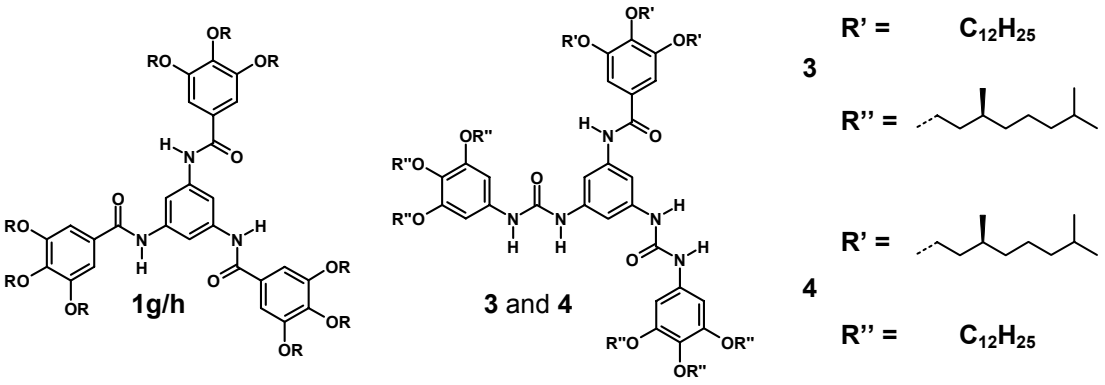

Figure 4.3. *Chemical structures of nitrogen centered triamides **1g/h** (left), and monoamide diureas **3** and **4** (right). R-groups of **1g/h** are similar to those of **1c/d** (see Scheme 4.2).*

Specific amide-amide and urea-urea interactions in asymmetrical 1,3,5-benzenetricarboxamides might be used to order functionalities. When 2 functionalities of the 1,3,5-trisubstituted benzene unit are provided with polymerizable groups, while the third is left for (solubilizing) side groups, the 1,3,5-unit becomes part of the main chain.[14] Using specific amide-amide urea-urea interactions, *meta*-phenylene-ureido foldamer[15] **5** might adopt a helical conformation (Figure 4.4). In addition to building blocks with 2 different functionalities, dinitro **6a/b** and diamino **7a/b**, monomers with 3 different functionalities, nitro/amine **8** and nitro/isocyanate **9**, are developed in order to build oligomeric 1,3,5-trisubstituted structures of defined length (Figure 5.1 in Chapter 5). For the synthesis of oligomers diamine building block **7a** is used in combination with mononitro monoisocyanate building block **9**. Generally, iterative nitro reduction, isocyanate formation and elongation to a nitro-blocked urea give access to oligomers **5**.

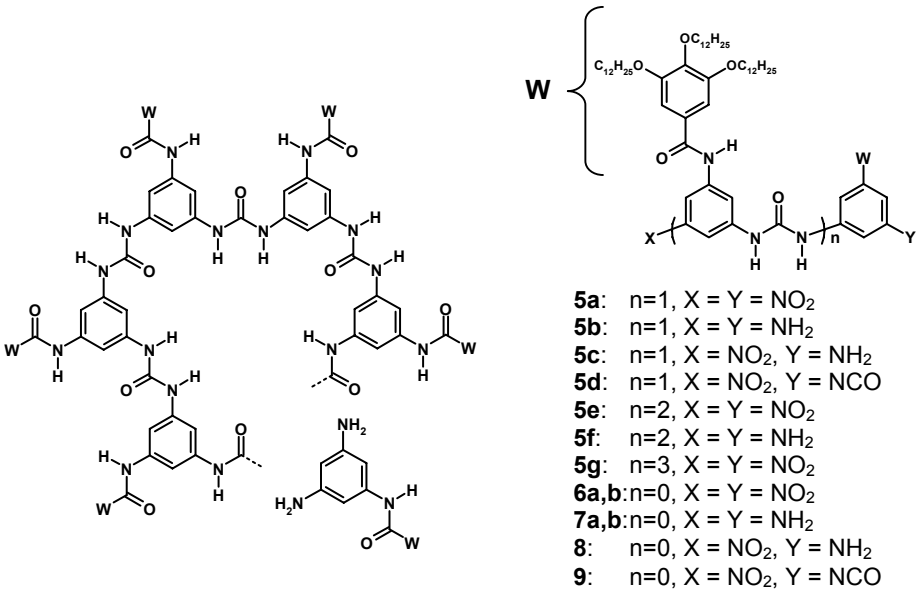

Figure 4.4. *Chemical structures of meta-phenylene-ureido foldamers **5**, next to the corresponding building blocks **6**-**9**. Building blocks **6b** and **7b** contain chiral (S)-3,7-dimethyloctyloxy chains instead of dodecyloxy groups (Scheme 4.1).*

4.2 Nitrogen centered triamides and asymmetrical disks

4.2.1 Synthesis

The synthesis of structures combining amide and urea functions requires introduction of asymmetry in the benzene-1,3,5-triamine core. First, the amine group of starting compound 3,5-dinitroaniline was converted to a solubilizing amide functionality using a 3,4,5-trialkoxybenzoyl chloride,[1a] in the presence of triethylamine (Scheme 4.1). Achiral compound **6a** contains dodecyloxy chains, while in chiral compound **6b** (*S*)-3,7-dimethyloctyloxy chains are present. The nitro groups of dinitro building blocks **6a/b** could be catalytically reduced with palladium on carbon, to give diamine building blocks **7a/b** quantitatively. Selective reduction could be ensured by use of formate as hydrogen source.[16] The reaction conditions for the selective reduction to give asymmetrical building block **8** are critical; the monoformamide and diamine **7a** are easily formed. The isocyanate functionality in asymmetrical building block **9** was introduced by treatment of mononitro monoamine **8** with an excess phosgene.

Scheme 4.1. *Synthesis of dinitro building blocks **6a/b**, diamino monomers **7a/b**, monoprotected unit **8**, and monoisocyanato mononitro unit **9** based on 3,5-dinitroaniline.*

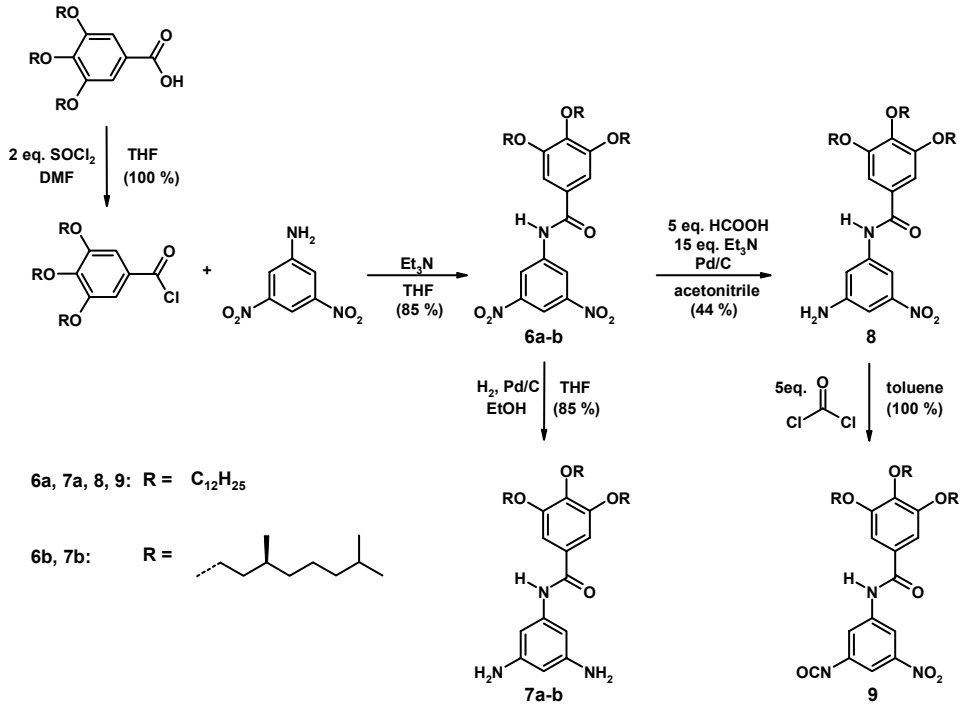

Diamino building blocks **7a/b** could be converted into discotics upon 'end capping' with acid chlorides (in case of **1g/h**) or isocyanates (in case of **3** and **4**). Both achiral (**1g**) and chiral (**1h**) nitrogen centered triamide disks were synthesized in good yield by treating diamine **7a/b** with 2 equivalents 3,4,5-trialkoxybenzoyl chloride (Scheme 4.2). Similarly, monoamide diurea disks **3** and **4** were obtained using 3,4,5-trialkoxybenzene isocyanate (Scheme 4.3).[17] Monoamide diurea disks **3** and **4** both contain one amide and two urea groups. Whereas disk **3** contains 6 chiral centers, which are connected to the core via the urea groups, disk **4** is equipped with 3 'chiral amide' functionalities.

Scheme 4.2. *Synthesis of nitrogen centered triamide disks **1g/h**.*

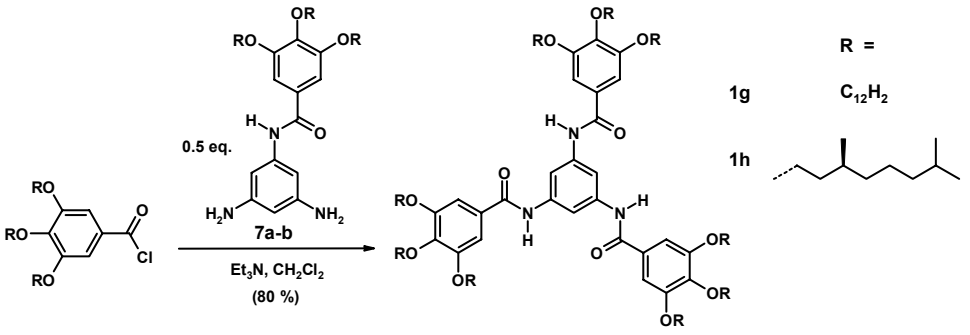

Scheme 4.3. *Synthesis of monoamide diurea disks **3** and **4**.*

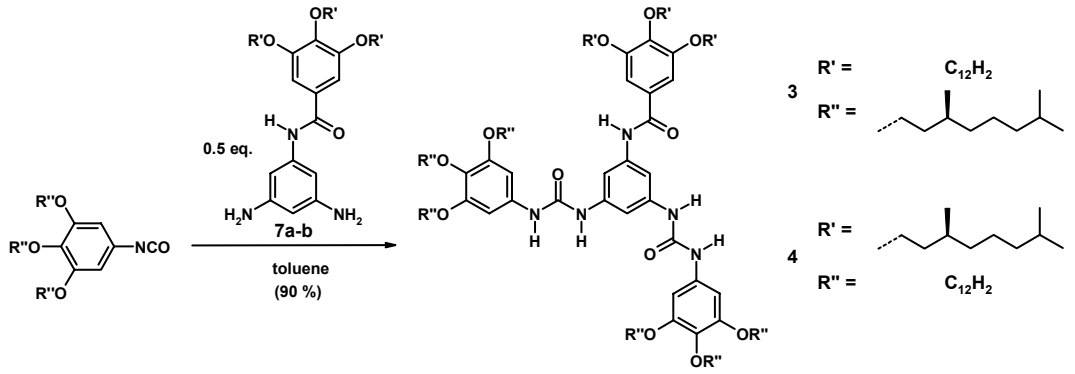

4.2.2 Self-assembly

Nitrogen centered C_3-symmetrical amide disk **1g** (achiral) shows liquid crystallinity (K (28 °C, 107 kJ/mol) M (154 °C, 53 kJ/mol) I), shown by the typical focal conic structures (Figure 4.5). Chiral nitrogen centered amide **1h** displays no liquid crystallinity and only one transition between the crystalline and isotropic phase was found (K (87 °C, 29 kJ/mol) I). Asymmetric disks **3** and **4** can be smeared and show birefringence from room temperature up to high temperatures, but no textures can be grown, as degradation occurs below the isotropization temperature (190 °C).

Figure 4.5. *Typical structure found in the liquid crystalline phase of nitrogen centered achiral amide disk **1g** (left) and crystals of chiral amide disk **1h** (right).*

The compounds were studied with IR spectroscopy by following the carbonyl stretch vibration in the solid state, and in 10^{-4} M heptane and chloroform solutions (Table 4.1). Carbonyl centered triamide **1c** is not (completely) aggregated in dilute apolar solution, while triurea **2c** is aggregated, as shown by similar carbonyl stretch vibrations in the solid state and in 10^{-4} M heptane solution. For nitrogen centered triamide **1g** a value is found in heptane, intermediate between that of the aggregated (solid) state and the molecularly dissolved one (chloroform). When monoamide diurea disk **3** was brought in heptane at a concentration of 10^{-2} M, a gel was formed. Unfortunately, no differentiation between the amide and urea signal was possible. Similar to triamide **1g**, the wavenumbers of monoamide diurea **3**, are not conclusive, at first glance.

Table 4.1. *Wavenumbers σ [cm^{-1}] of the carbonyl stretch vibrations of carbonyl centered triamide **1c**, triurea **2c**, nitrogen centered triamide **1g**, and monoamide diurea **3** in the solid state and in 10^{-4} M heptane or chloroform solutions.*

Compound	**1c**[a]	**2c**[a]	**1g**	**3**
σ solid state	1682 1664	1641	1645	1638
σ 10^{-4} M heptane	1670 1650	1641	1656	1650
σ 10^{-4} M chloroform	1676	1644 (1711)	1672	1681

[a] See Chapter 2.

However, in 10^{-2}–10^{-5} M tetrachloromethane solutions, infrared vibrations of monoamide diurea disk **3** are similar to those in the solid state (1644 cm^{-1}), indicating supramolecular architectures. In chloroform and toluene the molecules are only partly hydrogen bonded at higher concentrations (10^{-2} and 10^{-3} M). The (partial) aggregation in chloroform-*d1* was confirmed by ^{1}H-NMR spectroscopy, where broad signals were observed, in contrast to the sharp signals obtained in chloroform-*d1* / methanol-*d4* mixtures and in tetrahydrofuran-*d8*. As the NMR results of monoamide diurea disk **4** were comparable, the aggregation behavior in solution of asymmetrical disks **3** and **4** was judged similar at these concentrations.

C_3-symmetrical urea disks **2c/d** form supramolecular aggregates in dilute apolar solutions, while C_3-symmetrical carbonyl centered amide disks **1c/d** are not able to do so. Therefore, aggregate formation of the nitrogen centered C_3-symmetrical amide **1h** and the asymmetrical monoamide diurea disks **3** ('chiral urea') and **4** ('chiral amide'), was investigated with CD spectroscopy (Table 4.2).

Table 4.2[a]**.** *UV and CD data of carbonyl centered triamide **1d**, triurea **2d**, nitrogen centered triamide **1h**, and monoamide diureas **3** and **4**; λ_{max} [nm] = the absorption band most towards the red, and ε/Δε [l/mol.cm] = the intensity of the signal.*

No.	UV-Vis		CD	
	λ_{max}	ε	λ_{max}	Δε
1d[b]	308	2.1×10^4	-	-
2d[b]	259	5.1×10^4	275	-51.5
1h	286	4.8×10^4	-	-
3	261	4.0×10^4	265	-45.9
4	268	5.6×10^4	259	-45.1

[a] **1d**, **1h**, **3**, and UV of **4** measured at ~10^{-5} M and CD of **4** at ~10^{-4} M in heptane; **2d** measured at ~10^{-5} M in dodecane. [b] See Chapter 3.

Nitrogen centered amide **1h** does not show a Cotton effect in 10^{-4} M or 10^{-5} M heptane solutions. However, monoamide diurea disks **3** and **4** do show remarkable effects (Figure 4.6), resembling the signal of the C_3-symmetrical urea disk **2d** in shape and intensity. Temperature-dependent measurements with the C_3-symmetrical urea disk **2d** revealed that the compound was highly thermally resistant (135 °C) and that upon cooling 2 days were required for the original signal to restore. The Cotton effect of monoamide diurea **3** in a 10^{-5} M heptane solution has disappeared completely at 55 °C, and here also strong hysteresis was observed (approximately 2 days). The Cotton effect of monoamide diurea **4** in a 10^{-4} M heptane solution was only stable up to 30 °C. Furthermore, upon cooling not only kinetic effects were observed but also some irreversibility. After 2 days only ~25 % of the original intensity was reobtained.

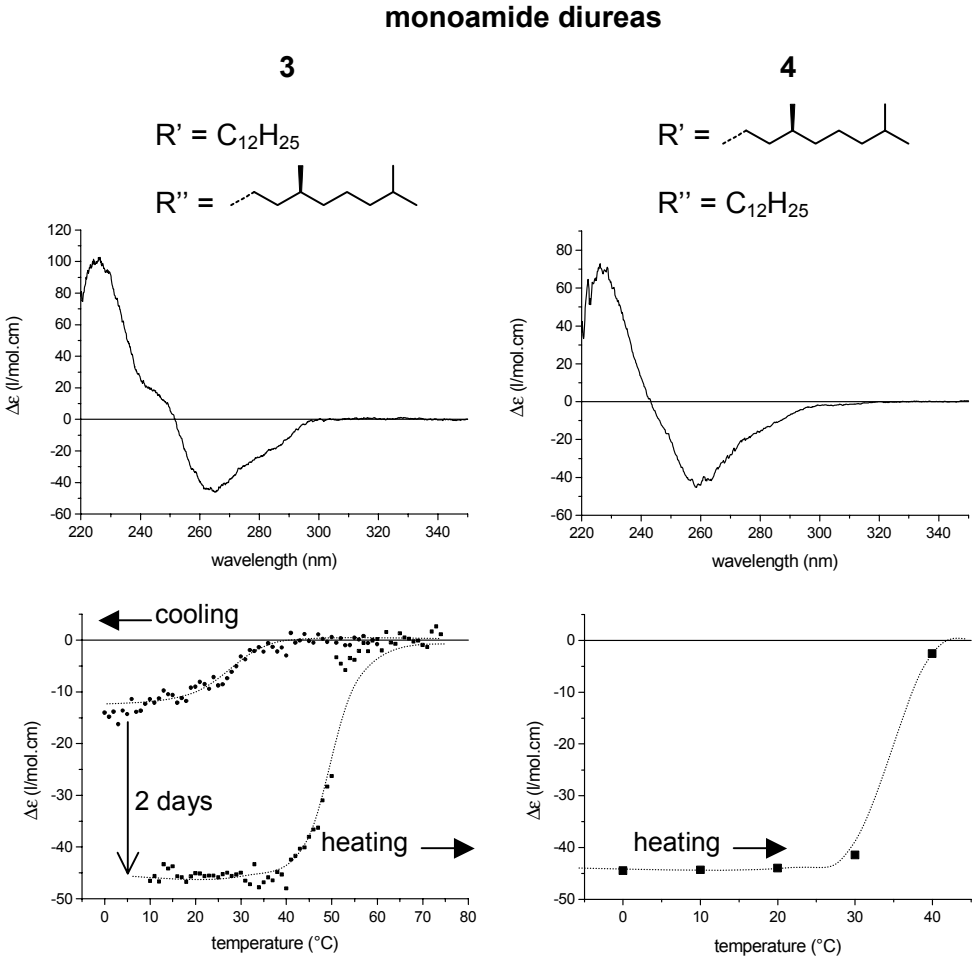

Figure 4.6. *CD spectra and temperature-dependent data of monoamide diurea disks **3** and **4** ('chiral urea' **3**: 10^{-5} M and 'chiral amide' **4**: 10^{-4} M in heptane).*

4.2.3 Asymmetrical scaffolds displaying specific amide-amide and urea-urea interactions

The absence of a liquid crystalline phase in nitrogen centered chiral amide **1h**, corresponds to the small liquid crystalline window shown by carbonyl centered chiral amide **1d** (Chapter 2). Achiral amide disks **1c** and **1g** both do form columnar liquid crystalline phases, but IR and CD measurements indicate that the (helical) columnar structure of medium-sized amide disks **1** is not retained in apolar solution. The similar behavior of the carbonyl centered triamides **1c/d** and the nitrogen centered triamides **1g/h** indicates that the difference in supramolecular aggregation between triamides **1c/d/g/h** and triureas **2c/d** is not caused by the difference in connectivity of the hydrogen bonding groups to the central benzene ring (via the carbonyl group or the nitrogen atom, respectively). Clearly, in comparison to triamide **1c/d**, the stronger hydrogen bonding of the urea groups in triurea **2c/d** increases the tendency to form helical, columnar architectures.

Asymmetrical disk **3**, with two 'chiral urea' groups and disk **4**, with one 'chiral amide' group, both show Cotton effects in CD spectroscopy and their absorptions are similar in shape and maxima. This means that the urea, as well as the amide part, is capable of transferring chirality to the ensemble of chromophores present in the molecule, implying that urea ánd amide groups are hydrogen bonded. The binding of all three groups is confirmed by the fact that the Cotton effects of monoamide diureas **3** and **4** resemble the effect displayed by triurea **2d** judged from shape, maxima, intensity and hysteresis (Table 4.2). As the intensity of the Cotton effect of **3** (6 chiral centers) is similar to that of **2d** (9 chiral centers), one might speak of a 'sergeants and soldiers' effect.[18] Presumably, asymmetrical disks **3** and **4** adopt conformations in which the amide and urea groups are tilted with respect to the central benzene ring in a propeller-like way, just like the symmetrical urea disks **2d** (Figure 4.7).

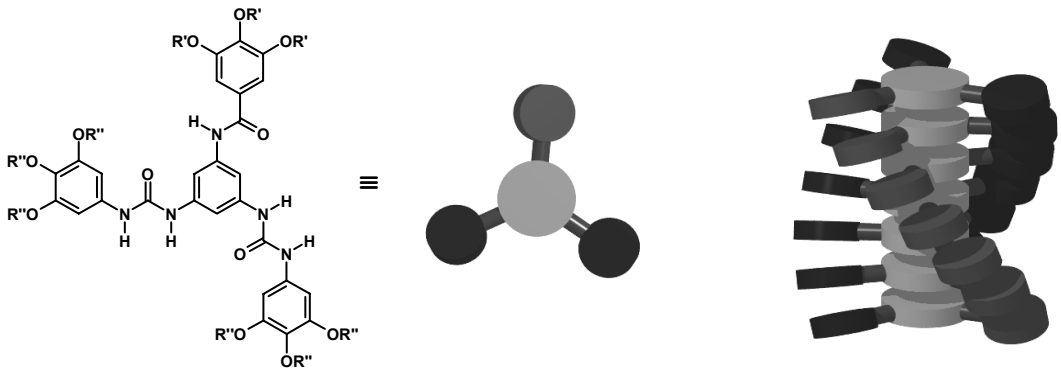

Figure 4.7. *Schemetical representation of the supposed conformations of monoamide diureas **3** and **4**, representing specific amide-amide and urea-urea interactions. Amide stacking is depicted in gray (top of disk and front of stack); urea stacking is depicted in black (bottom of disk and back of stack).*

From the presented CD data it is not obvious whether the monoamide diurea disks **3** and **4** are stacked urea by urea and amide by amide, or that also hydrogen bonds between amide and urea groups occur. From mixing experiments between triamides **1c/d** and triureas **2c/d** it was deduced that chiral amide disks **1d** (that do not form aggregates by themselves) cannot induce chirality when they

are mixed with achiral urea disks **2c** (Chapter 3). Assuming that this finding also applies to the asymmetrical disks **3** and **4**, this implies that only urea-urea and amide-amide hydrogen bonds occur. Presumably, aggregation is induced by the stronger urea interactions, and when in two superimposed disks two urea groups adopt a 'bent' conformation, the amide groups of the two disks are interacting, and a third hydrogen bond is formed, inducing the thermodynamically most favorable state. In conclusion, in asymmetrical 'medium' compounds **3** and **4** amide-amide hydrogen bonds can be formed, whereas in symmetrical 'medium' amide compounds **1g/h**, this is not possible.

Although the Cotton effects of monoamide diurea disks **3** and **4** are very similar, expression takes place at 10^{-5} M for 'chiral urea' **3**, while for 'chiral amide' **4** 10^{-4} M is needed. This could be rationalized by taking into account that **3** has 6 chiral centers and **4** has only 3, which renders transfer of chirality less efficient. However, when the UV maxima in 10^{-5} M solutions are examined (Table 4.2) , it is clear that values for the wavelength maximum and the intensity of 'chiral urea' **3** ($\lambda_{max,UV}$ = 261 nm, $\varepsilon = 4.0\times10^4$ l/mol.cm) are significantly smaller than those of 'chiral amide' **4** ($\lambda_{max,UV}$ = 268 nm, $\varepsilon = 5.6\times10^4$ l/mol.cm), suggesting that **3** is aggregated stronger than **4**.[19] This confirms that the stacking of the amides is induced by the stacking of the ureas. Supposedly, a stronger stack (a low $\lambda_{max,UV}$) is obtained when a 'propeller' is formed by rotation of both ureas and the amide in the same direction (either left or right). One can image that this is easier to achieve when 2 'chiral ureas' leave only 1 choice (left or right) for 1 'achiral amide', than when 1 'chiral amide' has to overrule the stronger interactions of 2 'achiral ureas'.The concepts postulated above, correspond to the behavior shown by the corresponding diurea [$\mathbf{4}^3$] (compound **4** in Chapter 3, Figure 4.8) The aggregate of diurea [$\mathbf{4}^3$] produces a Cotton effect of a completely different shape and of much less intensity (λ_{max} = 264 nm, $\Delta\varepsilon$ = +15 l/mol.cm). Furthermore, after the Cotton effect of the *m*-phenylene-diureido [$\mathbf{4}^3$] has disappeared at 80 °C, no hysteresis occurs upon cooling. This contrasts with the time-dependent behavior of triurea **2d**, and monoamide diureas **3** and **4**, providing additional evidence for the involvement of all three hydrogen bonding units in **3** and **4** in the supramolecular aggregate. It is supposed that another Cotton effect implies another supramolecular architecture. Probably, the urea groups of the *m*-phenylene-ureido [$\mathbf{4}^3$] adopt a 'linear' conformation, unlike the 'bent' position of the urea groups in **2d**, **3**, and **4**.

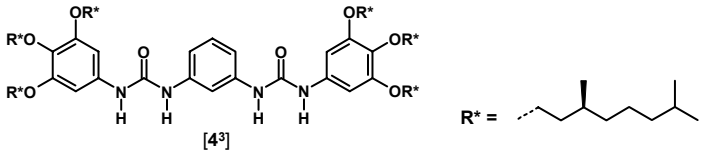

Figure 4.8. *Chemical structure of m-phenylene-diureido compound [$\mathbf{4}^3$] (compound **4** in Chapter 3).*

4.3 *meta*-Phenylene-ureido oligomers

4.3.1 Synthesis

Mononitro monoamine building block **8** could be converted in symmetrical dinitro monourea **5a** using half an equivalent of phosgene (Scheme 4.4). The nitro-groups of **5a** were reduced with hydrogen gas in the presence of palladium, yielding diamino monourea **5b**. This reduction took longer than the formation of corresponding dinitro building block **7a**, however. Asymmetrical monourea **5d** (one nitro and one isocyanato endgroup) is able to elongate the oligomers twice as fast as isocyanate **9**. Monourea **5c** (one nitro and one amino endgroup) was formed when symmetrical diamino building block **7a** was reacted only once with monoisocyanate **9**. Amine **5c** could be converted into isocyanate **5d**. However, to accomplish this, a large excess of phosgene and an elevated temperature were necessary. Combination of two equivalents isocyanate **9** with diamine **7a** gave the symmetrical nitro end capped diurea **5e**. The latter's nitro groups could only be reduced with H_2 under 3 atm. pressure, in the presence of active catalyst PtO_2 in an acidic environment and give diamine **5f**. Finally, treating monoamine **5c** with half an equivalent phosgene yielded the corresponding triurea **5g**. Urea oligomers **5** were characterized with ^{1}H-NMR, either in a mixture of chloroform-*d1* and methanol(-*d4*) or in tetrahydrofuran-*d8* at 50 °C, to obtain sharp signals. Remarkably, the amino substituted aromatic units of monourea **5f** are so electron rich that they undergo deuterium exchange along with urea and amide ones upon addition of methanol-*d4* to a chloroform-*d1* sample.

Scheme 4.4. *Synthesis of urea oligomers; monoureas **5a-d**, diureas **5e-f** and triurea **5g**.*

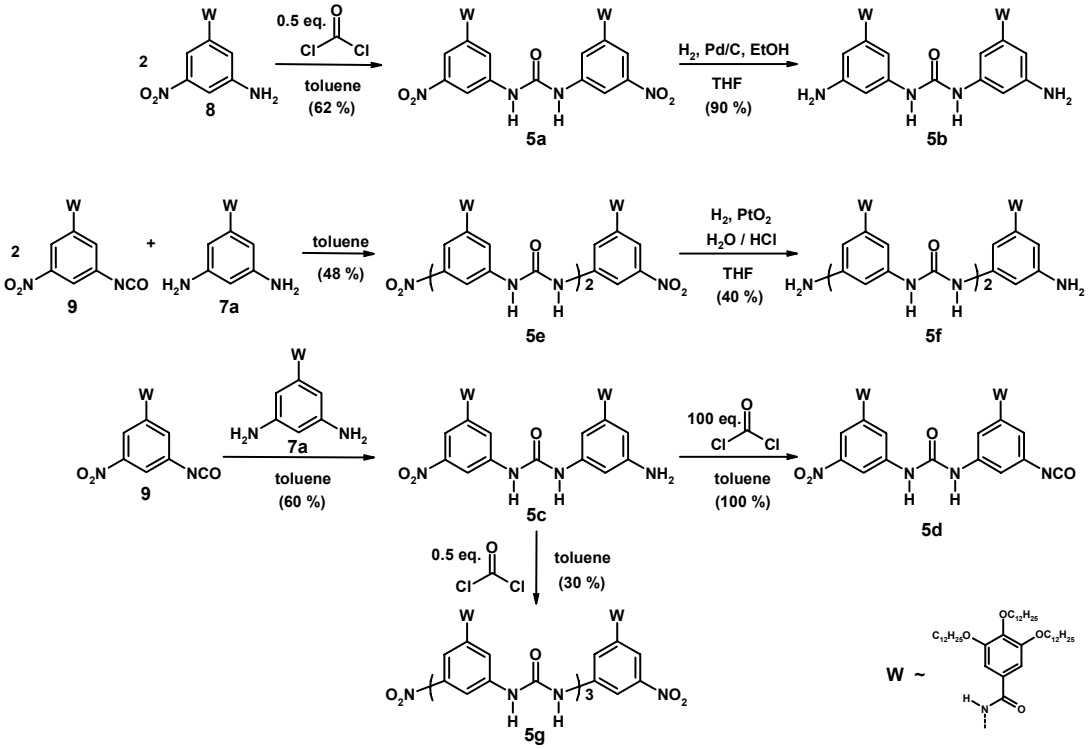

The synthesis of longer oligomers **5h,i,j** was persued by coupling two equivalents of monoisocyanate **5d** to one equivalent of diamines **7a**, **5b** and **5f**, respectively (Scheme 4.5). MALDI-TOF measurements show that the reaction mixtures contain not only the desired *m*-phenylene-ureido oligomers **5h-j**, but also starting materials and side products of lower molecular weight. After purifying tetraurea **5h** (chromatography BioBeads / tetrahydrofuran + 2.5 %v/v methanol), ^{1}H-NMR (THF-*d8*, 50 °C) shows only broad signals and in MALDI-TOF masses appear ranging from the diurea to the heptaurea (n=2 – n=7).

Scheme 4.5. *Attempted synthesis of longer oligomers **5h-j**.*

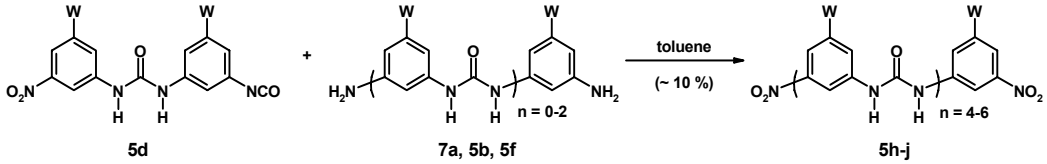

4.3.2 Conformational analysis

Achiral building blocks **6a**, **7a** and **8** show liquid crystalline mesophases, as follows from optical microscopy and DSC (Table 4.3). However, no indications for a mesophase of chiral dinitro building block **6b** could be found with these techniques. The cooling curve of chiral diamino building block **7b** shows 2 transitions (I (118 °C, -1.6 kJ/mol) M (36 °C, -0.2 kJ/mol) K), so this compound displays a thermotropic mesophase, despite the recrystallisation behavior in the heating run. In dinitro oligomers **5** liquid crystallinity is maintained, although no birefringent textures could be grown. The transition from the mesophase to the isotropic phase becomes less resolved for longer oligomers (**5h-j**).

Table 4.3.[a] *Transition temperatures T [°C] and corresponding enthalpies ΔH [kJ/mol] of building blocks **6a/b**, **7a/b**, and **8**; and m-phenylene-ureido oligomers **5a,e,g**.*

No.	K	T (*ΔH*)	M	T (*ΔH*)	M	T (*ΔH*)	I	No	K	T (*ΔH*)	M	T (*ΔH*)	I
6a	•	37 (*15*)	•			108 (*26*)	•	**5a**	•	-26 (*25*)	•	~100	•
6b	•	-	-			92 (*17*)	•	**5e**	•	-27 (*28*)	•	103 (*2.9*)	•
7a	•	-17 (*13*)	•	47 (*1.1*)	•	83 (*2.5*)	•	**5g**	•	-33 (*42*)	•	103 (*3.3*)	•
7b	•	44 (-8.4)	•	86 (*11.1*)	•	125 (*0.4*)	•						
8	•	-12 (*13*)	•			108 (*20*)	•						

[a] • = phase is observed; - = phase is not observed; K = crystalline phase; M = unidentified mesophase; I = isotropic phase.

Ureas **5c** (n=1), **5e** (n=2) and **5g** (n=3) are investigated with 2D-^{1}H-NMR (NOESY) in tetrahydrofuran-*d8* at 50 °C. With this technique a complete assignment of the signals is possible (Figure 4.9). Remarkably, proton **b** is positioned upfield with respect to proton **d**, although it is *ortho* to the nitro substituent. All three compounds show similar sets of cross-peaks. Only two interactions constrict the configuration in the backbone of this molecule. Firstly, a cross peak is observed between

urea protons **B** and **C** (Figure 4.9), showing that the urea protons are in a cisoid conformation. Secondly, near the nitro endgroups of the oligomer, rotation is restricted as well, judging from the absence of the crosspeak (**B**,**c**). In the molecularly dissolved state, the structure can rotate freely and may adopt numerous conformations.

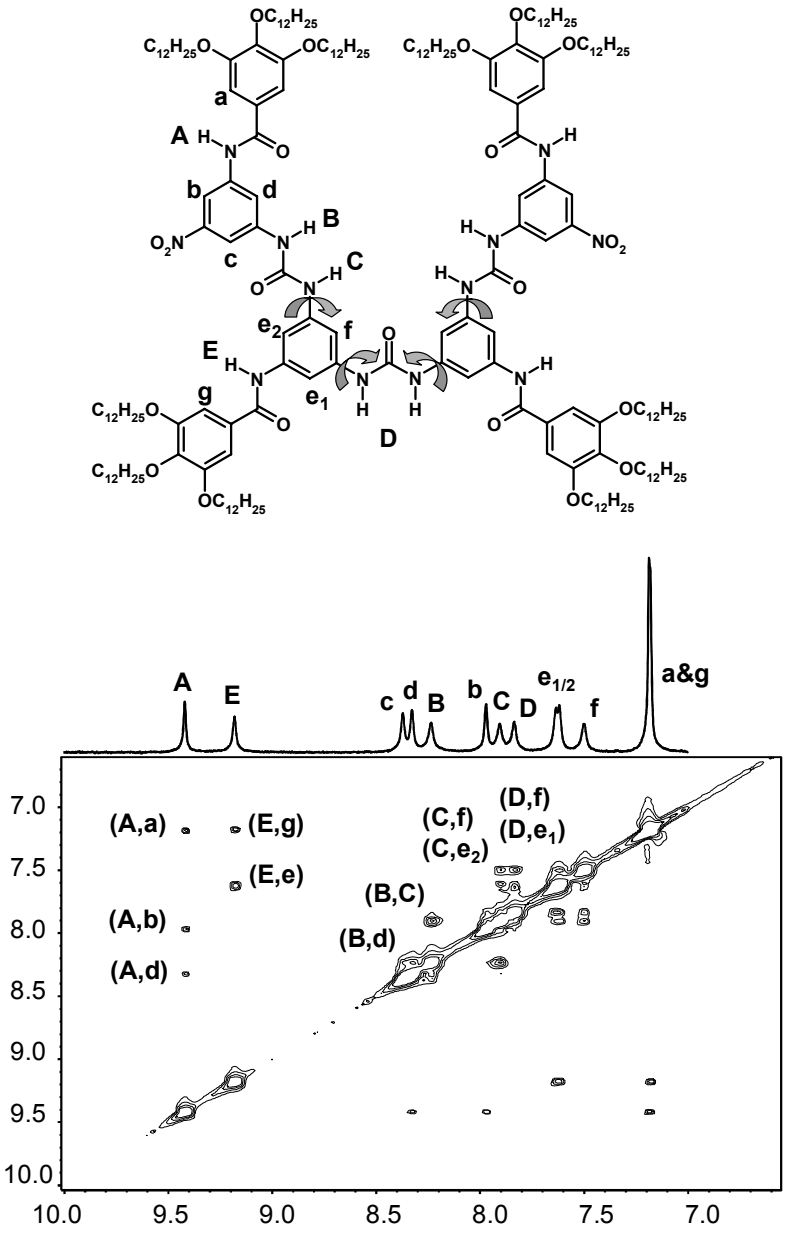

Figure 4.9. *Chemical structure and 2D ^{1}H-NMR spectrum of triurea oligomer **5g**.*

Apparently, in THF-*d8*, the *m*-phenylene-ureido oligomers are molecularly dissolved and possess rotational freedom. In $CDCl_3$, broad spectra are obtained, either due to aggregation phenomena, or because of the presence of many, slowly interconverting, conformations. Raising temperature or adding the hydrogen bond competitive solvent methanol does not sharpen the spectra, but both issues

might be overcome by complexation of the numerous amide and urea groups in the oligomers to negatively charged ions.[20] Indeed, sharp spectra were obtained upon addition of various tetrabutylammonium salts to chloroform solutions of dinitro monourea **5a**. In case of the the phosphate or the bromine, $(C_4H_9)_4N^+H_2PO_4^-$ and $(C_4H_9)_4N^+Br^-$, 2.5 eq. were sufficient. Also the nitrate (NO_3^-, 7.8 eq.), chloride (Cl^-, 10.5 eq.) or sulfate (HSO_4^-, ~15 eq.) could be used. One dimensional NOE proton NMR (Figure 4.10) indicates that dinitro monourea **5a** adopts a preferential, linear conformation in $CDCl_3$ solutions containing 17.9 eq. $(C_4H_9)_4N^+Cl^-$ (Figure 4.10). One aromatic proton (black triangle) undergoes through space interactions with both amide and urea protons, while the other two (black squares) do not interact with any other protons. In a $CDCl_3$ solution of **5a** containing 16.5 eq. $(C_4H_9)_4N^+NO_3^-$, also some additional interactions are observed (aromatic 8.45 ppm ■ and urea 10.4 ppm Δ), indicative of significant polulation of multiple conformations.

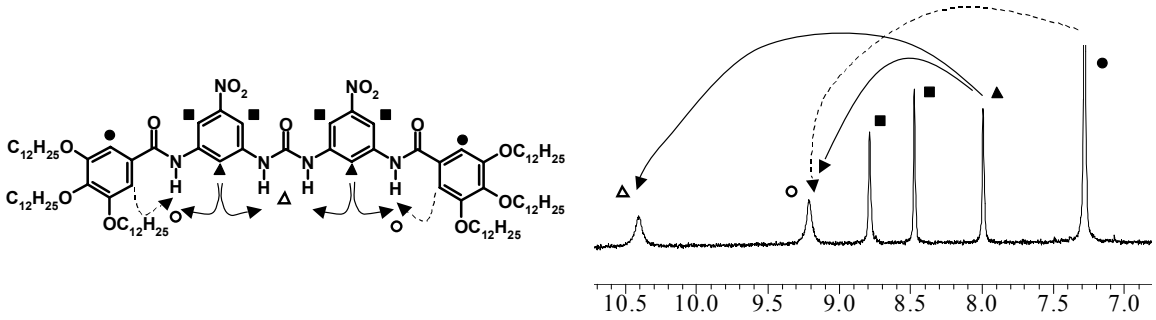

Figure 4.10. *One dimensional ^{1}H-NOE on dinitro monourea **5a** in $CDCl_3$ (2.5 mM) with 17.9 eq. $(C_4H_9)_4N^+Cl^-$.*

4.3.3 Undirectional aggregation

Typically, the reactive group interconversions of the *m*-phenylene-ureido oligomers **5** proceed considerably more difficult than those of the building blocks **6-9**. This is illustrated by the longer reaction time needed to reduce dinitro monourea **5a** to diamino monourea **5b**. Also, a more active catalyst is needed to reduce dinitro diurea **5e** to diamino diurea **5f**, and a large excess of phosgene has to be used to obtain monoisocyanate monourea **5d**. A possible explanation is that the reactive centers are more difficult to reach by the reagents because the substrates are larger and aggregate stronger. Not only the synthesis, but also the characterization becomes more tedious upon increasing the molecular weight. Where building blocks **6-9** were characterized by ^{1}H-NMR in chloroform, urea oligomers **5** only gave sharp signals in a mixture of chloroform and methanol or in tetrahydrofuran at 50 °C. Aggregation could also be the cause of the problems encountered in the synthesis and characterization of longer oligomers **5h-j**. Since peak broadening is already observed in ^{1}H-NMR spectra of mono-, di- and triureas **5a-g**, it is not surprising that raising temperature or addition of a hydrogen bond competitive solvent cannot overcome strong non-covalent interactions in long oligomers **5h-j**. Also the observation of longer and shorter chains in the MALDI-TOF spectrum of

tetraurea **5h** might be due to aggregation phenomena. Even after concentration of the tetraurea content by a size selective purification technique, the pure oligomer **5h** aggregates too strongly to be characterized with these analytical tools.

Although some order can be induced in *m*-phenylene-ureido oligomers **5**, resulting in thermotropic mesophases, no inherent preferential conformation is present in the molecularly dissolved state (THF-*d8*) of mono-, di-, and triureas **5c**, **5e**, and **5g**. Although a syn-conformation of the urea protons, and the ordering effect of the nitro endgroups is obvious, free rotation about the central urea groups is possible (Figure 4.9). Possibly, in a 'bad' solvent, e.g. heptane, that promotes hydrogen bonding, the conformation of the molecules becomes completely locked, but usually ^{1}H-NMR spectra become broad in the aggregated state, preventing 2D NMR techniques.[21] In chloroform the broad ^{1}H-NMR signals, either caused by aggregation or by the presence of multiple slowly interconverting conformers, can be sharpened by addition of negatively charged ions. Most probably the sharpening of the signals is due to complexation of these ions to the amide and urea groups. In case of a dinitro monourea **5a** solution in $CDCl_3$ with 17.9 eq. $(C_4H_9)_4N^+Cl^-$, this results in a single, extended conformation (Figure 4.10). Sharpening of the signal might also occur as a consequence of solvent polarity changes, because this extended conformation is also found in THF-*d8* in the absence of any salts.[22] However, the fact that methanol cannot change the spectral shape counteracts this. Furthermore, protons of dinitro monourea **5a** in $CDCl_3$ with 16.5 eq. $(C_4H_9)_4N^+NO_3^-$ display perfectly sharp signals, while NOE interactions still indicate some rotation around the central urea groups. In the preferred extended conformation, all 4 amide and urea protons are aligned. Since the largest ions (Br^- and $H_2PO_4^-$) display a stronger complexation than the smaller ions (Cl^- and NO_3^-), they might position themselves between amide and urea protons. More, and especially quantitative, investigations have to be performed to judge whether multiurea systems **5** would indeed make satisfactory ion sensors. Although the conformation of dinitro monourea **5a** seems linear upon addition of salts, the position of the nitro endgroups might be suitable for formation of a cavity, cycle, or helix.

4.3.4 Branched *m*-phenylene-ureido oligomers: mini-dendrimers

When diamine monourea **5b** is end capped with 2 equivalents of chiral 3,4,5-tri((*S*)-3,7-dimethyloctyloxy)benzoyl chloride, dumbbell molecule or mini-dendrimer **10** is obtained (Figure 4.11). Dumbbell **10** is a smearable solid at room temperature, and starts flowing at 70 °C. Upon cooling no structure is found with OPM, however. No CD-effect was found in heptane at 0.01 mM, although IR indicated at least partial hydrogen bonding (3350 cm^{-1} NH stretch and 1664 cm^{-1} CO stretch). When 1,3,5-benzenetriisocyanate (Chapter 2) is functionalized with 3 equivalents monoamine urea **5b**, branched hexa-urea **11** should be obtained. Because linear structures containing more than three urea groups could not be characterized due to excessive, kinetically hampered, intermolecular ordering, it is no surprise that 'dendrimer' **11** suffered from the same problems.

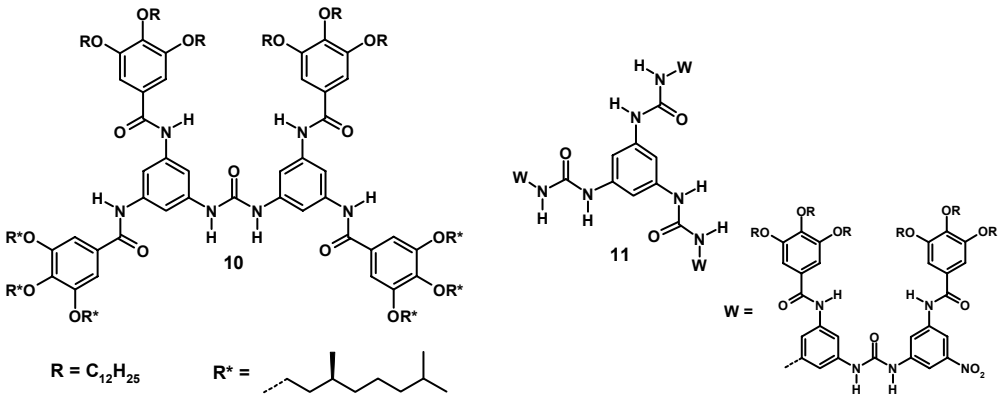

Figure 4.11. *Mini-dendrimers **10** and **11**.*

4.3.5 Considerations concerning the design of new helical oligomers

From the examples discussed above, it may become clear that expression of supramolecular chirality is not obvious for any structure being symmetrical and containing a substantial number of hydrogen bonds and/or π-π stacking groups. In medium-sized triamide disks (e.g. chiral carbonyl centered disk **1d**) the combination of amide-amide hydrogen bonding and π-π stacking between single benzene rings is not sufficient to form supramolecular assemblies in apolar solution. Most probably, the single additional urea group in mini-dendrimer **10** is not capable to raise intermolecular hydrogen bonding sufficiently for self-assemblies to be formed. Multiple urea groups are necesarry as present in triurea disks **2d** or asymmetrical disks **3** and **4**. In hexaurea mini-dendrimer **11**, intermolecular hydrogen bonding probably is very strong, trapping the structures in a kinetically determined situation. Imbalance between non-covalent interactions, which might be too weak or too strong, may prevent formation of ordered supramolecular architectures. Also a lack of directional interactions may prevent expression of supramolecular chirality. This is illustrated by dendritic fluorophores containing both phenylene vinylene and phenylene ethynylene moieties.[23]

These findings correspond to natural,[2,3] semi-natural,[24] as well as some synthetic foldamers[15] in which only 'weak' intramolecular hydrogen bonding is used to bend a foldamer into a helical conformation. Only when the chains are long enough, and contain enough of such 'weak' cooperative interactions, their 'native fold' becomes stable. In the next chapter, these leads will be discussed more elaborately, and followed upon in various new foldamer structures.

4.4 Conclusions

The library of discotics is expanded with nitrogen centered triamides **1g/h** and monoamide diureas **3** and **4**. Carbonyl centered triamides **1c/d** and nitrogen centered triamides **1g/h** show the same aggregation behavior. Only achiral compounds **1c/g** form columnar liquid crystalline phases in a reasonable temperature window, and no aggregation takes place in solution. This shows that connectivity of the hydrogen bonding groups does not greatly alter the aggregation behavior, implying that the stronger urea hydrogen bonding causes the triureas **2c/d** to form rigid rod-like aggregates, while the weaker amide hydrogen bonding prevents the triamides **1c/d** and **1g/h** to aggregate in dilute apolar solution.

Asymmetrical monoamide diurea disks **3** and **4** do show supramolecular aggregates in dilute apolar solution. The Cotton effects themselves and their time-dependent thermoreversible nature are reminescent of the behavior of triurea **2d**, and do not coincide with that of a *m*-phenylene-ureido moiety (compound **4** in Chapter 3). Furthermore, aggregates of disks **3**, containing 6 chiral centers connected via the urea groups, are formed easier than aggregates of disks **4**, containing only 3 chiral centers connected via the amide group. It is supposed that formation of helical supramolecular aggregates by asymmetrical disks **3** and **4** is initiated by urea-urea hydrogen bonding, and 'finetuned' by amide-amide intermolecular hydrogen bonding.

The concept of selective amide-amide and urea-urea stacking might prove helpful in ordering these functionalities. An attempt was made to apply the asymmetry in the helical folding of oligomeric *meta*-phenylene-ureido structures **5**. The structures were elongated via a stepwise approach, using diamino building block **7a** and nitro/isocyanate building block **9**. Tetra-, penta-, and hexaureas **5h-j** are expected to have the necessary length to complete one turn of a helix. However, they show strong but non-selective intermolecular interactions, despite the specific amide-amide and urea-urea intermolecular hydrogen bonding interactions displayed by asymmetrical disks **3** and **4**. The strong and undirectional interactions prevent endgroup reactivity, purification and characterization. NOESY ^{1}H-NMR cannot reveal any preferential conformation for monourea oligomer **5c**, diurea oligomer **5e** or triurea oligomer **5g** in THF-*d8*. Only restrictions are the *syn*-conformation of the urea protons, and those imposed by the nitro endgroups. On the other hand, amide and urea protons of dinitro monourea **5a** align in $CDCl_3$ upon complexation with tetrabutylammonium salts, particularly the bromide and phosphate. In this conformation, nitro groups might be positioned suitably to align functional groups, or extend the structure to a cavity, cycle or helix.

4.5 Experimental section

General. General aspects concerning synthesis, characterization, optical microscopy, DSC, and X-ray have been described in Chapter 2, whereas details about UV-Vis and CD spectroscopy can be found in Chapter 3. The syntheses of the following compounds have been described in Chapter 2: **1c/d**, **2c/d**, 3,4,5-tridodecyloxybenzoyl chloride, 3,4,5-tri((*S*)-3,7-dimethyloctyloxy)benzoyl chloride, 3,4,5-tridodecyloxybenzene isocyanate, and 3,4,5-tri((*S*)-3,7-dimethyloctyloxy)benzene isocyanate. ^{1}D-^{1}H-NOE experiments on dinitro monourea **5a** were performed using a dpfgnoe sequence (double pulse field gradient stimulated echo), with a 90° pulse of 7.45 and mixing times of 0.4 and 0.8 sec.

1,3,5-Tris-(3,4,5-tridodecyloxybenzoylamino)benzene (1g). A solution of 3,4,5-tridodecyloxybenzoyl chloride (0.49 g, 0.81 mmol) in dichloromethane (10 ml) was added dropwise to a solution of diamine **7a** (0.30 g, 0.38 mmol) and triethylamine (0.13 ml, 0.92 mmol) in dichloromethane (5 ml). After stirring overnight and evaporation of the dichloromethane, the crude product was purified using column chromatography (flash silica, gradient: chloroform / dichloromethane + 0-0.5 %v/v methanol, R_f = 0-0.3). Finally, white sticky solid **1g** (0.67 g, 83 %) was obtained: ^{1}H-NMR ($CDCl_3$) δ 8.24 (NH, s, 3H), 8.10 (H-ortho, s, 3H), 7.05 (H'-ortho, s, 6H), 3.98 (OCH_2, m, 18H), 1.80 (OCH_2CH_2, m, 18H), 1.46 ($OCH_2CH_2CH_2$, m, 18H), 1.26 ($(CH_2)_8$, m, 144H), 0.88 (CH_3, m, 27H) ppm; ^{13}C-NMR ($CDCl_3$) δ 165.9 (NHCO), 153.3 (C3'), 141.6 (C4'), 139.2 (C1), 129.1 (C1'), 107.1 (C2), 105.5 (C2'), 73.5, 69.3, 31.9, 30.4, 29.8, 29.7, 29.7, 29.7, 29.6, 29.5, 29.4, 26.1, 26.1, 22.7, 14.1 ppm; IR (ATR): 3278, 2921, 2852, 1645, 1615, 1581, 1536, 1499, 1455, 1385, 1332, 1220, 1112, 1003, 859, 760, 721, 677 cm^{-1}; Elemental analysis: calculated: $C_{135}H_{237}N_3O_{12}$ (2094.41): C, 77.42; H, 11.41; N, 2.01; found: C, 77.44; H, 10.66; N, 2.00; MALDI-TOF MS: calculated: 2093.81, found: 2116.63 (Na adduct).

1,3,5-Tris-[3,4,5-tri((*S*)-3,7-dimethyloctyloxy)benzoylamino]benzene (1h). Analogous to the previous procedure 3,4,5-tri((*S*)-3,7-dimethyloctyloxy)benzoyl chloride (1.0 g, 1.7 mmol) and diamine **7b** (0.56 g, 0.81 mmol), gave **1h** as a white sticky solid (1.18 g, 80 %): ^{1}H-NMR ($CDCl_3$) δ 8.05 (H-ortho, s, 3H), 8.01 (NH, s, 3H), 7.08 (H'-ortho, s, 6H), 4.07 (OCH_2, m, 18H), 1.88 - 0.86 (alkyl H, m, 171H) ppm; ^{13}C-NMR ($CDCl_3$) δ 165.8 (NHCO), 153.4 (C3'), 141.7 (C4'), 139.2 (C1), 129.2 (C1'), 106.7 (C2), 105.5 (C2'), 71.8, 67.7, 39.4, 39.3, 37.5, 37.4, 37.3, 36.4, 29.8, 29.7, 28.0, 24.7, 22.7, 22.6, 22.6, 19.6, 19.6 ppm; IR (ATR): 3284, 2954, 2925, 2870, 1650, 1616, 1583, 1551, 1501, 1464, 1429, 1384, 1329, 1216, 1110, 1045, 994, 956, 859, 753, 735, 687 cm^{-1}; Elemental analysis: calculated: $C_{117}H_{201}N_3O_{12}$ (1841.92): C, 76.30; H, 11.00; N, 2.28; found: C, 76.29; H, 10.46; N, 2.31; MALDI-TOF MS: calculated: 1841.52, found: 1864.59 (Na adduct).

N-{{3,5-Bis-{N'-[3,4,5-tri((*S*)-3,7-dimethyloctyloxy)-phenyl]-ureido}-phenyl}}-3,4,5-tridodecyloxybenzamide (3). A solution of 3,4,5-tri((*S*)-3,7-dimethyloctyloxy)benzoyl azide (0.59 g, 0.96 mmol) in dry toluene (9 ml) was refluxed for 2 h. The mixture was cooled to 80 °C, after which a solution of diamine **7a** (0.30 g, 0.38 mmol) in dry toluene (7 ml) was added dropwise. After stirring overnight the toluene was evaporated and the product dissolved in dichloromethane (15 ml). The solution was cooled with ice. This gave a precipitate that yielded white sticky solid **3** (0.70 g, 93 %) after filtration: ^{1}H-NMR ($CDCl_3$ / CH_3OH) δ 8.97 (amide NH, s, 1H), 8.14 (urea NH, s, 2H), 7.75 (urea NH, s, 2H), 7.54 (H-ortho, d, 2H), 7.27 (H-ortho, bs, 1H), 7.08 (H'-ortho, s, 2H), 6.64 (H''-ortho, s, 4H), 3.98 (OCH_2, m, 18H), 1.86 - 0.83 (alkyl H, m, 183 H) ppm; ^{13}C-NMR ($CDCl_3$ / CH_3OH) δ 166.7 (NHCO), 153.6 (C3'), 153.1 (C3''), 153.0 (NHCONH), 141.2 (C4''), 140.0 (C1), 138.9 (C3), 134.2 (C1''), 133.9 (C4''), 129.3 (C1''), 105.7 (C2/4), 105.3 (C2'), 98.6 (C2''), 73.5, 71.7, 69.2, 67.2, 39.3, 39.2, 37.5, 37.3, 37.2, 36.4, 31.8, 30.3, 29.7, 29.7, 29.6, 29.6, 29.6, 29.5, 29.4, 29.3, 29.3, 27.9, 26.0, 26.0, 24.7, 24.6, 22.6, 22.5, 22.5, 19.5, 19.3, 14.0 ppm; IR (ATR): 3319, 2954, 2923, 2854, 1638, 1603, 1555, 1504, 1457, 1427, 1383, 1329, 1224, 1117, 1003, 824, 754, 719 cm^{-1}; Elemental analysis: calculated: $C_{123}H_{215}N_5O_{12}$ (1956.11): C, 75.53; H, 11.08; N, 3.58; found: C, 74.52; H, 10.39; N, 3.52; MALDI-TOF MS: calculated: 1955.64, found: 1978.22 (Na adduct).

N-{{3,5-Bis-[N'-(3,4,5-tridodecyloxyphenyl)-ureido]-phenyl}-3,4,5-tri((*S*)-3,7-dimethyloctyloxy)benzamide (4). Analogous to the previous procedure 3,4,5-tridodecyloxybenzoyl azide (1.0 g, 1.4 mmol) and diamine **7b** (0.47 g, 0.68 mmol) afforded after additional column chromatography (flash silica, dichloromethane + 0-0.5 %v/v methanol, R_f = 0-0.1) white/brown sticky solid **4** (1.2 g, 87 %): ^{1}H-NMR (THF-*d8*) δ 9.27 (amide NH, s, 1H), 7.89 (urea NH, s, 2H), 7.56 (H-ortho, bs, 2H), 7.48 (urea NH, s, 2H), 7.34 (H-ortho, bs, 1H), 7.06 (H'-ortho, s, 2H), 6.56 (H''-ortho, s, 4H), 3.85 (OCH_2, m, 6H), 3.67 (OCH_2, m, 12H), 1.69 - 0.64 (alkyl H, m, 195 H) ppm; ^{13}C-NMR (THF-*d8*) δ 167.0 (NHCO), 155.0, 154.9 (C3', C3''), 154.5 (NHCONH), 143.2 (C4'), 142.6 (C1), 142.3 (C3), 137.4 (C1''), 135.7 (C4''), 132.2 (C1'), 108.3 (C2/4), 105.7 (C2'), 99.7 (C2''), 74.6, 72.9, 70.6, 69.1, 41.4, 71.3, 39.6, 39.5, 38.6, 33.9, 32.5, 31.9, 31.8, 31.8, 31.8, 31.7, 31.6, 31.6, 31.4, 30.0, 28.3, 28.2, 26.8, 26.8, 24.6, 24.2, 24.1, 21.2, 21.0, 15.5 ppm; IR (ATR): 3288, 2954, 2922, 2853, 1644, 1604, 1557, 1503, 1467, 1425, 1384, 1333, 1225, 1117, 1004, 826, 757, 719 cm^{-1}; Elemental analysis: calculated: $C_{129}H_{227}N_5O_{12}$ (2040.27): C, 75.94; H, 11.21; N, 3.43; found: C, 74.69; H, 10.39; N, 3.38; MALDI-TOF MS: calculated: 2039.73, found: 2039.85.

N,N'-Bis[5-Nitro-1-(3,4,5-tridodecyloxy)benzoylamino-3-phenyl]urea (5a). The mononitro monoamine building block **8** (0.20 g, 0. 25 mmol) was stirred for an hour in dry toluene (10 ml) while slowly adding a solution of phosgene in toluene (20 %w/w, 61 mg, 0.12 mmol). After evaporation of the solvent the yellow sticky product was purified using column chromatography (flash silica, CH_2Cl_2 + 1 % Et_3N + 0-2 % MeOH, R_f = 0.3). The yield of **5a** was quantitative (0.20 g, 100 %): ^{1}H-NMR (THF-*d8*) δ 9.49 (NHCO, s, 2H), 9.31 (NHCONH, bs, 2H), 8.39 (H4, s, 2H), 8.20 (H2, s, 2H), 8.01 (H6, s, 2H), 7.11 (H2', s, 4H), 3.90 (OCH_2, m, 12H), 1.67 (OCH_2CH_2, m, 12H), 1.43 ($OCH_2CH_2CH_2$, m, 12H), 1.25 ($(CH_2)_8$, m, 96H), 0.84 (CH_3, m, 18H) ppm; ^{13}C-NMR (THF-*d8*) δ 165.5 (NHCO), 153.1 (C3'), 152.3 (NHCONH), 149.0 (C5), 141.9 (C3), 141.5 (C4'), 141.4, 141.0 (C1), 129.4 (C1'), 114.5 (C2), 108.1, 107.6 (C6, C4), 106.6 (C2'), 72.9 (C4'O$\underline{C}H_2$), 69.1 (C3'O$\underline{C}H_2$), 32.1, 32.1, 30.6, 30.0, 29.9, 29.9, 29.8, 29.8, 29.8, 29.7, 29.6, 29.5, 29.5, 26.3, 22.7 ($(CH_2)_{10}$), 13.6 (CH_3) ppm; IR (ATR): 3299, 3094, 2921, 2852, 1715, 1651, 1603, 1581, 1531, 1499, 1465, 1427, 1333, 1211, 1114, 1001, 875, 746 cm^{-1}; Elemental analysis: calculated: $C_{99}H_{164}N_6O_{13}$ (1646.44): C, 72.22; H, 10.04; N, 5.10; found: C, 71.31; H, 9.87; N, 5.59; MALDI-TOF MS: calculated: 1646.24, found: 1669.05 (Na-adduct).

N,N'-Bis[5-Amino-1-(3,4,5-tridodecyloxy)benzoylamino-3-phenyl]urea (5b). The dinitro monourea **5a** (0.10 g, 0.061 mmol), palladium on carbon (10 %w/w, 6.4 mg, 0.0061 mmol), ethanol (0.6 ml) and THF (4.2 ml) were shaken overnight under a hydrogen atmosphere (~40 psi). The reaction mixture was diluted with CH_2Cl_2 and filtered over 3 paper filters to remove the catalyst. The solvent was evaporated and the product purified using column chromatography (flash silica, CH_2Cl_2 + 1 % Et_3N + 0-3 % MeOH, R_f = 0.1) yielding sticky white solid **5b** (0.087 g, 90 %): ^{1}H-NMR ($CDCl_3$ + 10 %v/v CD_3OD) δ 8.8 (residual NHCO, s, 2H), 8.2 (residual NHCONH, s, 2H), 7.12 (H2', s, 4H), 7.00 (H2, m, 2H), 6.94 (H6, m, 2H), 6.74 (H4, m, 2H), 4.05 (OCH_2, m, 12H), 3.15 (residual NH_2, s, 4H), 1.83, 1.76 (OCH_2CH_2, m, 12H), 1.49 ($OCH_2CH_2CH_2$, m, 12H), 1.27 ($(CH_2)_8$, m, 96H), 0.88 (CH_3, m, 18H) ppm; ^{13}C-NMR ($CDCl_3$ + 10 %v/v CD_3OD) δ 166.5 (NHCO), 153.4 (C3'), 152.7 (NHCONH), 146.3 (C5), 140.7 (C4'), 139.7 (C3), 139.1, 139.0 (C1), 129.5 (C1'), 105.8 (C2'), 102.6 (C2, C4, C6), 73.4 (C4'O$\underline{C}H_2$), 69.0 (C3'O$\underline{C}H_2$), 31.6, 30.0, 29.4, 29.4, 29.4, 29.4, 29.4, 29.3, 29.1, 29.1, 29.1, 29.1, 25.8, 25.8, 22.4 ($(CH_2)_{10}$), 13.7 (CH_3) ppm; IR (ATR): 3330, 2922, 2852, 1687, 1615, 1582, 1539, 1499, 1441, 1333, 1219, 1114, 1036, 851, 807, 752, 721 cm^{-1}; MALDI-TOF MS: calculated: 1586.29, found: 1609.21 (Na-adduct).

N-[5-Amino-1-(3,4,5-tridodecyloxy)benzoylamino-3-phenyl]-N'-[5-Nitro-1-(3,4,5-tridodecyloxy)benzoyl-amino-3-phenyl]urea (5c). Under cooling with an ice bath a solution of the isocyanate building block **9** (0.11 g, 0.098 mmol) in dry toluene (10 ml) was added to the diamine building block **7a** (0.094 g, 0.12 mmol) in dry toluene (10 ml). After 2 hours toluene was evaporated and the product was purified by column chromatography (flash silica, CH_2Cl_2 + 1 % Et_3N + 0-2 % MeOH, R_f = 0.3), which yielded 0.05 g (22 %) of dinitro diurea **5a** and 0.09 g (59 %) of the desired yellow sticky solid **5c**: ^{1}H-NMR (THF-*d8*) δ 9.59 ($NHCO_{NO2}$, s, 1H), 8.98 ($NHCO_{NH2}$, s, 1H), 8.70 ($NHCONH_{NO2}$, s, 1H), 8.42 ($H4_{NO2}$, s, 1H), 8.30 ($H2_{NO2}$, s, 1H), 8.11 ($H6_{NO2}$, s, 1H), 8.04 ($NHCONH_{NH2}$, s, 1H), 7.19 ($H2'_{NO2}$, s, 2H) , 7.15 ($H2'_{NH2}$, s, 2H), 7.14 ($H2_{NH2}$, s, 1H), 6.83 ($H6_{NH2}$, s, 1H), 6.63 ($H4_{NH2}$, s, 1H), 4.69 (NH_2, s, 2H), 3.96 (OCH_2, m, 12H), 1.77 (OCH_2CH_2, m, 12H,), 1.47 ($OCH_2CH_2CH_2$, m, 12H), 1.25 ($(CH_2)_8$, m, 96H), 0.83 (CH_3, m, 18H) ppm, ^{13}C-NMR ($CDCl_3$ + 10 %v/v CD_3OD) δ 166.6, 166.5 ($NHCO_{NO2}$, $NHCO_{NH2}$) ($C3'_{NO2}$, $C3'_{NH2}$), 152.9 (NHCONH), 148.6 ($C5_{NO2}$), 147.5 ($C5_{NH2}$), 141.3 ($C3_{NO2}$), 141.0 ($C4'_{NO2}$), 140.4 ($C3_{NH2}$), 139.6 , 139.5, 139.2 ($C4'_{NH2}$, $C1_{NO2}$, $C1_{NH2}$), 129.5, 128.7 ($C1'_{NO2}$, $C1'_{NH2}$), 115.6 ($C2_{NO2}$), 109.2, 108.7($C6_{NO2}$, $C4_{NO2}$), 106.0, 105.8 ($C2'_{NO2}$, $C2'_{NH2}$), 102.6, 102.2, 102.0 ($C6_{NH2}$, $C4_{NH2}$, $C2_{NH2}$), 73.5 (C4'O$\underline{C}H_2$), 69.2 (C3'O$\underline{C}H_2$), 31.8, 30.2, 29.6, 29.6, 29.6, 29.5, 29.5, 29.5, 29.3, 29.2, 29.2, 26.0, 26.0, 22.5 ($(CH_2)_{10}$), 13.9 (CH_3) ppm; IR (ATR): 3335, 2921, 2852, 1623, 1581, 1531, 1500, 1466, 1429, 1333, 1213, 1114, 1001, 851, 747, 721, 683 cm^{-1}.

N-[5-Isocyanato-1-(3,4,5-tridodecyloxy)benzoylamino-3-phenyl]-N'-[5-Nitro-1-(3,4,5-tridodecyloxy)-benzoylamino-3-phenyl]urea (5d). At 80 °C the mononitro monoamine monourea **5c** (20 mg, 0.021 mmol) in dry toluene (1 ml) was slowly added to a solution of phosgene in toluene (20 %w/w, 1.3 ml, 12.4 mmol) and stirred overnight. The solvent was evaporated and product **5d** (~20 mg, 100 %) used as such: ^{1}H-NMR (THF-*d8*) δ 9.59 ($NHCO_{NO2}$, s, 1H,), 9.31 ($NHCO_{NCO}$, s, 1H), 8.72 ($NHCONH_{NO2}$, s, 1H), 8.39 ($NHCONH_{NCO}$, $H4_{NO2}$, s, 2H), 8.31 ($H2_{NO2}$, s, 1H), 8.14 ($H6_{NO2}$, s, 1H), 7.83 ($H2_{NCO}$, s, 1H), 7.26 and 7.20 ($H6_{NCO}$ and $H4_{NCO}$, s, 2H), 7.20 ($H2'_{NO2}$, s, 2H), 7.15 ($H2'_{NCO}$, s, 2H), 3.96 (OCH_2, m, 12H), 1.75 (OCH_2CH_2, m, 12H), 1.47 ($OCH_2CH_2CH_2$, m, 12H), 1.25 ($(CH_2)_8$, m, 96H), 0.83 (CH_3, m, 18H) ppm; IR (ATR): 3300, 2921, 2852, 2260, 1720, 1650, 1606, 1582, 1533, 1501, 1465, 1427, 1334, 1260, 1207, 1115, 1017, 854, 801, 748, 720, 677, 664 cm^{-1}.

N-{{3,5-Bis{[5-nitro-1-(3,4,5-tridodecyloxy)benzoylamino]-3-phenyl-N'-ureido}-phenyl}}-3,4,5-tridodecyl-oxybenzamide (5e). The mononitro monoisocyanato building block **9** (0.20 g, 0.24 mmol) and the diamine building block **7a** (0.094 g, 0.12 mmol) were stirred during 2 hours in dry toluene (20 ml). After evaporation of the toluene and column chromatography both the mononitro monoamine monourea **5c** (flash silica, CH_2Cl_2 + 1 % Et_3N + 2 % MeOH, R_f = 0.3; 0.04 g, 21 %) and the desired sticky yellow solid **5e** (flash silica, CH_2Cl_2 + 0-1

% Et_3N, R_f = 0.9) (0.14 g, 48 %) were obtained: ^{1}H-NMR (THF-*d8*, 50 °C) δ 9.48 ($NHCO_{out}$, s, 2H), 9.30 ($NHCO_{in}$, s, 1H), 8.33 ($NHCONH_{out}$, s, 2H), 8.28 ($H4_{out}$, s, 2H), 8.26 ($H2_{out}$, s, 2H), 8.00 ($NHCONH_{in}$, s, 2H), 7.97 ($H6_{out}$, s, 2H), 7.66 ($H2_{in}$, s, 2H), 7.44 ($H4_{in}$, s, 1H), 7.18 (H-2', s, 6H), 3.94 (OCH_2, m, 18H), 1.73 (OCH_2CH_2, m, 18H), 1.45 ($OCH_2CH_2CH_2$, m, 18H), 1.26 ($(CH_2)_8$, m, 144H), 0.83 (CH_3, m, 27H) ppm; ^{13}C-NMR (THF-*d8*) δ 165.8, ($NHCO_{in}$), 165.6($NHCO_{out}$), 153.1, 153.0 ($C3'_{in}$, $C3'_{out}$), 152.4 (NHCONH), 148.9 ($C5_{NO2}$), 141.8, 141.6, 141.5, 140.7, 140.2, 140.2 ($C4'_{in/out}$, $C3_{NO2}$, C1, C3), 130.0, 128.8 ($C1'_{in}$, $C1'_{out}$), 114.8 ($C2_{NO2}$), 108.0 ($C6_{NO2}$), 107.7 ($C4_{NO2}$), 106.5 ($C2'_{in}$), 105.1 ($C2'_{out}$), 104.6 (C2, C4), 72.9, 72.9 (C4'O$\underline{C}H_2$), 69.1, 69.0 (C3'O$\underline{C}H_2$), 32.1, 30.6, 30.0, 30.0, 29.2, 29.9, 29.9, 29.8, 29.7, 29.7, 29.5, 26.4, 22.8 ($(CH_2)_{10}$), 13.7 (CH_3) ppm; IR (ATR): 3329, 2921, 2852, 1650, 1581, 1532, 1499, 1428, 1333, 1210, 1114, 1031, 874, 746, 721, 666 cm^{-1}; MALDI-TOF MS: calculated: 2451.87, found: 2474.29 (Na-adduct).

N-{{3,5-Bis{[5-amino-1-(3,4,5-tridodecyloxy)benzoylamino]-3-phenyl-N'-ureido}-phenyl}}-3,4,5-tridodecyloxybenzamide (5f). The dinitro diurea **5e** (0.10 g, 0.041 mmol), PtO_2 (10 mg, 0.044 mmol), THF (5 ml) and aqueous HCl-solution (0.5 ml, pH=1) were shaken for 2.5 days under a hydrogen atmosphere (~60 psi). The reaction mixture was diluted with CH_2Cl_2 (20 ml) and filtered over 3 paper filters to remove the catalyst. After evaporation of the solvent the product was purified using column chromatography (flash silica, CH_2Cl_2 + 1 % Et_3N + 0-1 % MeOH, R_f = 0.1). Finally, off-white solid **5f** (0.04 g, 41 %) was obtained: MALDI-TOF MS: calculated: 2391.92, found: 2414.24 (Na-adduct).

N,N'-Bis{1-(3,4,5-tridodecyloxybenzoylamino)-3-[1-(3,4,5-tridodecyloxybenzoylamino)-5-nitro-3-phenyl-N'-ureido]-5-phenyl}urea (5g). The mononitro monoamine monourea **5c** (0.22 g, 0.14 mmol) was stirred for 4 hours in dry toluene (10 ml) while slowly adding a solution of phosgene in toluene (20 %w/w, 34 mg, 0.068 mmol). The desired product **5g** was obtained in pure form (30 mg, 9 %) after repetitive column chromatography (flash silica, CH_2Cl_2 + 0-1 % Et_3N; Bio Beads S-X1, THF, followed by washing with MeOH to remove the stabilizer BHT or silica / CH_2Cl_2 filtration to remove THF degradation products): ^{1}H-NMR (THF-*d8*, 50 °C) δ 9.42 ($NHCO_{out}$, s, 2H), 9.18 ($NHCO_{in}$, s, 2H), 8.37 ($H4_{out}$, s, 2H), 8.33 ($H2_{out}$, s, 2H), 8.24 ($NHCONH_{out}$, s, 2H), 7.97 ($H6_{out}$, s, 2H), 7.91 ($NHCONH_{middle}$, s, 2H), 7.84 ($NHCONH_{in}$, s, 2H), 7.64 and 7.62 ($H2/6_{in}$, s, 4H), 7.50 ($H4_{in}$, s, 2H), 7.19 (H2', s, 8H), 3.97 (OCH_2, m, 24H), 1.74 (OCH_2CH_2, m, 24H), 1.47 ($OCH_2CH_2CH_2$, m, 24H), 1.25 ($(CH_2)_8$, m, 192H), 0.83 (CH_3, m, 36H) ppm; ^{13}C-NMR (THF-*d8*) δ 165.5, 165.5 (NHCO), 153.2, 153.1 (C3'), 152.2 (NHCONH), 149.2 ($C5_{NO2}$), 142.3, 141.9, 141.7, 140.8, 140.7, 140.4, 140.2, 130.4, 129.6 (C1'), 114.6 $C2_{out}$), 107.9, 107.0, 107.0, 104.6 ($C2/4_{in}$), 73.0, 72.9 (C4'O$\underline{C}H_2$), 69.4, 69.3 (C3'O$\underline{C}H_2$), 32.0, 30.6, 29.8, 29.8, 29.8, 29.7, 29.7, 29.6, 29.6, 29.4, 29.4, 29.3, 29.3, 22.6, 13.5 (CH_3) ppm; IR (ATR): 3317, 2921, 2852, 1648, 1615, 1581, 1532, 1500, 1456, 1429, 1334, 1259, 1211, 1114, 1016, 861, 797, 747, 721 cm^{-1}; MALDI-TOF MS: calculated: 3258.50, found: 3280.86 (Na-adduct).

N-(3,5-Dinitrophenyl)-3,4,5-tridodecyloxy-benzamide (6a). A solution of 3,4,5-tridodecyloxybenzoyl chloride (11.4 g, 16.4 mmol) in dry THF (150 ml) was added to 3,5-dinitroaniline (3.0 g, 16.4 mmol) and triethylamine (2.8 ml, 19.7 mmol) in dry THF (150 ml). After stirring overnight at 75 ºC the solvent was evaporated and the product purified with column chromatography (silica, hexane / ethyl acetate 8/2, R_f = 0.3) in combination with recrystallisation from hexane / ethyl acetate 9/1 to remove minor impurities or washing with methanol to remove 3,5-dinitroaniline. Finally, pure yellow solid **6a** (11.2 g, 81 %) was obtained: ^{1}H-NMR ($CDCl_3$) δ 8.94 (H2, d, 2H), 8.78 (H4, t, 1H), 8.46 (NHCO, s, 1H), 7.02 (H2', s, 2H), 4.01 (OCH_2, m, 6H), 1.79 - 1.72 (OCH_2CH_2, m, 6H), 1.44 ($OCH_2CH_2CH_2$, m, 6H), 1.26 ($(CH_2)_8$, m, 48H), 0.88 (CH_3, m, 9H) ppm; ^{13}C-NMR ($CDCl_3$) δ 166.0 (NHCO), 153.3 (C3'), 148.8 (C3), 142.2 (C1), 140.5 (C4'), 127.8 (C1'), 119.6 (C2), 113.6 (C4), 105.8 (C2'), 73.7, 69.5, 31.9, 30.3, 29.7, 29.6, 29.5, 29.4, 29.4, 29.3, 29.3, 26.1, 26.0, 22.7, 14.1 ppm; IR (ATR): 3418, 2916, 2848, 1676, 1585, 1541, 1498, 1467, 1429, 1347, 1336, 1202, 1120, 989, 894, 750, 726 cm^{-1}; Elemental analysis: calculated: $C_{49}H_{81}N_3O_8$ (840.19): C, 70.05; H, 9.72; N, 5.00; found: C, 70.45; H, 9.79; N, 4.86.

N-(3,5-Dinitrophenyl)-3,4,5-tri((*S*)-3,7-dimethyloctyloxy)-benzamide (6b). Analogous to the previous procedure 3,4,5-tri((*S*)-3,7-dimethyloctyloxy)benzoyl chloride (8.8 g, 14.4 mmol) gave yellow solid **6b** (9.5 g, 87 %): ^{1}H-NMR ($CDCl_3$) δ 8.94 (H2, d, 2H), 8.77 (H4, t, 1H), 8.43 (NHCO, s, 1H), 7.07 (H2', s, 2H), 4.05 (OCH_2, m, 6H), 1.89 - 0.86 (alkyl H, m, 57H) ppm; ^{13}C-NMR ($CDCl_3$) δ 166.0 (NHCO), 153.4 (C3'), 148.8 (C3), 142.3 (C1), 140.5 (C4'), 127.8 (C1'), 119.6 (C2), 113.6 (C4), 105.8 (C2'), 72.0, 67.8, 39.3, 39.2, 37.5, 37.3, 37.3, 36.3, 29.8, 29.7, 28.0, 24.7, 22.7, 22.6, 22.6, 22.6, 19.5 ppm; IR (ATR): 3282, 3105, 2954, 2927, 2870, 1662, 1582, 1546, 1499, 1466, 1429, 1383, 1341, 1212, 1116, 1074, 997, 902, 727 cm^{-1}; Elemental analysis: calculated: $C_{43}H_{69}N_3O_8$ (756.04): C, 68.31; H, 9.20; N, 5.56; found: C, 68.41; H, 8.77; N, 5.54.

N-(3,5-Diaminophenyl)-3,4,5-tridodecyloxy-benzamide (7a). The dinitro compound **6a** (0.84 g, 1,0 mmol) was shaken for 5 ½ h under hydrogen gas (150 ml, 6 mmol, 3 atm.) together with a 10 %w/w palladium on carbon catalyst (50 mg, 0.050 mmol), dissolved in ethanol (3 ml) and THF (22 ml). The reaction mixture was filtered over 3 paper filters to remove the catalyst. After column chromatography (flash silica, CH_2Cl_2 + 1 % Et_3N + 2 % MeOH, R_f = 0.3) **7a** was obtained as a sticky white/green solid (0.66 g, 85 %): ^{1}H-NMR ($CDCl_3$) δ

7.54 (NHCO, s, 1H), 7.00 (H2', s, 2H), 6.46 (H2, d, 2H), 5.83 (H4, t, 1H), 4.01 (OCH_2, m, 6H), 3.62 (NH_2, s, 4H), 1.80 (OCH_2CH_2, m, 6H), 1.46 ($OCH_2CH_2CH_2$, m, 6H), 1.26 (($CH_2)_8$, m, 48H), 0.88 (CH_3, m, 9H) ppm; ^{13}C-NMR ($CDCl_3$) δ 165.7 (NHCO), 152.9 (C3'), 148.0 (C3), 141.0 (C1), 139.8 (C4'), 130.0 (C1'), 105.7 (C2'), 98.2 (C2), 98.0 (C4), 73.4, 69.2, 31.8, 30.3, 29.7, 29.7, 29.6, 29.5, 29.4, 29.3, 26.0, 26.0, 22.6, 14.0 ppm; IR (ATR): 3343, 2921, 2852, 1615, 1582, 1544, 1497, 1453, 1335, 1223, 1113, 1002, 829 cm^{-1}; Elemental analysis: calculated: $C_{49}H_{85}N_3O_4$ (780.23): C, 75.43; H, 10.98; N, 5.39; found: C, 75.44; H, 10.57; N, 5.78.

N-(3,5-Diaminophenyl)-3,4,5-tri((*S*)-3,7-dimethyloctyloxy)-benzamide (7b). Analogous to the previous procedure dinitro compound **6b** (2.0 g, 2.7 mmol) gave **7b** as a sticky white/brown solid (0.69 g, 92 %): ^{1}H-NMR ($CDCl_3$) δ 7.51 (NHCO, s, 1H), 7.01 (H2', s, 2H), 6.46 (H2, s, 2H), 5.83 (H4, s, 1H), 4.05 (OCH_2, m, 6H), 3.62 (NH_2, bs, 4H), 1.88 - 0.86 (alkyl H, m, 57H) ppm; ^{13}C-NMR ($CDCl_3$) δ 165.6 (NHCO), 153.2 (C3'), 148.0 (C3), 141.3 (C1), 139.8 (C4'), 130.2 (C1'), 105.7 (C2'), 98.3 (C2), 97.9 (C4), 71.7, 67.7, 39.3, 39.2, 37.5, 37.3, 37.3, 36.3, 30.3, 29.8, 29.6, 27.9, 25.6, 24.7, 24.7, 22.7, 22.6, 19.5 ppm; IR (ATR): 3346, 2954, 2926, 2870, 1616, 1582, 1546, 1497, 1453, 1383, 1334, 1226, 1113, 996, 833, 757, 684 cm^{-1}; MALDI-TOF MS: calculated: 695.56, found: 696.55.

N-(3-Amino-5-nitro-phenyl)-3,4,5-tridodecyloxy-benzamide (8). In a two-neck flask the dinitro building block **6a** (1.5 g, 1.8 mmol), a 10%w/w palladium on carbon catalyst (40 mg, 0.040 mmol), and triethylamine (3.7 ml, 27 mmol) were heated to 80 ºC in acetonitrile (6 ml). Slowly formic acid (0.36 ml, 9.0 mmol) in acetonitrile (6 ml) was added. After 1 hour the reaction mixture was diluted with dichloromethane and filtered over 3 paper filters to remove the catalyst. The filtrate was diluted further and extracted with NH_4Cl solution (1 x) and saturated NaCl solution (2 x). The organic layer was dried over $MgSO_4$, filtered and evaporated. Column chromatography (flash silica, CH_2Cl_2 + 1 % Et_3N + 0-5 % MeOH, R_f = 0.3) gave yellow solid **8** (0.64 g, 44 %): ^{1}H-NMR ($CDCl_3$) δ 7.89 (NHCO, s, 1H), 7.71 (H6, t, 1H), 7.55 (H2, t, 1H), 7.25 (H4, t, 1H), 7.03 (H2', s, 2H), 4.08 (NH_2, bs, 2H,), 4.02 (OCH_2, m, 6H), 1.82 (OCH_2CH_2, m, 4H), 1.76(OCH_2CH_2, m, 2H), 1.46 ($OCH_2CH_2CH_2$, m, 6H), 1.26 (($CH_2)_8$, m, 48H), 0.88 (CH_3, m, 9H) ppm; ^{13}C-NMR ($CDCl_3$) δ 165.8 (NHCO), 153.3 (C3'), 149.4 (C5), 148.2 (C3), 141.8 (C1), 139.7 (C4'), 129.0 (C1'), 111.4 (C2), 105.6 (C2'), 104.9 (C6), 104.4 (C4), 73.6 (C4'O$\underline{C}H_2$), 69.4 (C3'O$\underline{C}H_2$), 31.9, 31.9, 30.3, 29.7, 29.7, 29.7, 29.6, 29.6, 29.4, 29.4, 29.3, 26.1, 22.7 (($CH_2)_{10}$), 14.1 (CH_3) ppm; IR (ATR): 3436, 3261, 2918, 2850, 1731, 1631, 1581, 1539, 1523, 1501, 1467, 1436, 1335, 1229, 1118, 745, 720 cm^{-1}; Elemental analysis: calculated: $C_{49}H_{83}N_3O_6$ (810.21): C, 72.64; H, 10.33; N, 5.19; found: C, 72.62; H, 10.44; N, 5.44.

N-(3-Isocyanato-5-nitro-phenyl)-3,4,5-tridodecyloxy-benzamide (9). The mononitro monoamine building block **8** (0.10 g, 0.12 mmol) in dry THF (6 ml) was added to a solution of phosgene in toluene (20%w/w, 0.33 ml, 0.62 mmol) in dry THF(1.5 ml) and stirred overnight at 80 °C. The solvent was evaporated and gaveproduct **9** (0.10 g, 100 %) that was used as such: ^{1}H-NMR ($CDCl_3$, 40 °C) δ 8.19 (H6, s, 1H), 8.03 (H2, s, 1H), 8.01 (NHCO, bs, 1H), 7.70 (H4, s, 1H), 7.04 (H2', s, 2H), 4.01 (OCH_2, m, 6H), 1.81 - 1.74 (OCH_2CH_2, m, 6H), 1.47 ($OCH_2CH_2CH_2$, m, 6H), 1.27 (($CH_2)_8$, m, 48H), 0.88 (CH_3, m, 9H) ppm; ^{13}C-NMR ($CDCl_3$) δ 166.1 (NHCO), 153.6 (C3'), 149.2 (C5), 142.3 (C1), 140.3 (C4'), 135.8 (C3), 128.6 (C1'), 125.8 (NCO), 122.0 (C2), 115.3 (C4), 112.1 (C6), 106.0 (C2'), 73.9 (C4'O$\underline{C}H_2$), 69.8 (C3'O$\underline{C}H_2$), 32.2, 32.2, 30.5, 30.0, 29.9, 29.9, 29.9, 29.8, 29.6, 29.6, 29.6, 29.3, 26.3, 22.9 ($CH_2)_{10}$), 14.3 (CH_3) ppm; IR (ATR): 3248, 2918, 2850, 2250, 1654, 1583, 1543, 1493, 1467, 1426, 1337, 1221, 1119, 908, 734 cm^{-1}.

N,N'-Bis{3-[3,4,5-tri((*S*)-3,7-dimethyloctyloxy)benzoylamino]-1-(3,4,5-tridodecyloxybenzoyl-amino)-5-phenyl} urea (10). To a solution of diamine monourea **5b** (0.13 g, 0.084 mmol) and triethylamine (0.028 ml, 0.20 mmol) in dry dichloromethane (2 ml), a solution of 3,4,5-tri((*S*)-3,7-dimethyloctyloxy)benzoyl chloride (0.14 g, 0.23 mmol) was added dropwise at room temperature. After two hours the dichloromethane was evaporated and the product purified by column chromatography (aluminiumoxide (II), dichloromethane + 1 %v/v methanol, Rf = 0.9 and flashsilica, dichloromethane + 0-3 %v/v methanol, Rf = 0-0.9). This yielded off-white sticky solid **10** (0.10 g, 44 %): ^{1}H-NMR (THF-*d8*) δ 9.22 (amide NH, s, 4H), 7.91 (urea NH, s, 2H), 7.79 (H2, s, 2H), 7.71 (H4, s, 4H), 7.15 (H2', s, 4H), 7.13 (H2', s, 4H), 3.98, 3.92, 3.87 (OCH_2, 3m, 4H, 16H, 4H), 1.79 - 0.75 (alkyl H, m, 252 H) ppm; ^{13}C-NMR (THF-*d8*): δ 166.7 (NHCO', NHCO''), 154.4 (NHCONH), 153.8 (C3', C3''), 142.8, 142.7 (C4', C4''), 142.0 (C5), 141.6 (C1, C3), 131.9, 131.8 (C1', C1''), 107.9, 107.9 (C4, C6), 107.1 (C2), 105.9 (C2', C2''), 74.3, 72.5, 70.4, 68.7, 41.0, 40.9, 39.1, 39.0, 39.0, 38.2, 33.5, 32.0, 31.4, 31.3, 31.3, 31.3, 31.2, 31.2, 31.1, 31.1, 31.0, 30.9, 29.5, 27.8, 27.8, 26.3, 26.3, 24.2, 23.7, 23.6, 23.6, 20.7, 20.6, 15.1 (alkyl C) ppm; IR (ATR): 3319, 2954, 2923, 2854, 1648, 1613, 1582, 1542, 1498, 1466, 1429, 1384, 1331, 1216, 1114, 1046, 998, 858, 754, 721, 684 cm^{-1}; Elemental analysis: calculated: $C_{173}H_{296}N_6O_{17}$ (2732.32): C, 76.05; H, 10.92; N, 3.08; found: C, 74.53; H, 10.02; N, 3.07.

4.6 References and notes

(1) For examples of helical stacks of discotics see Chapters 2 and 3. (a) Palmans, A.R.A.; Vekemans, J.A.J.M.; Havinga, E.E.; Meijer, E.W. *Angew. Chem. Int. Ed. Engl.* **1997**, *36*, 2648–2651. (b) Brunsveld, L.; Zhang, H.; Glasbeek, M.; Vekemans, J.A.J.M.; Meijer, E.W. *J. Am. Chem. Soc.* **2000**, *122*, 6175–6182.

(2) peptides: (a) Pauling, L.; Corey, R.B.; Branson, H.R. *Proc. Natl. Acad. Sci. USA* **1951**, *37*, 205–211. DNA: (b) Watson, J.D.; Crick, F.H.C. *Nature* **1953**, *171*, 737–738.

(3) Stryer, L.; *Biochemistry*, 4th ed, W. H. Freeman & Company: New York, 1995.

(4) (a) van Nostrum, D.F.; Picken, S.J.; Nolte, R.J.M. *Angew. Chem. Int. Ed. Engl.* **1994**, *33*, 2173–2175. (b) Engelkamp, H.; Middelbeek, S.; Nolte, R.J.M. *Science* **1999**, *284*, 785–788. (c) Lam, J.W.Y.; Dong, Y.; Cheuk, K.K.L.; Tang, B.Z. *Macromolecules* **2003**, *36*, 7927–7938. (d) Yasuda, Y.; Iishi, E.; Inada, H.; Shirota, Y. *Chem. Lett*. **1996**, 575–576. (e) Yasuda, Y.; Takebe, Y.; Fukumoto, M.; Inada, H.; Shirota, Y. *Adv. Mater.* **1996**, *8*, 740–741. (f) Osborn, E.J.; Schmidt, A.; Chau, L.-K.; Chen, S.Y.; Smolenyak, P.; Armstrong, N.R.; O'Brien, D.F. *Adv. Mater.* **1996**, *8*, 926–928. (g) Hanabusa, K.; Kawakami, A., Kimura, M.; Shirai, H.*Chem. Lett.* **1997**, 191–192. (h) Hanabusa, K.; Koto, C.; Kimura, M.; Shirai, H.; Kakehi, A. *Chem. Lett.* **1997**, 429–430.

(5) Masuda, M.; Jonkheijm. P.; Sijbesma, R.P.; Meijer, E.W. *J. Am. Chem. Soc.* **2003**, *125*, 15935–15940.

(6) See Chapter 2 for a definition of 'small', 'medium', and 'large' disks.

(7) Lohmeijer, B.G.G. *Graduation report: Supramolecular architectures in polar media*; Eindhoven University of Technology: Eindhoven, **2000**.

(8) van Gorp, J.J. *Graduation report: Supramoleculaire sturcturen opgebouwd uit 3,3'-diamino-2,2'-bipyridine en benzeen-1,3,5-tricarbonzuur*; Eindhoven University of Technology: Eindhoven, **1999**.

(9) (a) Chadda, S.K.; McCarry, B.E.; Childs, R.F. *J. Appl. Polym. Sci.* **1987**, *34*, 2713–2732. (b) Engel, M.; Burris, C.W.; Slate, C.A.; Erickson, B.W. *Tetrahedron* **1993**, *49*, 8761–8770.

(10) Kraft, A. *J. Chem. Soc., Perkin Trans. 1* **1999**, 705–714.

(11) Lukas, A.S.; Miller, S.E.; Wasielewski, M.R. *J. Phys. Chem. B* **2000**, *104*, 931–940.

(12) Klug, A. *Angew. Chem.* **1983**, *95*, 579–596.

(13) (a) Percec, V.; Schlueter, D.; Ronda, J.C.; Johansson, G.; Ungar, G.; Zou, J. P *Macromolecules* **1996**, *29*, 1464–1472. (b) Percec, V.; Cho, W.-D.; Mosier, P.E.; Ungar, G.; Yeardley, D.J.P. *J. Am. Chem. Soc.* **1998**, *120*, 11061–11070. (c) Percec, V.; Ahn, C.H.; Bera, T.K.; Ungar, G.; Yeardley, D.J.P. *Chem. Eur. J.* **1999**, *5*, 1070–1083.

(14) (a) Keizer, H.M.; Ramzi, A.; Sijbesma, R.P.; Meijer, E.W. *Polymer Preprints* **2003**, *44*, 596–597. (b) Keizer, H.M.*Thesis: Multi-component systems of hydrogen-bonded supramolecular polymers*; Eindhoven University of Technology: Eindhoven, **2004**.

(15) See Chapter 5, Hill, D.J.; Mio, M.J.; Prince, R.J.; Hughes, T.S.; Moore, J.S. *Chem. Rev.* **2001**, *101*, 3893–4011

(16) Terpko, M.O.; Heck, R.F. *J. Org. Chem.* **1980**, *45*, 4992–4993.

(17) Pieterse, K. *Thesis: Electron deficient materials based on azaheterocycles*; Eindhoven University of Technology: Eindhoven, **2001**.

(18) Green, M.M.; Reidy, M.P.; Johnson, R.D.; Darling, G.; O'Leary, D.J.; Wilson, G. *J. Am. Chem. Soc.* **1989**, *111*, 6452–6454.

(19) In UV-Vis measurements where the temperature is raised, the absorption maximum and intensity displayed by **3** become higher, like the ones displayed by **4** at 10^{-5} M in heptane.

(20) Snellink-Ruël, B.H.M.; Antonisse, M.M.G.; Engbersen, J.F.J.; Timmerman, P.; Reinhoudt, D.N. *Eur. J. Org. Chem.* **2000**, 165–170.

(21) (a) Palmans, A.R.A. *Thesis: Supramolecular structures based on the intramolecular H-bonding in the 3,3'-di(acylamino)-2,2'-bipyridine unit*; Eindhoven University of Technology: Eindhoven, **1997**. (b) Brunsveld, L. *Thesis: Supramolecular chirality, from molecules to helical assemblies in polar media*; Eindhoven University of Technology: Eindhoven, **2001**.

(22) See Chapter 5 for the structuring effect of THF on ureidophthalimide compounds.

(23) Unpublished results concerning: Diez-Barra, E.; Garcia-Martinez, J.C.; Rodriguez-Lopez, J. *J. Org. Chem.* **2003**, *68*, 832–838.

(24) Appella, D.H.; Christianson, L.A.; Karle, I.L.; Powell, D.R.; Gellman, S.H. *J. Am. Chem. Soc.* **1996**, *118*, 13071–13072.

Chapter 5

A chiral poly-ureidophthalimide helix showing both intra- and intermolecular ordering

Abstract: *A poly-ureidophthalimide **1,** which adopts a stable, helical conformation with about 7.5 units per turn, is designed, synthesized, and characterized. The design is based on the ordering of urea protons by intramolecular hydrogen bonding to imide oxygens, which is also illustrated in disk **2**, and monourea model compounds **3a-e**. Polymers **1** (**1-IIIa,** ~30 units) are formed in a single condensation step of diamino (**17**) and diisocyanato (**18**) functionalized monomers, equipped with a chiral phthalimide unit. Long, intermediate, and short oligomeric mixtures (**1a-c**) are obtained via column chromatography, while single oligomers (dimer upto octamer **1d-j**) are isolated by preparative, reversed phase high performance liquid chromatography. Temperature and concentration dependent CD measurements, as well as denaturation curves, involve time dependent effects (hysteresis). They demonstrate a high stability of the helical architecture, indicating an optimal balance between strength and reversibility. Intra- and intermolecular contributions to the folding of the helical polymer can clearly be distinguished by chain-length dependent CD studies in polar and apolar solvents. In tetrahydrofuran overall order is maximal (g=-0.012), although just mono-molecular folding takes place, while in heptane the folded helices stack to afford elongated aggregates.*

5.1 Introduction

5.1.1 Foldamers

Different approaches towards helix formation can be pursued,[1] one of them being the self-assembly approach described in Chapters 2 and 3.[2] However, in nature helices are formed by single (macro)molecules with the help of multiple intramolecular non-covalent interactions.[3] The self-assembly of (small) molecules implying intermolecular non-covalent interactions is more rare.[4] Structures that adopt ordered conformations with aid of multiple 'weak' intramolecular non-covalent interactions have been designated foldamers.[5] Because of the key role of natural helical foldamers in expressing biological activity, the expectations for the applications and features of synthetic foldamers is high. They might be even higher than expectations for synthetic helices formed via other approaches, such as the self-assembly or covalent helicene constructions.[1,6,7] Furthermore, polymers might prove advantageous in terms of accessibility, processability, and material properties.[8]

In contrast to rigid helicenes[7], where steric effects enforce a helical structure, synthetic foldamers[5] may use a variety of stabilizing intramolecular non-covalent interactions to adopt a biased conformation.[9] Just non-directional interactions like π-π stacking and solvophobic effects may suffice, like in *ortho*[10a,b]- or *meta*[10c-f]-phenylene vinylenes. Often, in combination with these non-directional interactions, directional intramolecular hydrogen bonding is incorporated.[11] It has been shown that aliphatic peptidometic homologues[12] as well as aromatic oligoamides[13], can mimic the helical structure, and possibly the concomitant functions, of natural α-peptides.[3a] It has to be noted that aliphatic peptidometic homologues resemble nature more closely, because hydrogen bonds between different pitches of the helix, i.e. between non-neighboring monomeric units are involved.[2b-j] In aromatic oligoamides hydrogen bonds appear 'perpendicular' to the direction of the helix, i.e. between two monomeric neighbors. Although not successful, an aromatic oligourea foldamer with hydrogen bonding between non-adjacent units was discussed in Chapter 4.

A variety of methods for the formation of elongated structures is known.[9] In foldamer research, often a stepwise strategy (method 4, Figure 5.1) is followed,[13] as this yields oligomers of well-defined length. This is favorable in terms of purification, characterization and interpretation of the folding behavior. However, the stepwise method is an elaborate one for obtaining structures of substantial length. Therefore, homo- or copolymerizations (method 1 and 2, Figure 5.1) can be applied alternatively.[14] Innumerous oligomers and polymers are obtained in one pot, so isolation of 'individual substances' might be elaborate.[15] Method 3, the semi-stepwise approach, can be regarded as a concession. When complementary monomers are used in a 1 to 2 ratio, ideally one length is found predominantly in the reaction mixture, which would simplify isolation of substances with this desired length.[16]

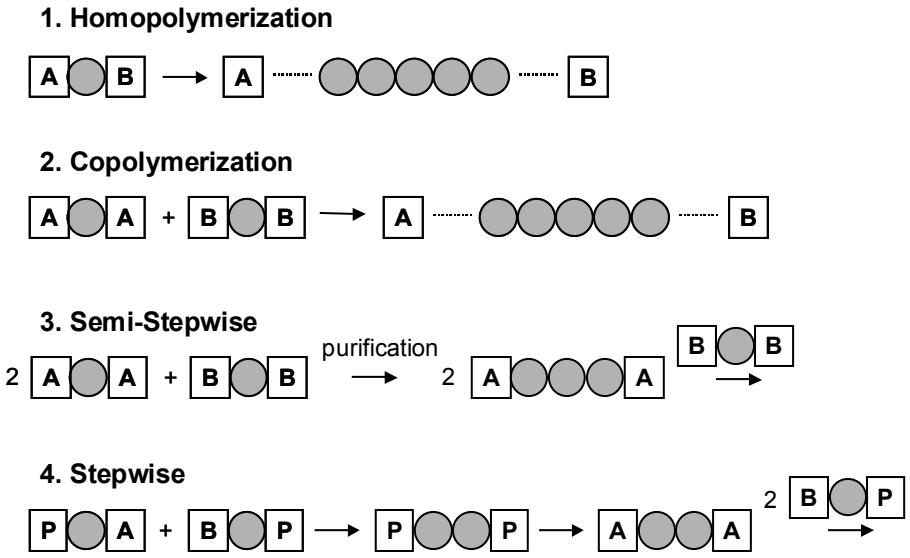

Figure 5.1. *Cartoon depicting 4 polymerization methods.*

A peculiarity in the formation of elongated structures, covalently as well as supramolecularly, is the formation of cycles.[17] Stacking of these rings, or ring-closed polymers, into hollow cores, might be regarded as an intermediate between the self-assembly and the foldamer approach.[18] Few examples are known, which show stacking between polymeric foldamers at high concentrations or low temperatures.[19a,b] Merging self-assembly (intermolecular) and foldamer (intramolecular) strategies possibly combines the best of both.[19c,d]

5.1.2 Design of a ureidophthalimide foldamer

In our design, findings concerning the self-assembly approach were translated to foldamer development. It has been learnt that urea groups may improve stability of supramolecular architectures with respect to amides. However, a delicate balance between different non-covalent interactions is needed, for the ordered architecture to maintain both reversibility and compactness.[20] A urea based aromatic polymer was aimed at, in which intramolecular hydrogen bonding between urea protons and carbonyl oxygens is used, to orient the urea groups.

Where amide groups cause aromatic oligomers to progress linearly,[21] urea groups[22] cause the chain to make a 120° bent.[23] Therefore, *para*-substituted monomeric aryl units are applied, instead of the *ortho*[13k]- or *meta*[13b-d,g-j]-substituted units used in amide based aromatic systems. Imide oxygens are found suitable to orient the *para*-positioned urea groups, and thereby induce a crescent or helical conformation with approximately 6 units per turn (Figure 5.2). Hydrogen bonds in a 5-membered ring are presumably not as strong as those in a 6-membered ring,[24] however, this might be favorable to the overall reversibility of the foldamer (Chapter 4).[9,20]

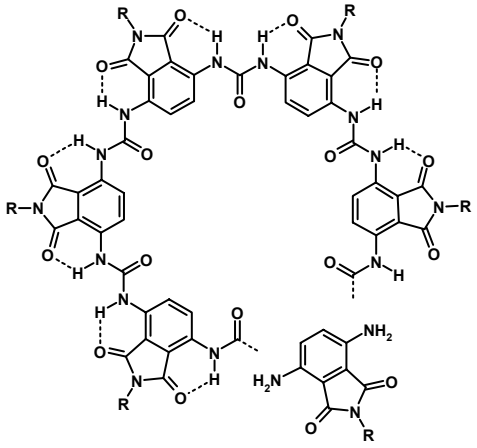

Figure 5.2. *Chemical structure of a turn of the polymer helix, together with that of the corresponding diamino functionalized monomer.*

Moreover, the imide function offers the possibility to incorporate any primary amine containing functionality. Indeed, this could imply application of this urea scaffold in a broad range of functional systems, expressing new material properties or biological activity.[6] In our case, a chiral amine will be incorporated into the polymer, to ensure solubility, phase separation, and the possibility to investigate the compounds with circular dichroism spectroscopy in dilute solution. Similar to self-assembled helices (Chapter 3), the helical twist sense of helical foldamers can be biased by a small, chiral perturbation to the side chains without disrupting the confomational stability of the oligomer[25,26] or polymer. In this chapter it is described how supramolecular chirality helped in creating a model for the intra- as well as intermolecular folding of the poly-ureidophthalimide in dilute apolar solution. In a similar way, such a model has been developed for the stacking of rigid helicenes in the liquid crystalline phase.[27]

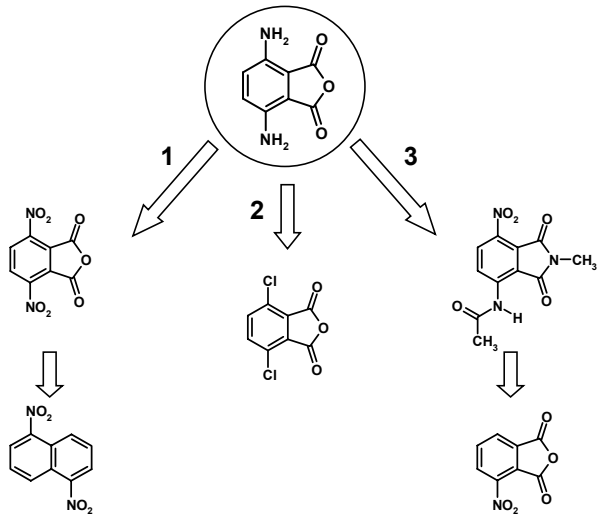

Figure 5.3. *Three routes towards the 3,6-diaminophthalic anhydride key-precursor.*

To obtain the ureidophthalimide elongated systems, 1,2,3,4-tetrasubstituted monomeric structures are necesarry. In general, the 1,2,3,4-substitution pattern is not common, and access to key precursor 3,6-diaminophthalic anhydride is limited (Figure 5.3). Since 3,6-dinitrophthalic anhydride was used in the past to derivatize sugars and peptides for analytical purposes,[28,29] route 1 was considered first. A primary amine of choice could easily be converted into the corresponding monomer by coupling to this 3,6-dinitrophthalic anhydride backbone building block, and reduction of the nitro groups. Consecutively, this diamino imide could hopefully give rise to a true polymer in a single condensation step. However, the synthetic procedure of 3,6-dinitrophthalic acid deals with nitration and oxidation of 1,5-dinitronaphthalene.[30] Although also route 2 via starting compound 3,6-dichlorophthalic anhydride was envisaged, initially route 3 seemed most promising. It would allow orthogonal substitution of the building block (a nitro and an acetylamino group),[31] that could enable synthesis of oligomers of defined length, which is probably helpful in characterization and synthesis of either cycles or polymers. Moreover, the starting compound of route 3 (3-nitrophthalic anhydride) is readily available.

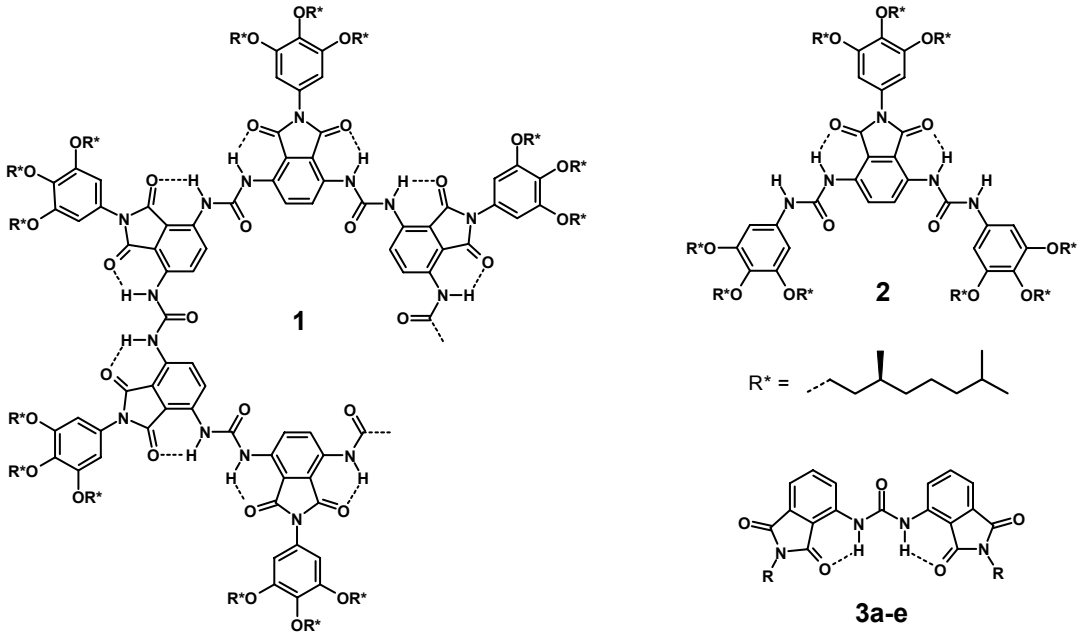

Figure 5.4. *Target compounds: Poly-ureidophthalimide **1**, phthalimide disk **2**, and monourea models **3a-e**. For **3a-e** R is depicted in Scheme 5.1.*

At first, route 3, concerning the orthogonally substituted building block, was explored and it was found that severe restrictions were involved. Route 1, in contrast, did give access to ureidophthalimide polymers **1** (Figure 5.4) via phthalimide monomers, and the 3,6-dinitro building block. To study the folding behavior of poly-ureidophthalimide **1** in more detail, oligomers of defined length were isolated with preparative, reversed phase HPLC. Also a phthalimide disk **2** and monourea models with varying R-groups **3a-e** were synthesized and investigated, in order to unambiguously explore relevant structural features.

5.2 Monourea phthalimide models

Initially, the phthalimide foldamer design was justified by demonstrating the feasibility of urea formation. Previously unknown monourea model compounds were synthesized and the preferential bent conformation of these dimers was shown with ^{1}H-NMR. The three-step procedure towards a monourea started with imide formation by reaction of 3-nitrophthalic anhydride and an amine in the bulk at 170 °C (Scheme 5.1).[32] Aqueous methylamine,[33] octylamine, *para*-methoxyaniline, as well as achiral and chiral gallic amines were used,[33] giving imides **4a-e**. Catalytic reduction of the nitro group in the presence of Pd/C (10%) yielded the corresponding 3-aminophthalimides **5a-e.** Finally, the 3-aminophthalimides were treated with half an equivalent of phosgene and the base 4-dimethylaminopyridine to give the monourea targets **3a-e**.

^{1}H-NMR spectroscopy has been selected to investigate whether the conformational freedom of monourea dimers **3a-e** is restricted by hydrogen bonding between the urea protons and the imide oxygens (Table 5.1). The chemical shift of ureas **3a-e** is compared to that of amides **6-8** (vide infra, Scheme 5.2). The NH protons of both urea and amide are positioned downfield (> 9 ppm). Furthermore, a remarkable downfield position (> 8.5 ppm) is found for the H-4 protons with respect to the other aromatic signals (7.7–7.5 ppm).

Scheme 5.1. *Synthesis of monourea dimers **3a-e**.*

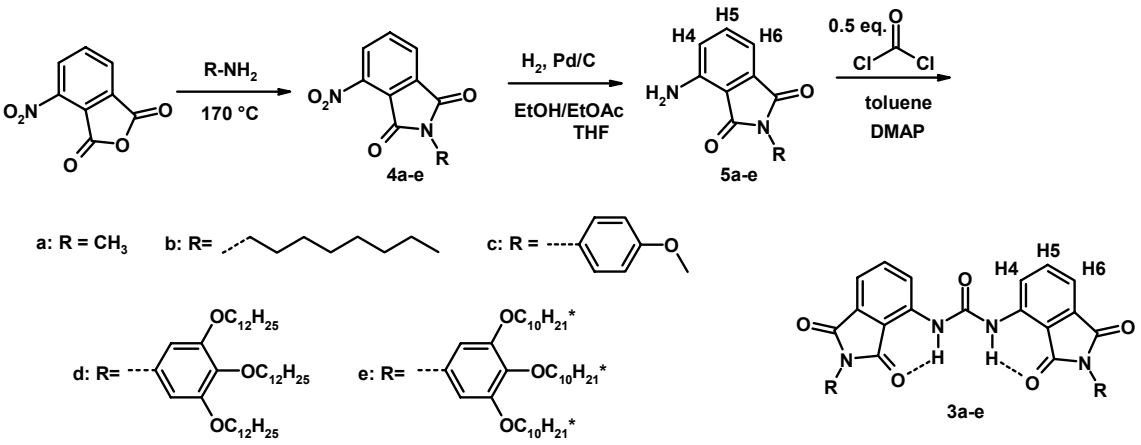

The specific aromatic signals are assigned using the mutual coupling patterns and constants. In acetylamino compounds **6** and **7** H-5 shows two large ortho-couplings, whereas H-4 and H-6 only show one. The difference between H-4 and H-6 becomes clear by combination of the different coupling constants with H-5 ($J_{4,5}$ = 8.5–9.2 Hz, being significantly larger than $J_{5,6}$ = 7.1–7.4 Hz), and comparison of the spectra of acetylamino derivatives **7** and **8** with that of amine derivative **5a**. They indicate that the absence of a coplanar carbonyl group induces a shift of the H-4 proton ($J_{4,5}$ = 8.5–9.2 Hz) of more than 1 ppm. These observations point to a close proximity of the H-4 protons and the urea carbonyl and, consequently, to intramolecular hydrogen bonding between the urea protons and the imide carbonyl.

Table 5.1. *^{1}H-NMR data [ppm] of amine **5a**, acetamides, **6**, **7** and **8**, and ureas **3a-c** (all in $CDCl_3$, except **3c** in DMSO-d6).*

No.	Amine **5a**	Acetyl **6**	Acetyl **7**	Acetyl **8**	Urea **3a**	Urea **3b**	Urea **3c**
NH	5.2	9.1	9.4	10.0	9.2	9.2	10.1
H-4	6.83	8.95	8.79	8.95	8.62	8.62	8.45

Also ^{13}C-NMR data (Table 5.2) support a structure in which the urea-function is somehow locked in a conformation that leads to a dramatic difference in shielding of C-2 versus C-4. Taking an incremental approach into account, the C-2 signal appears ~8.5 ppm upfield compared to the calculated position, whereas C-4 is found at the 'normal' position. Interestingly, the chemical shifts are not markedly influenced by the solvent ($CDCl_3$ or DMSO-*d6*). It is known that 3-D orientation may strongly affect ^{13}C-shifts. Such behavior was also observed in N-acylated 2,2'-bipyridine-3,3'-diamines. In these structures intramolecular H-bonding is undoubtedly responsible for the conformational locking of the molecule.[34]

Table 5.2. *^{13}C-NMR data [ppm] of phthalimide (DMSO-d6), urea **3c** (DMSO-d6), and urea **3d** ($CDCl_3$). The observed data of ureas **3c** and **3d** are compared to calculated data derived from the phthalimide shifts and the increment of the urea substituent.*

No.	Phthalimide	Urea Increment	Calculated	Observed	
				Urea **3c**	Urea **3d**
C-1	132.5	+0.5	133	132.8	131.3
C-2	*132.5*	*-9*	*123.5*	*114.8*	*115.2*
C-3	*123*	*+10*	*133*	*137.7*	*138.2*
C-4	134	-9	125	124.9	126.0
C-5	134	+0.5	134.5	136.1	136.2
C-6	123	-5	118	117.8	117.9

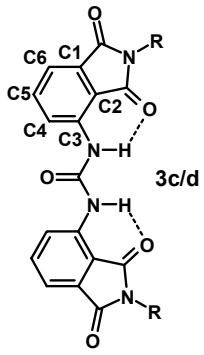

5.3 Orthogonally substituted 1,2,3,4-tetrasubstituted monomers

A 1,2,3,4-tetrasubstituted monomer **8** could be synthesized starting from 3-nitrophthalic anhydride. This was converted into the corresponding acetylamino compound **6** by treatment with hydrogen gas using palladium on carbon as a catalyst and acetic anhydride as the solvent (Scheme 5.2).[35] When anhydide **6** was treated with an aqueous methylamine solution and subsequently heated to 180 °C, N-methylimide **7** was obtained. The conditions needed for nitration of this imide **7** were critical.[31] When 12 equivalents of nitric acid in sulfuric acid were used at 0 °C, the reaction was complete within 2.5 hours. According to ^{1}H-NMR, next to the desired 3-acetylamino-6-nitro-N-methylphthalimide (**8**), only a minor amount of di-substituted product was formed, which could be removed by crystallization from acetone.

Scheme 5.2. *Synthetic route towards 3-acetylamino-N-methyl-phthalimide (**8**).*

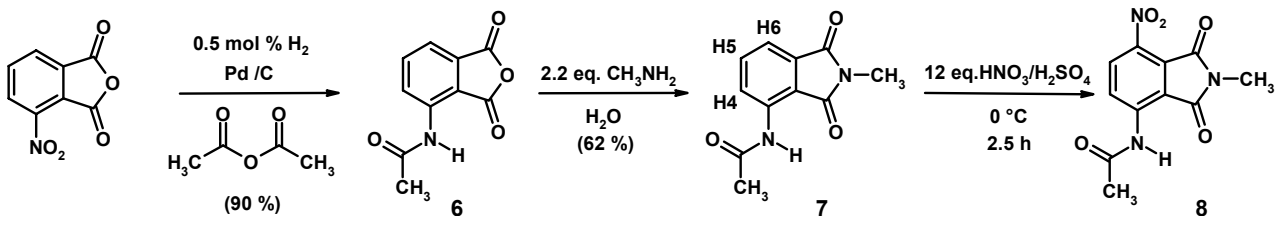

In principle, 3-acetylamino-6-nitro-N-methylphthalimide **8** could be deprotected, reduced and polymerized. However, doing so might yield severe solubility problems and, therefore, several methods were envisaged to replace the imide methyl by a longer alkyl or gallic-based group (R) to ensure solubility and phase separation. Three reaction types applied are designated '*nitration*', '*hydrolysis*', and '*transimidization*'.

In order to introduce the imide-R group as late as possible, *nitration* of 3-acetylaminophthalic anhydride **6** would be preferred (Scheme 5.3). It was found that the anhydride was not nucleophilic enough to be nitrated under the conditions applied for 3-acetylamino-N-methylphtalimide **7** (12 eq. HNO_3 / H_2SO_4, 0 °C). It has to be noted that the anhydride **6** could be brominated using either KBr and a Mo-catalyst[36] or Br_2 in basic medium.

Scheme 5.3. *Synthesis of 3-acetylamino-6-nitrophthalimide compounds **8** and **10** via nitration.*

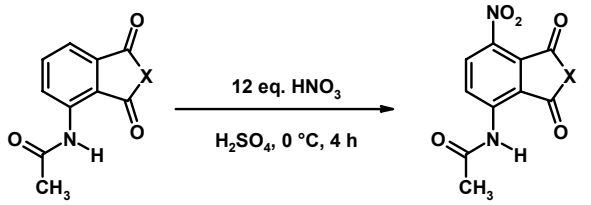

6: X =: O: no reaction
7: X = N-CH_3: reaction to **8**
9: X = N-C_8H_{17}: reaction to **10**

However, 3-acetylamino-N-octylphthalimide **9** could be nitrated to give 3-acetylamino-6-nitro-N-octylphthalimide **10** (R = C_8H_{17}) -albeit in lower yield- using the conditions mentioned previously. This in principle enables us to synthesize alkyl substituted oligomers (Scheme 5.3). It has to be noted that this route is not suitable for aromatic (gallic) amines, which will be nitrated more easily on the gallic nucleus. Finally, 3-acetylaminophthalimide **11** (R = H) was synthesized in 3 steps from 3-nitrophthalic acid (Scheme 5.4). If nitration and functionalization of the imide group would be possible, this is also an option for stepwise growth of oligomers in an orthogonal approach.

Scheme 5.4. *Anticipated approach using 3-acetylaminophthalimide **11**, an opening to stepwise growth of phthalimide oligomers via orthogonally substituted monomers.*

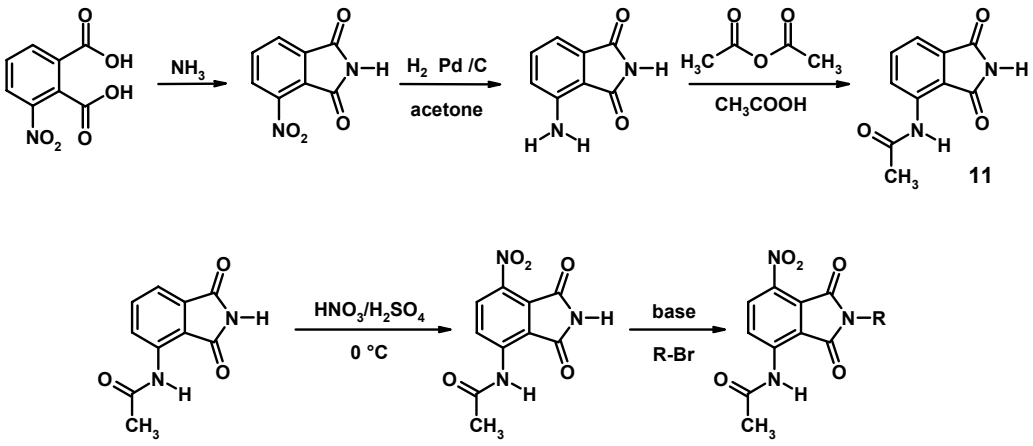

Were it possible to *hydrolyze* imide **8** to the anhydride **12**, the amine of choice could be reacted consecutively, to give a variety of imides.[37] The imide ring indeed opened readily under the influence of base (KOH), giving rise to two carboxylic salt – amide compounds (Scheme 5.5). Hydrolysis of the second carboxyl group proved difficult and required larger excess of base and higher temperatures. Apart from hydrolysis of the acetyl group, in this case decarboxylation took place, rendering this method unsuitable. In a final attempt it was tried to remove the methylamine fragment under acidic conditions, but only 3-amino-6-nitro-N-methylphthalimide was recovered.

Scheme 5.5. *Attempted hydrolysis of imide **8**.*

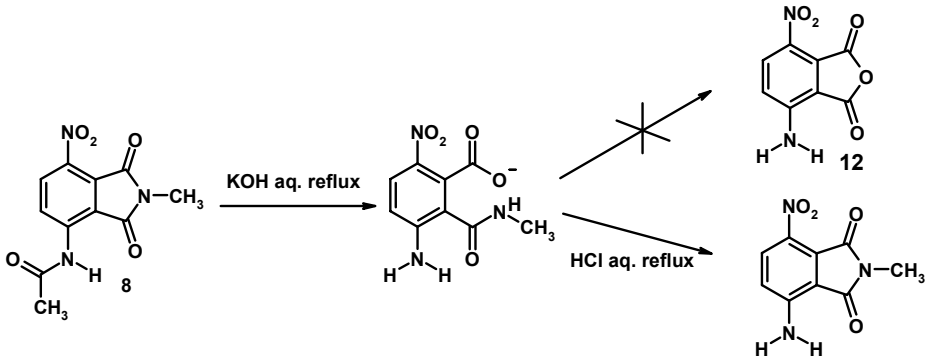

It is known that the amine fragment of an imide can be replaced by a more basic R-amine ('*transimidization*').[38] However, it was found that extremely high temperatures (240 °C) were needed to replace the imide methyl of **8** by the longer octadecyl tail to afford imide **13** ($R = C_{18}H_{37}$). Since the process was incomplete and concomitantly caused deacylation of the compound (Scheme 5.6), synthesis of these compounds via direct nitration might be preferred.

Scheme 5.6. *Transimidization of N-methylimide **8** to N-octadecylimide **13**.*

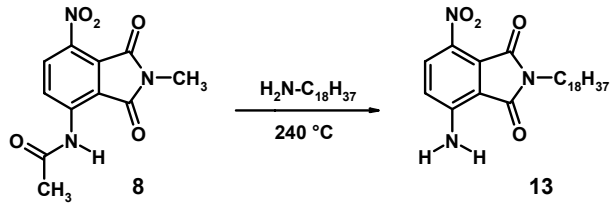

In conclusion, a stepwise growth of ureidophthalimide oligomers **1** is not straightforward. The difficulties encountered in the conversion of a suitable 1,2,3-trisubstituted building block to a dersired 1,2,3,4-tetrasubstituted monomer, have prompted us to embark for route 3, where the substitution pattern is already embedded in the commercially available starting compound 1,5-dinitronaphthalene.

5.4 A disk, oligomers, and polymers based on ureidophthalimidyl

5.4.1 Synthesis and fractionation

The desired starting compound for the synthesis of polymeric mixtures of **1**, 3,6-dinitrophthalic acid anhydride (**14**), was initially obtained from expensive and restrictedly available monopyridinium 3,6-dinitrophthalate (ICN Biomedicals). This was treated with respectively, a 6 M aqueous hydrochloric acid solution, and acetic anhydride, according to the procedure of Meek.[28] In view of required scale up, 3,6-dinitrophthalic acid was resynthesized by nitration and oxidation of 1,4-dinitronaphthalene, following the procedure of Momose.[30] As before, treatment of 3,6-dinitrophthalic acid with acetic anhydride gave the corresponding starting anhydride **14**.

Scheme 5.7. *Synthesis of diamino and diisocyanato phthalimide building blocks **17** and **18**.*

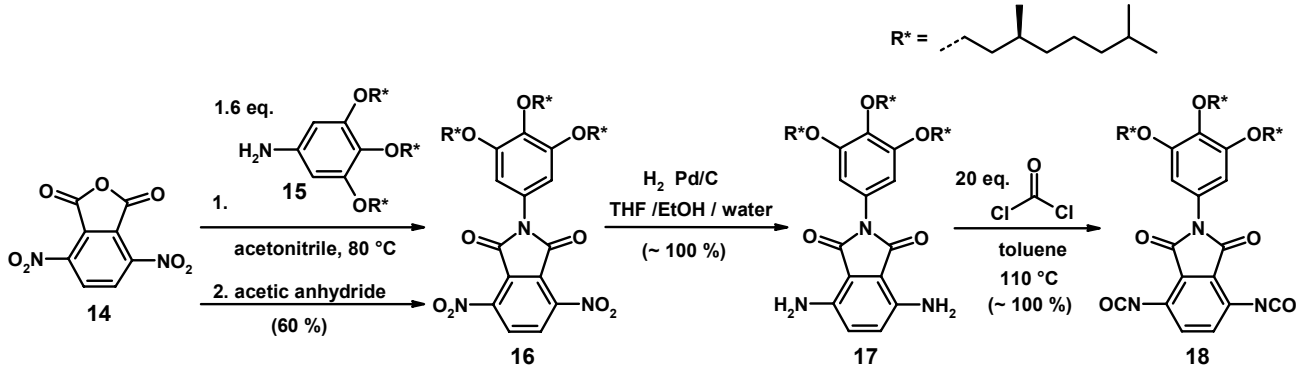

Anhydride **14** was reacted with an excess of chiral 3,4,5-tri((*S*)-3,7-dimethyloctyloxy)aniline **15**,[39] to afford 3,6-dinitrophthalimide **16** (Scheme 5.7) -after ring closure induced by acetic anhydride-[39] in 60 % yield. Dinitro compound **16** was catalytically hydrogenated on Pd to diamino monomer **17**. The diisocyanato monomer **18** was obtained by treating diamine **17** with an excess of phosgene. Both, reduction and isocyanate formation, proceeded quantitatively.

End capping of the diisocyanato building block **18** with 2 equivalents of 3,4,5-tri((*S*)-3,7-dimethyloctyloxy)aniline (**15**),[39] yielded phthalimide disk **2**. The base 4-dimethylaminopyridine was necessary for the condensation to take place (Scheme 5.8).

Scheme 5.8. *Synthesis of phthalimide disk **2**.*

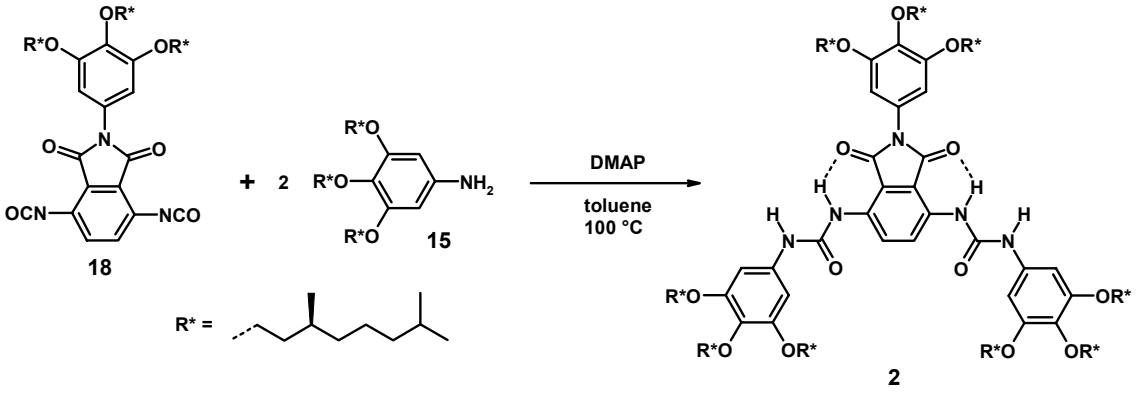

Equimolar amounts of diamine **17** and diisocyanate **18** were copolymerized in toluene, again in the presence of 4-dimethylaminopyridine (DMAP) to afford poly-ureidophthalimide **1** (Scheme 5.9). The reaction has been performed in triplo (**1-I**, **1-II**, and **1-III**).

Scheme 5.9. *Polymerization of diamino and diisocyanato phthalimide monomers **17** and **18** to give poly-ureidophthalimide **1**.*

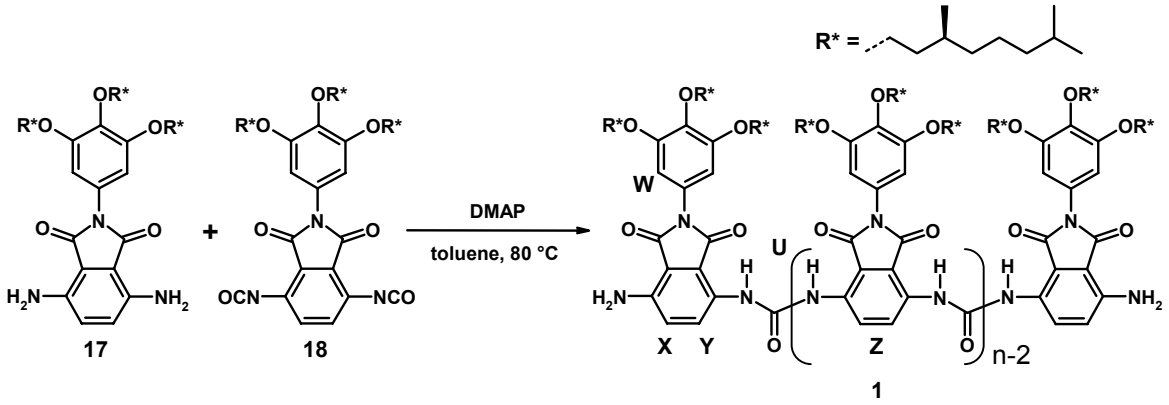

Initially, polymer **1** was submitted to column chromatography (silica, $CHCl_3/CH_3OH$) to remove DMAP, and to devide the polymer into 3 fractions. The longest molecules **1a** eluted readily, while the intermediate and short chains, **1b** and **1c**, were collected with a more polar eluting solvent. In this way, 9 polymeric mixtures (a long (**a**), intermediate (**b**), and short (**c**) one for 3 repetitive reactions (**I**, **II**, and **III**)) were obtained. Representative long, intermediate and short fractions are **1-IIIa**, **1-IIb** and **1-IIc**. The average chain length of the polymeric mixtures **1-Ia – 1-IIIc** was determined using ^{1}H-NMR endgroup analysis (Figure 5.5), relying on the integral ratio between the signals of the termini (amine protons at 5.18 ppm and aromatic phthalimide protons at 6.95 (X) and 8.48 (Y) ppm) and the

signals of the aromatic phthalimide protons in the main chain (Z, 8.73 ppm). For polymer **1-Ia**, a value as high as 30 units was calculated. Average values of 7 and 3.5 units were calculated for **1-IIb** and **1-IIc**, respectively (Table 5.3). In GPC chromatograms single peaks were obtained for long (**1-IIIa**) and intermediate (**1-IIb**) fractions, while separate oligomers got resolved in short fractions (**1-IIc**) (Figure 5.6).[40]

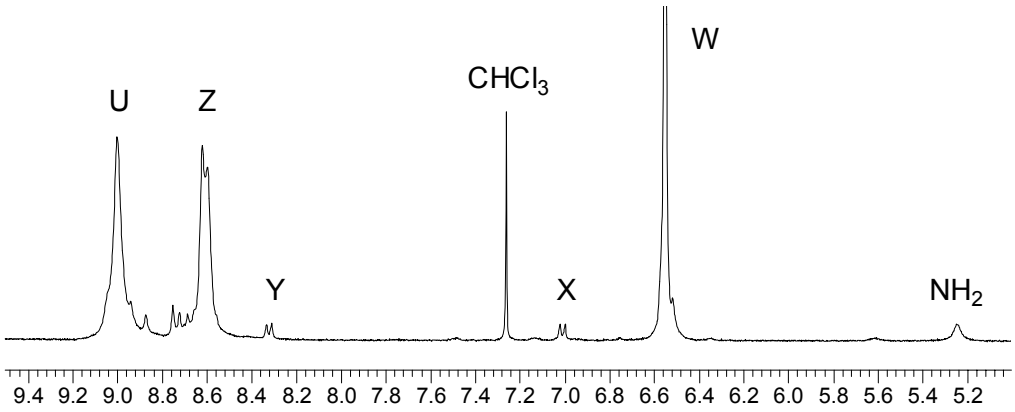

Figure 5.5. *^{1}H-NMR spectrum ($CDCl_3$/HFIP 2/1) of poly-ureidophthalimide **1-IIIa** (~30 units). See Scheme 5.9 for a chemical structure with the assignment of the peaks.*

Table 5.3. *Average degree of polymerization (n) of polymer fractions **1** (**1-Ia** – **1-IIIc**), determined by ^{1}H-NMR endgroup analysis.*

Reaction	Fractions		
	a (long)	**b** (intermediate)	**c** (short)
I	15	12	5
II	20	7	3.5
III	30	25 and 11[a]	5.5

[a] Two separate fractions are obtained due to extra chromotographic purification.

Single oligomers are obtained by preparative, reversed phase HPLC of oligomeric mixture **1-IIc** in a tetrahydrofuran/water mixture (Figure 5.7). The seven oligomers (**1d-j**) are characterized by combining analytical, reversed phase HPLC, MALDI-TOF mass spectrometry, and ^{1}H-NMR spectroscopy (see experimental section). Clearly, the different urea groups (2 for trimer **1e**, 3 for tetramer **1f**, and 4 for pentamer **1g**) could be distinguished in the ^{1}H-NMR spectra.

Strikingly, no indications for the presence of cyclic (hexameric) compounds are observed, in none of the fractions (**1Ia-1IIIc**, **1d-j**), with none of the techniques (MALDI-TOF, ^{1}H-NMR, GPC).

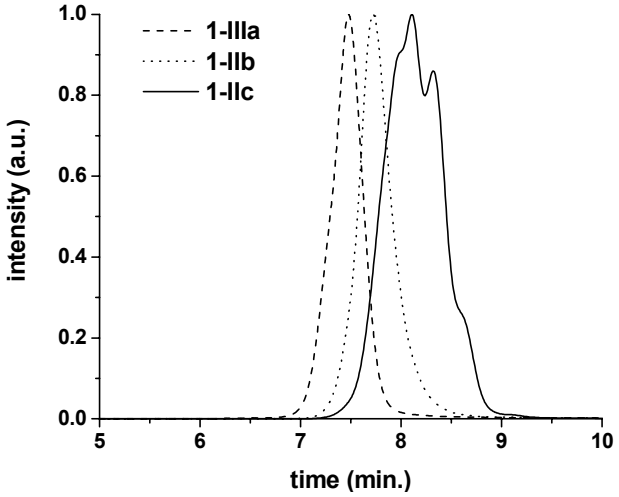

Fraction	t (min)	M_{top}	M_w/M_n
1-IIIa	7.42	10,677	1.41
1-IIb	7.67	6,951	1.16
1-IIc	8.05	3,521	1.28

Figure 5.6. *GPC traces (left) and data (right) of representative long (**1-IIIa**), intermediate (**1-IIb**), and short (**1-IIc**) polymer fractions.*

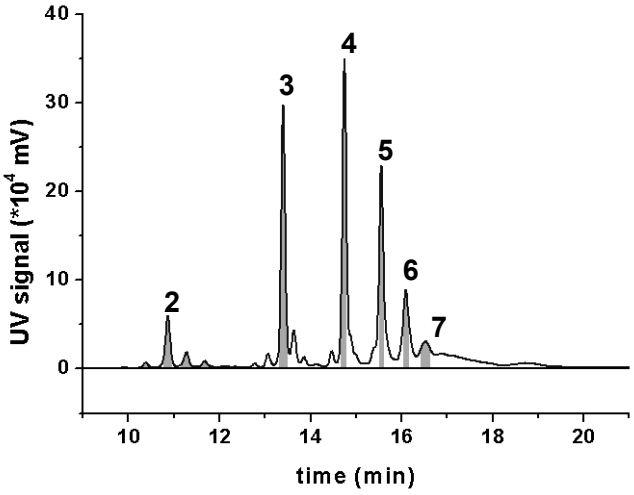

No.	n	purity
1d	2	'100 %'
1e	3	'100 %'
1f	4	'100 %'
1g	5	'100 %'
1h	6	3% 5-mer
1i	7	2% 5-mer, 9% 6-mer
1j	8	20% 6-mer, 30% 7-mer

Figure 5.7. *A preparative HPLC trace of oligomers **1d-j** (2-mer upto 8-mer, n = 2-8, respectively, left), and an overview of analytical HPLC data (right). See Scheme 5.9 for a definition of n.*

5.4.2 Stacking of phthalimide disks

In ^{1}H-NMR spectroscopy the inner urea proton of phthalimide disk **2** is clearly shifted downfield with respect to the outer one (8.74 versus 7.04 ppm), in agreement with intramolecular hydrogen bonding between the inner urea protons and the imide oxygens. These interactions give rise to a thermotropic liquid crystalline window, illustrated by DSC (K (47 °C, 8.1 kJ/mol) M (87 °C, 2.3 kJ/mol)), and birefringent textures in optical polarization microscopy. Although the temperature window is not large and transition enthalpies are low,[41] ordered architectures are observed in dilute (10^{-5} M) apolar solution (Figure 5.8). The UV-Vis spectrum in heptane is red shifted with respect to those in THF and chloroform (heptane: λ_{max} = 420 nm, λ_{onset} = 505 nm; THF: λ_{max} = 419 nm, λ_{onset} =

481 nm; chloroform: λ_{max} = 416 nm, λ_{onset} = 481 nm). Only in heptane a small[42] Cotton effect is observed. Heating from room temperature to 80 °C, causes the CD intensity to decrease gradually. Cooling down to 0 °C induces a change in shape of the Cotton effect. This behavior is reversible.

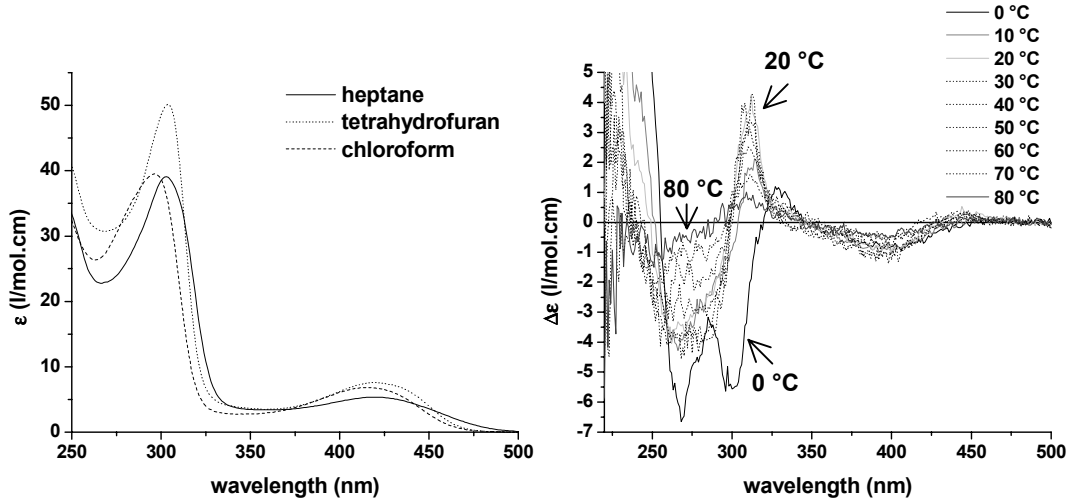

Figure 5.8. *UV-Vis spectra in different solvents (left), and temperature dependent CD spectra (right) of phthalimide disk **2** in heptane (3×10^{-5} M).*

5.4.3 Folding of the polymer

The first indication for the formation of a supramolecular architecture involving hydrogen bonding, was the large difference in solubility of polymer **1-IIIa** in chloroform (well soluble) and dichloromethane (poorly soluble). Peak broadening in ^{1}H-NMR ($CDCl_3$) only disappeared upon addition of the strong hydrogen bond competitor HFIP. In IR (Table 5.4) typically low positions of the carbonyl stretch vibrations are observed in the solid state (1644 cm^{-1}), as well as in solution (THF, heptane, chloroform). The NH and CO stretch vibrations display the lowest wavenumbers, so correspond to the strongest hydrogen bonding, in THF, followed by heptane and chloroform. The imide CO vibration appears at the highest wavenumbers in THF.

Table 5.4. *Wavenumbers σ [cm^{-1}] of the urea NH, urea CO, and imide CO stretch vibrations of poly-ureidophthalimide **1-IIIa** in the solid state and in different solvents.*

	urea NH	imide CO	urea CO
solid state	3346	1694	1645
THF	3340	1703	1641
heptane	3344	1694	1645
chloroform	3353	1696	1646

When a supramolecular architecture is indeed formed, one would expect the poly-ureidophthalimide polymer to fold into a helix with 6 units per turn, based on the chemical structure. However, from preliminary molecular modelling studies, it is deduced that 7.5 units are needed to complete one turn

(Figure 5.9). Most probably the hydrogen bonds between the urea protons and the imide oxygens lessen the angle between two monomeric units. In this way, no vertical stacks of urea or aromatic groups are formed, which would prevent an overall dipole moment within the helix. Diameters of 14 and 34 Å are estimated for the hollow core and the aromatic part of the helix,[43] respectively.

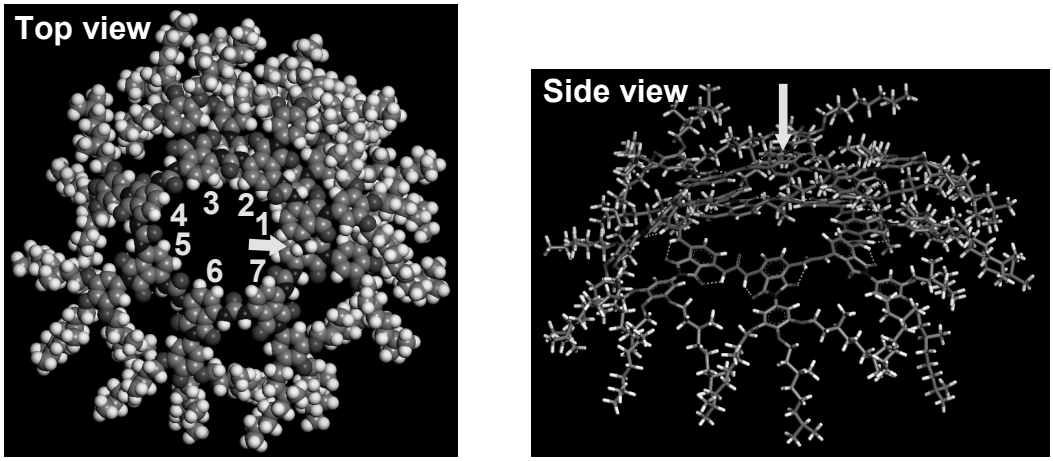

Figure 5.9. *Model of a decamer of ureidophthalimide **1**. In the top view (left,) the yellow arrow indicates the amine endgroup, and monomeric units of the helical pitch are numbered. In the side view (right), the yellow arrow indicates alternation of aromatic and urea groups in two consecutive turns of 7.5 units.*

Temperature dependent optical polarization microscopy indicates the presence of a liquid crystalline phase, although no textures can be grown, because the isotropization temperature (~300 °C) is well above the degradation point (~200 °C). However, a preliminary X-ray experiment showed two intense reflections, next to a broad halo (d = 4.9 Å) (Figure 5.10). One reflection is sharp (d_1 =42.4 Å), and might be attributed to the diameter of the helix. The other reflection is broad (d_2 = 26.3 Å), and might be assigned to regularity in the helix direction. No spectral changes are observed between 25 and 100 °C.

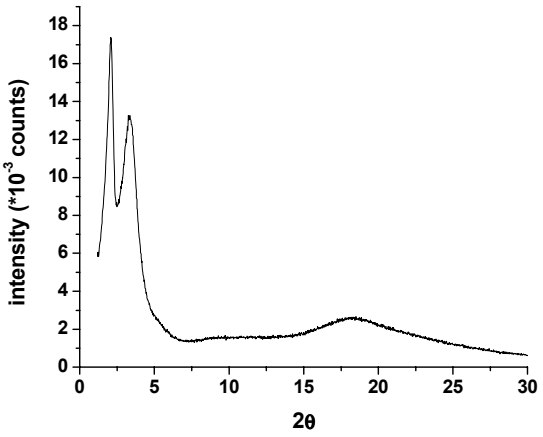

Figure 5.10. *X-ray spectrum of ureidophthalimide polymer **1-IIIa** at 100 °C.*

Ordered species are visualized beautifully using atomic force microscopy (Figure 5.11). Polymer **1-IIIa** is dropcast both from a dilute (0.03 mg/ml) tetrahydrofuran solution on mica, as well as from a heptane solution on graphite. In tetrahydrofuran straight rods are observed, indicating that the polymer chains lign up in a cylindrical aggregate, once they have adopted a circular conformation. Also the rods themselves align, showing a repetitive distance of 7 nm. Samples prepared from heptane show elongated aggregates, which are much more bent and flexible, pointing towards a somewhat less ordered architecture. Their width is estimated at 2 nm.

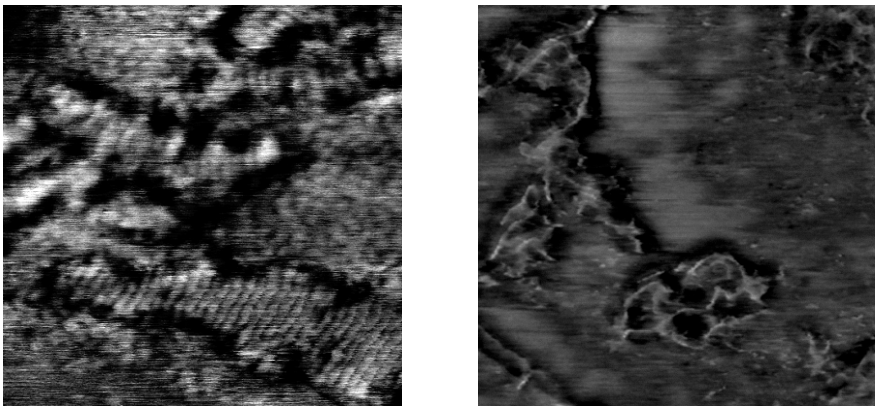

Figure 5.11. *AFM phase images (250 nm scale) of helical poly-ureidophthalimide **1-IIIa** dried from tetrahydrofuran on mica (left) and from heptane on graphite (right).*

The supramolecular architectures of long fraction **1-IIIa** are investigated further in dilute solution itself (0.03 mg/ml) using UV-Vis and CD spectroscopy (Figure 5.12). Consistent with the AFM images, it is found that chiral supramolecular architectures with a very high degree of ordering are present in the polar solvent tetrahydrofuran ($g = -1.2\times10^{-2}$). Less order is present in apolar solvents, such as heptane ($g = -5\times10^{-3}$), isooctane, methylcyclohexane and toluene, although the effect is still 10 times longer than that of phthalimide disk **2** ($\Delta\varepsilon = 5$ l/mol.cm). On the other hand, in the polar solvent chloroform, no Cotton effect is observed, suggesting a non-chiral, collapsed conformation of the polymer chains in this solvent. Differences in the UV spectra in the three solvents are very small (< 1 nm). Notably, in THF the UV and CD maximum coincide, while in heptane the UV maximum coincides with the CD zero crossing.

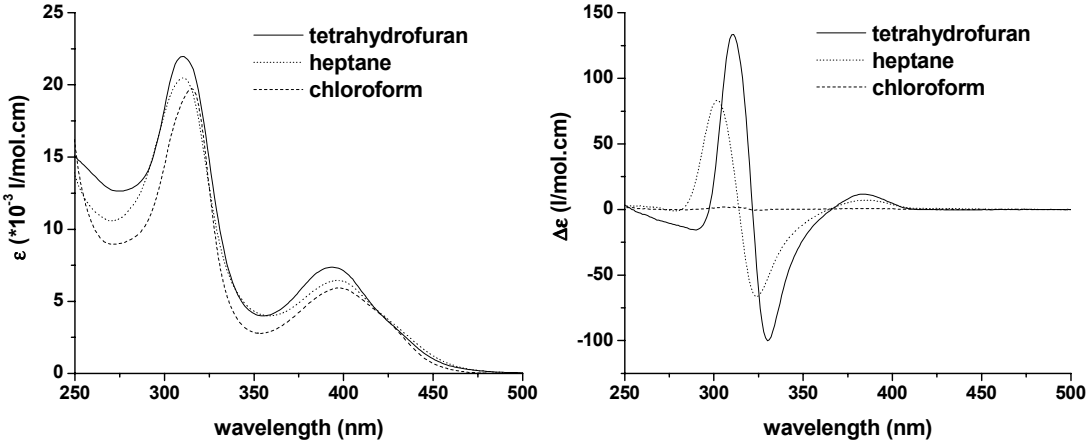

Figure 5.12. *UV-Vis (left) and CD (right) spectra (0.03 mg/ml, ε and Δε calculated per mole monomeric phthalimide units) of long ureidophthalimide fractions **1-IIIa** in THF, heptane, and chloroform.*

Both in heptane, as well as in tetrahydrofuran, order is hardly lost upon raising temperature (heptane 78 % at 90 °C, tetrahydrofuran 45 % at 55 °C, compared to 100 % at 20 °C). Again, a small shift in $\lambda_{max,\Delta\varepsilon}$ of the Cotton effects is found in heptane ($\lambda_{max,\Delta\varepsilon}$ = 325 nm at 10 °C, and 321 nm at 90 °C), while in THF no such shift occurs (Figure 5.13). Upon cooling, the architectures need at least several hours to regain their maximal amount of ordering. Both solvents feature a gradual decrease of λ_{max} in UV-Vis upon raising temperature ($\Delta\lambda_{max}$ = - 0.8 nm in THF and $\Delta\lambda_{max}$ = - 5 nm in heptane). The large decrease of λ_{max} in heptane, levels off at 90 °C.

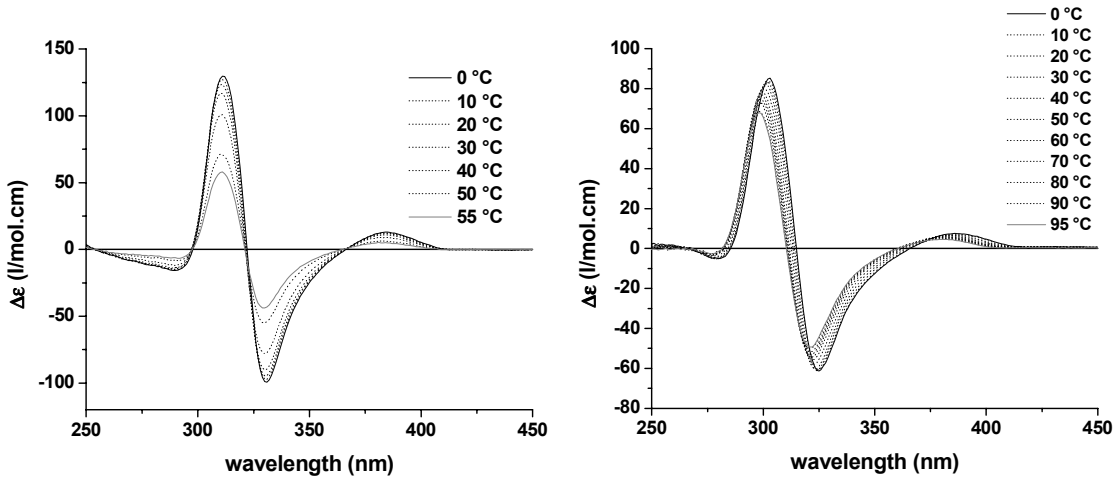

Figure 5.13. *Temperature dependent CD spectra (0.03 mg/ml, Δε calculated per mole monomeric phthalimide units) of long ureidophthalimide fractions **1-IIIa** in THF (left) and heptane (right).*

Preliminary concentration dependent measurements show a concentration independecy of ε, Δε, and g in a range between 5×10^{-4} and 5×10^{-6} in THF (Figure 5.14). At 1×10^{-6} Δε and g suddenly decrease significantly to half their original intensity (from 1×10^{-2} to 5×10^{-3}), but only for the band at 330 nm.In heptane both ε and Δε decrease gradually, while g stays constant (Figure 5.15).

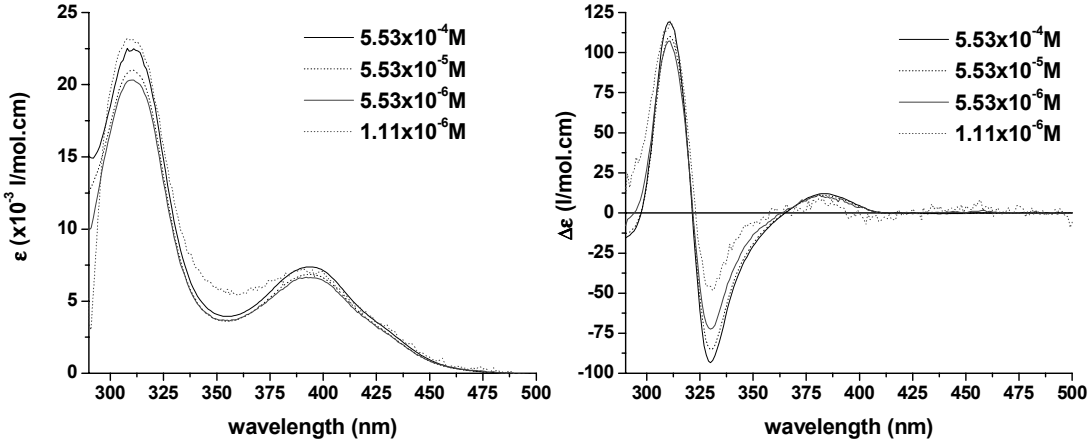

Figure 5.14. *Concentration dependent UV-Vis (left) and CD (right) spectra (0.03 mg/ml, ε and Δε calculated per mole monomeric phthalimide units) of long ureidophthalimide fractions* ***1-IIIa*** *in THF.*

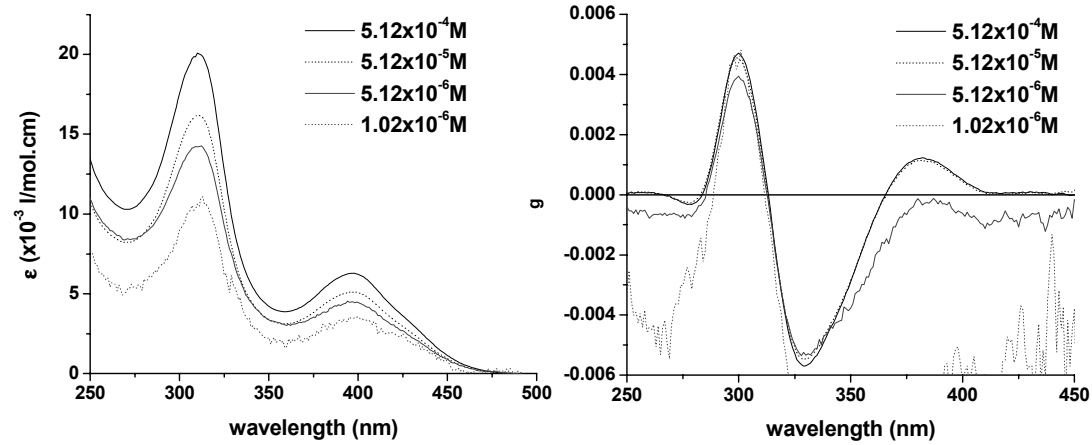

Figure 5.15. *Concentration dependent UV-Vis (left) and CD (right) spectra (0.03 mg/ml, ε and Δε calculated per mole monomeric phthalimide units) of long ureidophthalimide fractions* ***1-IIIa*** *in heptane.*

Denaturation experiments, in which chloroform is added stepwise to either a heptane or tetrahydrofuran solution, show that the chiral, helical conformations are unusually insensitive to the addition of chloroform. In THF, above 50 %v/v chloroform, a fairly sharp transition is observed, while in heptane, a much broader transition curve is found (Figure 5.16). It is found that the foldamer **1-IIIa** needs a long time (1 h), before equilibrium is reached upon addition of more chloroform, although this is not investigated elaborately yet. Changes in de UV-Vis maxima are extremely small ($\Delta\lambda_{max,UV}$ < 1 nm), but in heptane, a distinct shift of $\lambda_{max,\Delta\varepsilon}$ is found in the CD curves (0 % $CHCl_3$:

$\lambda_{max,\Delta\varepsilon}$ = 325 nm, and 90% $CHCl_3$: $\lambda_{max,\Delta\varepsilon}$ = 329 nm). Tetrahydrofuran denaturation curves show no such shift in $\lambda_{max,\Delta\varepsilon}$.

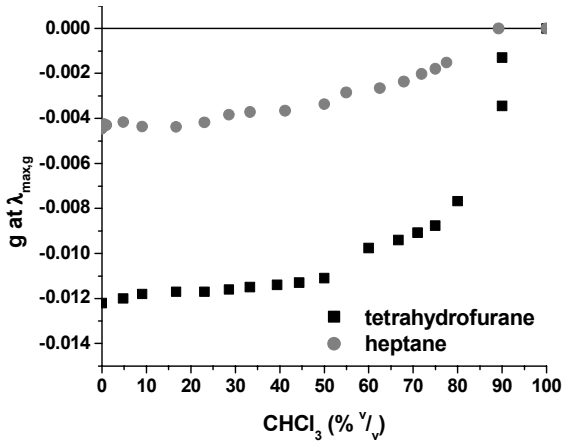

Figure 5.16. *Denaturation curves of poly-ureidophthalimide **6-IIIa** in THF (black squares) and heptane (gray circles) by stepwise addition of chloroform.*

5.4.4 Folding of the oligomers

Increasing stability of intramolecular hydrogen bonding upon chain-elongation is illustrated by a small downfield shift (0.05 ppm) of the protons of the inner urea groups (present in trimer **1e** and tetramer **1f**) compared to those of the outer ones (present in dimer, trimer and tetramer **1d-f**), which are typically positioned at 9.0 ppm. The folding of the oligomers is studied in more detail by monitoring the Cotton effect, and hence g, upon increasing chain length.

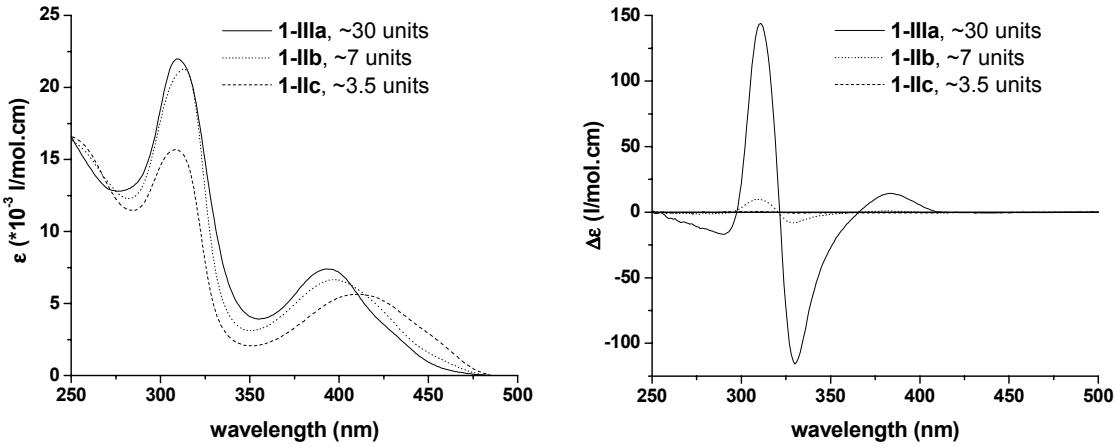

Figure 5.17. *UV-Vis (left) and CD spectra (right) in THF (~0.03 mg/ml), ε and Δε calculated per mole monomeric phthalimide units present in long (**1-IIIa**), intermediate (**1-IIb**), and short (**1-IIc**) ureidophthalimides*

This dependency is illustrated in THF by the representative long (**1-IIIa**), intermediate (**1-IIb**), and short (**1-IIc**) fractions. As described above (Figure 5.12), long fraction **1-IIIa** (~30 units) folds into a chiral structure with a very high degree of ordering in THF (g = -0.012). Remarkably, **1-IIb** (~7 units) shows only a minor Cotton effect, while **1-IIIa** (~3.5 units) shows no Cotton effect at all (Figure

5.17). The length (~7 units) at which supramolecular chirality starts to be expressed, coincides with the expected length of one pitch (Figure 5.9).

The correlation between expression of supramolecular chirality and a polymeric length of more than one pitch in THF, was elucidated in more detail by taking into account the CD intensities of all 9 polymeric fractions (**1-Ia** – **1-IIIc**, Table 5.3) and of the pure oligomers (**1d-j**, Figure 5.7). In tetrahydrofuran short oligomers (dimer **1d** upto pentamer **1g**) show no Cotton effect at all, while the hexa-, hepta- and octamer (**1h-j**) start showing a small amount of ordering. When the g values of the oligomers are compared to those of the 9 polymer batches with varying average length (Figure 5.18, left), clearly the intensity of the CD signal, and thereby the ordering in the architectures, keeps increasing, until it starts levelling off at approximately 30 units.

A strikingly different trend is found in heptane (Figure 5.18, right). Only the dimer and trimer (**1d,e**) do not show transfer of chirality, while the tetra- and pentamer (**1f,g**) already show g values in the range of that of the polymer mixture **1-IIIa** ($g = -4\times10^{-3}$). The hexa-, hepta-, and octamer (**1h-j**) yield intensities comparable to those found for the polymer **1-IIIa** in tetrahydrofuran ($g = -1\times10^{-2}$).

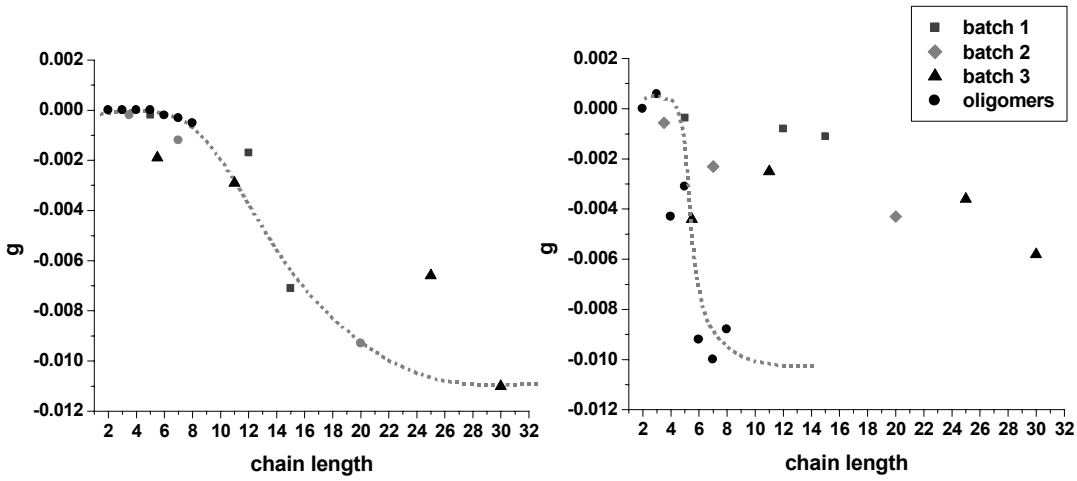

Figure 5.18. *Dependency of the Cotton effect on the chain length in tetrahydrofuran (left) and in heptane (right) (O.D. ~ 0.4 for **1a-h** and O.D.~0.05 for **1i-j**).*

Additional information for the final molecular picture, comes from mixing the tetramer **1f** and polymer **1-IIIa** in equimolar amounts, which resulted in a arithmetic average of the g value (**1f**: g = 0; **1-IIIa**: $g = -11.5\times10^{-3}$; 50/50 mixture: $g = -6.2\times10^{-3}$), when the experiment was performed in THF (Figure 5.19). In heptane, both g-values of the tetramer **1f** and polymer **1-IIIa** are in the order of -4.5×10^{-3}, and also the 50/50 mixture displays this value. Therefore, the tetramer **1f** was mixed with the octamer **1j**, also in a 50/50 mixture. Remarkably, the intensity of the negative signal around $\lambda = 330$ nm decreased more than linearly (**1f**: g ~ 0; **1g**: $g = -9.8\times10^{-3}$; 50/50 mixture: $g = -1.7\times10^{-3}$). This

experiment was repeated for the pentamer **1g** (**1g**: g ~ 0; **1-IIIa**: g = -9.8×10^{-3}; 50/ 50 mixture: g = -1.8×10^{-3}). For the positive signal around λ = 330 nm arithmetic averages were observed.

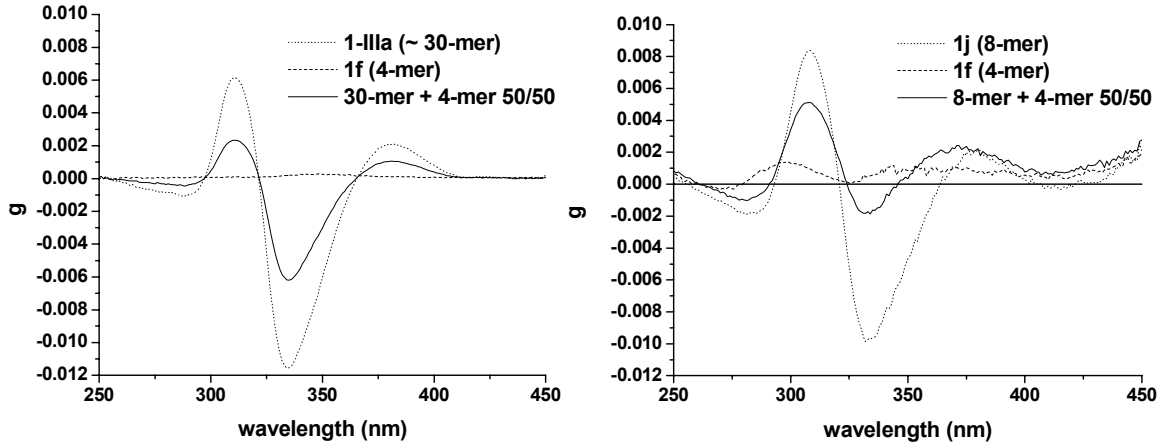

Figure 5.19. *Mixing experiments in THF (left, O.D. ~ 0.3), in which polymer **1-IIIa** is mixed with tetramer **1f** in a one to one ratio. In heptane (right, O.D. ~ 0.02), octamer **1j** and tetramer **1f** are mixed one to one.*

5.5 Chiral ureidophthalimide helices; folding and stacking

In dilute apolar solution, strong changes in the shape of the Cotton effect of phthalimide disk **2** are observed upon raising temperature. Together with the small overall intensity,[42] this indicates that transfer of chirality is not very eminent for this small structure. However, a modest expression of supramolecular chirality in the monomer, or model compound, might be promising for optimal supramolecular order in the corresponding polymer, where multiple of these 'weak' interactions are supposed to operate cooperatively.[3,12] Indeed, highly ordered architectures are observed for ureidophthalimide polymer **1,** as follows from the results above.

Remarkably, no cyclic structures are observed in reaction mixtures of **1** using GPC, ^{1}H-NMR or MALDI-TOF. It has to be noted that cyclic structures would not contain any primary amine functions, and might not get protonated, and thus not detected with MALDI-TOF in a mixture of amine end capped oligomers. However, the absence of cyclic structures is in congruence with the molecular model, which shows that two chain ends do not exactly match upon completion of one turn. In the future such macrocycles might be obtained by adjustment of the reaction conditions (use of a solvent favorable for helical conformation e.g. THF, low concentration, combination of suitable oligomers e.g. trimers, or a template e.g. triflate salt).[18]

The molecular model indicates that the aromatic cross section of the helical conformer of ureido polymer **1** amounts to 34 Å. In X-ray the corresponding sharp reflection is found at d_1 = 42.4 Å, which suggests a high degree of order. The difference of 11.6 Å between the estimation of the aromatic cross section, and the 'inter column distance' in X-ray spectroscopy corresponds to the distance taken up by one extended (*S*)-3,7-dimethyloctyl chain as found for C_3 symmetrical disks

(Chapter 2). Therefore, it is a strong indication for the architecture to be columnar. In AFM, columnar architectures are observed indeed, and their width is determined to be 2 nm (dropcast from heptane) and 7 nm (dropcast from THF), on average corresponding to the X-ray findings. The second, broad transition d_2 = 26.3 Å in X-ray could indicate order in the direction of the helix itself. Probably, the broadness is caused by the distribution of chain lengths present in mixture **1-IIIa**. The reflection corresponds to an estimated height of a molecular model of a ureidophthalimide 30-mer of 3 nm,[44] although 5 pitches of **1-IIIa**, only bridge 15 Å, when the π-π distance between two pitches is assumed to be 3.5 Å. The ureidophthalimides need to be investigated in more detail by comparing X-ray data on other oligomers and polymers **1**. In AFM pictures of polymer **1-IIIa** dropcast from THF, the rods are as long as 30 nm, and with an estimated length of 3 nm of the 30-mer helix, this would mean that 10 polymer helices are stacked on top of each other.

In dilute solution, CD spectroscopy reveals the folding of ureidophthalimides **1** in highly ordered architectures. The differences between various solvents might be rationalized by specific polymer-solvent interactions. IR spectroscopy on phthalimide **1-IIIa** indicates strongly hydrogen bonded urea groups in THF (lowest wavenumbers for NH and CO urea, Table 5.4). THF is a hydrogen bond acceptor and might increase syn-coplanarity of the two urea protons.[45] The higher wavenumber for the imide CO, subscribes formation of a 6-membered hydrogen bonded unit. In heptane, the g-value of **1-IIIa** is lower than in THF ($g = -1.2\times10^{-2}$ and -4×10^{-3}, respectively). Unlike THF, heptane is unable to co-structure the architecture inside the (poly-ureido) core, and it only interacts with the periphery of the architecture. This then has to find its optimal conformation by itself. Finally, in chloroform no Cotton effect is observed, most probably because this hydrogen bond donor disturbs the critical hydrogen bonds between polymer imide and urea groups to some extent.

The supramolecular chirality is stable upon raise of temperature, dilution, or addition of a 'good' solvent. In temperature dependent and denaturation experiments hysteresis is observed. This indicates that the maximal stability, and optimal strength of non-covalent interactions, is reached for this poly-ureidophthalimide structure. Stronger interactions will probably be at the expense of flexibilty and reversibility of the folded polymer.[20] Regrettably, insensitivity of CD intensity g towards dilution, prevents the gathering of additional evidence for the intra- and/or intermolecular folding behavior (*vide infra*). Such behavior is not uncommon for strong intermolecular hydrogen bonded interactions.[25,34]

Also the fact that the chloroform denaturation curve of poly-ureidophthalimide polymer **1-IIIa** shows a much sharper transition in THF than in heptane, indicates a higher degree of order in the former solvent, as a sharp transition generally corresponds to the unfolding of a highly ordered, 'crystalline like' foldamer conformation.[25] However in general, the ureidophthalimide folding process, might be considered as an elaborate one, comprising a range of (semi)ordered conformations, indicated by the broad denaturation curves, and the time dependent effect in these curves. The

findings of this ureido polymer **1-IIIa**, are in contrast to the behavior of phenylene ethynylene oligomers, which show distinct, gradual differences in $\lambda_{max,UV}$ upon denaturation, while the transition in CD is rather sharp.[25]

According to CD spectroscopy in dilute THF solution, a Cotton effect starts developing starting from a chain length of 6-8 (**1h-j**). It reaches a considerable value (-2×10^{-3}) at a chain length of 10, in agreement with the 7.5 units for one pitch in the molecular model. Chirality can only be transferred from the CD silent chiral alkyl chains in the periphery, to the CD active chromophores in the backbone, when an ordered architecture is formed. Therefore it is a probe for the presence of circular, helical supramolecular structures. Other examples displaying a similar chain-length 'treshold' for the helix to be stable and supramolecular chirality to be expressed are α- and β-peptides,[3a,12] and *meta*-phenylene ethynylenes.[25] The order in the helical phthalimide chains **1** keeps increasing, until a length of 30 is reached. In the 30-mer, already two pitches would be sandwiched between turns above and below. Therefore it is reasonable to accept that the phthalimide foldamer reaches its maximal amount of ordering at this point. This chain-length dependence indicates that the behavior in dilute THF solution is monomolecular. Also the proportional g value found for a 50/50 mixture of the tetramer (g = 0) and the polymer ($g = -1\times10^{-2}$) suggests that only intramolecular ordering occurs in dilute tetrahydrofuran solution. However, it can not be excluded totally, that in the 30-mer, when intramolecular stacking becomes optimal, intermolecular stacking is induced concomitantly. In long chains, stacking of helices might not be influenced by amine endgroups or by incorporation of shorter fragments. AFM illustrates that helices start stacking in THF at higher concentration, or at the surface.

In dilute heptane solution, the ordering phenomena are certainly not monomolecular; moreover, the intermolecular stacking of the helices seems to suffer from polydispersity. For apolar *meta*-phenylene ethynylene helices, intermolecular effects were also suspected to influence the expression of supramolecular chirality.[25] Reaching the hexa-, hepta- and octamer (**1h-j**), the g-value levels off at -1×10^{-2}, the same value found earlier for the polymer (**1-IIIa**) in tetrahydrofuran. This implicates that upon completion of one turn, maximal ordering is already reached. Circular oligomers (**1h-j**) are stabilized by other oligomers in an identical circular conformation, positioned above and below in the same stack (Figure 5.20). Having established that also in heptane 7.5-turn helices are formed, we may conclude that the Cotton effect produced by the tetra- and pentamer (**1f,g**) is originating from intermolecular stacking, leading also to a similar 7.5-turn helix. In those helices even a single turn comprises several molecules. From the fact that similar g-values are found for tetramer, pentamer and polymers (-4×10^{-3}), whereas much higher g-values are obtained for the hexa-, hepta- and octamer (-1×10^{-2}), one can conclude indeed that in the polymeric mixture intermolecular stacking is not perfect. This polydispersity effect was illustrated by mixing experiments. Mixing the tetramer or the pentamer in a 1 to 1 ratio with the octamer, yielded a Cotton effect for the mixture smaller than the

arithmetic average. This evidence is not overwhelming, since probably more lengths have to be mixed before the effect gets affected substantially. The octamer mixture itself, containing 20 % hexamer and 30 % heptamer (Figure 5.7), still shows a CD intensity of -1×10^{-2}.

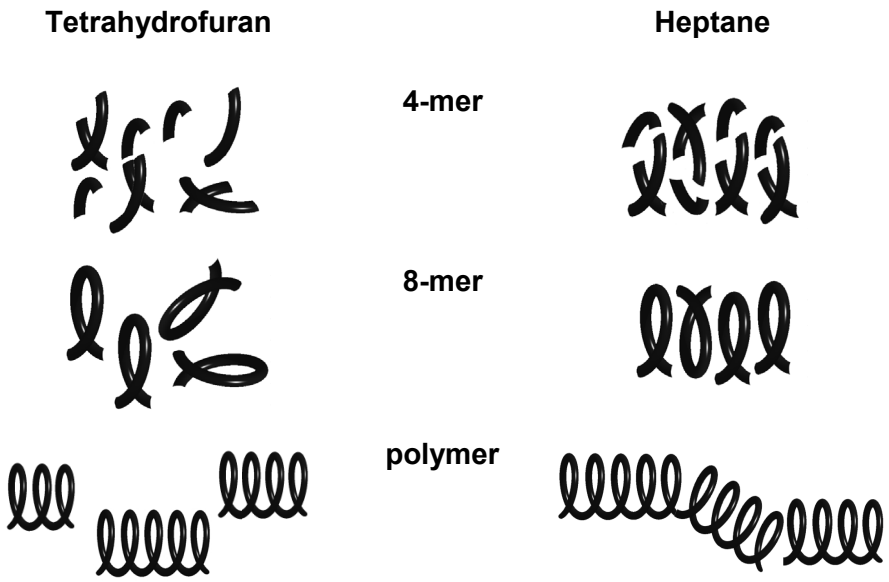

Figure 5.20. *Schematic representation of the folding in tetrahydrofuran and stacking in heptane of various poly-ureidophthalimide chain lengths.*

The fact that in heptane, $\lambda_{max,UV}$ (310.5 nm) corresponds with the zero crossing in CD (Figure 5.12), while in THF $\lambda_{max,UV}$ and $\lambda_{max,CD}$ coincide, could be an indication for intermolecular ordering in heptane. In heptane a single exciton coupled chromophore seems prominent. In THF, however, the signal seems a combination of two exciton coupled signals, indicating a different mode of ordering. Also, the shifts of $\lambda_{max,\Delta\varepsilon}$ in heptane during temperature dependent and denaturation experiments, might indicate intermolecular aggregation, because in tetrahydrofuran, these shifts do not occur. Furthermore, the drop in ε upon dilution is absent in THF. Finally, the g-value of the tetra- and pentamer **1f,g** is concentration dependent in heptane (4-mer **1f**: O.D.~0.4: $g = -4\times10^{-3}$; : O.D.~0.02: g ~ 0, Figures 5.18 and 5.19). For longer oligomers **1h-j** and polymers **1**, no such behavior is observed (Figures 5.14 and 5.15, in fig. 5.15: O.D.~0.64 to ~0.023: $g = -5.4\times10^{-3}$). This suggest that the expression of supramolecular chirality of tetra- and pentamer **1f,g** relies on intermolecular stacking, indeed.

For the polymer (~30 units, **1-IIIa**), the stacks of polymers have been actually visualized in AFM. In heptane, the intermolecular stacking seems to extend to dilute solutions (10^{-5} M) and short fragments (tetra- and pentamers). In THF, intermolecular aggregation is limited to higher concentrations and longer fragments. For example, octamers in a 10^{-5} M THF solution display a limited expression of supramolecular chirality ($g = 10^{-4}$), because the helical conformation is not

stabilized. In dodecane this conformation is more stable ($g = -4\times10^{-3}$), due to the intermolecular stacking (Figure 5.20, 8-mer). AFM/X-ray measurements and concentration dependent CD measurements on oligomers (**1d-j**) and various polymeric mixtures (**1-Ia – 1-IIIc**) might be helpful to elucidate the intra- and intermolecular folding and stacking.

5.6 Conclusions

Intramolecular hydrogen bonding between imide oxygens and urea protons, has been designed to order poly-ureidophthalimides **1**. The intramolecular hydrogen bonding is already supported by downfield positions of NH (9.0 ppm) and H-4 (8.6 ppm) signals in ^{1}H-NMR spectra of monourea phthalimide models **3a-e**. Also the strong upfield signal (115 ppm) of C-2 (*ortho* to the urea) illustrates the locked conformation of ureidophthalimides. Disk **2** shows that only two ureidophthalimide hydrogen bonding interactions, in combination with π-π stacking and phase separation, give already rise to liquid crystallinity. Also, a modest expression of supramolecular chirality in observed in dilute apolar solution. Multiple of these imide-urea hydrogen bonding interactions work cooperatively in ureidophthalimide polymers **1**, causing the structures to fold in highly ordered supramolecular architectures.

The columnar nature of the architectures is visualized by AFM microscopy, while a pitch of 6-8 units follows from the cross section determined with X-ray (d_1 = 42.4 Å). A convincing indication for helicity is the 'treshold' for expression of supramolecular chirality of 6-8 units in dilute THF solution, together with maximal order at about 30 units (~5 turns). Both in concentrated THF solution (on the surface), and in dilute solutions in heptane (10^{-5} M), on top of intramolecular folding, intermolecular stacking of the helices occurs, following from AFM pictures and chain-length dependent CD studies, respectively. In heptane, short oligomers (tetra- and pentamer) are able to self-assemble into circular aggregates, which concomitantly stabilize each other by alignment in an extended, helical architecture. However, the final order in these stacked polymers in heptane is lower than that of the monomolecular foldamers in THF ($g = -0.004$ and -0.012, respectively).

The helical conformation of the polymer is highly stable upon raising temperature, dilution, or addition of a hydrogen bond competitive solvent. Hysteresis is observed during these temperature dependent and denaturation experiments. Apparently, order and stability are optimally balanced for this poly-ureidophthalimide foldamer, since stronger hydrogen bonding and π-π stacking interactions may occur at the expense of reversibility and flexibility of the helical architecture.

The ureidopthalimide polymer is well accessible, as it is formed in a single condensation step, while a variety of amine-containing functionalities in principle can easily be incorporated into the monomeric unit. This renders this highly ordered poly-ureidophthalimide helix, enclosing an appealing hollow core, a supramolecular scaffold with potential applications in biological or materials science.

5.7 Experimental section

General. General aspects concerning synthesis, characterization, optical microscopy, DSC, and X-ray have been described in Chapter 2, whereas details about UV-Vis and CD spectroscopy can be found in Chapter 3. Phosgene is used as a commercial 20 %w/w solution in toluene. The synthesis of 3-acetylaminophthalic anhydride,[35] and 3,4,5-tris((*S*)-3,7-dimethyloctyloxy)aniline[39] has been described previously. Acetonitrile was dried on Merck molecular sieves (3 Å). Tetrahydrofuran was distilled from molecular sieves (4 Å) and toluene was distilled from Na. Matrix assisted laser desorption/ionization mass spectra were obtained using α-cyano-4-hydroxycinnamic acid or DCTB (*trans*-2-[3-(4-*tert*-butylphenyl)-2-methyl-2-propenylidene]malononitrile) as the matrix on a PerSeptive Biosystems Voyager-DE PRO spectrometer. GPC measurements on oligomeric mixtures 1a-c were performed on a mixed D column (Pl gel 5 μm, 200-400.000 g/mol), with a flow of 1 ml/min, and chloroform as the eluting solvent. The injection volume was 50 μl and UV detection (254 nm) was applied. Polydispersity indices were calculated from a polystyrene standard. Oligomeric mixtures of 1 were fractionated to yield oligomers **1d-j** on a semi-preparative, reversed phase HPLC column (Alltima C18, 5 μm; d = 10 mm, l = 150 mm), with a flow of 5 ml/min and a gradient from 80/20 %v/v THF/water to 100 %v/v THF as the eluting solvent. The injection volume was 10 μl and UV detection (315 nm) was applied. Oligomers were characterized on an analytical, reversed phase HPLC column (Alltima C18, 5 μm; d = 4.6 mm, l = 150 mm), with a flow of 1 ml/min and a gradient from 80/20 %v/v THF/water to 100 %v/v THF as the eluting solvent. The injection volume was 20 μl and again UV detection (315 nm) was applied. Atomic force microscopy images were recorded under ambient conditions using a Digital Instrument Multimode Nanoscope IV operating in the tapping mode regime. Micro-fabricated silicon cantilever tips (NSG01) with a resonance frequency of approximately 150 kHz and a spring constant of about 5.5 Nm^{-1} were used. The scan rate varied from 0.5 to 1.5 Hz. The set-point amplitude ratio ($r_{sp} = A_{sp}/A_o$, where A_{sp} is the amplitude setpoint, and A_o is the amplitude of the free oscillation) was adjusted to 0.9. All AFM images shown were subjected to a first-order plane-fitting procedure to compensate for sample tilt. AFM analysis was done off-line. AFM samples were prepared by drop casting the 1-IIIa solution under a solvent atmosphere on freshly cleaved highly oriented pyrolytic graphite (HOPG) or muscovite mica.

Amino terminated poly-{3-ureido-N-[3,4,5-tri((*S*)-3,7-dimethyloctyloxy)-phenyl]phthalimide-N',6-diyl} (1a-c). Diamino-monomer **17** (200 mg, 0.277 mmol) and diisocyanato-monomer **18** (214 mg, 0.277 mmol) were dissolved in toluene (3.5 ml) and 4-dimethylaminopyridine (15 mg, 0.12 mmol) was added. After stirring 1 h at 80 °C, the solvent was evaporated and DMAP removed by column chromatography (silica gel, chloroform + 0-0.75% methanol, R_f = 0.2–0.9). This yielded three fractions of ureidophthalimide polymer **1**, of which the high molecular weight material (**1a**, ~225 mg, ~55 %) eluted first, followed by an intermediate (**1b**, ~65 mg, ~15 %**)** and a low molecular weight fraction (**1c**, ~65 mg, ~15 %). **1a**: ^{1}H-NMR ($CDCl_3$) δ 9.04 (NHCONH, bs, 2nH), 8.73 (CHCNH, bs, 2nH), 8.48 (C<u>H</u>CHCNH_2, m, 2H), 6.95 (CHCNH_2, m, 2H), 6.57 (CHCN, s, 2nH), 5.18 (NH_2, bs, 4H), 4.00 (OCH_2, m, 6nH), 1.85 ($OCH_2C\underline{H}_A$, m, 3nH), 1.71 ($OCH_2C\underline{H}_B$, m, 3nH), 1.51 (C*H$CH_3C\underline{H}_2$, m, 6nH), 1.26 (C*H and C*H$CH_3CH_2C\underline{H}_2$, m, 9nH), 1.15 (C<u>H</u>$(CH_3)_2$ and C<u>H</u>$_2$CH$(CH_3)_2$, m, 9nH), 0.93 (C*CH_3, m, 9nH), 0.86 (CH_3, dd, 18nH) ppm; ^{13}C-NMR ($CDCl_3$) δ 168.6 (CO), 153.5 (C3'), 150.8 (NHCONH), 138.3 (C4'), 133.2 (C3), 127.0 (C4), 125.5 (C1'), 113.7 (C1), 105.1 (C2'), 71.7, 67.5 (OCH_2), 53.4, 39.4, 39.3, 37.5, 37.4, 37.4, 37.1, 36.3, 32.7, 31.9, 30.0, 29.8, 29.7, 29.4, 28.0, 28.0, 27.1, 24.7, 24.5, 22.7, 22.6, 22.6, 19.7, 19.6, 19.5, 14.1 (C_9H_{19}) ppm; IR (ATR): 3346, 2954, 2926, 2870, 1735, 1694, 1645, 1596, 1500, 1474, 1439, 1419, 1384, 1297, 1277, 1261, 1220, 1175, 1114, 1018, 928, 802, 763, 692 cm^{-1}; MALDI-TOF MS: calculated: dimer, 1470.06; trimer, 2217.58; tetramer, 2966.10; pentamer, 3713.62; found (Na-adducts): dimer, 1493.82; trimer, 2241.64; tetramer, 2990.34; pentamer, 3738.02.

Oligomers (1d-j). ($CDCl_3$): trimer: δ 8.99 (NHCONH, bs, 4H), 8.69 (C<u>H</u>CNH, bs, 2H), 8.55, and 8.48 (C<u>H</u>CHCNH_2, m, 2H), 6.97 (C<u>H</u>CNH_2, m, 2H), 6.58 and 6.57 (CHCN, m, 6H), 5.18 (NH_2, bs, 4H), 4.00 (OCH_2, bs, 18H), 1.85 - 0.86 (alkyl H, m, 171H) ppm; tetramer δ 9.06 (NHCONH, bs, 2H), 9.01 (NHCONH, bs, 2H), 8.99 (NHCONH, bs, 2H), 8.71 (C<u>H</u>CNH, bs, 4H), 8.55, and 8.48 (C<u>H</u>CHCNH_2, m, 2H), 6.97 (C<u>H</u>CNH_2, m, 2H), 6.58 and 6.56 (CHCN, m, 8H), 5.18 (NH_2, bs, 4H), 4.00 (OCH_2, bs, 24H), 1.85 - 0.86 (alkyl H, m, 228H) ppm; pentamer: δ 9.05 (NHCONH, bs, 4H), 9.00 (NHCONH, bs, 2H), 8.98 (NHCONH, bs, 2H), 8.72, and 8.73 (C<u>H</u>CNH, m, 6H), 8.55, and 8.48 (C<u>H</u>CHCNH_2, m, 2H), 6.97 (C<u>H</u>CNH_2, m, 2H), 6.58 and 6.57 (CHCN, m, 10H), 5.18 (NH_2, bs, 4H), 4.00 (OCH_2, bs, 30H), 1.85 - 0.86 (alkyl H, m, 285H); MALDI-TOF MS: calculated: dimer, 1470.06; trimer, 2217.58; tetramer, 2966.10; pentamer, 3713.62; hexamer, 4462.14; heptamer, 5209.66; octamer, 5958.18; found (Na-adducts): dimer, 1493.00; trimer, 2240.39; tetramer, 2989.10; pentamer, 3735.71; hexamer, 4484.51; heptamer, 5233.08; octamer, -.

3,6-Bis[3,4,5-tri((*S*)-3,7-dimethyloctyloxy)-phenylureido]-N-[3,4,5-tri((*S*)-3,7-dimethyloctyloxy)phenyl]-phthalimide (2). A solution of 3,6-diisocyanato-N-[3,4,5-tri((*S*)-3,7-dimethyloctyloxy)-phenyl]phthalimide

(161 mg, 0.208 mmol) in toluene (2 ml) was added dropwise to a solution of 3,4,5-tri((*S*)-2,7-dimethyloctyloxy)aniline (292 mg, 0.520 mmol) and 4-dimethylaminopyridine (5.0 mg, 0.041 mmol) in toluene (5 ml) at 100 °C. After 1 h the solvent was evaporated, and the product purified using column chromatography (silica gel, dichloromethane + 0-1 % $^{v}/_{v}$ methanol). Finally, phthalimide disk **2** was obtained as a sticky, orange solid (267 mg, 68 %): mp = 47 °C; ^{1}H-NMR ($CDCl_3$) δ 8.74 (inner urea NH, s, 2H), 8.62 (phthalimide CH, s, 2H), 7.04 (outer urea NH, s, 2H), 6.65 (COR*CH, s, 4H), 6.56 (COR*CH, s, 2H), 3.96 (OCH_2, m, 18H), 1.83 ($OCH_2C\underline{H}_A$, m, 9H), 1.68($OCH_2C\underline{H}_B$, m, 9H), 1.52 ($C^*HCH_3C\underline{H}_2$, m, 18H), 1.31 (C*H and $C^*HCH_3CH_2C\underline{H}_2$, m, 27H), 1.15 ($C\underline{H}(CH_3)_2$ and $C\underline{H}_2CH(CH_3)_2$, m, 27H), 0.90 ($C^*CH_3$, m, 27H), 0.87 ($CH_3$, m, 54H) ppm; ^{13}C-NMR ($CDCl_3$) δ 168.5 (CONRCO), 153.4 (C3'), 153.3 (C3''), 152.0 (NHCONH), 138.1 (C4'), 134.7 (C1''), 133.4 (C4''), 133.1 (C3), 127.0 (C4), 125.8 (C1'), 113.0 (C1), 105.4 (C2'), 99.3 (C2''), 71.7, 71.7, 67.5, 67.2 (OCH_2), 39.3, 39.3, 37.6, 37.4, 37.3, 36.4, 29.8, 29.7, 29.7, 28.0, 24.7, 24.7, 22.7, 22.6, 19.5, 19.5, 19.5, 19.4 (C_9H_{19}) ppm; IR (ATR): 3357, 2954, 2926, 2867, 1746, 1719, 1686, 1641, 1601, 1560, 1490, 1469, 1427, 1384, 1366, 1293, 1219, 1194, 1117, 1048, 1001, 930, 836, 762, 733, 694 cm^{-1}; Elemental analysis: calculated: $C_{118}H_{201}N_5O_{13}$ (722.07): C, 74.68; H, 10.67; N, 3.69; found: C, 74.10; H, 10.68; N, 3.68; MALDI-TOF MS: calculated: 1897.52, found: 1920.47 (Na-adduct).

3,3'-(N,N'-Ureido)-bis(N-methylphthalimide) (3a). 3-Amino-N-methylphtalimide (92 mg, 0.53 mmol) was added to a 20% phosgene solution in toluene (0.139 ml, 0.26 mmol) diluted in toluene (10 ml). After 30 min stirring at reflux temperature, DMAP (65 mg, 0.53 mmol) was added and a precipitate was formed. After 1 h the precipitate was filtered and washed with water (10 ml). Bringing the crude product in CH_2Cl_2, drying with $MgSO_4$, and filtration gave ureidophthalimide **3a** (53 mg, 53 %) as a white powder: mp = 312 °C (degradation); ^{1}H-NMR ($CDCl_3$) δ 9.22 (NHCONH, bs, 2H), 8.62 (H4, d, 2H), 7.68 (H5, t, 2H), 7.51 (H6, d, 2H), 3.19 (NCH_3, s, 6H) ppm; IR (ATR): 3460, 3346, 1751, 1689, 1629, 1597, 1537, 1477, 1443, 1376, 1328, 1279, 1224, 1188, 988, 806, 7452, 679 cm^{-1}.

3,3'-(N,N'-Ureido)-bis(N-octylphthalimide) (3b). A solution of 20% phosgene in toluene (0.39 ml, 0.73 mmol) was added dropwise to a solution of 3-amino-N-octylphthalimide (0.40 g, 1.5 mmol) in toluene (7 ml), which caused formation of a precipitate. After 1 h the reaction mixture was brought to reflux temperature to bring the precipitate into solution, and DMAP (18 mg, 0.15 mmol) was added. The reaction mixture was left for 1.5 h after which the solvent was evaporated. The crude product was treated with methanol to obtain ureidophthalimide **3b** (0.34 g, 82 %): mp = 172 °C; ^{1}H-NMR ($CDCl_3$) δ 9.23 (NHCONH, bs, 2H), 8.62 (H4, d, 2H), 7.67 (H5, t, 2H), 7.49 (H6, d, 2H), 3.66 (NCH_2, m, 4H), 1.67 ($NCH_2C\underline{H}_2$, d, 4H), 1.29 ($(CH_2)_5$, m, 20H), 0.87 (CH_3, m, 6H) ppm; ^{13}C-NMR ($CDCl_3$) δ 170.6 (CO), 168.1 (CO), 151.2 (NCONH), 137.9 (C3), 135.9 (C5), 132.0 (C1), 124.1 (C4), 117.6 (C6), 115.8 (C2), 38.3 (NCH_2), 32.0, 29.4, 29.4, 28.8, 27.1, 22.8 (C_6H_{12}), 14.3 (CH_3) ppm; IR (ATR): 3445, 3313, 3082, 2956, 2922, 2854, 1761, 1734, 1682, 1638, 1622, 1602, 1542, 1475, 1446, 1405 cm^{-1}.

3,3'-(N,N'-Ureido)-bis[N-(4-methoxyphenyl)phthalimide] (3c). A solution of 20% phosgene in toluene (0.47 ml, 0.90 mmol) was added dropwise to a solution of 3-amino-N-(4-methoxyphenyl)phthalimide (0.48 g, 1.8 mmol) in acetonitrile (25 ml), which caused formation of a precipitate and a color change from yellow to yellow/white. After 1.5 h, DMAP (22 mg, 0.18 mmol) was added, and the mixture was brought to reflux. After 1 night, the solvent was evaporated and the crude product washed with hot acetonitrile to obtain ureidophthalimide **3c** (60 mg, 12 %): mp = 300 °C; ^{1}H-NMR (DMSO-*d6*) δ 10.12 (NHCONH, bs, 2H), 8.46 (H4, d, 2H), 7.81 (H5, t, 2H), 7.57 (H6, d, 2H), 7.36 (H2', d, 4H), 7.06 (H3', d, 4H), 3.79 (OCH_3, s, 6H) ppm; ^{13}C-NMR (DMSO-*d6*) δ 168.1 (CO), 167.6 (CO), 159.6 (C4'), 152.9 (NHCONH), 137.7 (C3), 136.1 (C5), 132.8 (C1), 129.5 (C2'), 126.9 (C1'), 124.9 (C4), 118.1 (C3'), 117.8 (C6), 114.8 (C2), 56.1 (OCH_3) ppm; IR (ATR): 3318, 3121, 1769, 1756, 1738, 1696, 1616, 1591, 1541, 1517, 1474, 1435, 1426, 1397 cm^{-1}.

3,3'-(N,N'-Ureido)-bis[N-(3,4,5-tridodecyloxyphenyl)phthalimide] (3d). A solution of 3-isocyanato-N-(3,4,5-tridodecyloxyphenyl)phthalimide (0.52 g, 0.63 mmol) in toluene (30 ml) was added to a solution of 3-amino-phthalimide **5d** (0.47 g, 0.59 mmol) and 4-dimethylaminopyridine (15 mg, 0.12 mmol) in toluene (40 ml). The solution was stirred for 40 h at 110 °C, allowed to cool and evaporated to dryness. The obtained residue was dissolved in THF (5 ml) and precipitated from 50% ethyl acetate / hexane (100 ml). The solution was filtrated and the residue was washed with 50% ethyl acetate / hexane (2 × 10 ml) and methanol (3x 2 ml). Finally, column chromatography (silica gel, CH_2Cl_2, R_f = 0.4) afforded the achiral bisurea (**3d**) as a sticky yellow solid (0.30 g, 33%): mp: 100-101 °C; ^{1}H-NMR ($CDCl_3$) δ 9.30 (NH, s, 2H), 8.72 (H4, d, 2H), 7.75 (H5, t, 2H), 7.58 (H6, d, 2H), 6.57 (H2', s, 4H), 3.98 (OCH_2, m, 12H), 1.80-1.68 ($OCH_2C\underline{H}_2$, m, 12H), 1.46-1.41 ($OCH_2CH_2C\underline{H}_2$, m, 12H), 1.26 ($(CH_2)_8$, m, 96H), 0.88 ($CH_3$, t, 18H); ^{13}C-NMR ($CDCl_3$) δ 169.4 (imide CO_{in}), 166.8 (imide CO_{out}), 153.4 (C3'), 151.0 (urea CO), 138.2 (C3), 138.1 (C4'), 136.2 (C5), 131.3 (C1), 126.0 (C4), 124.4 (C1'), 117.9 (C6), 115.2 (C2), 105.3 (C2') 73.5, 69.2 (OCH_2), 32.0, 31.9, 31.8, 30.3, 30.0, 29.7, 29.6, 29.4, 29.3, 26.2, 26.1, 22.7, 14.1, 14.0 (alkyl C) ppm; IR(ATR): 3336, 2918, 2850, 1770, 1756, 1727, 1695, 1615, 1599, 1531,

1507, 1475, 1468, 1437, 1416, 1392, 1307, 1279, 1235, 1204, 1116, 1050, 1015, 991, 910, 880, 824, 777, 745, 721, 698 cm^{-1}; MALDI-TOF MS: calculated: 1608.23 found: 1608.31;

3,3'-(N,N'-Ureido)-bis{N-[3,4,5-tri((*S*)-3,7-dimethyloctyloxy)phenyl]phthalimide} (3e). A solution of 3-isocyanato-N-[3,4,5-((*S*)-3,7-dimethyloctyloxy)phenyl]phthalimide. (0.10 g, 0.14 mmol) in toluene (10 ml) was added to a solution of 3-amino-phthalimide (**5e**, 0.12 g, 0.17 mmol) and 4-dimethylaminopyridine (12 mg, 0.10 mmol) in toluene (10 ml). The solution was stirred for 10 h at 110 °C, allowed to cool and evaporated to dryness. The obtained residue was dissolved in toluene (1 ml) and precipitated from acetone (25 ml) which afforded chiral (**5e**) (0.14 g, 65%): mp: 67-70 °C; ^{1}H-NMR ($CDCl_3$) δ 9.23 (NH, s, 2H), 8.63 (H4, d, 2H), 7.67 (H5, t, 2H), 7.50 (H6, d, 2H), 6.58 (H2', s, 4H), 3.98 (OCH_2, m, 12H), 1.84 ($OCH_2C\underline{H}$, m, 12H), 1.62 ($OCH_2C\underline{H}$, bs, 12H), 1.53 ($C^*HCH_3C\underline{H}_2$, m, 12H), 1.33 (C^*H and $C^*HCH_3CH_2C\underline{H}_2$, m, 18H), 1.16 ($C\underline{H}(CH_3)_2$ and $C\underline{H}_2CH(CH_3)_2$, m, 18H), 0.94 ($C^*CH_3$, m, 18H), 0.88 ($CH_3$, dd, 36H) ppm; ^{13}C-NMR ($CDCl_3$) δ 169.4 ($imideCO_{in}$), 166.8 ($imideCO_{out}$), 153.4 (C3'), 150.9 (urea CO), 138.2 (C3), 138.1 (C4'), 136.2 (C5), 131.3 (C1), 126.0 (C4), 124.3 (C1'), 117.8 (C6), 115.1 (C2), 105.3 (C2'), 71.8, 67.5 (OCH_2), 39.4, 39.2, 37.5, 37.4, 36.3, 29.8, 29.7, 28.0, 28.0, 24.7, 22.7, 22.7, 22.6, 22.6, 19.6, 19.5 (alkyl C) ppm; IR(ATR): 3357, 2954, 2925, 1773, 1697, 1596, 1524, 1505, 1475, 1436, 1412, 1384, 1305, 1273, 1238, 1199, 1113, 820, 744 cm^{-1}; MALDI-TOF: calculated: 1440.04, found: 1462.6 (Na adduct).

3-Nitro–N-octylphthalimide (4b). 3-Nitrophthalic anhydride (1.0 g, 5.1 mmol) and octylamine (0.78 g, 5.4 mmol) were mixed at 180 °C. The reaction was stopped when no water evolved anymore. The crude product was purified by column chromatography (silica, CH_2Cl_2, R_f = 0.3) to give 3-nitro-N-octylphenylphthalimide (**4b**, 0.7 g, 45 %): ^{1}H-NMR ($CDCl_3$) δ 8.10 (H4, d, 1H), 8.09 (H6, d, 1H), 7.88 (H5, t, 1H), 3.70 (NCH_2, m, 2H), 1.68 ($NCH_2C\underline{H}_2$, m, 2H), 1.28 ((CH_2)$_5$, m, 10H), 0.86 (CH_3, m, 3H) ppm; ^{13}C-NMR ($CDCl_3$) δ 166.1 (C1-CO), 163.2 (C2-CO), 145.3 (C3), 135.5 (C5), 134.4 (C1), 128.6, 127.1, 124.0 (C2, C4, C6), 39.0 (NCH_2), 32.0, 29.3, 29.3, 28.5, 27.0, 22.8, 22.7, 14.3 (CH_3) ppm.

3-Nitro–N-(4-methoxyphenyl)phthalimide (4c).[32] The powders 3-nitrophthalic anhydride (1.0 g, 5.2 mmol) and 4-methoxyaniline (0.67 g, 5.4 mmol) were mixed at 170 °C. Water condensed at the top of the flask, and after 10 min the reaction was stopped. The crude product could be crystallized from THF or acetonitrile. Also precipitation from THF or acetonitrile upon addition of ethanol gave 3-nitro-N-(4-methoxyphenyl)phthalimide (**4c**, 0.94 g, 61 %): ^{1}H-NMR ($CDCl_3$) δ 8.21 (H4, d, 1H), 8.14 (H6, d, 1H), 7.97 (H5, t, 1H), 7.34 (H2', d, 2H), 7.02 (H3', d, 2H), 3.86 (OCH_3, s, 3H) ppm.

3-Amino-N-methylphthalimide (5a). 3-Acetylamino-N-methylphthalimide (**7**, 0.28 g, 1.3 mmol) was stirred in HCl aq. (36 %, 3 ml) for 5 min. at 120 °C. The reaction mixture was cooled in an ice bath, dissolved in dichloromethane, and neutralized with K_2CO_3 (2.5 g). After extraction of the salts with water, the organic layer was dryed with Na_2SO_4 and filtered. Evaporation of the solvent gave amine **5a** which was used as such (0.16 g, 72 %): mp = 219 °C; ^{1}H-NMR ($CDCl_3$) δ 7.42 (H5, dd, 1H), 7.14 (H6, d, 1H, $J_{6,5}$ = 7.1), 6.83 (H4, d, 1H, $J_{4,5}$ = 8.3), 5.2 (NH_2, bs, 2H), 3.12 (NCH_3, s, 3H) ppm; IR (ATR): 3463, 3348, 1751, 1683, 1631, 1597, 1478, 1441, 1375, 1329, 1275, 1245, 1187, 998, 745 cm^{-1}.

3-Amino-N-octylphthalimide (5b). 3-Nitro-N-octylphthalimide (0.40 g, 1.3 mmol) was shaken in a mixture of 80% ethylacetate and 20%ethanol (10 ml) together with a 10% Pd/C catalyst (14 mg, 0.014 mmol) for 4 h under an atmosphere of hydrogen gas (4 atm.). After removal of the solvent, **5b** (0.4 g, ~100 %) was isolated as an oil and used as such: ^{1}H-NMR ($CDCl_3$) δ 7.38 (H5, t, 1H), 7.13 (H6, d, 1H), 6.83 (H4, d, 1H), 5.20 (NH_2, bs, 2H), 3.60 (NCH_2, m, 2H), 2.04 ($NCH_2C\underline{H}_2$, m, 2H), 1.27((CH_2)$_5$, m, 10H), 0.86(CH_3, t, 3H) ppm.

3-Amino-N-(4-methoxyphenyl)phthalimide (5c). 3-Nitro-N-(4-metoxyphenyl)phthalimide (0.94 g, 3.0 mmol) was shaken for 4 h in THF (30 ml) together with a 10% Pd/C catalyst (38 mg, 0.037 mmol) under an atmosphere of hydrogen gas (4 atm.). The solvent was evaporated and the amine **5c** (0.9 g, ~100 %) was used as such: ^{1}H-NMR ($CDCl_3$) δ 7.46 (H5, t, 1H), 7.31 (H2', d, 2H), 7.24 (H6, d, 1H), 7.01 (H3', d, 2H), 6.89 (H4, d, 1H), 5.30 (NH_2, bs, 2H), 3.84(OCH_3, s, 3H) ppm.

3-Acetylamino-N-(3,4,5-tridodecyloxyphenyl)phthalimide. At 100 °C, 3,4,5-tridodecyloxyaniline (1.49 g, 2.23 mmol) was dissolved in dioxane (15 ml) and a solution of 3-acetylaminophthalic anhydride (0.39 g, 1.9 mmol) in dioxane (10 ml) was added. After stirring for 19 h at 100 °C the dioxane was evaporated and the reaction mixture redissolved in dioxane (20 ml) and acetic anhydride (2 ml). After stirring for 10 min at 100 °C, the solvent was removed in vacuo and the product purified by column chromatography (silica gel, CH_2Cl_2 + 1% EtOAc, R_f =0.3). Finally, the achiral acetylamino-phthalimide was obtained as a yellow sticky solid (1.38 g, 87%): mp: 106-108 °C; ^{1}H-NMR ($CDCl_3$) δ 9.63 (NHCO, s, 1H), 8.84 (H4, d, 2H), 7.67 (H5, t, 1H), 7.58 (H6, d, 1H), 6.57 (H2', s, 2H), 3.98 (OCH_2, m, 6H), 2.26 (CH_3CO, s, 3H), 1.80-1.68 ($OCH_2C\underline{H}_2$, m, 6H), 1.46-1.41 ($OCH_2CH_2C\underline{H}_2$, m, 6H), 1.26 (($CH_2$)$_8$, m, 48H), 0.88 ($CH_3$, t, 9H) ppm; ^{13}C NMR ($CDCl_3$): δ 169.4 (C1-CO), 169.2 (NHCO), 166.8 (C2-CO), 153.3, 153.3 (C3'), 138.1 (C3), 137.7 (C4'), 136.3 (C5), 131.1 (C1), 125.9 (C1'), 125.0 (C4), 118.3 (C6), 115.2 (C2), 105.3 (C2'), 73.5, 69.2, 32.0, 31.9, 30.3, 29.8, 29.7, 29.6, 29.4, 29.3, 26.1, 26.0, 25.0, 22.6, 14.1 ppm; IR (ATR): 3361, 2919, 2851, 1764, 1698, 1621, 1597, 1533, 1505, 1481, 1468,

1437, 1413, 1390, 1377, 1307, 1260, 1233, 1180, 1118, 1016, 903, 868, 798, 747, 720, 684 cm^{-1}; MALDI-TOF MS: calculated: 832.63, found: 832.60.

3-Amino-N-(3,4,5-tridodecyloxyphenyl)phthalimide (5d). 3-Acetylamino-N-(3,4,5-tridodecyloxy-phenyl)phthalimide (1.23 g, 1.47 mmol) was dissolved in 12 M HCl (4.2 ml) / dioxane (45.8 ml) and stirred for 3h at 100 °C. Afterwards, the mixture was neutralized with ammonia (13.3 M, 6 ml) at 0 °C and dioxane was evaporated. Brine (60 ml) was added and the mixture was extracted with dichloromethane (3 × 70 ml). The organic layers were combined and dried with Na_2SO_4. The residue was purified by column chromatography (silica, CH_2Cl_2, R_f = 0.3) and amino-phthalimide **5d** was obtained as a bright yellow solid (1.0 g, 86%): mp: 115-117 °C; ^{1}H-NMR ($CDCl_3$) δ 7.47 (H5, t, 1H), 7.23 (H6, d, 1H), 6.90 (H4, d, 1H), 6.58 (H2', s, 2H), 5.30 (NH_2, s, 2H), 3.98 (OCH_2, m, 6H), 1.80-1.68 ($OCH_2C\underline{H}_2$, m, 6H), 1.46-1.41 ($OCH_2CH_2C\underline{H}_2$, m, 6H), 1.26 ($(CH_2)_8$, m, 48H,), 0.88 ($CH_3$, t, 9H,) ppm; IR (ATR): 3471, 3348, 2918, 2850, 1743, 1702, 1640, 1595, 1509, 1482, 1467, 1439, 1415, 1389, 1309, 1238, 1190, 1131, 1096, 1025, 939, 878, 820, 814, 775, 739, 722, 704 cm^{-1}; MALDI-TOF MS: calculated: 790.62 found: 791.65.

3-Isocyanato-N-(3,4,5-tridodecyloxyphenyl)phthalimide. A solution of 3-amino-phthalimide (**5d**, 0.49 g, 0.63 mmol) in toluene (40 ml) was added dropwise to a 20 % solution of phosgene in toluene (6.7 ml, 13 mmol) at room temperature. After 30 minutes the mixture was heated to 110 ^{0}C for 7 h Evaporation of the solvent and excess phosgene gave the desired 3-isocyanato-phthalimide which was used as such: IR (ATR): 2921, 2852, 1771, 1707, 1600, 1507, 1467, 1438, 1417, 1391, 1362, 1307, 1237, 1188, 1119, 904, 824, 746, 721 cm^{-1} .

3-Acetylamino-N-[3,4,5-tri((*S*)-3,7-dimethyloctyloxy)phenyl]phthalimide. Analogous to the previous procedure 3,4,5-tri((*S*)-3,7-dimethyloctyloxy)aniline (1.00 g, 1.78 mmol), 3-acetylaminophthalic anhydride (0.30 g, 1.48 mmol), and acetic anhydride (1.6 ml) gave the chiral acetylamino-phthalimide (0.74 g, 66%) as a yellow sticky solid: mp: 98-99 °C; ^{1}H-NMR ($CDCl_3$) δ 9.64 (NH, s, 1H), 8.84 (H4, d, 2H), 7.67 (H5, t, 1H), 7.58 (H6, d, 1H), 6.55 (H2', s, 2H), 3.98 (OCH_2, m, 6H), 2.26 (CH_3CO, s, 3H), 1.84 ($OCH_2C\underline{H}$, m, 3H), 1.62 ($OCH_2C\underline{H}$, bs, 3H), 1.53 ($C^*HCH_3C\underline{H}_2$, m, 6H), 1.33 (C^*H and $C^*HCH_3CH_2C\underline{H}_2$, m, 9H), 1.16 ($C\underline{H}(CH_3)_2$ and $C\underline{H}_2CH(CH_3)_2$, m, 9H), 0.94 ($C^*CH_3$, m, 9H), 0.88 ($CH_3$, dd, 18H) ppm; ^{13}C NMR ($CDCl_3$): δ 169.4 (C1-CO), 169.3 (NHCO), 166.8 (C2-CO), 153.4 (C3'), 138.2 (C3), 137.8 (C4'), 136.3 (C5), 131.1 (C1), 126.0 (C1'), 125.0 (C4), 118.3 (C6), 115.2 (C2), 105.3 (C2'), 71.8, 67.5, 53.4, 39.4, 39.3, 37.5, 37.4, 37.3, 36.3, 29.8, 29.7, 28.0, 25.0, 24.7, 22.7, 22.7, 22.6, 22.6, 19.6 ppm; IR (ATR): 3359, 2954, 2926, 2870, 1769, 1703, 1621, 1595, 1528, 1504, 1478, 1439, 1410, 1384, 1366, 1301, 1233, 1181, 1116, 1047, 1034, 997, 903, 867, 820, 744, 683 cm^{-1}; MALDI-TOF MS: calculated: 748.53, found: 748.35.

3-Amino-N-[3,4,5-tri((*S*)-3,7-dimethyloctyloxy)phenyl]phthalimide (5e). Analogous to the previous procedure 3-acetylamino-N-[3,4,5-((*S*)-3,7-dimethyloctyloxy)phenyl]phthalimide (0.74 g, 0.99 mmol), 12 M HCl (2.8 ml), and ammonia (13.3 M, 4.1 ml) gave bright yellow solid **5e** (0.58 g, 83%): mp: 67-68 °C; ^{1}H-NMR ($CDCl_3$) δ 7.47 (H5, t, 1H), 7.23 (H6, d, 1H), 6.90 (H4, d, 1H), 6.58 (H2', s, 2H), 5.36 (NH_2, s, 2H), 3.98 (OCH_2, m, 6H), 1.84 ($OCH_2C\underline{H}$, m, 3H), 1.62 ($OCH_2C\underline{H}$, bs, 3H), 1.53 ($C^*HCH_3C\underline{H}_2$, m, 6H), 1.33 (C^*H and $C^*HCH_3CH_2C\underline{H}_2$, m, 9H), 1.16 ($C\underline{H}(CH_3)_2$ and $C\underline{H}_2CH(CH_3)_2$, m, 9H), 0.94 ($C^*CH_3$, m, 9H), 0.88 ($CH_3$, dd, 18H) ppm; ^{13}C NMR ($CDCl_3$): δ 169.3 (C1-CO), 167.7 (C2-CO), 153.3, 153.2(C3'), 145.8 (C3), 137. 8 (C4'), 135.5 (C5), 132.4 (C1), 126.8 (C1'), 121.3 (C4), 113.0 (C6), 110.8 (C2), 105.4 (C2'), 71.8, 67.4 (OCH_2), 39.4, 39.3, 37.6, 37.4, 37.4, 37.3, 36.4, 29.9, 29.8, 28.0, 24.8, 24.7, 22.8, 22.7, 22.7, 22.6, 19.6, 19.6 (alkyl C) ppm; IR (ATR): 3478, 3368, 2953, 2926, 2869, 1765, 1701, 1635, 1593, 1504, 1482, 1466, 1438, 1411, 1384, 1366, 1301, 1233, 1190, 1168, 1115, 1047, 1027, 996, 937, 911, 877, 816, 781, 745, 704, 679 cm^{-1}; MALDI-TOF MS: calculated: 706.53, found: 706.44.

3-Isocyanato-N-[3,4,5-tri((*S*)-3,7-dimethyloctyloxy)phenyl]phthalimide. Analogous to the previous procedure chiral 3-amino-phthalimide (**5e**, 0.1 g, 0.14 mmol) in toluene (1 m1), together with 20 % phosgene in toluene (1.5 ml, 2.8 mmol) gave the chiral 3-isocyanato-phthalimide, which was used as such: IR(ATR): 2954, 2925, 2870, 2251, 1773, 1708, 1633, 1617, 1596, 1506, 1464, 1438, 1413, 1384, 1365, 1304, 1239, 1187, 1117, 1048, 909, 877, 823, 786, 744, 723, 696 cm^{-1}.

3-Acetylaminophthalic anhydride (6).[34] mp = 188.5-191 °C; ^{1}H-NMR ($CDCl_3$) δ 9.10 (NHCO, bs, 1H), 8.94 (H4, d, 1H, $J_{4,5}$ = 8.5), 7.86 (H5, dd, 1H), 7.66 (H6, d, 1H, $J_{6,5}$ = 7.4), 2.32 ($COCH_3$, s, 3H) ppm; ^{13}C-NMR ($CDCl_3$) δ 169.2 (imide CO), 164.6 (amide CO), 161.8 (imide CO), 138.8 (C3), 138.3 (C5), 130.6 (C1), 126.0 (C4), 120.0 (C6), 115.4 (C2), 24.9 (NHCO$\underline{C}$H3) ppm; IR (ATR): 3352, 3130, 1837, 1759, 1696, 1622, 1603, 1524, 1476, 1421, 1367, 1287, 1258, 1234, 1203, 1163, 1132, 1012, 900, 826, 739, 678 cm^{-1}; Elemental analysis: calculated: $C_{10}H_7NO_4$ (205.17): C, 58.54; H, 3.44; N, 6.83; found: C, 58.62; H, 3.19; N, 6.77; GCMS (205.17): M^+ = 205, 163, 43.

3-Acetylamino-N-methylphthalimide (7). A mixture of 3-acetylaminophthalic anhydride (3.03g, 14.6 mmol) and a 35% solution of methylamine in water (3.18 ml, 36 mmol) was stirred for 1,5 h at room temperature (exothermic), after which water was removed via coevaporation with 2-propanol. Ring closure was induced by heating for 1 h at 180 °C. The crude product was purified by column chromatography (silica, CH_2Cl_2, R_f = 0.3) and recrystallization from chloroform to give acetylaminophthalimide **7** (2.0 g, 63 %): mp = 159 °C; ^{1}H-NMR

($CDCl_3$) δ 9.4 (NHCO, s, 1H), 8.79 (H4, d, 1H, $J_{4,5}$ = 8.5), 7.62 (H5, dd, 1H), 7.51 (H6, d, 1H, $J_{6,5}$ = 7.1), 3.19 (NCH_3, s, 3H), 2.32 ($COCH_3$, s, 3H) ppm; ^{13}C-NMR ($CDCl_3$) δ 170.2 (imide CO), 169.2 (amide CO), 167.8 (imide CO), 137.2 (C3), 135.7 (C5), 131.6 (C1), 124.6 (C4), 117.9 (C6), 115.7 (C2), 24.9 ($NHCOCH_3$), 23.7 (NCH_3) ppm; IR (ATR): 3344 , 1759, 1693, 1619, 1525, 1476 1439, 1417, 1364, 1351, 1290, 1256, 1233, 1160, 1035, 996, 824, 740 cm^{-1}; Elemental analysis: calculated: $C_{11}H_{10}N_2O_3$ (205.17): C, 60.55; H, 4.62; N, 12.84; found: C, 60.48; H, 4.10; N, 12.97; GCMS (218.21): M^+ = 218, 176, 43.

3-Acetylamino-6-nitro-N-methylphthalimide (8).[31] 3-Acetylamino-N-methylphthalimide (**7**, 0.70 g, 3.2 mmol) was added slowly to sulfuric acid (7.0 ml). After cooling to 0 °C, a mixture of sulfuric acid (2.22 ml) and nitric acid (d = 1.52 g/ml, 1.76 ml, 42 mmol) was added dropwise. After 5.5 h the red reaction mixture was poured into ice water (17.5 g) and the precipitate extracted with $CHCl_3$. Drying of the organic layer with Na_2SO_4, filtration, and evaporation of the solvent, gave the brownish crude product, which could be recrystallized from aceton to give tetrasubstituted **8** (0.50 g, 60 %): ^{1}H-NMR ($CDCl_3$) δ 9.98 (NHCO, s, 1H), 8.94 (H4, d, 1H $J_{4,5}$ = 9.2), 8.13 (H5, d, 1H), 3.19 (NCH_3, s, 3H), 2.32 ($COCH_3$, s, 3H) ppm; GCMS (263.21): M^+ = 263, 221, 191, 43.

Note: The reaction was monitored by sampling via extraction using ethyl acetate/heptane 1/1 followed by analysis with TLC (color change from blue to pink with UV detection (254 nm)) and GCMS.

3-Acetylamino-N-octylphthalimide (9). A mixture of 3-acetylaminophthalic anhydride (**6**, 2.00 g, 9.75 mmol) and octylamine (1.27 g, 9.85 mmol) was heated at 185 °C for 45 min. The crude product was purified with column chromatography (silica, CH_2Cl_2 + 0-2 % EtOAc R_f = 0-0.5), yielding octyl compound **9** as a light yellow solid (2.4 g, 78 %): ^{1}H-NMR ($CDCl_3$) δ 9.54 (NHCO, bs, 1H), 8.74 (H4, d, 1H), 7.65 (H5, t, 1H), 7.51 (H6, d, 1H), 3.64 (NCH_2, t, 2H), 2.27 ($COCH_3$, s, 3H), 1.66 ($NCH_2C\underline{H}_2$, m, 2H), 1.27 (($(CH_2)_5$, m, 10H), 0.87 (CH_3, t, 3H) ppm; ^{13}C-NMR ($CDCl_3$) δ 170.6 (imide CO), 169.5 (amide CO), 168.1 (imide CO), 137.6 (C3), 136.0 (C5), 131.8 (C1), 124.9 (C4), 118.2 (C6), 116.0 (C2), 38.3 (NCH_2), 32.0, 29.4, 28.8, 27.1, 25.2, 22.9, 14.3 (CH_3) ppm; IR (ATR): 3340, 2926, 2851, 1767, 1704, 1683, 1612, 1525, 1480, 1398, 1348, 1292, 1243, 1171, 1054, 1008, 939, 825, 745 cm^{-1}; GCMS (316.40): M^+ = 316, 274, 175, 43.

3-Acetylamino-6-nitro-N-octylphthalimide (10). N-Octyl-phthalimide **9** (0.15 g, 0.32 mmol) was added slowly to H_2SO_4 (1.1 ml), after which a mixture of H_2SO_4 (0.31 ml) and HNO_3 (d = 1.52 g/ml, 0.16 ml, 3.84 mmol) was added at 0 °C. After 4 h the red reaction mixture was poured into icewater (3 g) and the precipitate extracted with $CHCl_3$. Drying of the organic layer with Na_2SO_4, filtration, and evaporation of the solvent, gave brownish product **10** (95 mg, 82 %, purity ~80%): ^{1}H-NMR ($CDCl_3$) δ 10.0 (NHCO, s, 1H), 8.9 (H4, d, 1H), 8.2 (H5, d, 1H), 3.7 (NCH_2, m, 2H), 2.5 – 0.8 ($(CH_2)_6CH_3$) ppm.

3,6-Dinitro-N-[3,4,5-tri((*S*)-3,7-dimethyloctyloxy)phenyl]phthalimide (16). At 80 °C, 3,4,5-tri((*S*)-3,7-dimethyloctyloxy)aniline (**2**, 1.00 g, 1.78 mmol) was dissolved in acetonitrile (2 ml) and a solution of 3,6-dinitrophthalic anhydride (279 mg, 1.17 mmol) in acetonitril (1 ml) was added. After stirring for 1 h the acetonitrile was evaporated and the reaction mixture redissolved in acetic anhydride (4 ml). After stirring for 2 h at 100 °C, the solvent was removed in vacuo, and the product purified with column chromatography (silica gel, heptane / ethyl acetate 8/2, R_f = 0.3). Finally, chiral dinitro-phthalimide **3** was obtained as an orange/brown sticky solid (0.55 g, 60 %): mp = 72-73 °C; ^{1}H-NMR ($CDCl_3$) δ 8.18 ($CHCNO_2$, s, 2H), 6.57 (CHCN, s, 2H), 3.98 (OCH_2, m, 6H), 1.84 ($OCH_2C\underline{H}_A$, m, 3H), 1.62 ($OCH_2C\underline{H}_B$, m, 3H), 1.53 ($C^*HCH_3C\underline{H}_2$, m, 6H), 1.33 (C*H and $C^*HCH_3CH_2C\underline{H}_2$, m, 9H), 1.16 ($C\underline{H}(CH_3)_2$ and $C\underline{H}_2CH(CH_3)_2$, m, 9H), 0.94 ($C^*CH_3$, m, 9H), 0.88 ($CH_3$, dd, 18H) ppm; ^{13}C-NMR ($CDCl_3$) δ 159.9 (CO), 153.4 (C3'), 146.3 (C3), 138.7 (C4'), 130.0 (C4), 125.1, 125.0 (C1 and C1'), 105.2 (C2'), 71.8, 67.6 (OCH_2), 39.3, 39.2, 37.5, 37.3, 36.2, 29.8, 29.7, 27.9, 24.7, 22.7, 22.6, 22.6, 19.5 (C_9H_{19}) ppm; IR (ATR): 2954, 2926, 2870, 1734, 1596, 1541, 1502, 1467, 1440, 1417, 1383, 1349, 1304, 1232, 1125, 1046, 991, 852, 822, 690 cm^{-1}; Elemental analysis: calculated: $C_{44}H_{67}N_3O_9$ (782.04): C, 67.58; H, 8.64; N, 5.37; found: C, 67.85; H, 8.74; N, 5.33; MALDI-TOF MS: calculated: 781.49, found: 781.50.

3,6-Diamino-N-[3,4,5-tri((*S*)-3,7-dimethyloctyloxy)phenyl]phthalimide (17). Under an atmosphere of hydrogen gas (1 atm.), dinitro-phthalimide **3** (0.50 g, 0.64 mmol) was stirred for 3 h in a mixture of tetrahydrofuran (6 ml), ethanol (1.2 ml) and water (0.1 ml) together with Pd/C 10 %w/w (68 mg, 0.064 mmol). After removal of the catalyst by filtration, the solvents were evaporated and minor impurities were separated from the product with column chromatography (silica gel, dichloromethane, R_f = 0.3). Finally, diamino-phthalimide **4** was obtained as an orange/yellow sticky solid (0.39 g, 85 %): mp = 85.5-87 °C; ^{1}H-NMR ($CDCl_3$) δ 6.78 ($C\underline{H}CNH_2$, s, 2H), 6.61 (CHCN, s, 2H), 5.29 (NH_2, bs, 4H), 3.99 (OCH_2, m, 6H), 1.83 ($OCH_2C\underline{H}_A$, m, 3H), 1.62 ($OCH_2C\underline{H}_B$, m, 3H), 1.54 ($C^*HCH_3C\underline{H}_2$, m, 6H), 1.33 (C*H and $C^*HCH_3CH_2C\underline{H}_2$, m, 9H), 1.16 ($C\underline{H}(CH_3)_2$ and $C\underline{H}_2CH(CH_3)_2$, m, 9H), 0.94 ($C^*CH_3$, m, 9H), 0.87 ($CH_3$, dd, 18H) ppm; ^{13}C-NMR ($CDCl_3$) δ 168.6 (CO), 153.1 (C3'), 138.4 (C3), 137.5 (C4'), 127.0 (C4), 125.1 (C1'), 109.1 (C1), 105.3 (C2'), 71.7, 67.3 (OCH_2), 39.3, 39.2, 37.5, 37.3, 36.3, 29.7, 29.6, 27.9, 24.7, 22.6, 22.5, 22.5, 19.5, 19.5 (C_9H_{19}) ppm; IR (ATR): 3475, 3366, 2954, 2927, 2870, 1736, 1687, 1657, 1617, 1593, 1494, 1468, 1436, 1384, 1294, 1235,

1187, 1117, 941, 821, 704 cm^{-1}; Elemental analysis: calculated: $C_{44}H_{71}N_3O_5$ (722.07): C, 73.19; H, 9.91; N, 5.82; found: C, 73.24; H, 10.01; N, 5.54; MALDI-TOF MS: calculated: 721.54, found: 721.55.

3,6-Diisocyanato-N-[3,4,5-tri((*S*)-3,7-dimethyloctyloxy)phenyl]phthalimide (18). A solution of diamino-monomer **4** (150 mg, 0.208 mmol) in toluene (2.4 ml) was added dropwise to a 20 %w/w solution of phosgene in toluene (2.2 ml, 4.16 mmol) at room temperature. After 30 min the reaction mixture was heated to 110 °C for 4 h. Evaporation of the solvent and excess phosgene, gave the diisocyanato-monomer **5** (161 mg, ~100 %), which was used as such: ^{1}H-NMR ($CDCl_3$) δ 7.28 (CHCNCO, s, 2H), 6.56 (CHCN, s, 2H), 3.99 (OCH_2, m, 6H), 1.85 ($OCH_2C\underline{H}_A$, m, 3H), 1.70 ($OCH_2C\underline{H}_B$, m, 3H), 1.56 ($C^*HCH_3C\underline{H}_2$, m, 6H), 1.31 (C*H and $C^*HCH_3CH_2C\underline{H}_2$, m, 9H), 1.16 ($C\underline{H}(CH_3)_2$ and $C\underline{H}_2CH(CH_3)_2$, m, 9H), 0.92 ($C^*CH_3$, m, 9H), 0.87 ($CH_3$, dd, 18H) ppm; ^{13}C-NMR ($CDCl_3$) δ 166.0 (CONHCO), 153.4 (C3'), 138.5 (C4'), 132.1 (C4), 128.8 (C1), 126.9 (C3), 125.4 (C1'), 123.4 (NCO), 105.5 (C2'), 71.8, 67.5 (OCH_2), 39.4, 39.2, 37.5, 37.3, 36.3, 29.8, 29.7, 29.4, 28.0, 24.7, 22.7, 22.6, 22.6, 19.6 (C_9H_{19}) ppm; IR (ATR): 2954, 2926, 2870, 2241, 1705, 1596, 1539, 1505, 1464, 1436, 1383, 1365, 1302, 1261, 1238, 1179, 1119, 1021, 902, 842, 804, 760, 702 cm^{-1}.

Caution: The poisonous and volatile phosgene should be carefully handled in a fumehood.

5.8 References and notes

(1) Schmuck, C. *Angew. Chem. Int. Ed.* **2003**, *42*, 2448–2452.

(2) Note: (a) One strategy towards helix formation is the self-assembly of molecules with the help of intermolecular non-covalent interactions. In this text this strategy is called the self-assembly approach, while in ref. 1 this strategy is called the supramolecular approach. We wish to prevent confusion with the foldamer approach, as in both the self-assembly and foldamer approach non-covalent or supramolecular interactions are used, intermolecularly in case of self-assembly, and intramolecularly in case of foldamers. Examples: (b) Gardiner, K.M.; Khoury, R.G.; Lehn, J.-M. *Chem. Eur. J.* **2000**, *6*, 4124–4131. (c) Petitjean, A.; Cuccia, L.A., Lehn, J.-M.; Nierengarten, H.; Schmutz, M.; *Angew. Chem. Int. Ed.* **2002**, *41*, 1195–1198. (d) Berl, V.; Krische, M.J.; Huc, I.; Lehn, J.-M.; Schmutz, M. *Chem. Eur. J.* **2000**, *6*, 1938–1946. (e) Schmuck, C.; Wienand, W. *Angew. Chem. Int. Ed.* **2001**, *40*, 4363–4369. (f) Scherrington, D.C.; Tashkinen, K.A. *Chem. Soc. Rev.* **2001**, *30*, 83–93. (g) Zeng, F.; Zimmerman, S.C., Kolotuchin, S.V.; Reichert, D.E.C.; Ma, Y. *Tetrahedron* **2002**, *58*, 825–843. (h) Sijbesma, R.P.; Meijer, E.W. *Chem. Commun*. **2003**, 5–16. (i) Brunsveld, L.; Vekemans, J.A.J.M.; Hirschberg, J.H.K.K.; Sijbesma, R.P., Meijer, E.W. *Proc. Natl. Acad. Sci. USA* **2002**, *99*, 4977. (j) Würthner, F.; Yao, S.; Beginn, U. *Angew. Chem. Int. Ed.* **2003**, *42*, 3247–3250.

(3) peptides: (a) Pauling, L.; Corey, R.B.; Branson, H.R. *Proc. Natl. Acad. Sci. USA* **1951**, *37*, 205–211. DNA: (b) Watson, J.D.; Crick, F.H.C. *Nature* **1953**, *171*, 737–738.

(4) tobacco mosaic virus: (a) Klug, A. *Angew. Chem.* **1983**, *95*, 579 – 596. (b) Stryer, L.; *Biochemistry*, 4th ed, W. H. Freeman & Company: New York, **1995**.

(5) Appella, D.H.; Christianson, L.A.; Karle, I.L.; Powell, D.R.; Gellman, S.H. *J. Am. Chem. Soc.* **1996**, *118*, 13071–13072.

(6) Nakano, T.; Okamoto, Y. *Chem. Rev.* **2001**, *101*, 4013–4038.

(7) (a) Meurer, K.P.; Vögtle, F. *Top. Curr. Chem.* **1985**, *127*, 1. (b) Kiupel, B.; Niederalt, C.; Nieger, M.; Grimme, S.; Vögtle, F. *Angew. Chem. Int. Ed.* **1998**, *37*, 3031–3034. (c) Urbano, A. *Angew. Chem. Int. Ed.* **2003**, *42*, 3986–3989. (d) Chou, H.-C.; Hsu, C.-H.; Cheng, Y.-M.; Cheng, C.-C.; Liu, H.-W.; Pu, S.-C.; Chou, P.-T. *J. Am.Chem. Soc.* **2004**, *126*, 1650–1651.

(8) (a) Folmer, B.J.B.; Sijbesma, R.P.; Versteegen, R.M.; van der Rijt, J.A.J.; Meijer, E.W. *Adv. Mater.* **2000**, *12*, 874–878. (b) Keizer, H.M.; Sijbesma, R.P.; Jansen, J.F.G.A.; Pasternack, G.; Meijer, E.W. *Macromolecules* **2003**, *36*, 5602–5606.

(9) Hill, D.J.; Mio, M.J.; Prince, R.B.; Hughes, T.S.; Moore, J.S. *Chem. Rev.* **2001**, *101*, 3893-4011.

(10) (a) Jones, T.V.; Blatchly; R.A.; Tew, G.N. *Org Lett.* **2003**, *5*, 3297–3299. (b) Arnt, L; Tew, G.N. *Macromolecules* **2004**, *37*, 1283–1288. (c) Prince, R.B.; Moore, J.S.; Brunsveld, L.; Meijer, E.W *Chem. Eur. J.* **2001**, *7*, 4150–4154. (d) Brunsveld, L.; Meijer, E.W.; Prince, R.B.; Moore, J.S. *J. Am. Chem. Soc.* **2001**, *123*, 7978–7984. (e) Matsuda, K.; Stone, M.T.; Moore, J.S. *J. Am. Chem. Soc.* **2002**, *124*, 1836–11837. (f) Zhao, D.; Moore, J.S. *Macromolecules* **2003**, *36*, 2712–2720.

(11) (a) Cary, J.M.; Moore, J.S *Org. Lett.* **2002**, *4*, 4663–4666. (b) Yang, X.; Brown, A.L.; Furukawa, M., Li, S.; Gardiner, W.E., Bukowski, E.J.; Bright, F.V.; Zheng, C.; Zeng, X.C.; Gong, B. *Chem. Commun.* **2003**, 56–57. (c) Yang, X.; Yuan, L.; Yamato, K.; Brown, A.L.; Feng, W.; Furukawa, M.; Zeng, X.C.; Gong, B. *J. Am. Chem. Soc.* **2004**, *126*, 3148–3162.

(12) (a) Cheng, R.P.; Gellman, S.H.; DeGrado, W.F. *Chem Rev.* **2001**, *101*, 3219–3232. (b) Huck, B.R.; Fisk, J.D.; Gellman, S.H. *Org. Lett.* **2000**, *2*, 2607–2610. (c) Gademann, K.; Häne, A.; Rueping, M.; Jaun, B.; Seebach, D. *Angew. Chem. Int. Ed*. **2003**, *42*, 1534–1537. (d) Seebach, D.; Schaeffer, L.; Brenner, M.; Hoyer, D. *Angew. Chem. Int. Ed*. **2003**, *42*, 776–778. (e) Seebach, D.; Matthews, J. L. *Chem. Commun.* **1997**, 2015–2022.

(13) (a) Huc, I. *Eur. J. Org. Chem.* **2004**, 17–29. (b) Berl, V.; Huc, I.; Khoury, R.G.; Lehn, J.-M.; *Chem. Eur. J.* **2001**, *7*, 2798–2809. (c) Dolain, C.; Maurizot, V.; Huc, I. *Angew. Chem. Int. Ed.* **2003**, *42*, 2738–2740. (d) Kolomiets, E.; Berl, V.; Odriozola, I.; Stadler, A.-M.; Kyritsakas, N.; Lehn, J.-M. *Chem. Commun.* **2003**, 2868–2869. (e) Jiang, H.; Léger, J.-M.; Huc, I. *J. Am. Chem. Soc.* **2003**, *125*, 3448–3449. (f) Jiang, H.; Dolain, C.; Léger, J.-M.; Gornitzka, H.; Huc, I. *J. Am. Chem. Soc.* **2004**, *126*, 1034–1035. (g) Berl, V.; Huc, I.; Khoury, R.G.; Krische, M.J.; Lehn, J.-M. *Nature* **2000**, *407*, 720–723. (h) Acocella, A.; Venturini, A.; Zerbetto, F. *J. Am. Chem. Soc.* **2004**, *126*, 2362–2367. (i) Gong, B. *Chem. Eur. J.* **2001**, *7*, 4336–4342. (j) Zhu, J.; Parra, R.D.; Zeng, H.; Skrzypczak-Jankun, E.; Chen Zeng, X.; Gong, B. *J. Am. Chem. Soc.* **2000**, *122*, 4219–4220. (k) Hamuro, Y.; Geib, S.J.; Hamilton, A.D. *J. Am. Chem. Soc.* **1997**, *119*, 10587–10593. (l) Odriozola, I.; Kyritsakas, N.; Lehn, J.-M. *Chem. Commun.* **2004**, 62–63.

(14) (a) Cornelissen, J.J.L.M.; Graswinckel, W.S.; Rowan, A.E.; Sommerdijk, N.A.J.M.; Nolte, R.J.M. *J. Polym. Sci., Part A: Polym. Chem* **2003**, *41*, 1725–1736. (b) Cheuk, K.K.L.; Lam, J.W.Y.; Ming Lai, L.; Dong, Y.; Tang, B.Z. *Macromolecules* **2003**, *36*, 9752–9762. (c) Yashima, E.; Maeda, K.; Okamoto, Y.

Nature **1999**, *399*, 449–451. (d) Mayer, S.; Maxein, G.; Zentel, R. *Macromolecules* **1998**, *31*, 8522–8525. (e) Gu, H.; Nakamura, Y.; Sato, T.; Teramoto, A.; Green, M.M.; Jha, S.K.; Andreola, C.; Reidy, M.P. *Macromolecules* **1998**, *31*, 6362–6368. (f) Schlitzer, D.S.; Novak, B.M. *J. Am. Chem. Soc.* **1998**, *120*, 2196–2197.

(15) Groenendaal, L. *Thesis: The Chemistry of oligopyrroles, Design, synthesis and characterization of well-defined and functional α,α-linked oligomers*; Eindhoven University of Technology: Eindhoven, **1996**.

(16) (a) Aratani, N.; Osuka, A. *Bull. Chem. Soc. Jpn*. **2001**, *74*, 1361–1379. (b) Aratani, N.; Osuka, A. *Macromol. Rapid Commun.* **2001**, *22*, 725–740.

(17) (a) Folmer, B.J.B.; Sijbesma, R.P.; Kooijman, H.; Spek, A.L.; Meijer, E.W. *J. Am. Chem. Soc.* **1999**, *121*, 9001–9007. (b) ten Cate, A.T.; Dankers, P.Y.W.; Kooijman, H.; Spek, A.L.; Sijbesma, R.P.; Meijer, E.W. *J. Am. Chem. Soc.* **2003**, *125*, 6860–6861.

(18) cyclic peptides: (a) Bong, D.T.; Clark, T.D.; Granja, J.R.; Ghadiri, M.R. *Angew. Chem. Int. Ed.* **2001**, *40*, 989–1011. guanosines: (b) Gottarelli, G.; Proni, G.; Spada, G.P.; Bonazzi, S.; Garbesi, A.; Ciuchi, F.; Mariani, P. *Biopolymers* **1997**, *42*, 561–574. (c) Giorgi T.; Lena S.; Mariani P.; Cremonini M.A; Masiero S.; Pieraccini S.; Rabe J.P; Samori P.; Spada G.P.; Gottarelli G. *J. Am. Chem. Soc.* **2003**, *125*, 14741–14749. heterocyclic base / crown ether: Fenniri, H.; Deng, B.-L.; Ribbe, A.E.; *J. Am. Chem. Soc.* **2002**, *124*, 11064–11072. (d) UPy hexamers: (e) Keizer, H.M.; Ramzi, A.; Sijbesma, R.P.; Meijer, E.W. *Polymer Preprints* **2003**, *44*, 596–597. folic acids: (f) Kanie, K.; Nishii, M.; Yasuda, T.; Taki, T.; Ujiie, S.; Kato, T. *J. Mater. Chem.* **2002**, *11*, 2875–2886. π-π macrocycles: (g) Tobe, Y.; Utsumi, N.; Kawabata, K.; Nagano, A.; Adachi, K.; Araki, S.; Sonoda, M.; Hirose, K.; Naemura, K. *J. Am. Chem. Soc.* **2002**, *124*, 5350–5364. (h) Lahiri, S.; Thompson, J.L.; Moore, J.S. *J. Am. Chem. Soc.* **2000**, *122*, 11315–11319. (i) Höger, S.; Bonrad, K.; Mourran, A.; Beginn, U.; Möller, M. *J. Am. Chem. Soc.* **2001**, *123*, 5651–5659. (j) Höger, S. *Chem. Eur. J.* **2004**, *10*, 1320–1329.

(19) (a) Berl, V; Huc, I.; Khoury, R.G.; Lehn, J.-M. *Chem. Eur. J.* **2001**, *7*, 2810–2820. (b) Cuccia, L.A.; Lehn, J.-M.; Homo, J.-C.; Schmutz, M. *Angew. Chem. Int. Ed.* **2000**, *39*, 233–237. (c) Prince, R.B.; Brunsveld, L.; Meijer, E.W.; Moore, J.S. *Angew. Chem. Int. Ed.* **2000**, *39*, 228–231. (d) See chapter 4 for or a discussion about 'tertiary structures' of 'secondarily ordered' self-assembled helices.

(20) van Gorp, J.J.; Vekemans, J.A.J.M.; Meijer, E.W. *J. Am. Chem. Soc.* **2002**, *124*, 14759–14769.

(21) (a) Estroff, L.A.; Incarvito, C.D.; Hamilton, A.D. *J. Am. Chem. Soc.* **2004**, *126*, 2–3. (b) Ernst, J.T.; Becerril, J.; Park, H.S.; Yin, H.; Hamilton, A.D. *Angew. Chem. Int. Ed.* **2003**, *42*, 535–539. (c) Hamuro, Y.; Hamilton, A.D. *Bioorg. Med. Chem.* **2001**, *9*, 2355–2363. (d) Nowick, J.S.; Pairish, M.; Quen Lee, I.; Holmes, D.L.; Ziller, J.W. *J. Am. Chem. Soc.* **1997**, *119*, 5413–5424.

(22) (a) Hemmerlin, C.; Marraud, M.; Rognan, D.; Graff, R.; Semetey, V.; Briand, J.-P.; Guichard, G.; *Helv. Chim. Acta* **2002**, *85*, 3692–3710. (b) Semetey, V.; Rognan, D.; Hemmerlin, C.; Graff, R.; Briand, J.-P.; Maraud, M. Guichard, G. *Angew. Chem. Int. Ed.* **2002**, *41*, 1893–1895.

(23) Usually, urea groups adopt a 'transoid' conformation. (a) Corbin, P.S.; Zimmerman, S.C.; *J. Am. Chem. Soc.* **2000**, *122*, 3779–3780. (b) Corbin, P.S.; Zimmerman, S.C.; Thiessen, P.A.; Hawryluk, N.A.; Murray, T.J. *J. Am. Chem. Soc.* **2001**, *123,* 10475–10488.

(24) Parra, R.D.; Gong, B.; Zeng, X.C. *J. Chem. Phys*. **2001**, *115*, 6036–6041.

(25) (a) Brunsveld, L. *Thesis: Supramolecular chirality, from molecules to helical assemblies in polar media*; Eindhoven University of Technology: Eindhoven, **2001**. (b) Prince, R.B. Thesis: *Phenylene ethynylene foldamers: cooperative conformational transition, twist sense bias, molecular recognition properties, and solid-state organization*; Southeast Missouri State University: Urbana, Illinois, **2000**.

(26) (a) Green, M.M.; Peterson, N.C.; Sato, T.; Teramoto, A.; Cook, R.; Lifson, S. *Science* **1995**, *268*, 1860–1866. (b) Moore, J.S.; Gorman, C.B.; Grubbs, R.H. *J. Am. Chem. Soc* **1991**, *113*, 1704–1712.

(27) Vyklický, L.; Eichhorn, S.H.; Katz, T.J. *Chem Mater.* **2003**, 15, 3594–3601.

(28) Meek, J.L. *J. Chromatogr.* **1983**, *266*, 401–408.

(29) (a) Momose, T.; *Chem. Pharm. Bull.* **1960**, *8*, 514–516. (b) Momose, T.; Nakamura, M. *Talanta* **1963**, 10, 115.

(30) Momose, T.; Torigoe, M. *J. Pharm. Soc. Jpn.* **1951**, *71*, 977–979.

(31) (a) Reznikova, I.I.; Veselova, T.V. *Zhurnal Organicheskoi Khimii* **1970**, *6*, 840–845. (b) Nekhoroshev, A.A.; Sevbo, D.P.; Ginzburg, O.F. *Zhurnal Organicheskoi Khimii* **1980**, *17*, 369–374.

(32) Alexander, J.W.; McElvain, S.M. *J. Am. Chem. Soc.* **1938**, *60*, 2285–2287.

(33) In principle imides **4a**, **4d**, and **4e** could be synthesized as described, directly from imide introduction in 3-nitrophthalic anhydride and reduction of the nitro compound to the amine. However, imides **4a**, **4d**, and **4e** are formed via conversion of 3-nitrophthalic anhydride to the corresponding acetyl compound (Scheme 5.2), followed by introduction of the solubilizing group at the imide position, and removal of the acetyl group in concentrated HCl (aq). These experiments show that the acetyl group can be hydrolyzed without ring opening of the imide functionality. See Experimental section and: (a) Oona, J. *Report: Monourea*

phthalimides; Eindhoven University of Technology: Eindhoven, **2001**. (b) Greeven A. *Report: Monourea phthalimides*; Eindhoven University of Technology: Eindhoven, **2002**. Further results will appear in: (c) de Greef, T.F.A., *Graduation report*; Eindhoven University of Technology: Eindhoven, **2004**.
(34) Palmans, A.R.A. *Thesis: Supramolecular structures based on the intramolecular H-bonding in the 3,3'-di(acylamino)-2,2'-bipyridine unit*; Eindhoven University of Technology: Eindhoven, **1997**.
(35) Biniecki, S.; Moll, M.; Rylski, L. *Ann. Pharm. Franc.* **1958**, 421–428.
(36) (a) Sana, S.; Rajanna, K.C.; Moazzam Ali, M.; Saiprakash, P.K. *Chem. Lett.* **2000**, 48–49. (b) Choudary, B.M.; Sudha, Y.; Reddy, P.N. *Synlett.* **1994**, 450.
(37) (a) Nagao, Y.; Naito, T.; Abe, Y.; Misono, T. *Dyes and Pigments* **1996**, *32*, 71–83. (b) Kaiser, H.; Lindner, J.; Langhals, H. *Chem. Ber.* **1991**, *124*, 529–535. (c) Neuteboom, E.E.; Beckers, E.H.A.; Meskers, S.C.J.; Meijer, E.W.; Janssen, R.A.J. *J. Org. Biomol. Chem.* **2003**, *1*, 198–203.
(38) (a) Bender, T.P.; Wang, Z.Y. *J. Polym. Sci., Part A: Polym. Chem.* **2000**, *38*, 3991–3996. (b) MacKinnon, S.M.; Bender, T.P.; Wang, Z.Y. *J. Polym. Sci., Part A: Polym. Chem.* **2000**, *38*, 9–17. (c) Herbert, C.G.; Ghassemi, H,; Hay, A.S. *J. Polym. Sci., Part A: Polym. Chem.* **1997**, *35*, 1095–1104.
(39) Pieterse, K. *Thesis: Electron deficient materials based on azaheterocycles*; Eindhoven University of Technology: Eindhoven, **2001**.
(40) Better separation of monomer upto pentamer for fraction **1-IIc** are obtained using a mixed E column, however, no comparison with fractions **1-IIIa** and **1-IIb** can be made, nor estimations of the molecular weight (distribution).
(41) As described in Chapter 2, medium amide disk **1c** and urea disk **2c** show liquid crystallinity over a window of at least 150 °C, and transition enthalpies of 44 and 65 kJ/mol, respectively.
(42) For phthalimide disk **2**, $\Delta\varepsilon$ = 5 l/mol.cm, while for medium and large urea disks **2d** and **2f**, $\Delta\varepsilon$ = 120 and 300 l/mol.cm, respectively (Chapter 3).
(43) The aromatic cross section is measured between two oxygens of two opposite 3,4,5-tris((S)-dimethyloctyloxy)benzene units (See also C_3-symmetrical disks in Chapter 2).
(44) Koen Pieterse, results to be published.
(45) See Chapter 4 for the structuring effect of THF on dintro *m*-phenylene-ureido oligomers.

Chapter 6

Supramolecular scaffolds for new materials; helical dyes

Abstract: *In this chapter, a first exploration is undertaken into the potential applications of helical poly-ureidophthalimides in biological or materials science. One of the opportunities would be the incorporation of dyes in the helix, in order to achieve stacked dyes for molecular wires. In a first attempt, 1-ureidoanthraquinone units (**3**) are incorporated in a helical copolymer **1**, together with 3-ureido-N-[3,4,5-tris((S)-3,7-dimethyloctyloxy)phenyl]-phthalimide units (**5**). To interpret the self-assembly of the anthraquinone/phthalimide copolymer **1**, banana-shaped bisurea anthraquinones **2a/b** are synthesized and investigated in the solid state (DSC, TOPM), as well as in dilute solution (UV-Vis, CD). The banana-shaped mesogens **2a/b** show bright red mesophases, while in dilute apolar solution modest Cotton effects are observed. From a single condensation reaction, anthraquinone phthalimide chains of 20 repeating units on average (**1a**), as well as chains of only oligomeric length (**1c**) could be obtained. Supramolecular chirality is expressed in copolymers **1a** and **1c**, although limited. This could be caused by too strong intramolecular hydrogen bonding between anthraquinone oxygens and urea protons. Other reasons for limited expression of chirality could be the asymmetrical hydrogen bonding of the urea groups to anthraquinone and phthalimide units or the presence of dimeric phthalimide units in the polymer chains.*

6.1 Introduction

6.1.1 Supramolecular scaffolds for new materials

Secondary interactions are widespread, and the mesoscopic ordering they cause, is essential to the function of natural macromolecules,[1] as well as to the properties of plastics and performance materials.[2] Understanding of the mesoscopic ordering at a typical 5-100 nm length scale, has proven to be helpful in linking the chemical structure (Å-length scale) to the biological function or material properties (μm-length scale). For this reason, the well-accessible ureidophthalimide polymer (Figure 5.4), which beautifully folds into a helical conformation, could find its application in either biological systems, or in materials chemistry.

The spatially ordered urea oxygens probably render the inner surface of the helix slightly negatively charged, while the alkyl side chains create a lipid like periphery. Therefore, the helical ureidophthalimide structurally resembles natural ion channels,[3a] for example gramicidine.[3b] Another possibility is a carrier function of the folded polymer,[4] provided it is water soluble.[5] This would be achieved by replacing the alkyl side chains by oligo(ethylene oxide) ones.[6] The guest molecule inside the cavity might use the internal urea oxygens as handles and act as a template,[7] thereby increasing the stability of the helical conformation even further.

Mesoscopic ordering has also been found to strongly influence the performance of plastic electro-optical devices, such as light-emitting diodes, and solar cells.[8] Such devices consist of π-conjugated materials, of which the optical and semi-conducting properties are not only a result of π-electron delocalisation along the backbone, but also of interchain electron transfer.[9] Both processes proceed more controlled in well-defined oligomers, than in polymeric mixtures.[10] The interchain electron transfer is enhanced by self-assembly of the rod-like π-conjugated oligomers into stacks.[11] However, more complicated hierarchical assembly processes are desired to render charge transport even more efficient.[12] To achieve this, hydrogen bonding functionalities might be incorporated in the π-conjugated oligomers.[13] These bonds possibly induce formation of highly ordered cylindrical or tubular aggregates.[14] Also, π-conjugated supramolecular polymers are supposed to be easily processible while being free of defects and behaving well-defined.[10] Furthermore, hydrogen bonded π-conjugated architectures combining both p- and n-type units come into scope.[15] Finally, due to their mesoscopic length scale (5-100 nm), π-conjugated supramolecular architectures might contribute to the miniaturization of electro-optical devices.[16] Since optical lithography and etching techniques have limited resolutions due to the wavelength of the applied light, supramolecular architectures might be helpful for the development of even smaller, and faster devices, that are able to store information in an even higher density.[16b]

6.1.2 Design of a molecular wire

Previously, a variety of π-conjugated dyes have been incorporated in both inter- and intramolecularly hydrogen bonded architectures. Discotics were functionalized at the periphery, to give columns of discotics flanked with stacks of ordered dyes.[17] Also in the foldamer, or polymeric helix approach, it can be envisaged to functionalize the periphery of the molecule, attached via the imide group. However, functionalities can also be incorporated in the backbone of the polymer. For this, the blue, n-type dye 1,4-diaminoanthraquinone[18] is a suitable candidate, since its carbonyl groups could order urea functionalities in a way similar to the phthalimide units. In view of the anticipated lack of solubility of oligo(1-ureido-anthraquinones), it was aimed to copolymerize the 1,4-diaminoanthaquinone with solubilizing 3,6-diisocyanatophthalimide units (Scheme 5.7). If this anthraquinone/phthalimide copolymer would be prone to helix formation, it is reasonable to aim for an improved, three layered, molecular wire.[19] Such a wire would contain an n-type center, p-type interior (e. g. oligo(phenylene vinylene)), and insulating exterior (Figure 6.1).

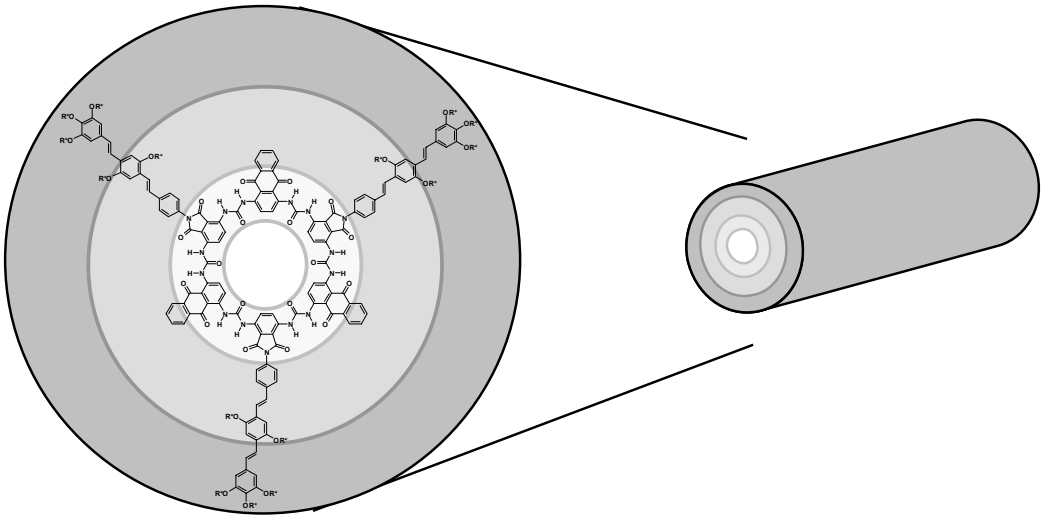

Figure 6.1. *Design of a three-layered molecular wire, consisting of an n-type anthraquinone center (light gray), p-type oligo(phenylene vinylene) interior (gray), and insulating exterior (dark gray).*

The synthesis of anthraquinone/phthalimide copolymer **1** (Figure 6.2) starts from 1,4-diaminoanthraquinone and 3,6-diisocyanato-N-[3,4,5-tris((*S*)-3,7-dimethyloctyloxy)phenyl]-phthalimide. It requires transformation of a less nucleophilic anthraquinone amine into a urea functionality. To test this condensation, banana-shaped 1,4-bisurea anthraquinones **2a/b**, end capped with 3,4,5-trialkoxybenzene units, were synthesized. The behavior of these 'small' models will facilitate understanding of the folding behavior of copolymer **1**. In addition, bent-core, or banana-shaped mesogens are a new class of liquid crystals,[20] that might display columnar phases,[21] similar to disc-like molecules.[22]

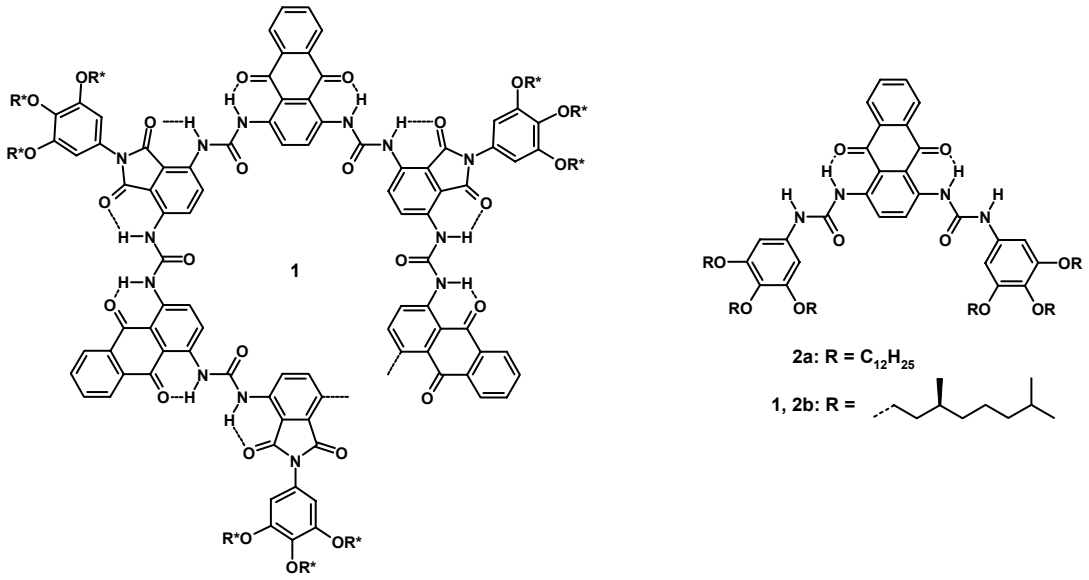

Figure 6.2. *Chemical structures of anthraquinone/phthalimide copolymer **1** and banana-shaped mesogens **2a/b**.*

6.2 An anthraquinone copolymer and banana-shaped mesogens

The amines of 1,4-diaminoanthraquinone (**3**) were found reactive enough to form urea groups with 3,4,5-tridodecyloxybenzene isocyanate **4a** or 3,4,5-tri((*S*)-3,7-dimethyloctyloxy)benzene isocyanate **4b**.[23] Elevated temperatures (110 °C) and a base (4-dimethylaminopyridine) were applied (Scheme 6.1), similar to the phthalimide condensations of diamino and diisocyanato phthalimide building blocks (see Chapter 5). Remarkable was the color change from blue (1,4-diaminoanthraquinone (**3**)) to red (bisurea anthraquinones **2a/b**). Similar conditions were also applied in the synthesis of copolymer **1**, which was obtained in a condensation of 1,4-diaminoanthraquinone and 3,6-diisocyanato-N-[3,4,5-tris((*S*)-3,7-dimethyloctyloxy)phenyl]phthalimide (**5**) in a one to one ratio (Scheme 6.2). After column chromatography, a long (**1a**), intermediate (**1b**), and short (**1c**) fraction of the copolymer were obtained, in which long fraction **1a**, comprised 80 % of the reaction mixture.

Scheme 6.1. *Synthesis of banana-shaped mesogens **2a/b** based on anthraquinone.*

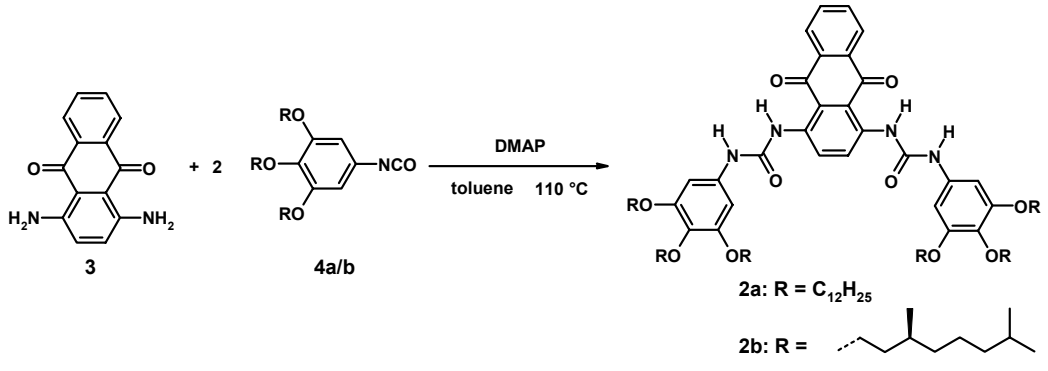

Scheme 6.2. *Synthesis of ureido-anthraquinone - ureido-phthalimide copolymer **1**.*

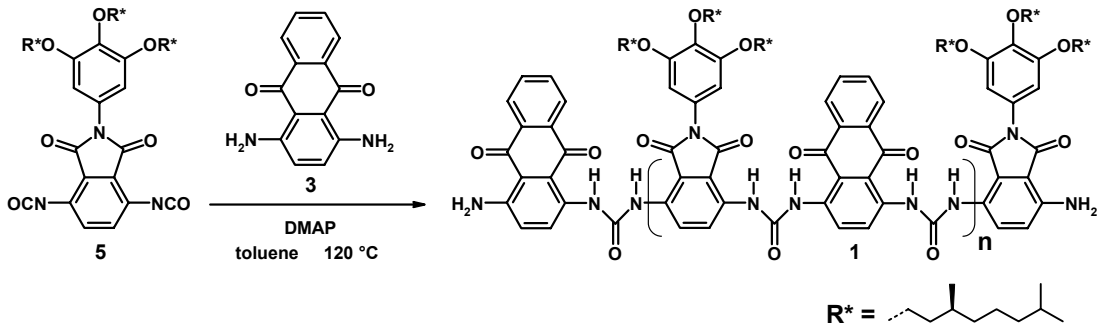

The ^{1}H-NMR spectra of anthraquinone models **2a/b** display the signal of the central urea proton at 11.8 ppm. The outer urea proton signal shifts with concentration and solvent ($CDCl_3$ with or without CH_3OH), but generally appears around 8.5 ppm. This indicates intramolecular hydrogen bonding, stronger than in case of the phthalimide compounds (urea proton at 9.0 ppm). In ^{13}C-NMR the conformational locking of the urea groups with respect to the anthraquinone moiety becomes obvious from the dramatically different shielding of C-4A (-9.5 ppm) *versus* C-2 (+1 ppm) compared to calculated values. This phenomenon has been observed previously in phthalimide analogues (see Table 5.2).[24] Also typically low wavenumber positions of NH and CO stretch vibrations in IR (3288, and 1636 cm^{-1}, respectively) point towards this direction. Indeed, both the achiral and chiral anthraquinone models show a thermotropic liquid crystalline window in DSC (**2a**: heating run 40 °C/min; K (82 °C, 33 kJ/mol) M (184 °C, 21 kJ/mol) I; **2b**: heating run 10 °C/min; K (95 °C, ~0.9 kJ/mol) M (182 °C, ~9 kJ/mol) I)). The aromatic urea groups start to decompose well below the isotropization temperature (~140 °C, and 184/182 °C, respectively), which makes the calculated transition enthalpies less reliable. Nevertheless, liquid crystalline textures could be grown with the aid of temperature dependent optical polarization microscopy (Figure 6.3).

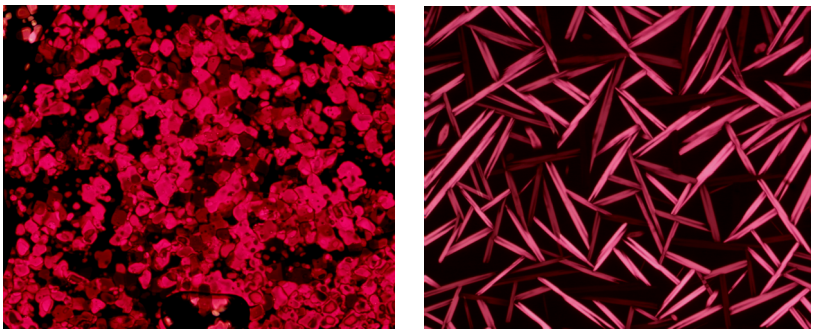

Figure 6.3. *Optical microscopy pictures of achiral banana-shaped anthraquinone **2a** (left, 166 °C, after pressing of the sample between two glass plates), and chiral banana-shaped anthraquinone **2b** (right, 130 °C).*

In apolar dilute solution, ordered architectures of bisurea anthraquinone **2b** are maintained, as indicated by a drop in the absorption coefficient ε in the UV spectrum in heptane, compared to spectra in chloroform or THF. Furthermore, in heptane a small blue shift and the appearance of a shoulder at λ = 573 nm are detected (heptane: λ_{max} = 526 nm, chloroform or THF: λ_{max} = 533 nm; Figure 6.4, left). In chloroform and THF no Cotton effect is observed, while in heptane ordered, supramolecular aggregates are present. Also the anthraquinone units are involved in the ordering process, as a bisignate CD signal is centered around 530 nm (Figure 6.4, right). The effect is small,[25] which is expected to be favorable in oligomeric structures **1a-c**, when cooperativity of multiple similar interactions is required. Bisurea anthraquinone **2b** shows a reversible temperature dependent behavior between 0 and 60 °C, where the Cotton effect disappears.

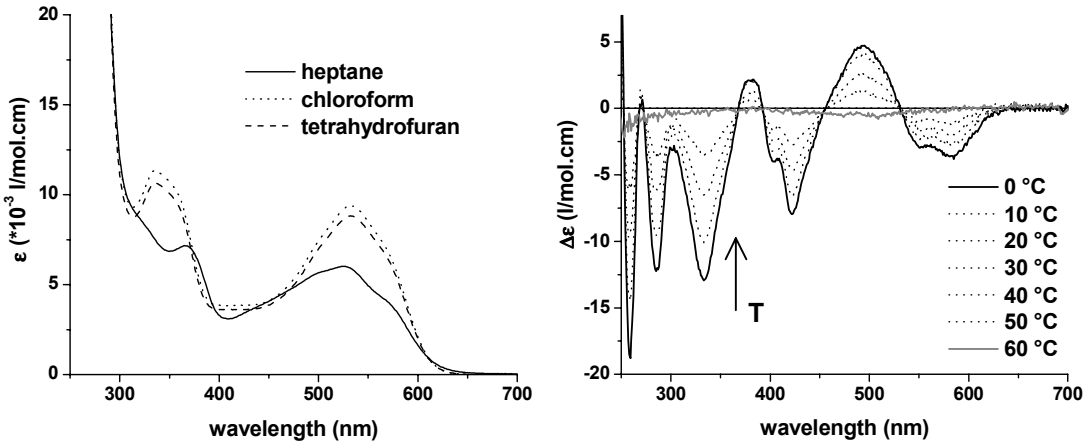

Figure 6.4. *UV-Vis spectra in different solvents (left), and temperature dependent CD spectra (right) in heptane (3×10^{-5} M) of bisurea anthraquinone **2b**.*

The anthraquinone/phthalimide copolymer **1** was characterized by GPC. Clearly, the long and intermediate fractions **1a** and **1b** (elution times 7.60, and 7.62 min, respectively), contain 'longer' chains. In short fraction **1c** the phthalimide monomer, and species consisting of one or two anthraquinone/phthalimide units seem present (elution times 7.65, 7.92, 8.10, 8.37, and 8.95 (diamino phthalimide) min). MALDI-TOF spectrometry on the three fractions **1a-c**, showed similar results, most probably because of the limited degree of ionization of the longer molecules. The longest oligomer observed in MALDI-TOF was the hexamer (n = 5). Besides strictly alternating structures of anthraquinone and phthalimide $(A–Ph)_n$, molecules containing dimeric phthalimide units $(A\text{-}Ph\text{-}Ph)_n$ are present in the reaction mixture (see experimental section). This is caused by hydrolysis of some of the isocyanato groups of the diisocyanato phthalimide monomer during the reaction, by water that comes primarily with the DMAP.[26] In IR, the NH_2 stretch vibration (3439 cm^{-1}) is more intense in short fraction **1c**, while for long fraction **1a**, the NH stretch and CO stretch urea vibrations are more resolved. They are found at low wavenumbers (3349/3304 cm^{-1}, and 1645/1631cm^{-1}, respectively),

similar to the hydrogen bonding in phthalimide homo-polymers (Chapter 5). More information about the composition of the polymeric mixtures **1a** and **1c** was obtained from ^{1}H-NMR. In both cases spectra had to be recorded in a 2/1 mixture of $CDCl_3$ and HFIP, in order to obtain resolved peaks (Figure 6.5). Still, hydrogen bonded urea protons are observed, indicated by the signals between 12.5 and 13.0 ppm (anthraquinone, A_U) and around 9.0 ppm (phthalimide, Ph_U), proving that indeed elongated structures have been formed.

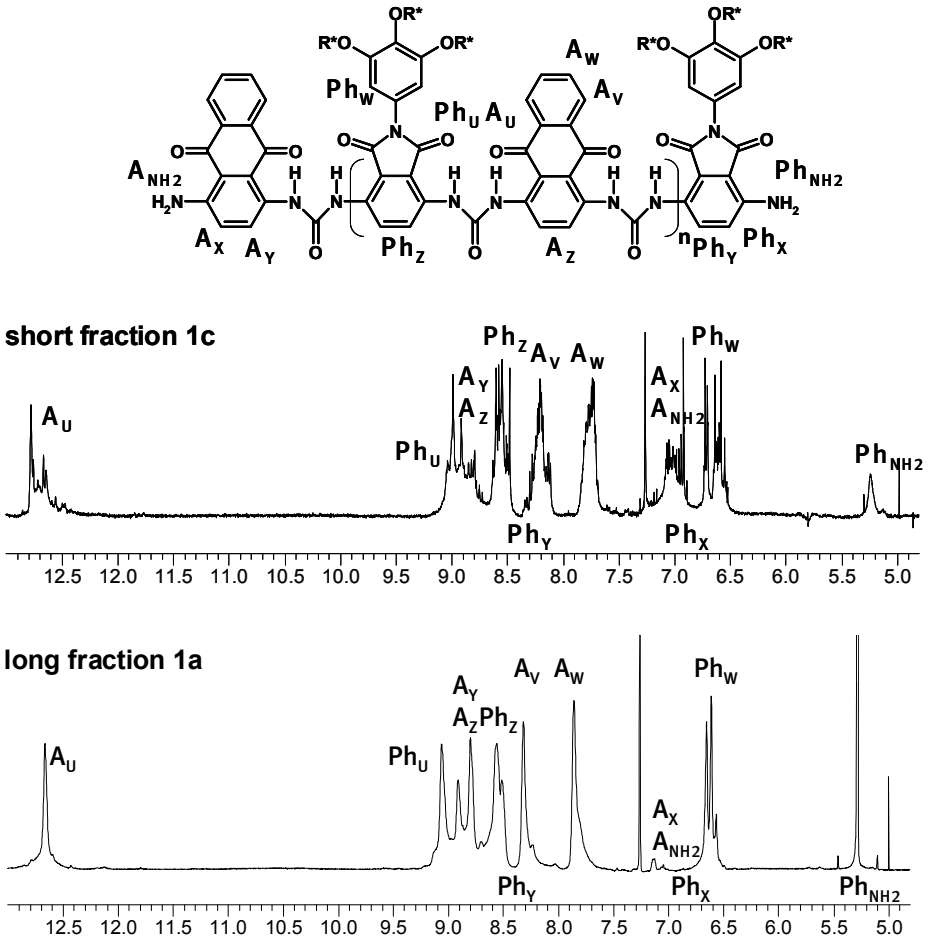

Figure 6.5. *Chemical structure and ^{1}H-NMR spectra ($CDCl_3$/HFIP 2/1) of anthraquinone/ phthalimide copolymer fractions **1a** (long, bottom), and **1c** (short, top).*

In short fraction **1c**, substantial signals were found at 5.2 ppm of the phthalimide amino endgroups Ph_{NH2} (2H), and at 7.0 ppm, where the anthraquinone amino endgroups A_{NH2} (2H), are expected. Also the aromatic protons adjacent to these amino endgroups Ph_X (1H) and A_X (1H) appear at 7.0 ppm. In the spectrum of long **1a**, these signals have almost disappeared. Clearly resolved are the anthraquinone aromatic multiplets A_V (2H) and A_W (2H). Therefore, the ratio between the integrals of Av (2H) and that of the endgroups (Ph_{NH2}, A_{NH2}, Ph_X and A_X, 6H) was used to estimate the average length of the oligomers for mixtures **1a** and **1c** ($(Ph_{NH2}+A_{NH2}+Ph_X+A_X)/6$) / ($(A_v/2)$). For short

cooligomers **1c**, a ratio of 3 is found, while in case of a dimer (n = 1), the ratio would be 1. This is rationalized by the presence of a substantial amount of diamino phthalimide. For long fraction **1a**, the ratio endgroup/anthraquinone monomer was approximately 1/20, which corresponds to structures, long enough to complete an estimated 6 turns in a helical conformation. Considering that in the copolymer the repeating unit (n) comprises two aromatic units (anthraquinone and phthalimide), the degree of polymerization is judged similar to that of the phthalimide homopolymer (Chapter 5).

Because the degradation temperature of these aromatic urea structures **1a-c** (~140 °C) is expected to be much lower than the isotropization temperature (~ 300 °C), they have not been studied yet in the solid state (TOPM / DSC). In dilute solution, the UV spectrum in heptane of short **1c** shows a drop in the absorption coefficient ε, and a blue shift in the onset, compared to spectra in chloroform and THF (heptane: λ_{onset} = 700 nm, chloroform or THF: λ_{onset} = 643 nm; Figure 6.6, left). In contrast to the blue shift in $\lambda_{max,UV}$ of bisurea anthraquinone **2b** in heptane, oligomers **1c**, show a red shift in $\lambda_{max,UV}$ in both heptane and THF compared to chloroform (heptane and THF: λ_{max} = 540 nm, chloroform: λ_{max} = 530 nm). In all three solvents a shoulder is visible (heptane λ = 591 nm; THF: λ = 583 nm; chloroform: λ = 572 nm).

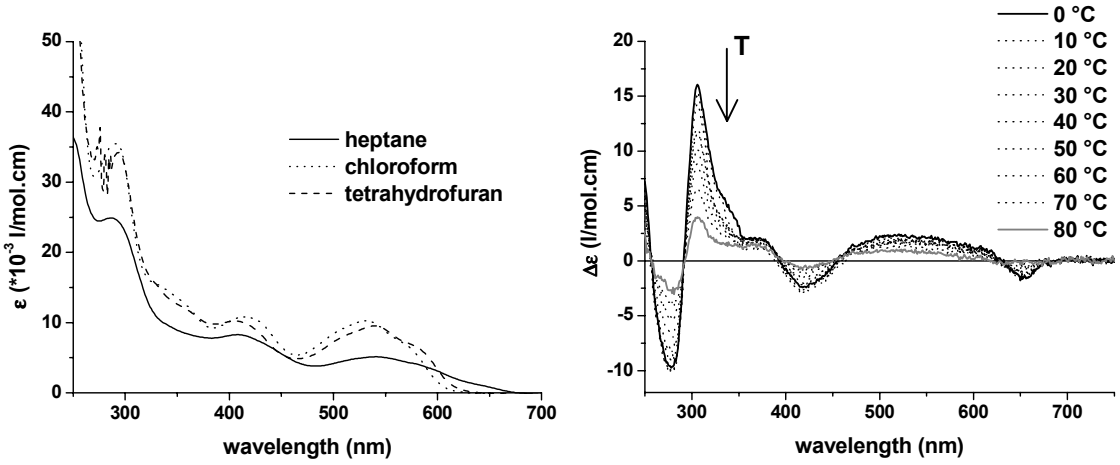

Figure 6.6. *UV-Vis spectra in different solvents (left), and temperature dependent CD spectra (right) in heptane (0.03 mg/ml, ε and Δε calculated per mole monomeric units) of short anthraquinone/phthalimide oligomers **1c**.*

Similar to bisurea models **2b**, in chloroform and THF no Cotton effect is observed for polymer **1a-c**, while in heptane ordered, supramolecular aggregates are present (Figure 6.6, right). Both phthalimide ($\lambda_{max,UV}$ = 408 nm) and anthraquinone units ($\lambda_{max,UV}$ = 540 nm) are involved in the aggregation. Although the UV spectrum of **1c** in THF clearly differs from that in chloroform, supramolecular chirality is not expressed, in contrast to the situation for phthalimide homopolymers (Chapter 5). The supramolecular ordering of **1c** in heptane is remarkably stable upon heating to 80 °C,

but upon cooling the signal is not reobtained. This indicates that order is not maximal in this foldamer, which is in line with the small overall Cotton effect.[25]

The Cotton effect has decreased even further in long copolymers **1a**; Δε is about 2, similar to short **1c** in heptane at 80 °C. To dissolve **1a** in dodecane, temperature has to be raised to 80 °C, and from the irreversible temperature behavior of **1c**, it follows that the effect of long **1a** will not return to its 'hypothetical' value at 20 °C. Therefore, it is logical that the intensity of the effects of **1a** (at 80 °C, or after cooling to 20 °C) and **1c** (at 80 °C) in these apolar solvents are similar (Figure 6.7, right). In all other solvents investigated, similar spectra with a Δε of 2 are obtained (not depicted), no matter their ε or λ_{max} in UV-Vis (Figure 6.7, left).

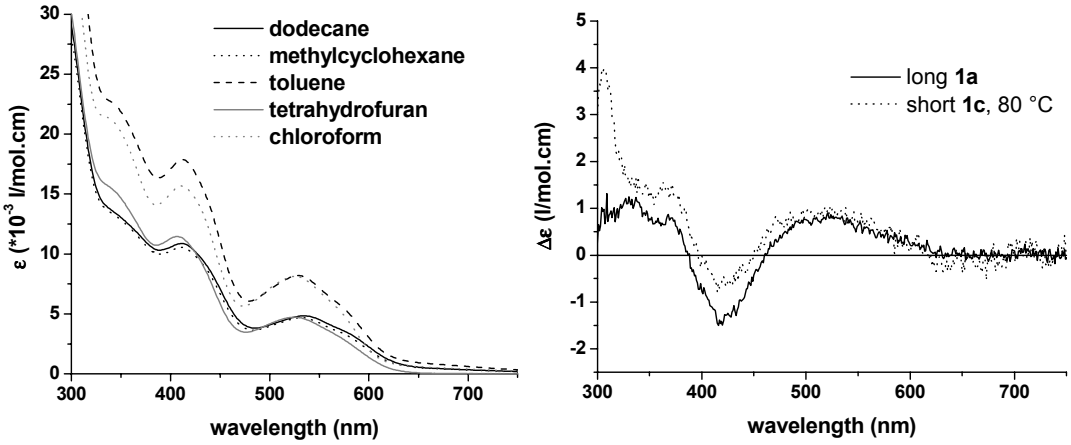

Figure 6.7. *UV-Vis spectra in different solvents (left), and temperature dependent CD spectra (right) in dodecane (0.04 mg/ml, ε and Δε calculated per mole monomeric units) of long anthraquinone/phthalimide oligomers **1a**. (UV spectrum **1c** in heptane.)*

6.3 Ordered dyes in stacks and helices

Although supramolecular ordering in dilute apolar solution does not seem optimal in anthraquinone banana mesogens **2a/b** and anthraquinone/phthalimide copolymers **1**, stacks and helices of dyes are formed. Regarding the low degree of order, together with the limited length (6 turns), 'donut' might describe the shape of the supramolecular aggregates of **1** probably better than 'helix'. It would be revealing to characterize the mesophase of banana mesogens **2a/b** with X-ray spectroscopy. Also the anthraquinone/phthalimide copolymeric structures **1** need to be investigated in more detail, to pin point the exact reason for the lack of supramolecular ordering. The liquid crystallinity of models **2a/b**, and their modest supramolecular aggregation in apolar solution, look very promising for optimal ordering in the corresponding copolymer **1**. Also in case of the homo-phthalimide structures, modest self-assembly of the model compound (disk), gave stable, as well as reversible, folding of similar

polymeric structures (Chapter 5). This is also in agreement with intermolecular interactions of (semi) natural macromolecules.[27]

It has to be noted that the hydrogen bonded anthraquinone urea proton signals appear much more downfield than the phthalimide urea proton signals (12.5, and 9.0 ppm, respectively). This corresponds to their chemical structures, which show that in case of the anthraquinone unit, the positions of the urea proton and imide oxygen with respect to each other, are much more favorable for intramolecular hydrogen bonding, than in case of the phthalimide unit. Indeed, multiple of these stronger anthraquinone hydrogen bonding interactions might be too much, preventing the structure to move (back) to its most ordered, thermodynamically stable conformation (Chapter 3).

On the other hand, order in this copolymeric structure is inherently smaller than in the phthalimide-based homopolymer. The urea groups are 'twisted', since they are hydrogen bonded on one side to a 5-membered ring (phthalimide), and on the other to a 6-membered one (anthraquinone). Also, it is hard to judge the influence of (π-π) interactions between stacked phthalimide, anthraquinone, and urea units. Finally, the synthetic procedure may be optimized, in order to exclude dimeric phthalimide fragments $(A\text{-}Ph\text{-}Ph)_n$, which make the chains less regular, and thus decrease their ordering capabilities.

6.4 Conclusions

Banana-shaped anthraquinone bisureas **2a/b** appear as bright red thermotropic mesophases. They display modest self-assembly in dilute apolar solution, in which the anthraquinone unit is clearly involved. Although such behavior in the model compound seems a prerequisite for optimal folding of a corresponding foldamer,[27] supramolecular order in anthraquinone/phthalimide copolymers **1** comes not to full expression. A reason for this might be too strong intramolecular hydrogen bonding between anthraquinone oxygens and urea protons. Other explanations can be found in twisting of the urea groups between anthraquinone and phthalimide units, or the fact that not all polymer chains are strictly alternating. Nonetheless, the results are promising with respect to further development of helical dyes, in for example molecular wires.

6.5 Experimental section

General. General aspects concerning synthesis, characterization, and optical techniques have been described in Chapter 2, 3, and 5. 1,4-Diaminoanthraquinone (**3**) is commercially available. Syntheses of 3,4,5-tridodecyloxybenzene isocyanate (**4a**), and 3,4,5-tri((*S*)-3,7-dimethyloctyloxy)benzene isocyanate (**4b**) have been described previously.[23] 3,6-Diisocyanato-N-[3,4,5-tri((*S*)-3,7-dimethyloctyloxy)phenyl]phthalimide (**5**) is described in Chapter 5 as compound **18**.

Amino terminated copolymer of 3-ureido-N-[3,4,5-tris((*S*)-3,7-dimethyloctyloxy)-phenyl]phthalimidyl and 1-ureidoanthraquinone (1). 3,6-Diisocyanato-N-[3,4,5-tris((*S*)-3,7-dimethyloctyloxy)phenyl]phthalimide (**5**, 101 mg, 0.130 mmol), 1,4-diaminoanthraquinone (**3**, 15.5 mg, 0.065 mmol), and 4-dimethylaminopyridine (16.0 mg, 0.130 mmol) were stirred in refluxing toluene (5 ml) for 1 h, after which a solution of 1,4-diaminoanthraquinone (15.5 mg, 0.065 mmol) in toluene (5 ml) was added portion wise. After one night, the solvent was evaporated, and DMAP removed by column chromatography (flash silica gel, chloroform + 0 - 3 % $^{v}/_{v}$ methanol, R_f = 0.2 - 0.9). This yielded three fractions of red ureidophthalimide/anthraquinone copolymer **1**, of which the high molecular weight material (**1a**, ~120 mg, ~80 %) eluted first, followed by an intermediate (**1b**, ~8 mg, ~5 %**)** and low molecular weight fraction (**1c**, ~25 mg, ~15 %): **1a**: ^{1}H-NMR ($CDCl_3$/HFIP 2/1) δ 12.66 (A_U, bs, (2n+1)H), 9.06 (Ph_U, bs, (2n+1)H), 8.90, 8.80 (A_Y, A_Z, m, 1H +2nH), 8.55, 8.53 (P_Z, m, 2nH), 8.32, 7.86 (A_V, A_W, m, 4(n+1)H),7.05 (A_X, Ph_X, A_{NH2}, m, 4H) 6.65, 6.60, 6.55 (Ph_W, s, 2(n+1)H), 5.20 (Ph_{NH2}, bs, 2H), 4.08 (OCH_2, m, 6(n+1)H), 1.90 – 0.88 ((C_9H_{19}), m, 57(n+1)H) ppm; ^{13}C-NMR ($CDCl_3$/HFIP 2/1) δ 187.7 (CO_A), 169.3, 169.0 (imide CO), 153.7 153.2 (C3', urea CO), 138.5 (C4'), 136.9, 135.4, 133.7, 133.5, 133.2, 132.8, 128.6, 127.4, 126.3, 121.9, 121.0, 117.6, 115.2 (C4aA), 114.7 (C1), 105.5 (C2'), (OCH_2 not visible), 39.4, 39.4, 37.5, 37.5, 36.8, 36.2, 30.0, 28.1, 24.9, 24.8, 22.5, 22.4, 22.4, 22.3, 19.3, 19.1, 19.1 (C_9H_{19}) ppm; IR (ATR): 3349, 3304, 2953, 2925, 2869, 1724, 1694, 1645, 1631, 1591, 1474, 1398, 1384, 1365, 1274, 1262, 1216, 1166, 1114, 998, 932, 884, 842, 762, 728, 687 cm^{-1}; GPC elution times: **1a**, 7.60; **1b**, 7.62; **1c**, 7.65, 7.92, 8.10, 8.37, and 8.95 min. (3,6-diamino-N-[3,4,5-tris((*S*)-3,7-dimethyloctyloxy)phenyl]phthalimide, 9.03 min); MALDI-TOF MS: see below.

1,4-Bis(3,4,5-tridodecyloxyphenylureido)anthraquinone (2a). A solution of 3,4,5-tridodecyloxybenzene isocyanate (478 mg, 0.710 mmol), 1,4-diaminoanthraquinone (84.8 mg, 0.356 mmol) and 4-dimethylaminopyridine (86 mg, 0.710 mmol) was stirred for 1 h in refluxing toluene (5 ml). After evaporation of the solvent, the product was purified using column chromatography (silica gel, dichloromethane + 2 % $^{v}/_{v}$ ethyl acetate, R_f = 0.25). Finally, banana-shaped anthraquinone **2a** was obtained as a sticky, dark red solid (68 mg, 12 %, together with a mixture of mono- and di-substituted products, 100 mg): mp = 82 °C; ^{1}H-NMR ($CDCl_3$ + CD_3OD) δ 11.95 (inner urea NH, s, 2H residual), 8.81 (anthraquinone CH, s, 2H), 8.25 (outer urea NH, s, 2H residual), 8.05, 7.67 (anthraquinone CH, m, 4H), 6.75 (gallic ar. H, s, 4H), 3.92 (OCH_2, m, 12H), 1.76 ($OCH_2C\underline{H}_2$, m, 12H), 1.45 (OCH_2 $CH_2C\underline{H}_2$, m, 12H), 1.27 ((CH_2)$_8$, m, 96H), 0.87 (CH_3, m, 18H) ppm; ^{13}C-NMR ($CDCl_3$ + CD_3OD) δ 185.5 (anthraquinone CO), 153.0, 152.9 (C3', urea CO), 152.8, 139.1 (C1), 138.9 (C1'), 134.0 (C6), 133.6 (C8a), 133.1 (C4'), 128.3 (C5), 126.6 (C2), 115.4 (C4a), 98.8 (C2'), 73.5, 68.9 (OCH_2), 31.8, 30.2, 29.7, 29.6, 29.4, 29.3, 26.1, 22.6, 14.0 ($C_{11}H_{23}$) ppm; IR (ATR): 3281, 2921, 2852, 1668, 1635, 1595, 1581, 1552, 1491, 1468, 1428, 1385, 1263, 1214, 1115, 1008, 820, 720 cm^{-1}; Elemental analysis: calculated: $C_{100}H_{164}N_4O_{10}$ (1582.44): C, 75.90; H, 10.45; N, 3.54; found: C, 75.92; H, 10.58; N, 3.36; MALDI-TOF MS: calculated: 1582.25, found: 1605.28 (Na-adduct).

1,4-Bis[3,4,5-tri((*S*)-3,7-dimethyloctyloxy)-phenylureido]anthraquinone (2b). A solution of 3,4,5-tris((*S*)-3,7-dimethyloctyloxy)benzene isocyanate (523 mg, 0.890 mmol), 1,4-diaminoanthraquinone (84.8 mg, 0.356 mmol) and 4-dimethylaminopyridine (109 mg, 0.890 mmol) was stirred for one night in refluxing toluene (10 ml). After evaporation of the solvent, the product was purified using column chromatography (flash silica gel, dichloromethane + 0 - 2 % $^{v}/_{v}$ ethyl acetate, R_f = 0 - 0.3). Finally, banana-shaped anthraquinone **2b** was obtained as a sticky, dark red solid (430 mg, 85 %): mp = 95 °C; ^{1}H-NMR ($CDCl_3$ + CH_3OH) δ 11.78 (inner urea NH, s, 2H), 8.77 (outer urea NH, s, 2H residual), 8.62 (anthraquinone CH, s, 2H), 7.86, 7.53 (anthraquinone CH, m, 4H), 6.69 (gallic ar. H, s, 4H), 3.92 (OCH_2, m, 12H), 1.83 - 0.64 ((C_9H_{19}), m, 114H) ppm; ^{13}C-NMR ($CDCl_3$ +CH_3OH) δ 185.0 (anthraquinone CO), 152.9, 152.7 (C3', urea CO), 138.6 (C1, C1'), 134.4 (C6), 133.3 (C8a), 132.7 (C4'), 127.9 (C5), 126.2 (C2), 115.3 (C4a), 98.0 (C2'), 71.5, 66.7 (OCH_2), 39.1, 39.0, 37.3, 37.1, 37.0, 36.1, 29.5, 29.4, 27.6, 24.4, 22.3, 20.5, 19.2, 19.1 (C_9H_{19}) ppm; IR (ATR): 3288, 2953, 2926, 2869, 1670, 1636, 1596, 1582, 1552, 1492, 1429, 1383, 1263, 1211, 1114, 1002, 820, 735, 720 cm^{-1}; Elemental analysis: calculated: $C_{88}H_{140}N_4O_{10}$ (1414.12): C, 74.74; H, 9.98; N, 3.96; found: C, 74.74; H, 10.08; N, 3.88; MALDI-TOF MS: calculated: 1413.06, found: 1436.29 (Na-adduct).

MALDI-TOF MS of copolymer 1.

Oligomer	Mass		
	Adduct	**calculated**	**found**
A (diamino anthraquinone)	Na	261.06	
Ph (diamino phthalimide)	Na	744.53	
A-Ph	Na	1008.58	1010.72
A-Ph-A	Na	1272.64	1274.59
Ph-Ph	*Na*	*1493.05*	*1493.31*
Ph-A-Ph	Na	1757.10	1757.67
A-Ph-A-Ph	Na	2021.16	2021.40
A-Ph-A-Ph-A	Na	2285.21	2284.88
Ph-Ph-A-Ph	*Na*	*2504.62*	*2504.94*
Ph-A-Ph-A-Ph	Na	2768.68	2768.13
A-Ph-A-Ph-A-Ph	Na	3033.73	3031.52
cycle	Na	3059.71	
Ph-Ph-A-Ph-Ph	*Na*	*3253.14*	*3251.49*
Ph-Ph-A-Ph-A-Ph	*Na*	*3517.20*	*3513.28*
Ph-A-Ph-A-Ph-A-Ph	Na	3781.25	3778.26
A-Ph-A-Ph-A-Ph-A-Ph	Na	4045.31	4041.03
Ph-Ph-A-Ph-A-Ph-Ph	*Na*	*4265.72*	*4258.98*
A-Ph-A-Ph-A-Ph-A-Ph-A	Na	4310.36	4301.71
Ph-Ph-A-Ph-A-Ph-A-Ph	*Na*	*4529.77*	*4523.09*
Ph-A-Ph-A-Ph-A-Ph-A-Ph	Na	4793.83	4787.43
A-Ph-A-Ph-A-Ph-A-Ph-A-Ph	Na	5057.88	5049.09
Ph-A-Ph-A-Ph-A-Ph-A-Ph-A-Ph	Na	5806.40	5798.20

6.6 References and notes

(1) spider silk: (a) Simmons, A.H.; Michal, C.A; Jelinski, L. *Science* **1996**, *271*, 84-87. Eles, P.T.; Michal, C.A. *Macromolecules* **2004**, *37*, 1342–1345. elastin: (b) Ayres, L.;Vos, M.R.J.; Adams, P.J.H.M.; Shklyarevskiy, I.O.; van Hest, J.C.M. *Macromolecules* **2003**, *36*, 5967–5973.

(2) thermoplastic elastomers: (a) Versteegen, R.M.; Sijbesma, R.P.; Meijer, E.W. *Angew. Chem. Int. Ed.* **1999**, *38*, 2917–2919. (b) Versteegen, R.M. *Thesis: Well-defined thermoplastic elastomers; Reversible networks based on hydrogen bonding*; Eindhoven University of Technology: Eindhoven, **2003**. advanced block copolymers: (c) Zubarev, E.R.; Pralle, M.U.; Li, L.; Stupp, S.I. *Science* **1999**, *283*, 523–526. (d) Hartgerink, J.D.; Beniash, E.; Stupp, S.I. *Science* **2001**, *294*, 1684–1688. (e) Hulvat, J.F.; Stupp, S.I *Angew. Chem. Int. Ed.* **2003**, *42*, 778–781.

(3) (a) Bong, D.T.; Clark, T.D.; Granja, J.R.; Ghadiri, M. R. *Angew. Chem. Int. Ed.* **2001**, *40*, 989–1011. (b) Duax, W.L.; Burkhart, B.M.; Pangborn, W.A.; Pletnev, V.; Wawrzak, Z.; Glowka, M. *Adv. Supramol. Chem.* **2002**, *8*, 245–282.

(4) (a) Inouye, M.; Waki, M.; Abe, H. *J. Am. Chem. Soc.* **2004**, *126*, 2022–2027. (b) Heemstra, J.M.; Moore, J.S. *J. Am. Chem. Soc.* **2004**, *126*, 1648–1649.

(5) (a) Baars, W.P.L.; Kleppinger, R.; Koch, M.H.J.; Yeu, S.-L.; Meijer, E.W. *Angew. Chem. Int. Ed*. **2000**, *39*, 1285–1288. (b) Tomalia, D.A.; Durst, H.D. *Top. Curr. Chem.* **1993**, *165*, 193–313. Boas, U.; Heegaard, P.M.H. *Chem. Soc. Rev.* **2003**, *33*, 43–63.

(6) (a) Brunsveld, L.; Zhang, H.; Glasbeek, M.; Vekemans, J.A.J.M.; Meijer, E.W. *J. Am. Chem. Soc.* **2000**, *122*, 6175–6182. (b) Kilbinger, A.F.M.; Schenning, A.P.H.J.; Goldoni, F.; Feast, W.J.; Meijer, E.W. *J. Am. Chem. Soc.* **2000**, *122*, 1820–1821. (c) Janssen, H.M. *Thesis: Chiral ethylene oxide derivatives in supramolecular assemblies*; Eindhoven University of Technology: Eindhoven, **1997**.

(7) (a) Berl, V.; Krische, M.J.; Huc, I.; Lehn, J.-M.; Schmutz, M. *Chem. Eur. J.* **2000**, *6*, 1938–1946. An example of templating in nature is the tobacco mosaic virus: (b) Klug, A. *Angew. Chem.* **1983**, *95*, 579–596. (c) Stryer, L.; *Biochemistry*, 4th ed, W. H. Freeman & Company: New York, **1995**.

(8) van Duren, J.K.J. *Thesis: Polymer:fullerene bulk-heterojunction solar cells*; Eindhoven University of Technology: Eindhoven, **2004**.

(9) Brédas, J.L.; Cornil, J.; Beljonne, D.; Dos Santos, D.A.; Shuai, Z. *Acc. Chem. Res.* **1999**, *32*, 267–276.

(10) (a) Schenning, A.P.H.J.; Jonkheijm, P.; Peeters, E.; Meijer, E.W. *J. Am. Chem. Soc.* **2001**, *123*, 409–416. (b) Peeters, E. *Thesis: Mesoscopic order in π-conjugated materials*; Eindhoven University of Technology: Eindhoven, **2000**.

(11) thiophenes: Schenning, A.P.H.J.; Kilbinger, A.F.M.; Biscarini, F; Cavallini, M.; Cooper, H.J.; Derrick, P.J.; Feast, W.J.; Lazzaroni, R.; Leclere, Ph.; McDonell, L.A.; Meijer, E.W.; Meskers, S.C.J. *J. Am. Chem. Soc.* **2002**, *124*, 1269–1275.

(12) Percec, V.; Glodde, M.; Bera, T.K.; Mlura, Y.; Shlyanovskaya, I.; Singer, K.D.; Balagurusamy, V.S.K.; Helney, P.A.; Schnell, I.; Rapp, A.; Spiess, H.-W.; Hudson, S.D.; Duan, H. *Nature* **2002**, *417*, 384–387.

(13) perylenes: Thalacker, C.; Würthner, F. *Adv. Funct. Mat.* **2002**, *12*, 209–218.

(14) Jonkheijm, P.; Miura, A.; Zdanowska, M.; Hoeben, F.J.M.; De Feyter, S.; Schenning, A.P.H.J.; De Schryver, F.C.; Meijer, E.W. *Angew. Chem. Int. Ed.* **2004**, *43*, 74–78.

(15) triad: (a) Ramos, A.M.; Meskers, S.C.J.; van Hal, P.A.; Knol, J.; Hummelen, J.C.; Janssen, R.A.J. *J. Phys. Chem.* A **2003**, *107*, 9269–9283. OPV with pendant fullerene: (b) Ramos, A.M.; Rispens, M.T.; van Duren, J.K.J.; Hummelen, J.C.; Janssen, R.A.J. *J. Am. Chem. Soc.* **2001**, *123*, 6714–6715. (c) Upy-OPV and Upy-fullerene: Beckers, E.H.A.; Schenning, A.P.H.J.; van Hal, P.A.; El-Ghayoury, A.; Sanchez, L.; Hummelen, J.C.; Meijer, E.W.; Janssen, R.A.J. *Chem. Commun.* **2002**, 2888–2889.

(16) (a) Balzani, V.; Credi, A.; Raymo, F.M.; Stoddart, J.F. *Angew. Chem. Int. Ed.* **2000**, *39*, 3348–3391. (b) Goldhaber-Gordon, D.; Montemerlo, M.S.; Love, J.C.; Opiteck, G.J.; Ellenbogen, J.C *Proc. IEEE* **1997**, *85*, 521–540.

(17) C_3-symmetrical OPV's: (a) van Herrikhuyzen, J. *Graduation report: Supramolecular p- and n-type stacks; construction, manipulation, and application*; Eindhoven University of Technology: Eindhoven, **2003**. triazine OPV's: (b) Jonkheijm, P.; Hoeben F.J.M.; Kleppinger, R.; van Herrikhuyzen, J.; Schenning, A.P.H.J.; Meijer, E.W. *J. Am. Chem. Soc.* **2003**, *125*, 15941–15949. fullerene Upy: (d) Rispens, M.T.; Sanchez, L.; Beckers, E.H.A.; van Hal, P.A.; Schenning, A.P.H.J.; El-Ghayoury, A.; Peeters, E.; Meijer, E.W.; Janssen, R.A.J.; Hummelen, J.C. *Synth. Met.* **2003**, *135-136*, 801–803.

(18) anthraquinone metallo mesogen: (a) Naidu, J.J.; Kumar. S. *Mol. Cryst. Liq. Cryst.* **2003**, *397*, 17–24. anthracene organogellator: (b) Brotin, T.; Utermöhlen, R.; Fages, F.; Bouas-Laurent, H.; Desvergne, J.-P. *J. Chem. Soc., Chem. Commun.* **1991**, 416–418. 1,8-diureidoanthraquinone: (c) Kang, S.O.; Jeon, S.; Nam K.C. *Supramol. Chem.* **2002**, *14*, 405–410.

(19) (a) Eichhorn, S.H.; Adavelli, A.; Sheng Li H.; Fox, N. *Mol. Cryst. Liq. Cryst.* **2003**, *397*, 47–58. (b) Pieterse, K.; van Hal, P.A.; Kleppinger, R.; Vekemans, J.A.J.M.; Janssen, R.A.J.; Meijer, E.W. *Chem. Mater.* **2002**, *13*, 2675–2679. (c) Boden, N.; Borner, R.C.; Bushby; R.J.; Clements, J. *J. Am. Chem. Soc.* **1994**, *116*, 10807–10808.

(20) (a) Strzelecka, H.; Jallabert, C.; Verber, M. *Mol. Cryst. Liq. Cryst.* **1988**, *156*, 355–359. (b) Strzelecka, H.; Jallabert, C.; Verber, M.; Davidson, P.; Levelut, A.M.; Malthête, J.; Sigaud, G.; Skoulios, A.; Weber, P. *Mol. Cryst. Liq. Cryst.* **1988**, *161*, 403–411. (c) Pelzl, G.; Diele, S; Weissflog, W. *Adv. Mater.* **1999**, *11*, 707–724. (d) Walba, D.M.; Körblova, E.; Shao, R.; Maclennan, J.E.; Link, D.R.; Glaser, M.A.; Clarck, N.A. *Science* **2000**, 288, 2180–2184. (e) Prasad, V.; Shankar Rao, D.S.; Krishna Prasad, S. *Mol. Cryst. Liq. Cryst.* **2003**, *397*, 79–88. (f) Dierking, I. *Textures of Liquid Crystals*; WILEY-VCH: Weinheim, **2003**. (g) Choi, E-J.; Ahn, J.-C.; Chien, L.-C.; Lee, C.-K.; Zin, W.-C.; Kim, D.-C.; Shin, S.-T. *Macromolecules* **2004**, *37*, 71–78.

(21) Shen, D.; Pegenau, A.; Diele, S.; Wirth, I.; Tschierske, C. *J. Am. Chem. Soc.* **2000**, *122*, 1593–1601.

(22) (a) Wu, J.; Watson, M.D.; Zhang, L.; Wang, Z.; Müllen, K. *J. Am. Chem. Soc.* **2004**, *126*, 177–186. (b) Lemaur, V.; da Silvo Filho, D.A.; Coropceanu, V.; Lehman, M.; Geerts, Y.; Piris, J.; Debije, M.G.; van de Craats, A.M.; Senthilkumar, K.; Siebbeles, L.D.A.; Warman, J.M.; Brédas, J.-L.; Cornil, J. *J. Am. Chem. Soc.* **2004**, *126*, 3271–3279. (c) Bushey, M.L.; Hwang, A.; Stephens, P.W.; Nuckolls, C. *Angew. Chem. Int. Ed.* **2002**, *41*, 2828–2831. (d) Palmans, A.R.A.; Vekemans, J.A.J.M.; Fischer, H.; Hikmet, R.A.; Meijer, E.W. *Chem. Eur. J.* **1997**, *3*, 300–307. (e) Palmans, A.R.A.; Vekemans, J.A.J.M.; Hikmet, R.A.; Fisher, H.; Meijer, E.W. *Adv. Mater.* **1998**, *10*, 873–876. (f) Praefcke, K.; Eckert, A. *Mol. Cryst. Liq. Cryst.* **2003**, *396*, 265–299. (g) Chandrasekhar, S. *Handbook of liquid crystals: Low molecular weight liquid crystals II*; Vol. 2B, 749–780; Demus, D.; Goodby, J.; Gray, G.W.; Spiess, H.W., Vill, V. (Eds.), WILEY-VCH: Weinheim, **1998**.

(23) Pieterse, K. *Thesis: Electron deficient materials based on azaheterocycles*; Eindhoven University of Technology: Eindhoven, **2001**.

(24) Vekemans, J.A.J.M., unpublished results.

(25) For C_3-symmetrical disks (Chapter 3), and poly-ureidophthalimides (Chapter 5) $\Delta\varepsilon$ = 275, and 150 l/mol.cm, respectively.

(26) The optimization of urea condensations using 4-dimethylaminopyridine will be reported in: de Greef, T.F.A., *Graduation report*; Eindhoven University of Technology: Eindhoven, **2004**.

(27) (a) Cheng, R.P.; Gellman, S.H.; DeGrado, W.F. *Chem. Rev.* **2001**, *101*, 3219–3232. (b) Gademann, K.; Häne, A.; Rueping, M.; Jaun, B.; Seebach, D. *Angew. Chem. Int. Ed.* **2003**, *42*, 1534–1537. (c) Seebach, D.; Schaeffer, L.; Brenner, M.; Hoyer, D. *Angew. Chem. Int. Ed.* **2003**, *42*, 776–778. (d) Stryer, L.; *Biochemistry*, 4th ed, W. H. Freeman & Company: New York, **1995**.

Summary

Self-assembly of synthetic, organic structures may open new opportunities in both the fields of biology and materials science. In principle supramolecular chemistry allows rapid formation of, nano-sized, well-defined architectures, while their reversible nature is maintained. A supramolecular architecture needs an optimal balance between stability and reversibility. When non-covalent interactions are too strong, movement of building blocks might be hampered by kinetic factors, thus making it difficult to reach the ordered thermodynamic equilibrium situation.

To find an optimal balance between the stability and the reversibility in the supramolecular architecture, an optimal interplay between non-covalent interactions in the architecture has to be achieved. To judge the contribution of each specific secondary interaction (e.g. hydrogen bonding, π-π stacking), a thorough understanding of the relationship between the chemical structure and the material properties (liquid crystallinity, gel formation) is essential. For various compounds (Figure 1), a coherent molecular picture has emerged over the complete concentration range from the bulk, via the gel, to the isolated molecules. A variety of techniques has been applied, among which DSC, optical microscopy, and X-ray in the solid state. In the concentrated gel phase AFM and SANS have been used. In dilute solution isolated supramolecular architectures are present. To recognize, and to determine the degree of ordering in, these supramolecular architectures, supramolecular chirality has been incorporated via information in the chiral peripheral chains. Circular dichroism spectroscopy is the appropriate tool that has provided insight into and understanding of the behavior of new chiral architectures.

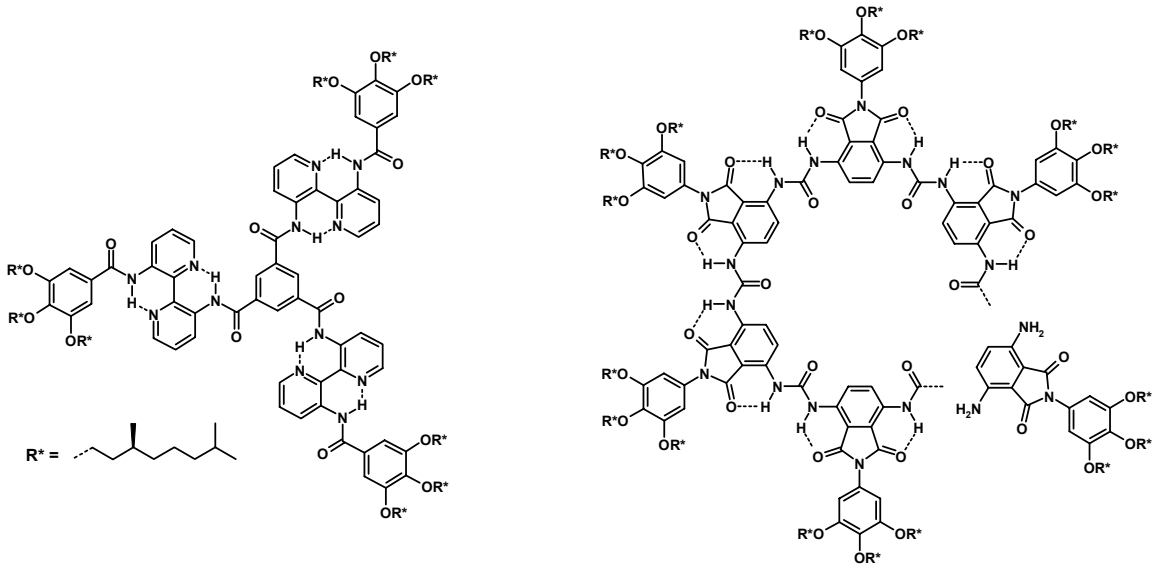

Figure 1. *Chemical structures of a C_3-symmetrical disk (left) and of a ureidophthalimide 'foldamer' (right).*

This research is focusing on the helix-architecture, in view of its key role in expressing functions of proteins. Recently, C_3-symmetrical discotics have been developed, that suitably self-assemble into columns. In the column, helicity has been introduced by 'locking' the disks in a mutually rotated position with the aid of *inter*molecular hydrogen bonding and π-π stacking interactions. To optimally tune these interactions, a series of twelve C_3-symmetrical discotics, varying in hydrogen bonding unit (amide or urea), π-π stacking (small, medium, large), and chirality in the lipophilic chains, has been compared. The disks show a coherent behavior over the whole concentration range, indeed. In dilute solution (CD), single molecules self-assemble into helical columns. These columns form a network in the gel phase (AFM, SANS), and are hexagonally ordered in the liquid crystalline phase (X-ray). At all concentrations it has been found that urea hydrogen bonding provides a higher stability than amide hydrogen bonding. At the same time, kinetic effects become apparent in building the most ordered architecture, indicated as hysteresis. Amide disks seem to form an ordered helix directly, while urea disks initially form an ill-defined stack that subsequently transforms slowly in a well-ordered, chiral column. The rigidity of the urea stack enables the formation of an *n*-heptane solvent shell around the stack, in an environment of branched *iso*-octane.

Asymmetry in abovementioned disks, in principle allows incorporation of the 'secondary' helices in 'tertiary' architectures. Monoamide diurea disks stack into helices via specific amide-amide and urea-urea interactions. However, an attempt to thread monoamide diurea disks to a foldamer adopting a helical conformation failed. Lengths above five or six units show irreversible and disordered aggregation induced by the 'strong' hydrogen bonding interactions.

Nonetheless, the 'foldamer approach' is a strategy towards helix formation closer to the natural α-helix than the 'self-assembly strategy'. Like natural macromolecules, foldamers are covalent polymeric molecules that adopt a helical conformation by *intra*molecular, non-covalent interactions. A poly-ureidophthalimide with 'weak' intramolecular hydrogen bonding has been designed, synthesized and investigated. From microscopic and optical measurements follows that this polymer (~30 units) folds into an ordered, chiral, supramolecular helix in various solvents and at low concentration (10^{-5} M). After isolation of the oligomers (2 up to 8 units) with chromatography, intra- and intermolecular 'folding' processes could be identified.

Aiming at application of the ureidophthalimide scaffold in new materials, a first attempt is undertaken to incorporate the dye anthraquinone in the phthalimide helix. Indeed, ordered architectures are found, that may contribute to a more efficient charge transport in supramolecular electronics.

Samenvatting

Zelfassemblage van synthetische, organische structuren leidt tot nieuwe ontwikkelingen, zowel binnen het vakgebied van de biologie, als dat van de materiaalkunde. In principe maakt het zelfassemblageproces het mogelijk op nano-schaal, snel goed-gedefinieerde architecturen op te bouwen, die hun reversibele karakter behouden. In een supramoleculaire architectuur is een optimale balans tussen stabiliteit en reversibiliteit essentieel. Wanneer niet-covalente interacties te sterk worden, belemmeren kinetische factoren de bewegingsvrijheid van de individuele bouwstenen. De supramoleculaire architectuur kan dan zijn optimaal geordende thermodynamische evenwichtssituatie niet meer bereiken.

Een optimale balans tussen stabiliteit en reversibiliteit in de supramoleculaire architectuur houdt een optimale afstemming in van de verschillende niet-covalente interacties (bijvoorbeeld waterstofbrug-vorming en π-π interacties). Om de bijdrage van iedere specifieke interactie in te kunnen schatten, is een diepgaand begrip van de relatie tussen de chemische structuur en de materiaaleigenschappen (vloeibaar kristalliniteit, gelvorming) noodzakelijk. Voor verschillende verbindingen (Figuur 1) is een samen-hangend moleculair beeld gevormd over het totale concentratiegebied, van bulk, via gel tot geïsoleerd molecuul. Hierbij is gebruik gemaakt van een scala aan technieken, waaronder DSC, optische microscopie en röntgen diffractie in de vaste fase, terwijl in de gel fase AFM en SANS zijn gebruikt. In verdunde oplossing zijn geïsoleerde supramoleculaire architecturen aanwezig. Om (de mate van) ordening hierin te herkennen, is gebruik gemaakt van supramoleculaire chiraliteit, geïntroduceerd via chirale informatie in de perifere ketens. Circulair dichroïsme spectroscopie is het aangewezen instrument gebleken om inzicht en begrip te verkrijgen in het gedrag van de nieuwe chirale architecturen.

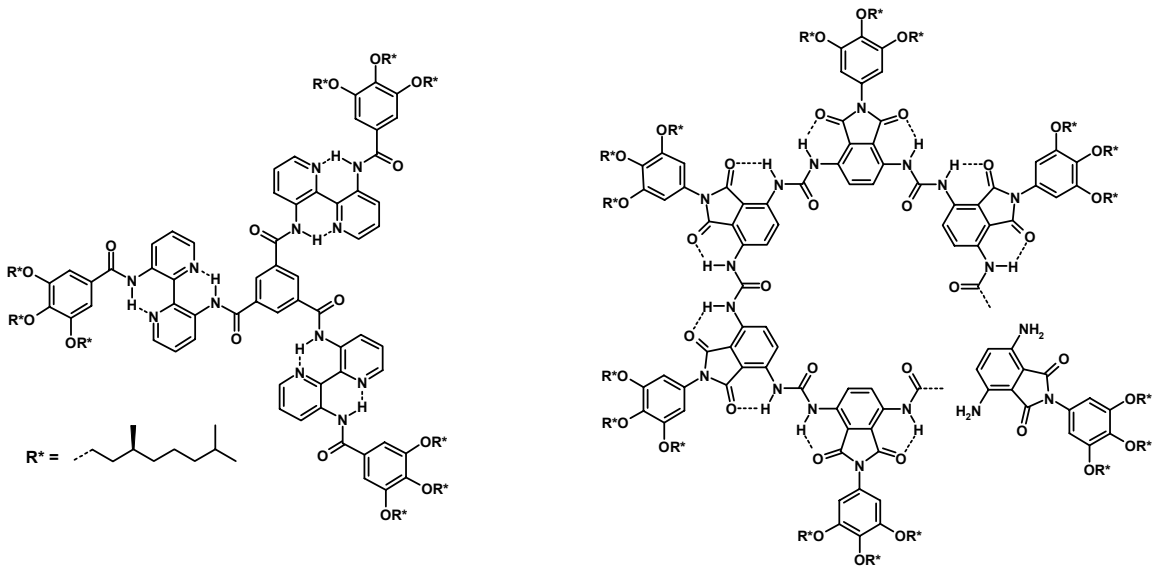

Figuur 1. *Chemische structuren van een C_3-symmetrische disk (links) en van een ureïdoftaalimide 'foldamer' (rechts).*

In dit onderzoek ligt de nadruk op de helix-architectuur, mede vanwege de essentiële rol die de α-helix speelt in de expressie van eiwitfuncties. Recent zijn C_3-symmetrische schijfvormige moleculen ontwikkeld, die zelf-assembleren tot kolommen. Heliciteit is gegenereerd door de schijven ten opzichte van elkaar te roteren met behulp van *inter*moleculaire waterstofbrugbinding en π-π stapeling. Om een optimale afstemming van deze interacties te verkrijgen is een reeks van twaalf C_3-symmetrische schijven vergeleken, variërend in hun mogelijkheid tot waterstofbrugbinding (amide of ureum) en tot π-π stapeling (klein, gemiddeld, groot), al dan niet voorzien van een stereogeen centrum in de lipofiele zijstaarten. De schijven vertonen inderdaad een samenhangend gedrag over het hele concentratiegebied. In verdunde oplossing (CD) zelf-assembleren ze tot helische kolommen. Deze kolommen vormen een netwerk in de lyotrope gelfase (AFM, SANS), terwijl ze in de vloeibaar kristallijne fase hexagonaal geordend zijn (X-ray). Bij alle concentraties is gebleken dat ureum waterstofbruggen een grotere stabiliteit geven dan amide waterstofbruggen. Tegelijkertijd wordt de kinetiek zichtbaar in het opbouwen van de meest geordende architectuur, een fenomeen aangeduid als hysterese. Amide schijven lijken direct een geordende helix te vormen. De ureum schijven vormen aanvankelijk een slecht gedefinieerde stapel, die vervolgens langzaam in een goed-geordende, chirale kolom verandert. De rigiditeit van de ureum kolom maakt de formatie van een *n*-heptaan solvent schil om de kolom mogelijk, in een medium van vertakt *iso*-octaan.

Asymmetrie in de bovengenoemde disks, maakt het in principe mogelijk de 'secundaire' helices te incorporeren in 'tertiaire' architecturen. Monoamide diureum disks vormen helices via uitsluitend amide-amide en ureum-ureum interacties. Echter, een poging de monoamide diureum disks 'aaneen te rijgen' tot een 'foldamer' in een helixconformatie faalde. Al bij een lengte van vijf tot zes eenheden trad irreversibele en dus ongeordende aggregatie op door 'sterke' waterstofbruginteracties.

Niettemin ligt de 'foldamer' aanpak tot helixformatie dichter bij de natuurlijke α-helix dan de 'self-assembly' benadering. Hier wordt immers gebruik gemaakt van covalente polymeermoleculen, die een helixconformatie aannemen met behulp van *intra*moleculaire, niet-covalente interacties. Een poly-ureïdoftaalimide met 'zwakkere' intramoleculaire waterstofbruggen is ontworpen, gesynthetiseerd en onderzocht. Uit microscopische en optische metingen blijkt dat dit polymeer (~ 30 eenheden) een geordende, chirale supramoleculaire helix vormt in diverse oplosmiddelen en bij lage concentratie (10^{-5} M). Na chromatografische isolatie van de oligomeren (2 tot en met 8 eenheden), konden intra- en intermoleculaire opvouwprocessen geïdentificeerd worden.

Met het oog op toepassing van het ureïdoftaalimide platform in nieuwe materialen is een eerste poging ondernomen om de kleurstof antrachinon op te nemen in de ftaalimide helix. Er zijn inderdaad geordende architecturen gevonden die zouden kunnen bijdragen aan een efficiënter ladingstransport in supramoleculaire elektronica.

Curriculum Vitae

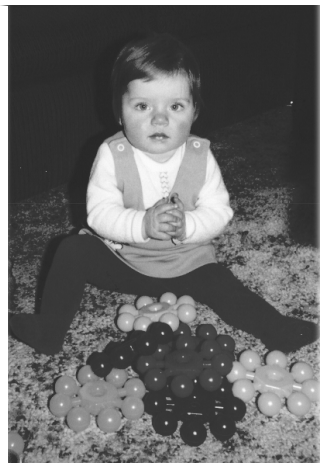

Judith van Gorp werd geboren op 12 mei 1976 te Eindhoven. Na de VWO-opleiding aan de Gemeentelijke Scholengemeenschap Woensel, het tegenwoordige Stedelijk College Eindhoven, werd in 1994 begonnen aan de studie Scheikundige Technologie aan de Technische Universiteit Eindhoven. Haar externe stages werden uitgevoerd aan de Universiteit van Osaka (prof.dr. Akira Harada) in de zomer van 1997 en bij SHELL Research and Technology Centre (Louvain-la-Neuve, België) in het eerste kwartaal van 1998. In augustus 1999 rondde ze haar afstudeerproject af binnen de capaciteitsgroep Macromoleculaire en Organische Chemie. Na deze datum bleef ze werkzaam als promovendus in deze groep, onder leiding van prof.dr. E.W. Meijer en dr. J.A.J.M. Vekemans. De belangrijkste resultaten van dit onderzoek staan beschreven in dit proefschrift. Tijdsafhankelijke fluorescentiemetingen zijn uitgevoerd in september 2002 aan de Universiteit van Amsterdam samen met prof.dr. Max Glasbeek, dr. Hong Zhang en drs. Paul Toele. X-ray data waren het resultaat van een bezoek aan prof. Takashi Kato en drs. Yuko Kamikawa aan de Universiteit van Tokio in december 2003. Vanaf juni 2004 zal ze werkzaam zijn bij DuPont, tot oktober in Wuppertal (Duitsland), daarna in Wilmington (Delaware, Verenigde Staten).

Judith van Gorp was born in Eindhoven, the Netherlands on May 12th, 1976. She attended the Gemeentelijke Scholengemeenschap Woensel, the present Stedelijk College Eindhoven, where she obtained her VWO-degree (pre-university degree). In 1994 she started the study of Chemical Engineering and Chemistry at the Eindhoven University of Technology. Her external traineeships were performed at Osaka University (prof.dr. Akira Harada) in the summer of 1997 and at SHELL Research and Technology Centre (Louvain-la-Neuve, Belgium) in the first quarter of 1998. She obtained her Master of Science degree in August 1999 with a graduation project at the laboratory of Macromolecular and Organic Chemistry. She stayed in this group as a Ph.D. student under the supervision of prof.dr. E.W. Meijer and dr. J.A.J.M. Vekemans. The most important results of the investigations are described in this thesis. Time dependent fluorescence measurements were performed in September 2002 at the University of Amsterdam in cooperation with prof.dr. Max Glasbeek, dr. Hong Zhang en drs. Paul Toele. X-ray data were the result of a visit to prof. Takashi Kato en drs. Yuko Kamikawa at Tokyo University in December 2003. As of June 2004 she will be working with DuPont, until October in Wuppertal (Germany), afterwards in Wilmington (Delaware, United States of America).

Dankwoord

Waar de promovendus stopt met schrijven, wordt doorgaans begonnen met lezen. Het dankwoord is dan ook de plaats waar de betrokkenheid bij het promotieonderzoek wordt gedeeld met de mensen die onmisbaar zijn geweest in het realiseren ervan.

Mijn onderzoeksbegeleiders, prof.dr. Bert Meijer en dr. Jef Vekemans, zijn allebei verliefd op moleculen, of tenminste toch op het ontwerpen en synthetiseren ervan. Wanneer je jullie kamers 'langs gaat' voor advies in deze, kom je altijd met meer energie weer naar buiten. Maar ook jullie begrip voor allerlei andere obstakels, die een promovendus zo op zijn levenswandel tegenkomt, is ongekend. Ik zal jullie altijd dankbaar blijven voor het voorbeeld dat jullie gesteld hebben, vooral zoals jullie vastgelegd zijn op de 'familiekiekjes'. Hierbij denk ik terug aan een frisse ochtendduik in de Zeeuwse wateren of een pose als koningin in een Duits toneelstuk. Maar ook de filtreerpapieren overvol poeders in het laboratoriumkastje van Jef zal ik nooit vergeten, evenmin als het vol structuren gekrijte bord op de kamer van Bert.

I thank prof. Takashi Kato and drs. Yuko Kamikawa for their help with X-ray measurements on columnar 'Eki Sho', and above all for the warm welcome they gave me in Tokyo. Een paar 'donkere dagen' in Amsterdam hebben geleid tot de tijdsafhankelijke fluorescentieresultaten. Hiervoor wil ik prof.dr. Max Glasbeek, dr. Hong Zhang en drs. Paul Toele bedanken. Prof.dr. Max Glasbeek en prof.dr.ir. René Janssen hebben het proefschrift gecontroleerd op zijn fysische correctheid. I also thank prof. Steven Zimmerman for his improvements and suggestions. Naast de leden van de leescommissie gaat mijn dank vanzelfsprekend uit naar de totale promotiecommissie, gecompleteerd door prof.dr. Roeland Nolte, prof.dr. Thijs Michels en dr. Rint Sijbesma.

De mensen van 'lab 2' zijn rotsen in de branding van de Dommel. Van Emiel Peeters en Koen Pieterse leerde ik snel de kneepjes van het vak. Zelfstandig werken kon ik al ras, aangezien ze in het aangrenzende PPP-kamertje doorgaans meer aandacht voor elkaar hadden dan voor mij. Sindsdien heb ik lief en leed gedeeld met Jolanda Spiering, van labbrillen en glasscherven tot chirale galluszuurderivaten. Ook René Sinkeldam is een dappere ridder in de 'Orde van lab 2', die ik geweldig (met zachte g) veel succes wens met het vervolg van het 'foldamer' onderzoek. Hierin hebben stagiaires Jaana Oona en Andrea Greven verschillende bouwstenen en modelverbindingen gesynthetiseerd, en heeft afstudeerder 'Tosti' Tom de Greef zich vermaakt met oligomeren van gedefinieerde lengte. Research stagiaire Kristie Spijker is zo moedig geweest de wilde ideeën van een 'solvent shell' rondom de stacks van C_3-symmetrische discoten te toetsen. Ook Spinoza studenten Marloes Langelaan, Bram Coolen en Peter van den Broek hebben in dit opzicht menig meting uitgevoerd. I had many pleasant discussions with 'disc man' Mitsutoshi Masuda. It will only be a matter of time before the stacks become as high as Tokyo Tower.

Het werk van Anja Palmans en Luc Brunsveld heeft ons hierbij enorm op weg geholpen. Ik zou bijna zeggen dat jullie proefschriften voor mij als het oude en het nieuwe testament zijn geweest. Ze staan er grijsgelezen en verfomfaaid bij in vergelijking met de overige proefschriften in mijn kast.
Daan Wouters en Pascal Jonkheijm zijn verantwoordelijk voor de AFM foto's. Ralf Kleppinger wil ik bedanken voor de SANS metingen. Serge Söntjens is behulpzaam geweest bij de 2D NOESY metingen. Koen Pieterse heeft de aanzet gegeven tot het modelleren van de poly-ureïdoftaalimiden. Joost van Dongen, Xianwen Lou en Ralf Bovee bedank ik voor al hun hulp op analytisch gebied. Ralf heeft heel wat moeite moeten doen de ftaalimide oligomeren klein te krijgen. Handmatig (!) hebben we menig fractie opgevangen.

Alle vroegere en huidige leden van de capaciteitsgroep Macromoleculaire en Organische Chemie wil ik bedanken voor het creëren van een sfeer waarin wederzijdse interesse en behulpzaamheid centraal staan. De wetenschappelijke betrokkenheid van deelnemers aan de 'Supra'- en 'Sixma'-werkbesprekingen heeft zeker bijgedragen aan de diverse projecten. Bij Henk Eding en Hannie van der Lee denk ik aan de vele babbeltjes, vooral diegene boven de stofzuiger of vaatwasser uit. Ook Joke, Hanneke, Ingrid (2x), Carien en Dianne 'op' het secretariaat en Hans 'in' het magazijn hebben er aan bijgedragen dat het mij aan niets ontbrak.

Vele niet-wetenschappelijke bevliegingen kon ik delen met mijn mede-SMO-cabaretiers. In de eerste plaats noem ik 'Helmond Zapt', met onder andere 'Petazzie', 'Ricardo', 'Beppie', 'Paul Jambers' en 'Willibrord Frequin'. De professionaliteit van het avondvullend programma van 'JuPaJo-productions' kent zijn weerga niet, al had het gastoptreden van de 'Nuenense Broekkabouter' voor mij niet gehoeven. De samenwerking met 'Meneer Cactus', 'Mevrouw Stemband' en 'Kweetniet' was al net zo onvergetelijk. Ook 'Plastic Fantastic Barbie en Ken' behoren tot dit illustere gezelschap, evenals de Friese Helmondse. Bij deze laatste dient opgemerkt te worden dat een samenwerking met jezelf een aparte gewaarwording is.

Daarom ben ik de mensen bij wie ik dag en nacht mijn hart uit kan storten nog het meest dankbaar. Jeroen, de overkant van de oceaan voelt net zo dichtbij als het eind van de gang. Zodra ik m'n ogen dicht doe, kan ik je horen en zien. Plien en Jo, jullie zijn kanjers van 'Chemical Sisters' en ik kan me gewoonweg geen andere paranimfen voorstellen. Een broer die met je meeleeft geeft enorm veel steun, Joost. Ik weet 'waar je huis woont'. 'Ons mam' is mijn alles. Regelmatig zeg ik tegen haar: 'Als ik jou toch niet had...', waarop zij dan antwoordt: '....dan was je er niet.'

Judith.